N71-13494
CR-115806

OAKLAND UNIVERSITY SCHOOL OF ENGINEERING

FINAL REPORT

NASA/ERC Contract No. NGR 23-054-003
March 15, 1969 to June 30, 1970

BIOSYSTEMS ENGINEERING RESEARCH

Volume III Pattern Recognition of Biological Photomicrographs Using Coherent Optical Techniques.

R.E. Haskell, Associate Professor of Engineering

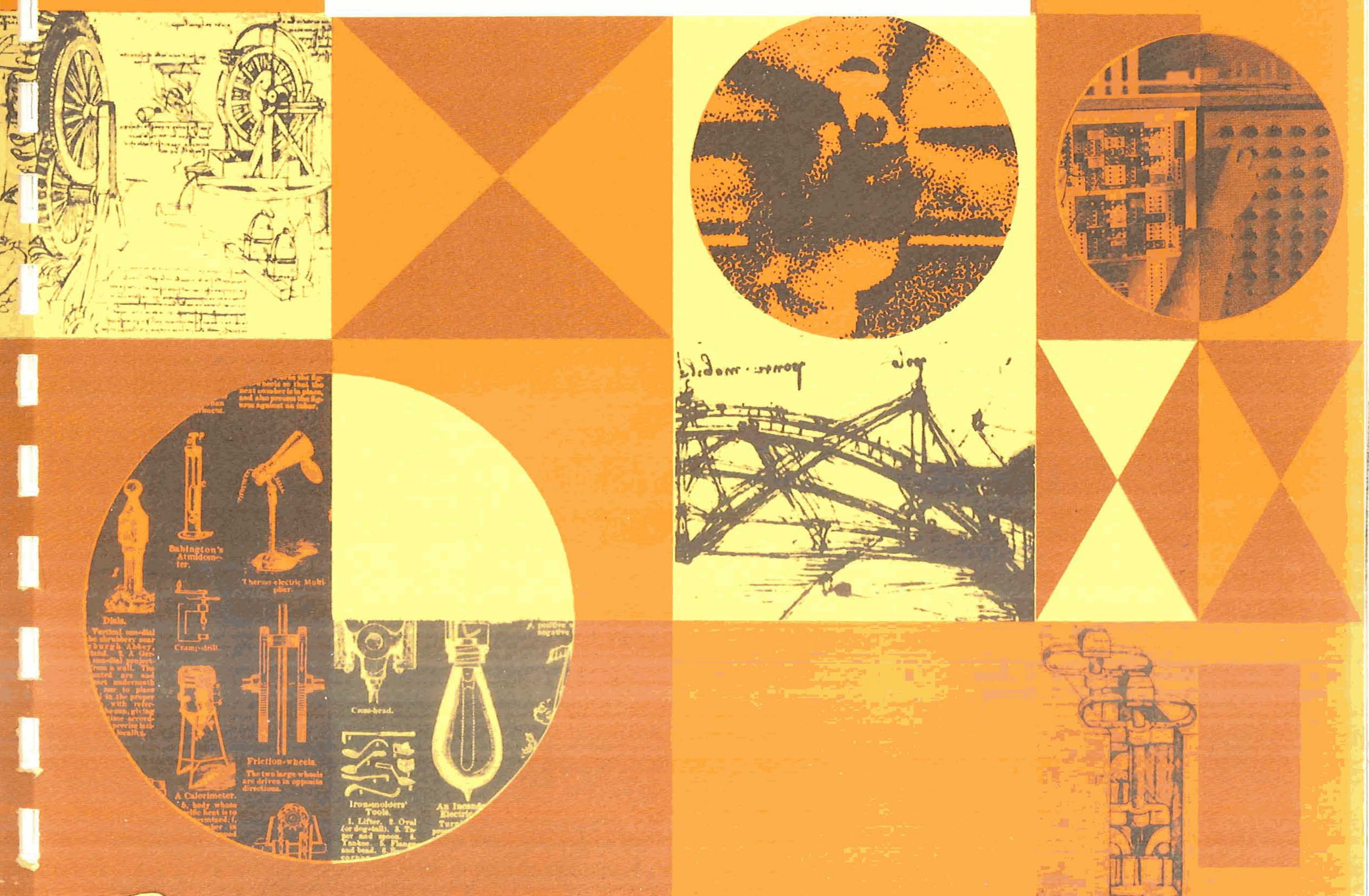

FINAL REPORT

NASA/ERC Contract No. NGR 23-054-003
March 15, 1969 to June 30, 1970

BIOSYSTEMS ENGINEERING RESEARCH

Volume III Pattern Recognition of Biological Photomicrographs Using Coherent Optical Techniques.

R.E. Haskell, Associate Professor of Engineering

Project Staff:

J.E. Gibson, Principal Investigator
J.C. Hill, Principal Investigator
R.E. Haskell
G.A. Jackson
R.H. Edgerton

SCHOOL OF ENGINEERING
OAKLAND UNIVERSITY
ROCHESTER, MICHIGAN 48063

Technical Report 70-7
November, 1970

VOLUME III

PATTERN RECOGNITION OF BIOLOGICAL PHOTOMICROGRAPHS USING COHERENT OPTICAL TECHNIQUES

R.E. Haskell, Associate Professor of Engineering

Oakland University

Rochester, Michigan 48063

FOREWORD

This report was prepared under NASA Contract NGR 23-054-003, which provided institutional support for biosystems research conducted by the Oakland University School of Engineering, and is one of four volumes reporting research conducted during the period March 15, 1969 to June 31, 1970.

The four volumes of the series, together with their principal authors are listed below:

Volume I	A Dynamic Model of the Human Postural Control System (J.C. Hill).
Volume II	An Investigation of Two Hybrid Computer Identification Techniques for Use in Manual Control Research (G.A. Jackson).
Volume III	Pattern Recognition of Biological Photomicrographs Using Coherent Optical Techniques (R.E. Haskell).
Volume IV	Augmentation of the Focus Control System of the Human Eye through Index of Refraction Variation of Liquid Crystal Materials (R.H. Edgerton).

Professors J.C. Hill and J.E. Gibson, Dean of the School of Engineering, were principal investigators on the contract.

ABSTRACT

Random patterns in photomicrographs can be recognized by studying the nature of coherent light diffracted by the spatial pattern. Techniques for measuring the power spectrum and autocorrelation function of random spatial signals are described. These techniques include both holographic and non-holographic methods. A computer program for generating random patterns with known statistics is presented. Results of power spectrum and autocorrelation measurements are given together with theoretical curves for a variety of spatial signals.

ACKNOWLEDGMENT

A number of students have contributed to this research by developing the computer programs and performing the experimental measurements. These students are:

Graduate Students: William Gelbach
Y.Y. Hung
John Moran

Undergraduate Students: Fred Levko
Larry Peck
Nader Safai

PATTERN RECOGNITION OF BIOLOGICAL

PHOTOMICROGRAPHS USING COHERENT OPTICAL TECHNIQUES

PATTERN RECOGNITION OF BIOLOGICAL PHOTOMICROGRAPHS USING COHERENT OPTICAL TECHNIQUES

1. Introduction

This research in pattern recognition was stimulated by a desire to obtain quantitative statistical information about certain types of random spatial patterns such as might occur in biological or metallographic photomicrographs. Examples of photomicrographs of the rabbit lens epithelimin are shown in Figs. 1 and 2. The basic idea is to analyze the manner in which coherent light is diffracted by a two-dimensional random pattern and from such measurements to infer certain statistical quantities such as mean cell size, shape, and distribution. Lendaris and Stanley[1] have recently reported on a quasi-automatic device for sampling the diffraction pattern in an attempt to recognize patterns in aerial photographs. In addition to diffraction pattern or power spectrum measurements we show in this report that autocorrelation and cross-correlation measurements we show in this report that autocorrelation and cross-correlation measurements can also be useful in recognizing patterns, particularly those of a random nature.

Progress has been made in three areas of this research. The first is concerned with power spectrum measurements of spatial signals. While it is well known that lenses can produce Fourier Transforms of spatial signals, in the attached Technical Report No. 70-3 we show that a single lens or a single spherical mirror can not only be used to produce a power spectrum of spatial signals but can be used as a complete optical processing system in which a filtered version of the input signal can be obtained in the output plane. The use of a large spherical mirror in such an optical processing system allows one to use spatial signals of a larger size than is possible with common lens systems.

In addition to power spectrum measurements made with lenses and

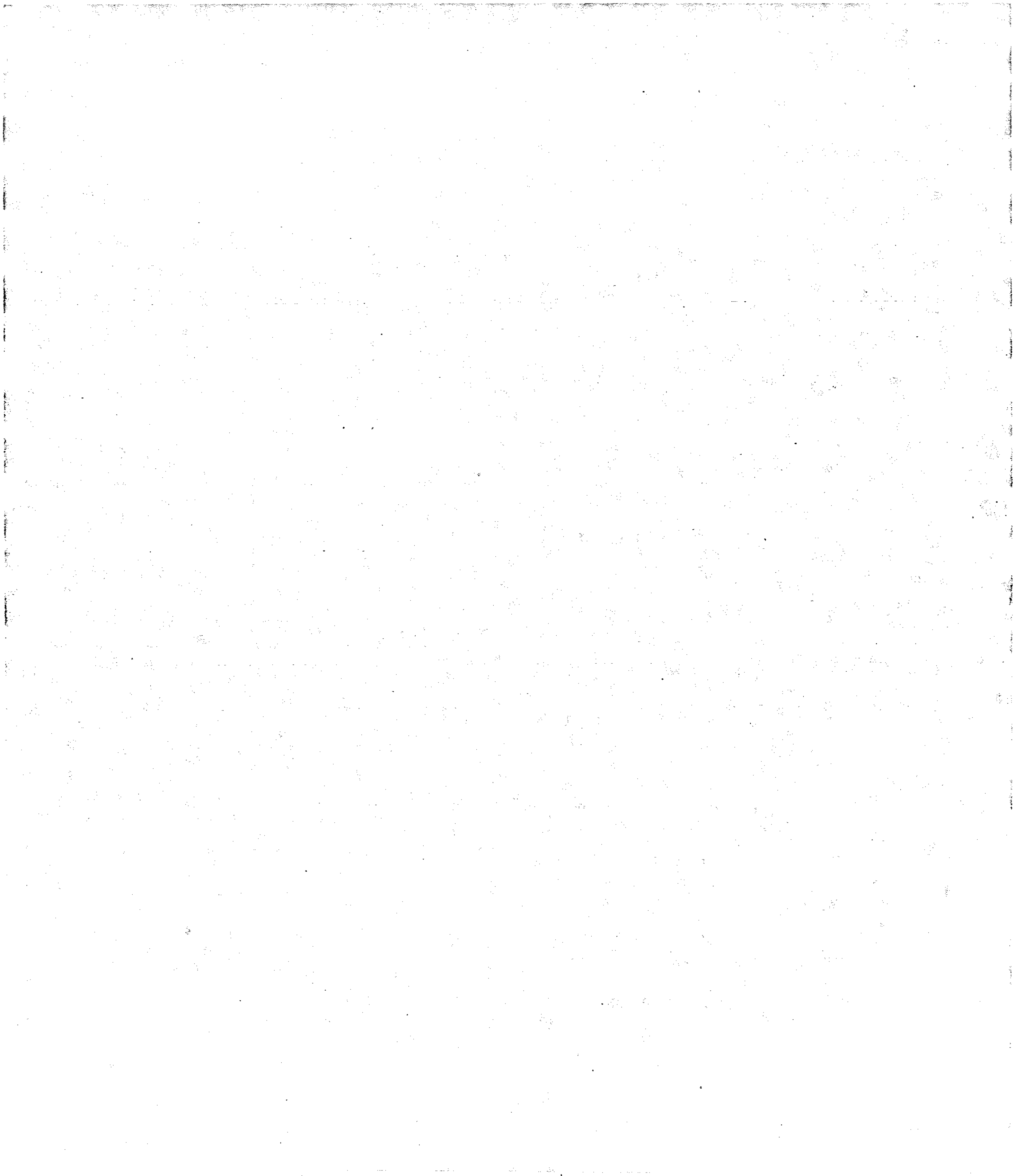

Fig. 1 Photomicrograph of the middle region of rabbit lens epithelmin.

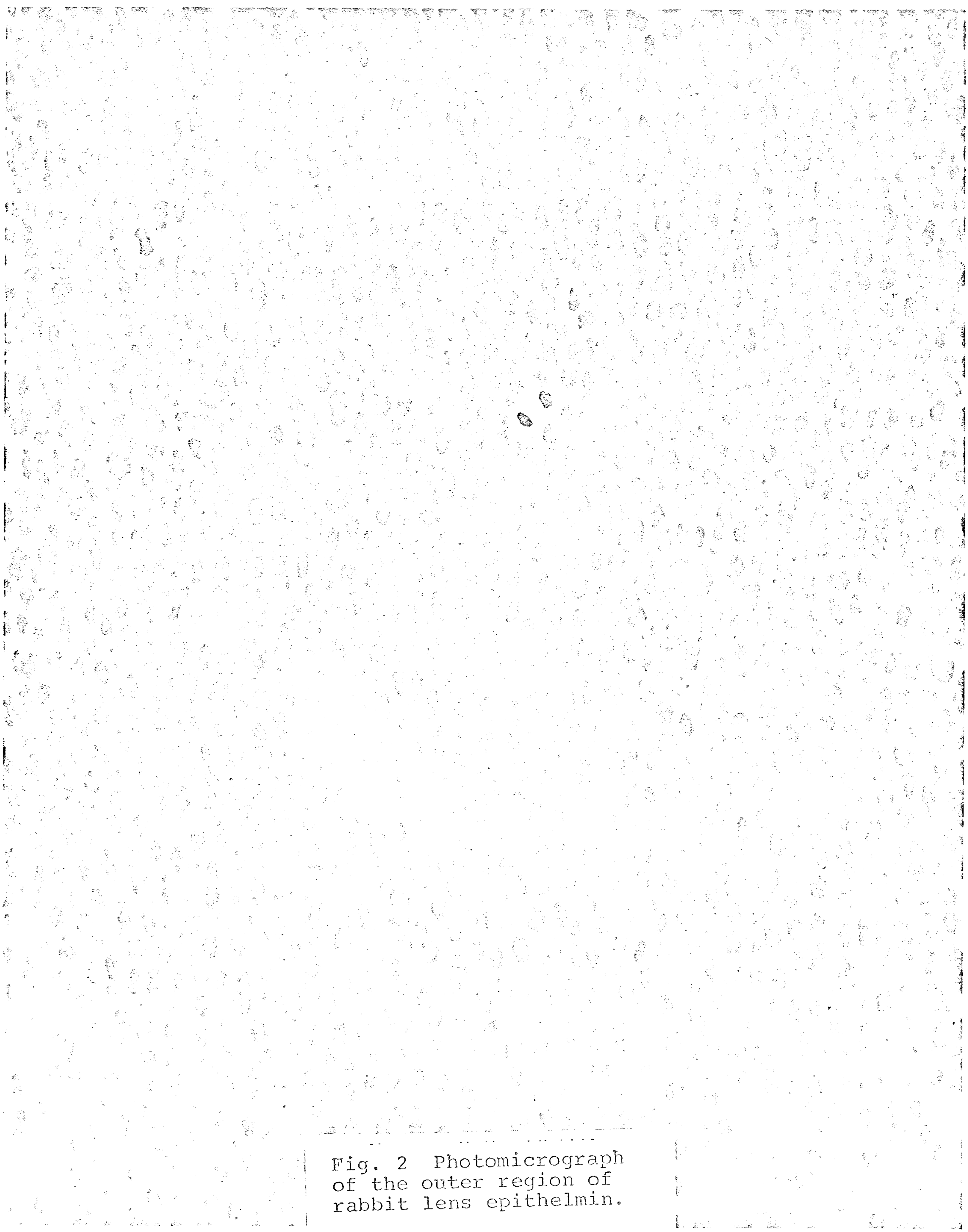

Fig. 2 Photomicrograph of the outer region of rabbit lens epithelmin.

spherical mirrors it has been shown in this laboratory for the first time that power spectrum measurements can be made holographically without the use of any lenses. This work is described in the attached Technical Report No. 70-4 entitled "Fourier Transforming Properties of Holograms" by Richard E. Haskell which was presented at the Optical Society of America meeting in Hollywood, Florida, September 28-October 2, 1970. The location of Fourier transform planes in holographic imaging is greatly facilitated by the use of two nomographs which are described in the attached Technical Report No. 70-1.

The second area of progress is related to autocorrelation, cross-correlation, and convolution measurements of spatial signals. One method of measuring the autocorrelation function of a spatial signal is to record the power spectrum of the signal on photographic film in the transform plane of an optical processing system. A positive transparency is made from this first negative transparency and is then used as the signal in a similar processing system. The Fourier transform of the power spectrum is equal to the autocorrelation function of the original signal and is measured in the transform plane of the optical system. Some measurements made in this way are shown in Section 4 of this report.

An alterante method of measuring the autocorrelation function of a spatial signal is to use a holographic technique. This technique can also be used to measure the cross-correlation and convolution of two different spatial signals and has the potential of being adaptable to real-time measurements. A detailed analysis of this technique together with experimental results is given in the attached Technical Report No. 70-2.

The third area of progress concerns the development of a computer program that will automatically plot a variety of random patterns made up of dots and circles. This computer program is described in Section 3 of this report and a number of different random plots are presented. These random spatial signals are recorded on 35 mm film and are then used as test signals in the various optical processing systems. The basic statistical description of random spatial signals is discussed in the following section.

2. Diffraction of Coherent Light by Random Spatial Signals

Figure 3 shows coherent light incident from the left on a transparency of a random spatial signal which is located in the x-y plane and acts as a diffracting screen. If $\underset{\sim}{U}(x,y)$ is the complex amplitude of light just to the left of the screen then the light amplitude just to the right of the screen is given by

$$\underset{\sim}{U}'(x,y) = \underset{\sim}{g}(x,y)\ \underset{\sim}{U}(x,y) \qquad (1)$$

where

$$\underset{\sim}{g}(x,y) = A(x,y)e^{j\phi(x,y)} \qquad (2)$$

is the complex transmittance of the transparency. The amplitude and phase of this transmittance, $A(x,y)$ and $\phi(x,y)$ are considered to be two-dimensional random functions of the coordinates x and y. For convenience the position vector $r = x\underset{\sim}{u}_x + y\underset{\sim}{u}_y$ can be introduced so the (2) can be written as

$$\underset{\sim}{g}(\underset{\sim}{r}) = A(\underset{\sim}{r})e^{\,j\phi(\underset{\sim}{r})} \qquad (3)$$

The random functions $A(\underset{\sim}{r})$ and $\phi(\underset{\sim}{r})$ are characterized by the one dimensional probability densities $p(a;\underset{\sim}{r})$ and $p(\phi;\underset{\sim}{r})$. Thus, for example, $p(a;\underset{\sim}{r})da$ is the probability that at the position $\underset{\sim}{r}$, the amplitude $A(\underset{\sim}{r})$ has a value between a and a + da. These one dimensional probability densities can be used to find the mean values, variances, and higher moments of the random functions $A(r)$ and $\phi(r)$. However, they by no means give a complete description of these random functions. The most important information in the transparency concerns the spatial distribution of the particular objects photographed (cells, nuclei, grain structure, etc). The statistical properties of these spatial disbributions are characterized by higher order probability density functions. The most important of these are the two-dimensional probability densities $p(a_1,a_2;\underset{\sim}{r}_1,\underset{\sim}{r}_2)$ and $p(\phi_1,\phi_2;\underset{\sim}{r}_1,\underset{\sim}{r}_2)$. Thus, for example, $p(\phi_1,\phi_2,\underset{\sim}{r}_1,\underset{\sim}{r}_2)d\phi_1 d\phi_2$ is the probability that at the position $\underset{\sim}{r}_1$ the phase $\phi(\underset{\sim}{r}_1)$ has a value between ϕ_1 and $\phi_1+d\phi_1$ <u>and</u> at the position $\underset{\sim}{r}_2$ the phase $\phi(\underset{\sim}{r}_2)$ has a value between ϕ_2 and $\phi_2 + d\phi_2$.

These two-dimensional probability densities can be used to calculate the correlation functions $B_A(\underset{\sim}{r}_1,\underset{\sim}{r}_2)$ and $B_\phi(\underset{\sim}{r}_1,\underset{\sim}{r}_2)$. Thus, for example

$$\begin{aligned} B_A(\underset{\sim}{r}_1,\underset{\sim}{r}_2) &= \left\langle A(\underset{\sim}{r}_1)A(\underset{\sim}{r}_2) \right\rangle \\ &= \iint a_1 a_2 p(a_1,a_2;\underset{\sim}{r}_1,\underset{\sim}{r}_2)da_1 da_2 \end{aligned} \tag{4}$$

If the transparency is a photomicrograph, a particular photomicrograph will represent a certain realization of the random processes $A(\underset{\sim}{r})$ and $\phi(\underset{\sim}{r})$. The ensemble associated with these random processes might consist of a collection of similar photomicrographs from different specimens or photomicrographs of different regions of the same specimen. The random processes $A(\underset{\sim}{r})$ and $\phi(\underset{\sim}{r})$ are said to be stationary in the wider sense if the expected values $\langle A \rangle$ and $\langle \phi \rangle$ are independent of $\underset{\sim}{r}$ and the correlation functions $B_A(\underset{\sim}{\rho})$ and $B_\phi(\underset{\sim}{\rho})$ depend only on the coordinate difference $\underset{\sim}{\rho}=\underset{\sim}{r}_2 - \underset{\sim}{r}_1$.

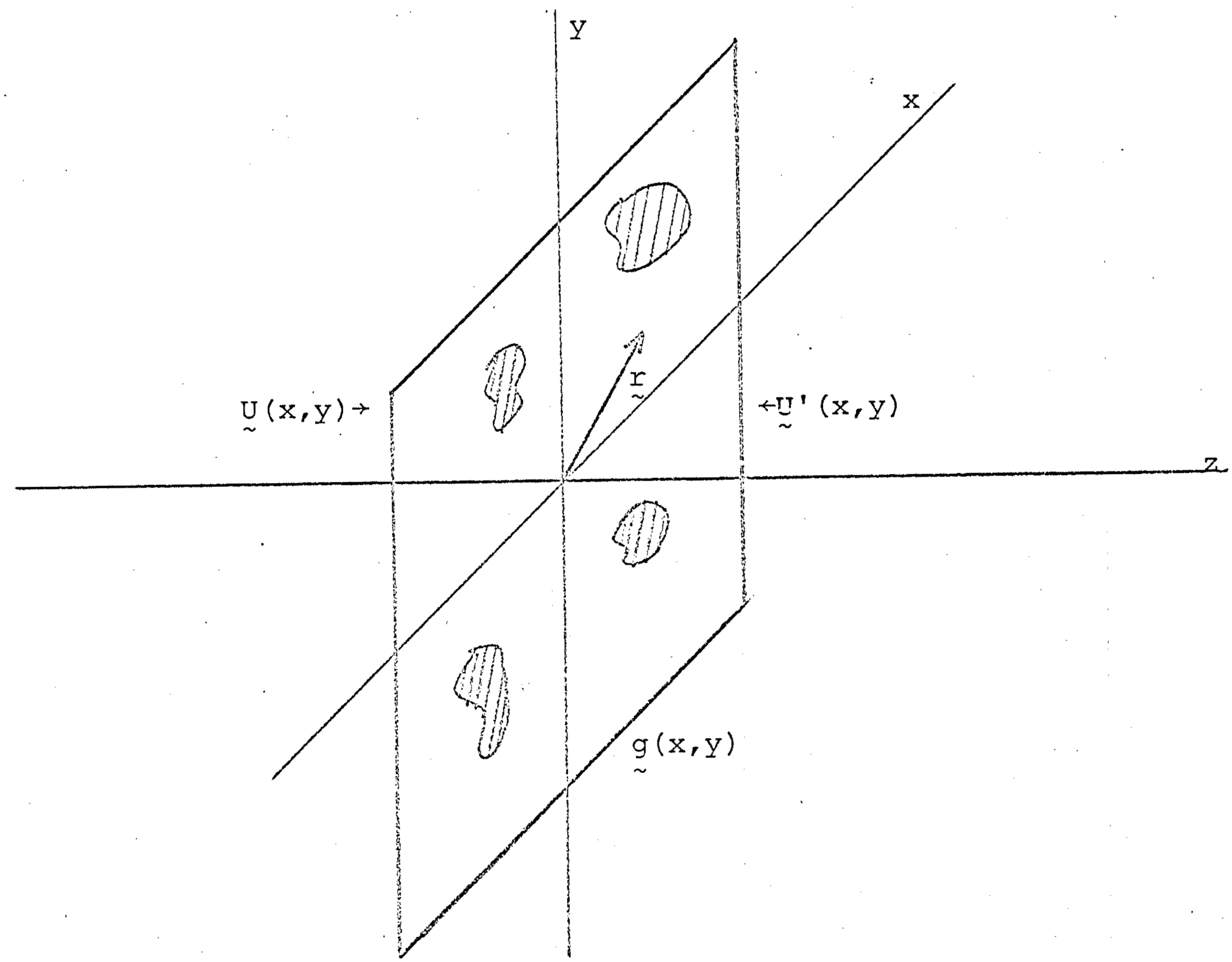

Fig. 3

Random Diffracting Screen

The space average of a given function $A(r)$ is defined as

$$\overline{A(\underset{\sim}{r})} = \lim_{\substack{X\to\infty \\ Y\to\infty}} \frac{1}{XY} \int_{-\frac{X}{2}}^{\frac{X}{2}} \int_{-\frac{Y}{2}}^{\frac{Y}{2}} A(\underset{\sim}{r})\,d\underset{\sim}{r} \tag{5}$$

where $d\underset{\sim}{r} = dxdy$. If the ensemble average $\langle A \rangle$ is equal to the space average $\overline{A(\underset{\sim}{r})}$ the process is said to be ergodic. For a stationary random process $A(\underset{\sim}{r})$, if the correlation function $B_A(\underset{\sim}{\rho}) = \langle A(\underset{\sim}{r})\, A(\underset{\sim}{r} + \underset{\sim}{\rho})\rangle$ is equal to the space correlation function $\overline{B_A(\underset{\sim}{\rho})} = \overline{A(\underset{\sim}{r})\, A(\underset{\sim}{r} + \underset{\sim}{\rho})}$ the process is said to be ergodic with respect to its correlation function. The optical methods for measuring the correlation function generally measure the space correlation function. An important consideration as will be illustrated below is that the detail of the photomicrograph be fine enough so that a space average over the entire photomicrograph is a good approximation to the ensemble average.

An optical system such as that shown in Fig. 4 can be used to produce the Fourier transform of a given spatial signal. Thus if $g(\underset{\sim}{r})$ is the complex transmittance of a particular transparency whose total area is XY then the complex light amplitude in the transform plane (the p-q plane of Fig. 4) will be proportional (to within a quadratic phase factor) to the Fourier transform of $\underset{\sim}{g}(x,y)$, denoted by $\underset{\sim}{G}_{XY}(f_x, f_y)$, where f_x and f_y are the spatial frequencies in the x and y directions. The light intensity in the transform plane will be proportional to $\left|\underset{\sim}{G}_{XY}(\underset{\sim}{f})\right|^2 = \underset{\sim}{G}_{XY}(\underset{\sim}{f})\underset{\sim}{G}^*_{XY}(\underset{\sim}{f})$ where $\underset{\sim}{f}$ is used to denote the spatial frequency vector $\underset{\sim}{f} = f_x\underset{\sim}{u}_x + f_y\underset{\sim}{u}_y$.

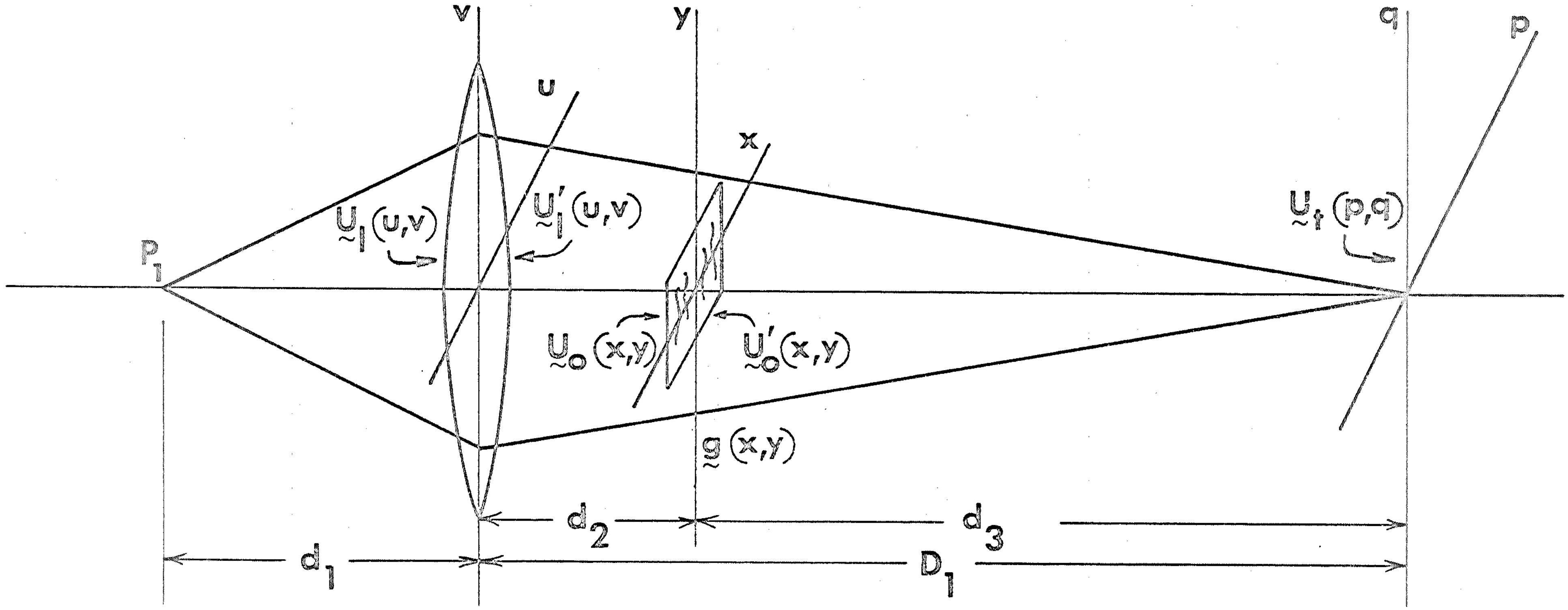

Fig. 4 Fourier Transforming Property of a Lens.

For the complex random signal $\underset{\sim}{g}(\underset{\sim}{r})$ (assumed to be stationary) the autocorrelation function $B_g(\underset{\sim}{\rho})$ is defined as

$$B_g(\underset{\sim}{\rho}) = \left\langle \underset{\sim}{g}(\underset{\sim}{r})\ \underset{\sim}{g}^*(\underset{\sim}{r} + \underset{\sim}{\rho}) \right\rangle \tag{6}$$

The power spectral density $S_g(\underset{\sim}{f})$ of the random process $\underset{\sim}{g}(\underset{\sim}{r})$ is defined as the two-dimensional Fourier transform of the autocorrelation function $B_g(\underset{\sim}{\rho})$. Thus

$$S_g(\underset{\sim}{f}) = \int_{-\infty}^{\infty} B_g(\underset{\sim}{\rho}) e^{-j2\pi \underset{\sim}{f}\cdot\underset{\sim}{\rho}} d\underset{\sim}{\rho} \tag{7}$$

One can show that $S(\underset{\sim}{f})$ is also related to the Fourier transform of $\underset{\sim}{g}(\underset{\sim}{r})$ by the expression

$$S_g(\underset{\sim}{f}) = \lim_{\substack{X\to\infty \\ Y\to\infty}} \left\langle \frac{1}{XY}\ \underset{\sim}{G}_{XY}(\underset{\sim}{f})\ \underset{\sim}{G}^*_{XY}(\underset{\sim}{f}) \right\rangle \tag{8}$$

In the case of the optical experiment $S_g(\underset{\sim}{f})$ is seen to be proportional to the limit of an ensemble average of the intensity measured in the transform plane. This effect will be shown in some experimental results discussed below.

The autocorrelation function $B_g(\underset{\sim}{\rho})$ is given from (7) by the inverse relation

$$B_g(\underset{\sim}{\rho}) = \int_{-\infty}^{\infty} S_g(\underset{\sim}{f}) e^{j2\pi \underset{\sim}{f}\cdot\underset{\sim}{\rho}} d\underset{\sim}{f} \tag{9}$$

$S_g(\underset{\sim}{f})$ can be recorded on photographic film in the transform plane of $\underset{\sim}{g}(\underset{\sim}{r})$. This new signal can be transformed optically to give the autocorrelation function according to (9). Examples of this type of measurement will be described below. Often the photomicrograph will be characterized by only its amplitude transmittance $A(\underset{\sim}{r})$ or by only its phase transmittance $\phi(\underset{\sim}{r})$. In general it will be necessary to relate the statistical properties of $A(\underset{\sim}{r})$ and $\phi(\underset{\sim}{r})$ to the measured statistical properties of $\underset{\sim}{g}(\underset{\sim}{r})$.

3. Computer Generation of Random Patterns

In order to generate random spatial patterns with a known statistical disbribution a computer program was developed that would automatically plot a variety of random patterns on an oscilloscope or an x-y plotter. These patterns are then photographically reduced and used as signals in the optical processing system.

The program will generate from 1 to 225 patterns either uniformly or randomly spaced. The patterns may be:

(a). Single spots with random rotation about a fixed point from 0° to 360°.

(b). Same as above with random distance from fixed point.

(c). Double spots with random orientation.

(d). Double spots with random orientation and random radius.

(e). Circles alone.

(f). Circles around any of the above patterns.

(g). Any of the random patterns may be overlapped or not overlapped as desired.

(h). Circle and spot sizes may be varied randomly for any of the above combinations.

The program consists of a mainline and six subroutines: PTLOC, DSPOT, CIRCL, OVLAP, RANC, RANS.

(1). PTLOC (IRAN, NCALL, XH1, YH1, XH2, YH2, IRAD).

IRAN - Integer from 1 to 32767 used as a seed for the random number generator.

NCALL - Integer which should equal 1 the first time PTLOC is called; any other number for further calls.

XH1, YH1 and XH2, YH2 - Coordinates of two points with random rotation.

IRAD - If 1, spots have random radius.

If 2, spots have fixed radius.

This subroutine assumes a coordinate axis centered at (0,0) and generates the x and y coordinates of two spots located symmetrically with respect to the origin. The line of centers between the two spots has a random orientation which is uniformly distributed between 0 and 2π. The distance between the two spots may also be varied randomly with a uniform distribution between two arbitrary distances.

(2). DSPOT (X,Y)

X - x coordinate of spot center

Y - y coordinate of spot center.

This subroutine will draw and fill in a 1/8 inch circle on an x-y plotter centered about the point x,y. This is done by initially plotting the 1/8 inch circle, and then plotting smaller concentric circles to fill in the spot. Circles are drawn using Lissajous figures and its circumference is divided into 25 points.

(3). CIRCL (X,Y)

X - x coordinate of circle center.

Y - y coordinate of circle center.

This subroutine is similar to DSPOT but draws a circle 0.6 inches in diameter and does not fill it in. This circle is also drawn using Lissajous figures and its circumference is divided into 125 points.

(4). MAINLINE

The mainline program handles the generation of the pattern locations and calls the appropriate subroutines depending on the data switch configuration.

The program is broken into two parts . One generates a uniform pattern distribution drawing spots and circles as desired, the other generates a random pattern distribution also with spots and circles. All of these options are selected by data switches. The data switch subroutine CALL DATSW (No., IVAL) reads the data switch number and returns IVAL = 2 if off and IVAL = 1 if on. Executable GO TO statements make the logical decisions based on the data switches.

For a uniform pattern the number of rows and the number of columns desired is entered via the typewriter. These will be spaced equally in both the x and y directions. For the random pattern, the number of patterns only is entered.

(5). OVLAP (X,Y,IGO,K)

X - x coordinate of pattern center.

Y - y coordinate of pattern center.

IGO - is 1 if pattern overlaps previous one, and is 2 if no overlap occurs.

K - is set equal to 1 if overlap is desired, and is set equal to 2 if no overlap is desired.

This subroutine stores all of the patterns plotted in the random mode and as a new pattern is to be plotted, computes its distance from all of the previous ones to determine if overlap will occur, and sets IGO equal to 1 or 2 if K is 2. If K is 1, IGO is always 2 and overlap is allowed.

(6). RANC,RANS

These are function subroutines which generate random circle and spot radii and these values are placed in common and used by all the subroutine.

The subroutines as written for use on an IBM 1130 are contained in Appendix 1. A number of different patterns produced by these programs are presented in Figs. 5 - 12.

```
// JOB T
// FOR
*ONE WORD INTEGERS
*LIST ALL
      FUNCTION RANS(K7,IRAN,NCALL)
      GO TO (5,10),K7
5     IF(NCALL-1) 7,6,7
6     IX=IRAN+10
7     CALL RANDU(IX,IY,TFL)
      IX=IY
      RANS=.0625*TFL+.0625
      RETURN
10    RANS=.0625
      RETURN
      END
// DUP
*STORE       WS   UA   RANS
```

```
// FOR
*ONE WORD INTEGERS
*LIST ALL
      FUNCTION RANC(K6,IRAN,NCALL)
      GO TO (5,10),K6
5     IF(NCALL-1) 7,6,7
6     IX=IRAN+8
7     CALL RANDU(IX,IY,YFL)
      IX=IY
      RANC=.1*YFL+.2
      RETURN
10    RANC=.3
      RETURN
      END
// DUP
*STORE       WS   UA   RANC
```

```
// FOR
*ONE WORD INTEGERS
*LIST ALL
      SUBROUTINE OVLAP(X,Y,INC,IGO,KO)
      DIMENSION PT(225,2)
      GO TO (35,1),KO
1     PT(INC,1)=X
      PT(INC,2)=Y
      IF(INC-1) 10,5,10
5     IGO=2
      RETURN
10    N=INC-1
      IGO=2
      DO 30 I=1,N
      IF(IGO-1) 15,30,15
15    DIST=SQRT((PT(INC,1)-PT(I,1))**2 + (PT(INC,2)-PT(I,2))**2)
      IF(DIST-.65) 20,20,25
20    IGO=1
      GO TO 30
25    IGO=2
30    CONTINUE
      RETURN
35    IGO=2
      RETURN
      END
// DUP
*STORE      WS  UA  OVLAP
```

```
// FOR
*ONE WORD INTEGERS
*LIST ALL
      SUBROUTINE PTLOC(IRAN,NCALL,XH1,YH1,XH2,YH2,IRAD,NSPOT)
      COMMON CRAD,SPOT
      PI=3.1415926
 42   FSTOD=PI/2.
      IF(NCALL-1) 10,5,10
 5    IX=IRAN
 10   CALL RANDU (IX,IY,YFL)
      IX=IY
      GO TO (60,15),NSPOT
C     DOUBLE SPOT
 15   ANGLE=PI*YFL
      GO TO (20,21),IRAD
 20   CALL RANDU(IX,IY,TFL)
      IX=IY
      R=TFL*(CRAD-(SPOT+.005))+(SPOT+.005)
      GO TO 14
 21   R= CRAD-(SPOT+.005)
 14   IF(ANGLE-FSTOD) 16,22,25
C      COMPUTE POINT COORDINATES
 16   XH1=  R*COS(ANGLE)
      YH1=  R*SIN(ANGLE)
C      ADJUST POINTS TO PROPER QUADRANT
      XH2=-XH1
      YH2=-YH1
      RETURN
 22   XH1=0.
      YH1=  R
      XH =0.
      YH2=-  R
      RETURN
 25   ANG=PI-ANGLE
      XH1=-  R*COS(ANG)
      YH1=  R*SIN(ANG)
      XH2=-XH1
      YH =-YH1
      RETURN
C      SINGLE POINT COORDINATE LOCATION
 60   ANGLE=2.*PI*YFL
      GO TO (65,70),IRAD
 65   CALL RANDU(IX,IY,TFL)
      IX=IY
      R=TFL*(CRAD-(SPOT+.005))
      GO TO 75
 70   R=CRAD-(SPOT+.005)
 75   XH1=R*COS(ANGLE)
      YH1=R*SIN(ANGLE)
      XH2=0.0
      YH2=0.0
      RETURN
 35   END
// DUP
*STORE        WS  UA  PTLOC
```

```
// FOR
*ONE WORD INTEGERS
*LIST ALL
      SUPROUTINE DSPOT(X,Y)
      COMMON CRAD,SPOT
C      PEN UP (PRECATUION)
      CALL RSCL(1,IER)
      R=SPOT
      XSTRT=(X+.0625)*3276.7
      IXSTR=XSTRT
      YSTRT=Y*3276.7
      IYSTR=YSTRT
C      MOVE PEN TO INITIAL POINT
      CALL LTDA(6,IXSTR,IER)
      CALL LTDA(7,IYSTR,IER)
      CALL DELAY(.4)
C      PEN DOWN
      CALL SSCL(I,IER)
      CALL DELAY(.1)
      DIV=(2.*3.14159)/20.
C      DRAW FOUR CONCENTRIC CIRCLES
      IF(R-.1250) 20,15,15
15    L=25
      GO TO 55
20    IF(R-.1093) 30,25,25
25    L=21
      GO TO 55
30    IF(R-.0937) 40,35,35
35    L=18
      GO TO 55
40    IF(R-.0718) 50,45,45
45    L=15
      GO TO 55
50    L=12
55    DO 10 J=1,L
      THETA=0.0
      DO 5 I=1,20
      X1=R*COS(THETA)
      Y1=R*SIN(THETA)
       XOUT=(X+X1)*3276.7
       YOUT=(Y+Y1)*3276.7
      IXOUT=XOUT
      IYOUT=YOUT
      CALL LTDA(6,IXOUT,IER)
      CALL LTDA(7,IYOUT,IER)
      THETA=THETA+DIV
5     CONTINUE
      R=R+.005
10    CONTINUE
C      PEN UP
      CALL RSCL(1,IER)
      CALL DELAY(.1)
      RETURN
      END
// DUP
*STORE      WS  UA  DSPOT
```

```
// FOR
*ONE WORD INTEGERS
*LIST ALL
      SUBROUTINE CIRCL(X,Y)
      COMMON CRAD,SPOT
C      PEN UP (PRECAUTION)
      CALL RSCL(1,IER)
      PI=3.1415926
      DIV=(2.*PI)/125.
      THETA=0.0
      R=CRAD
      IXOUT=(X+ R )*3276.7
      IYOUT=Y*3276.7
C      MOVE PEN TO FIRST POINT
      CALL LTDA(6,IXOUT,IER)
      CALL LTDA(7,IYOUT,IER)
      CALL DELAY(.4)
C      PEN DOWN
      CALL SSCL(1,IER)
      CALL DELAY(.1)
C      PLOT CIRCLE
      DO 20 I=1,125
      Y1=  R*SIN(THETA)
      X1=  R*COS(THETA)
      IXOUT=(X+X1)*3276.7
      IYOUT=(Y+Y1)*3276.7
      CALL LTDA(6,IXOUT,IER)
      CALL LTDA(7,IYOUT,IER)
      THETA=THETA+DIV
   20 CONTINUE
C      PEN UP
      CALL RSCL(1,IER)
      CALL DELAY(.1)
      RETURN
      END
// DUP
*STORE      WS  UA  CIRCL
```

```
// FOR
*IOCS(1132 PRINTER,DISK,CARD,TYPEWRITER,KEYBOARD)
*ONE WORD INTEGERS
*LIST ALL
      INTEGER ROWS,COLS
      DIMENSION KEY(16)
      COMMON CRAD,SPOT
C      WRITE SWITCH CONFIGURATION
4     WRITE(1,2000)
      WRITE(1,2001)
      WRITE(1,2005)
      WRITE(1,2010)
      WRITE(1,2015)
      WRITE(1,2020)
      WRITE(1,2025)
      WRITE(1,2030)
      WRITE(1,2031)
      WRITE(1,2032)
      WRITE(1,2035)
      PAUSE 1111
C      READ SWITCHES
      DO 5 I=1,10
5     CALL DATSW(I,KEY(I))
      CALL DATSW(0,K0)
      K1=KEY(1)
      K2=KEY(2)
      K3=KEY(3)
      K4=KEY(4)
      K5=KEY(5)
      K6=KEY(5)
      K7=KEY(7)
       K8=KEY(8)
      K9=KEY(9)
      K10=KEY(10)
      WRITE(1,2040)
      WRITE(1,2041)
      READ(6,2045) IRAN
C      PEN UP
      CALL PSCL(1,IER)
C      SELECT STATIC TEST MODE
6     CALL SAMO(3,IER)
      II=0
C      LOAD DACS WITH ZEROES
      CALL LTDA(6,II,IER)
      CALL LTDA(7,II,IER)
      WRITE(1,2050)
      PAUSE 2222
      GO TO (130,10),K8
10    GO TO (12,11),K9
11    WRITE(1,2055)
      READ(6,2060) ROWS
      WRITE(1,2065)
      CALL LTDA(6,III,IER)
      READ(6,2060) COLS
C      UNIFORM PATTERN GENERATION SECTION
12    DO 120 I=1,ROWS
      R=ROWS+1
      CALL DATSW(1,K1)
      GO TO (120,15),K1
15    IF(I-1) 25,20,25
20    YINC=10./R
```

```
      GO TO 30
25    YINC=YINC+10./R
30    DO 100 J=1,COLS
      NCALL=I+J-1
      CRAD=RANC(K6,IRAN,NCALL)
      C=COLS+1
      CALL DATSW(1,K1)
      GO TO (100,31),K1
31    IF(J-1) 40,35,40
35    XINC=10./C
      GO TO 45
40    XINC=XINC+10./C
45    GO TO (50,55),K5
50    CALL CIRCL(XINC,YINC)
55    GO TO (65,60),K2
60    GO TO (65,100),K3
65    SPOT=RANS(K7,IRAN,NCALL)
      CALL PTLOC(IRAN,NCALL,XH1,YH1,XH2,YH2,KEY(4),K2)
      VOLX1=XINC+XH1
      VOLY1=YINC+YH1
      CALL DSPOT(VOLX1,VOLY1)
      GO TO (70,100),K3
70    VOLX2=XINC+XH2
      VOLY2=YINC+YH2
      CALL DSPOT(VOLX2,VOLY2)
100   CONTINUE
120   CONTINUE
130   GO TO (129,201),K8
C      RANDOM PATTERN GENERATION SECTION
129   JRAN=IRAN+2
      KRAN=JRAN+2
      GO TO(132,131),K9
131   WRITE(1,2056)
      READ(6,2060) ROWS
      NF=0
132   DO 200 K=1,ROWS
      NCALL=K
      CRAD=RANC(K6,IRAN,NCALL)
133   CALL DATSW(1,K1)
      GO TO (200,135),K1
135   CALL RANDU(JRAN,IY,Y)
136   JRAN=IY
      YO=Y*9.4+.3
      CALL RANDU(KRAN,IX,X)
141   KRAN=IX
      XO=X*9.4 +.3
      CALL OVLAP(XO,YO,K,IGO,KO)
      GO TO (143,144),IGO
143   NF=NF+1
      GO TO 133
144   WRITE (3,1234) XO,YO
1234  FORMAT ('CORDINATE OF THE CIRCLE',2X,F10.5,4X,F10.5)
      GO TO (145,150),K5
145   CALL CIRCL(XO,YO)
150   GO TO (160,155),K2
155   GO TO (160,200),K3
160   SPOT=RANS(K7,IRAN,NCALL)
      CALL PTLOC(IRAN,NCALL,XH1,YH1,XH2,YH2,KEY(4),K2)
      VOLX1=XO+XH1
      VOLY1=YO+YH1
```

```
      CALL DSPOT(VOLX1,VOLY1)
      GO TO (165,200),K3
165   VOLX2=XO+XH2
      VOLY2=YO+YH2
      CALL DSPOT(VOLX2,VOLY2)
200   CONTINUE
      NT=NF+ROWS
      WRITE(1,2080) ROWS,NT
201   WRITE(1,2070)
      PAUSE 3333
C      REPLOT OR NEW PLOT
      CALL DATSW(9,K9)
      GO TO(6,205),K9
205   WRITE(1,2075)
      PAUSE 4444
      CALL DATSW(10,K10)
      GO TO (4,210),K10
2000  FORMAT('T U R N  O N',4X,'F O R'/)
2001  FORMAT(4X,'SW 0',6X,'OVERLAP')
2005  FORMAT(4X,'SW 1',6X,'INTERUPT')
2010  FORMAT(4X,'SW 2',6X,'SINGLE RANDOM SPOTS')
2015  FORMAT(4X,'SW 3',6X,'PAIRS OF RANDOM SPOTS')
2020  FORMAT(4X,'SW 4',6X,'RANDOM SPOT LOCATION RADIUS')
2025  FORMAT(4X,'SW 5',6X,'CIRCLES AROUND PATTERNS')
2030  FORMAT(4X,'SW 6',6X,'RANDOM CIRCLE RADIUS')
2031  FORMAT(4X,'SW 7',6X,'RANDOM SPOT SIZE')
2032  FORMAT(4X,'SW 8',6X,'RANDOM PATTERN LOCATION'/)
2035  FORMAT('SELECT SWITCHES *** PUSH START'/)
2040  FORMAT('ENTER RANDOM VARIABLE')
2041  FORMAT('ODD NUMBER(      ) 1 TO 32750')
2045  FORMAT(11X,I5)
2050  FORMAT('POSITION THE PEN IN THE LOWER LEFT CORNER OF GRID'/'X-Y SC
     1ALES 1V/IN'/'PUSH START'/)
2055  FORMAT('ENTER NUMBER OF PATTERNS'/'ROWS(    ) MAX-15')
2056  FORMAT('ENTER NUMBER OF PATTERNS'/'NO. (    ) MAX-225')
2060  FORMAT(5X,I3)
2065  FORMAT('COLS(    ) MAX-15')
2070  FORMAT(/'SW 9 ON TO REPLOT *** PUSH START'/)
2075  FORMAT(/'SW 10 ON FOR NEW PLOT *** PUSH START'/)
2080  FORMAT('TOTAL TRIALS FOR ',I3,' POINTS IS ',I4/)
210   CALL EXIT
      END
// XEQ
```

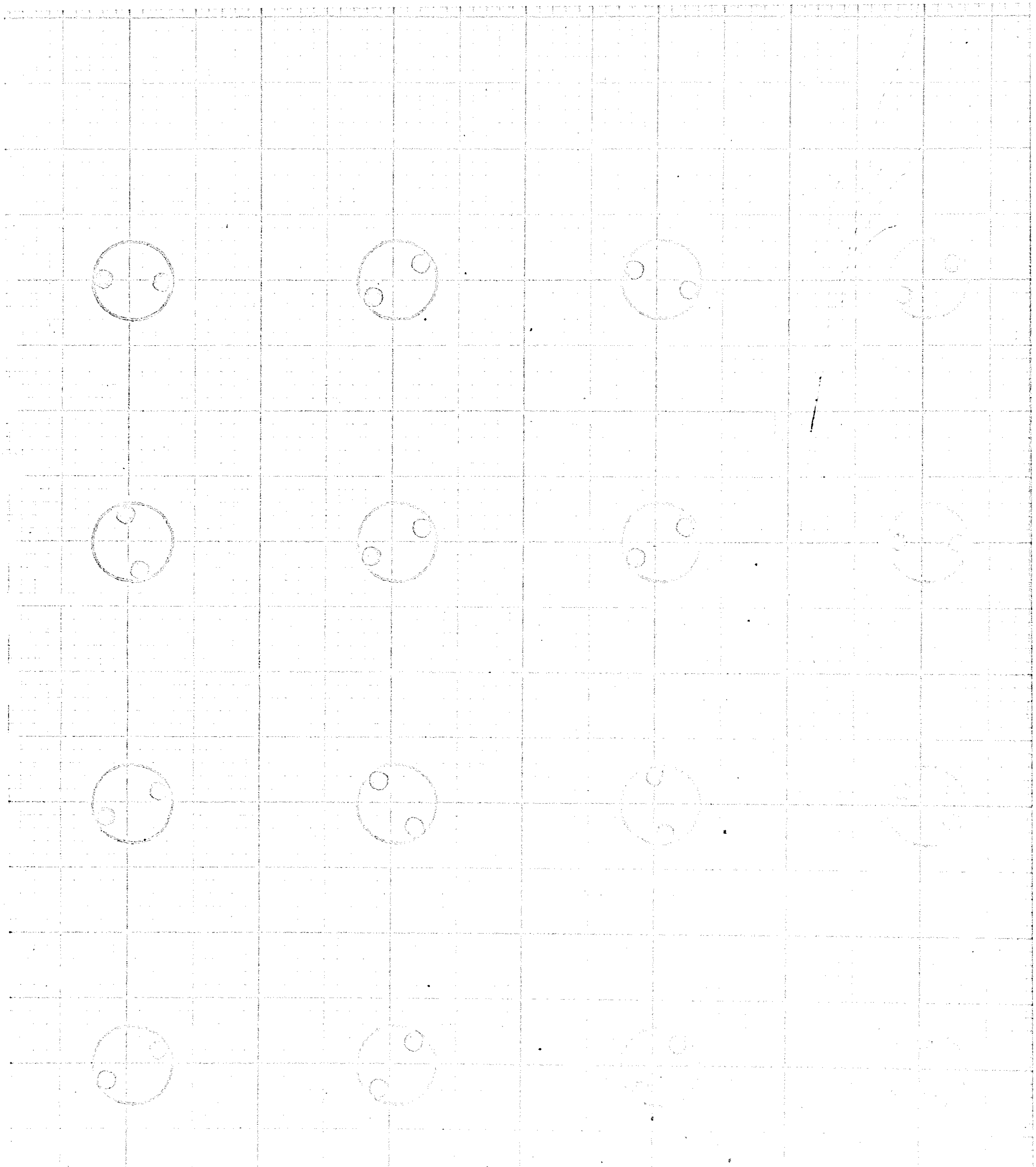

Fig. 5 Periodic array of circles with two dots oriented randomly within the circle.

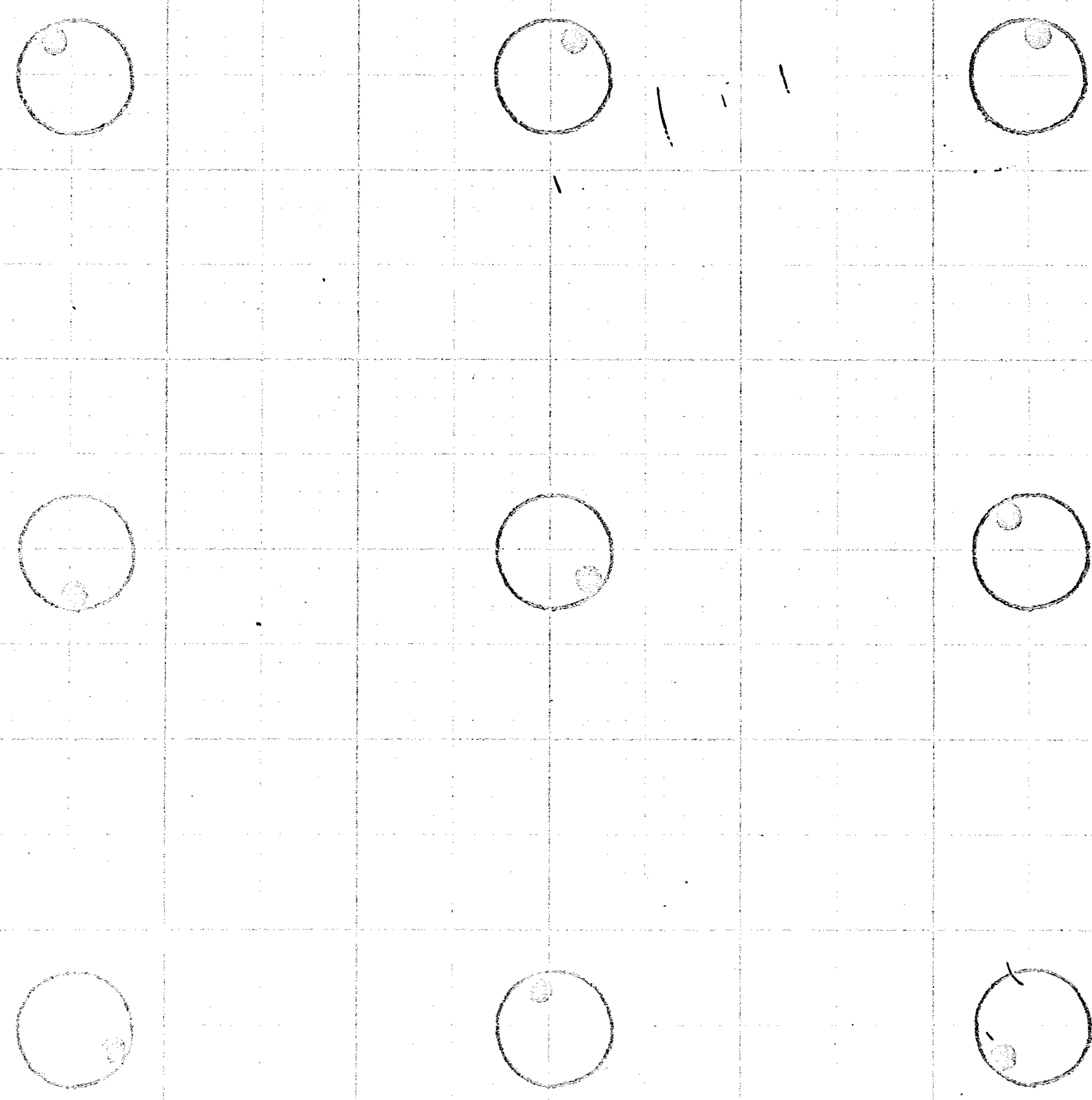

Fig. 6 Periodic array of circles
with single dot located randomly
on circumference of circle.

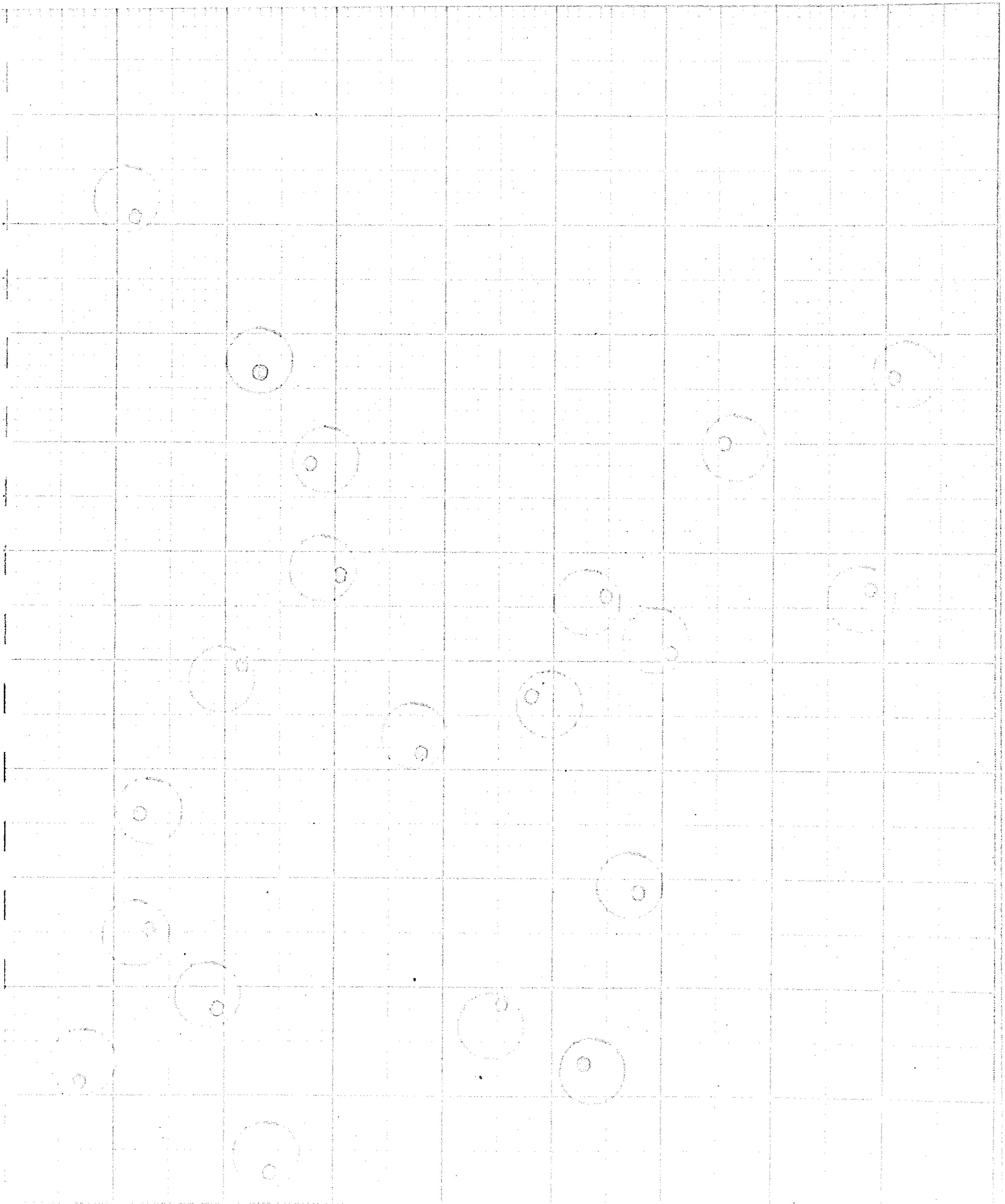

Fig. 7 Random array of non-overlapping circles with single dot located randomly within the circles.

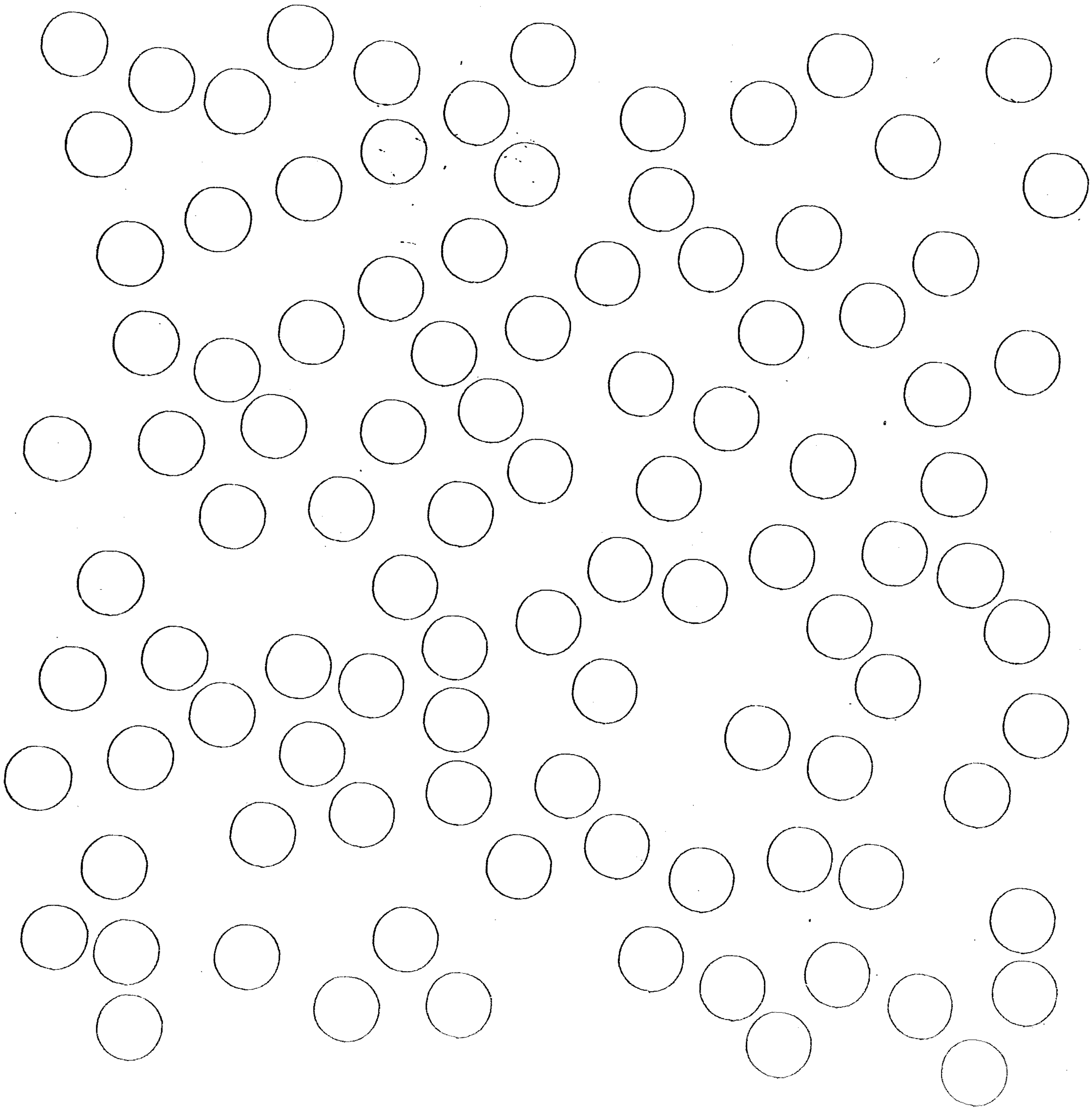

Fig. 8 Random array of non-overlapping circles.

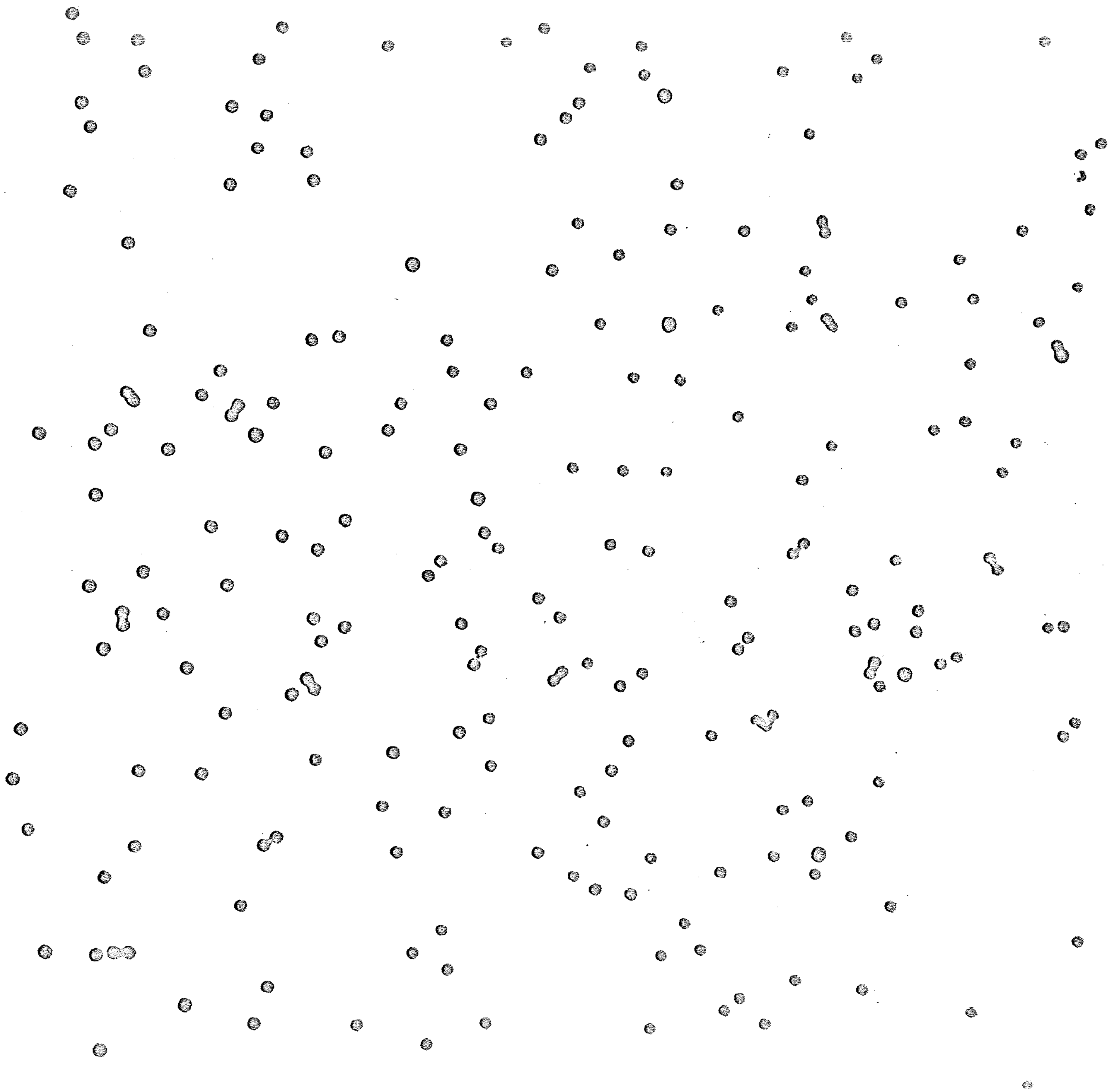

Fig. 9 Random array of single
overlapping dots.

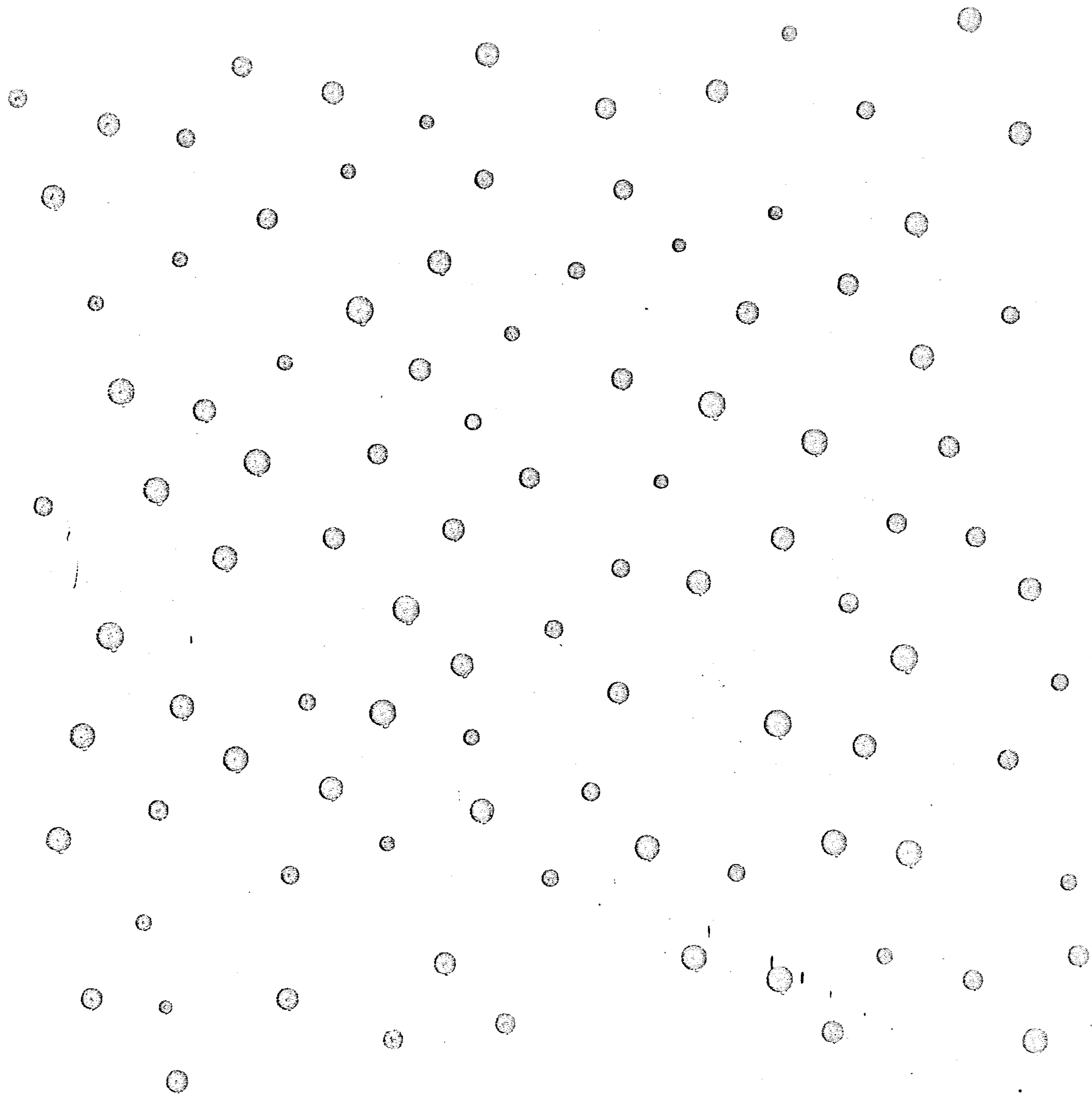

Fig. 10 Random array of non-overlapping dots of random size.

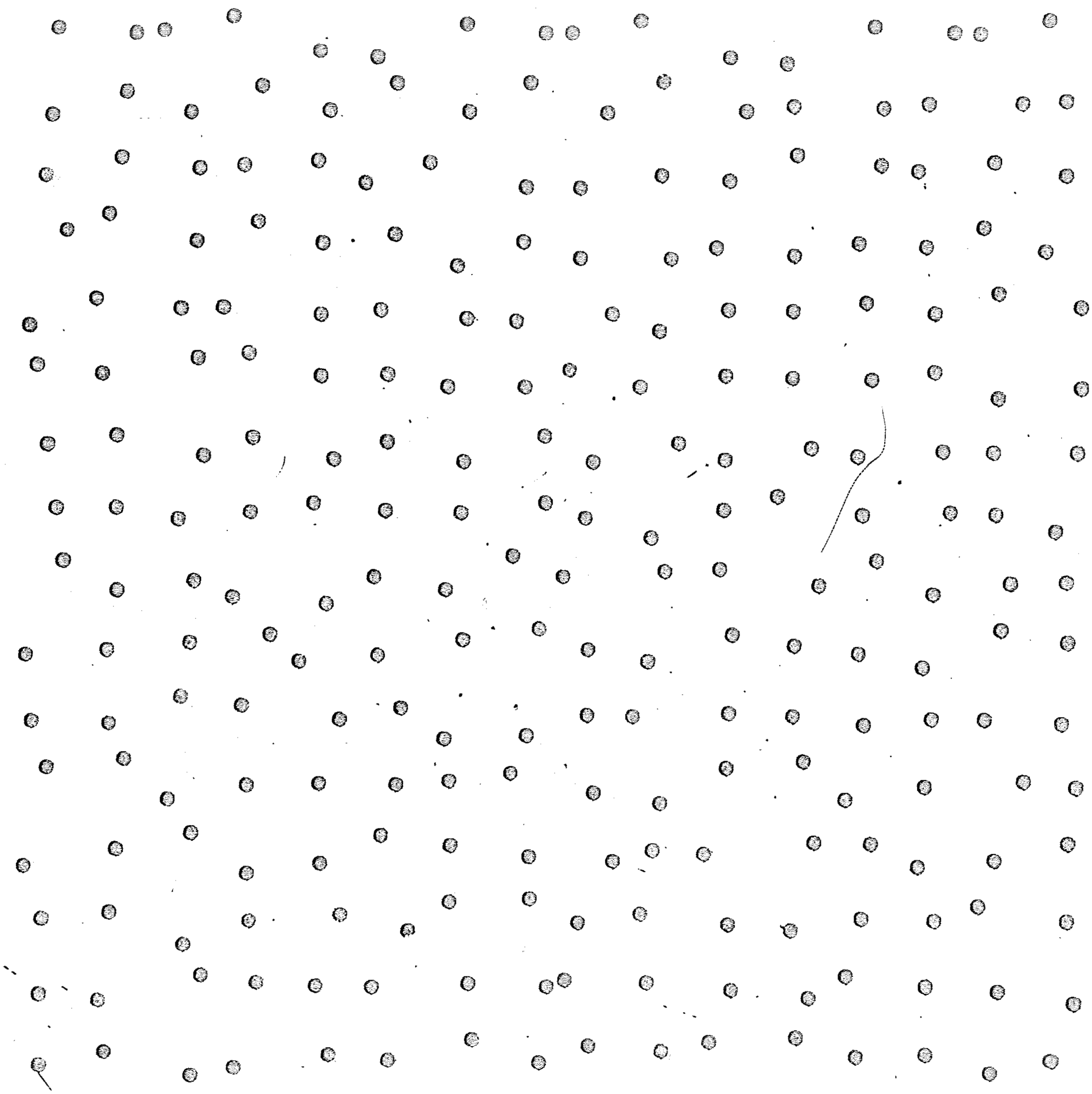

Fig. 11 Dots are located randomly within a periodic array of circles that are not drawn.

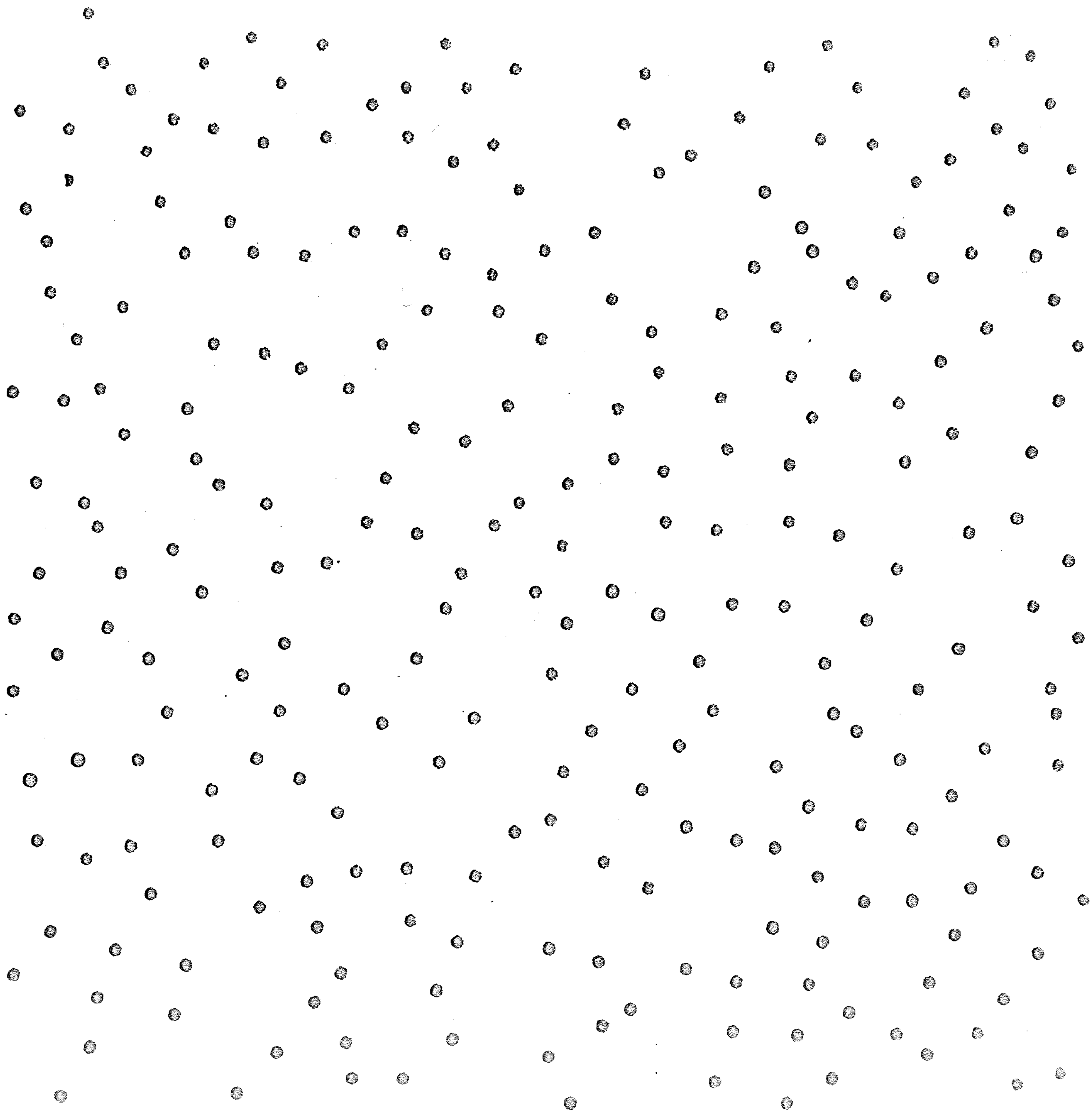

Fig. 12 Random array of two-dot patterns. In each two-dot pattern the distance between the dots is constant and the orientation of the two dots is random

4. Power Spectrum and Autocorrelation Measurements

In this section a number of theoretical and experimentally measured power spectra and autocorrelation functions of various random spatial patterns are presented. All of the patterns are made up of circular dots or circular rings or combinations of both. In Section 4.1 the power spectrum and autocorrelation function of a single circular dot and a single circular ring will be considered.

4.1 Circular dots and rings

When photographically reproduced a circular dot becomes a circular aperture in a diffracting screen. Such a circular aperture can be written as circ(r) where

$$\mathrm{circ}(r) = \begin{cases} 1 & r \leq 1 \\ 0 & \text{otherwise} \end{cases} \tag{10}$$

The two-dimensional Fourier transform of circ(r) is well known [2] and is $J_1(2\pi f)/f$ where J_1 is a Bessel function of the first kind, order one, and $f = (f_x{}^2+f_y{}^2)^{1/2}$ where f_x and f_y are the spatial frequencies in the x and y directions. One can therefore write the Fourier transform pair

$$\mathrm{circ}(r) \longleftrightarrow J_1(2\pi f)/f \tag{11}$$

Using the scaling theorem one can write the Fourier transform of a circular aperture of radius R. Thus,

$$\mathrm{circ}\left(\frac{r}{R}\right) \longleftrightarrow R^2\,\frac{J_1(2\pi Rf)}{Rf} \tag{12}$$

The Fourier transform in (12) will be designated as $G_R(f)$. Thus, the power spectrum of a circular aperture of radius R is given by

$$\left| G_R(f) \right|^2 = \pi^2 R^4 \left[2 \frac{J_1(2\pi Rf)}{2\pi Rf} \right]^2 \tag{13}$$

A theoretical plot of $[2J_1(2\pi Rf)/2\pi Rf]^2$ vs. 2Rf is shown in Fig. 13. For experimental comparison, the light diffracted by a circular aperture was scanned in the transform plane by a photomultiplier tube behind a 10μ pinhole. The result is shown in Fig. 14.

An aperture in the form of a circular ring can be written as $\mathrm{ring}_a(r)$ and defined as

$$\mathrm{ring}_a(r) = \begin{cases} 1 & a \leq r \leq 1 \\ 0 & \text{otherwise} \end{cases} \tag{14}$$

Thus,

$$\mathrm{ring}_a(r) = \mathrm{circ}(r) - \mathrm{circ}(r/a) \tag{15}$$

and the Fourier transform of $\mathrm{ring}_a(r)$ can be written as

$$\mathrm{ring}_a(r) \longleftrightarrow \frac{J_1(2\pi f) - a\,J_1(2\pi af)}{f} \tag{16}$$

If the outer radius of the ring is A, then

$$\mathrm{ring}_a\left(\frac{r}{A}\right) \longleftrightarrow A^2 \left[\frac{J_1(2\pi Af) - aJ_1(2\pi aAf)}{Af} \right] \tag{17}$$

The Fourier transform in Eq. (17) will be designated as $G_{aA}(f)$. Thus, the power spectrum of a circular ring of outer radius A and whose ratio of inner to outer diameter is a is given by

$$\left| G_{aA}(f) \right|^2 = \pi^2 A^4 \left[2 \frac{J_1(2\pi Af) - a\,J_1(2\pi aAf)}{2\pi Af} \right]^2 \tag{18}$$

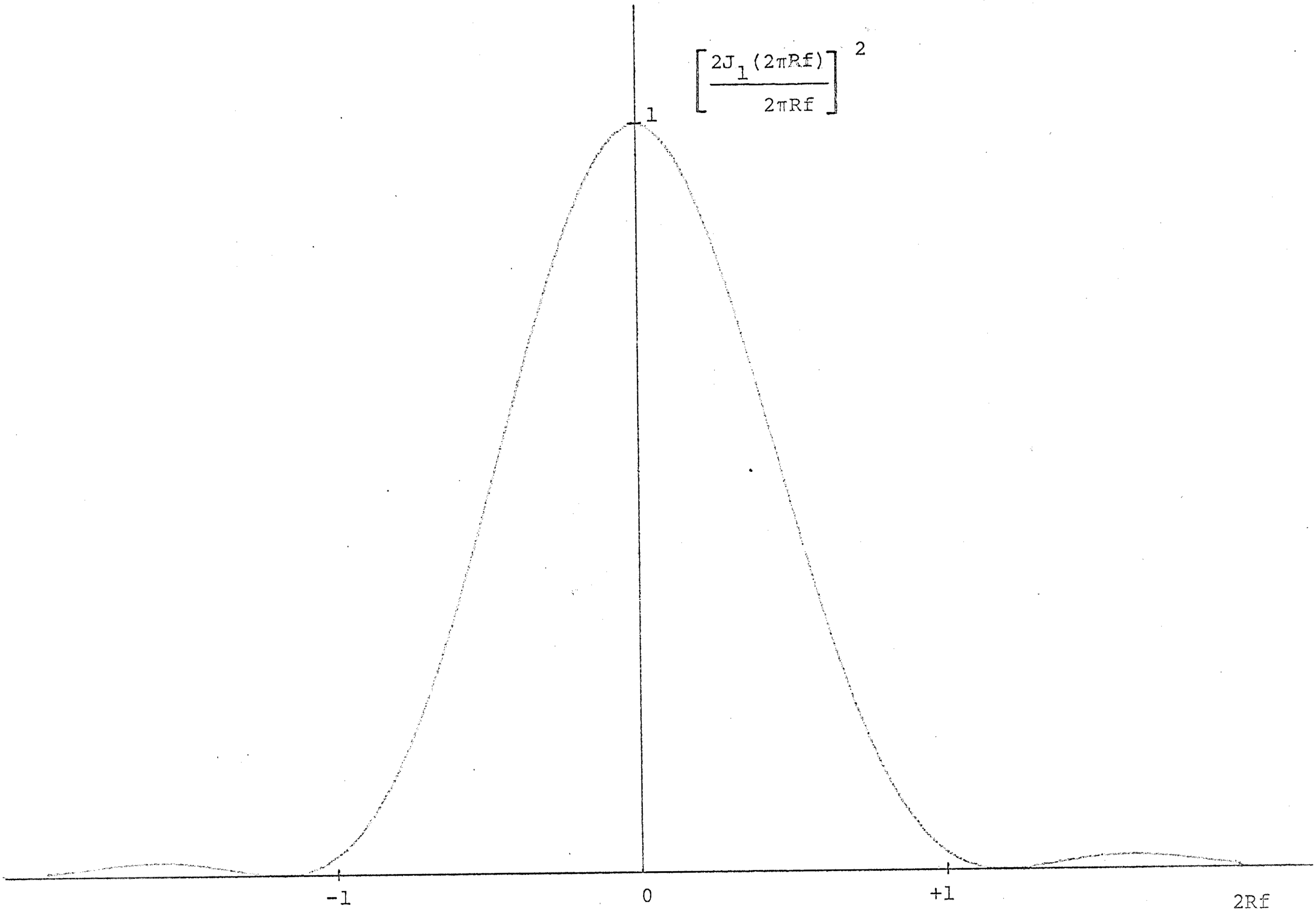

Fig. 13

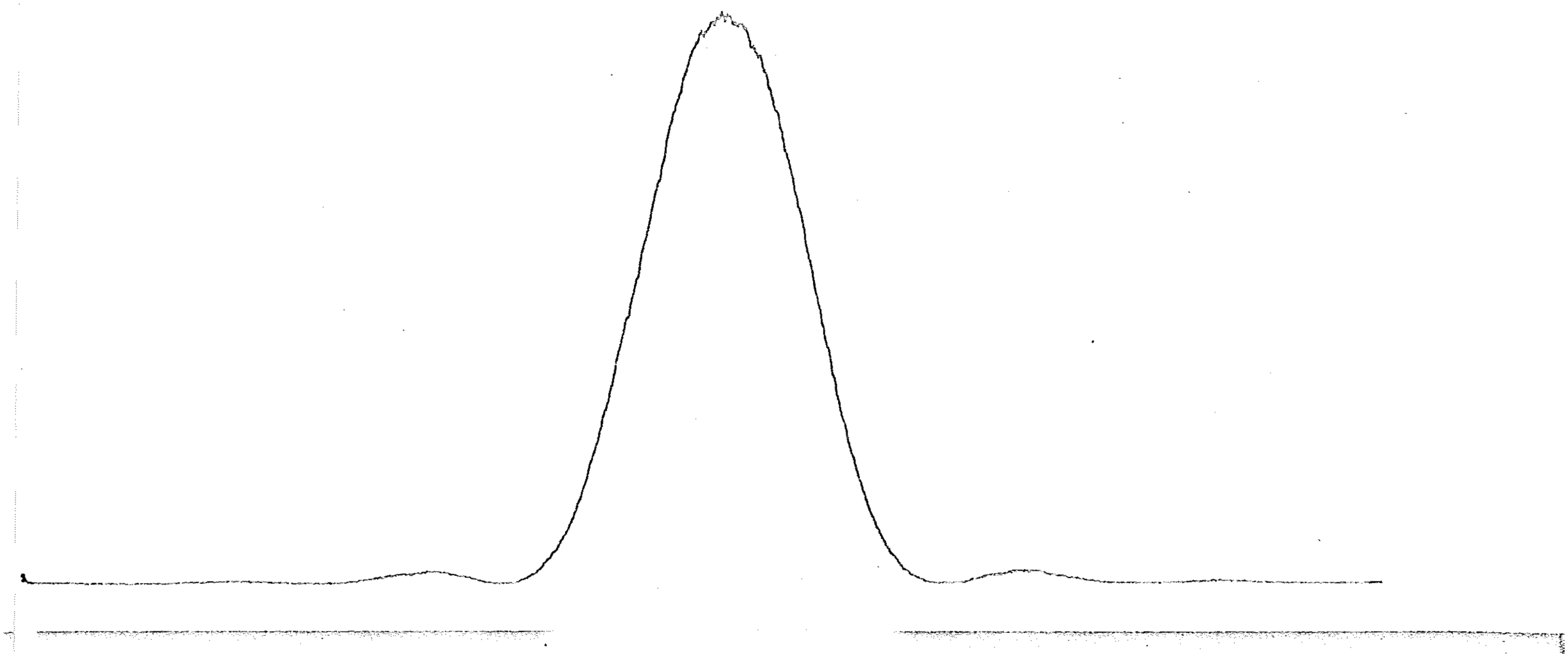

Fig. 14 Photograph and photo-
multiplier scan of power spec-
trum of circ (r).

Plots of $\left|G_{aA}(f)\right|^2 / \pi^2 A^4$ vs. $2Af$ for different values of a are shown in Figs. 15-19. A photomultiplier scan of the light diffracted in the transform plane by a circular ring with a value of $a = .96$ is shown in Fig. 20.

The two-dimensional autocorrelation function $\phi_{gg}(x,y)$ of a real function $g(x,y)$ is defined by the integral

$$\phi_{gg}(x,y) = \iint_{-\infty}^{\infty} g(x_1,y_1)g(x_1+x,y_1+y) \; dx_1 dy_1 \tag{19}$$

If $g(x,y)$ represents an aperture -- i.e. has a value of one inside the aperture and a value of zero outside the aperture, then (19) represents the area of overlap as $g(x_1,y_1)$ is slid across itself. The autocorrelation function for circ(r/R) can therefore be calculated from Fig. 21. The area of overlap in Fig. 21a is four times the area of B in Fig. 21b. It follows that the autocorrelation function $\phi_{RR}(x)$ of circ(r/R) will be circularly symmetric and can be written in the x-direction as

$$\begin{aligned}\phi_{RR}(x) &= 4 \text{ area}(B) \\ &= 4 \, [\text{area}(A+B) - \text{area}(A)] \\ &= 4\left\{\left(\frac{\theta}{2\pi}\right) [\pi R^2] - \frac{1}{2}\left(\frac{x}{2}\right)\sqrt{R^2 - \left(\frac{x}{2}\right)^2}\right\}\end{aligned} \tag{20}$$

From Fig. 21 $\theta = \cos^{-1}(x/2R)$. If the function $F(S)$ is defined as

$$F(S) = \frac{2}{\pi}\left[\cos^{-1}(S) - S\sqrt{1 - S^2}\right] \tag{21}$$

then from (20) $\phi_{RR}(x)$ can be written as

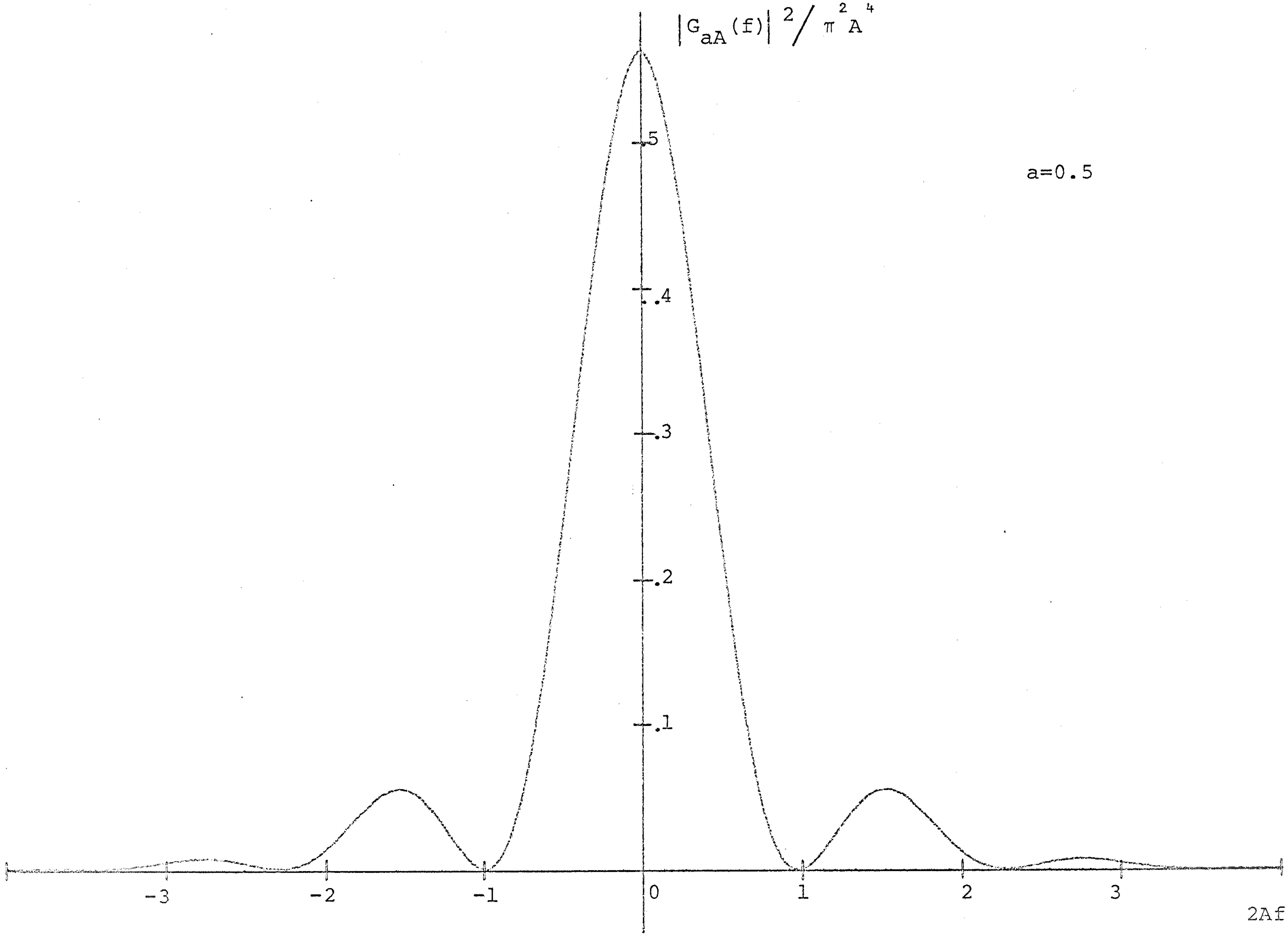

Fig. 15

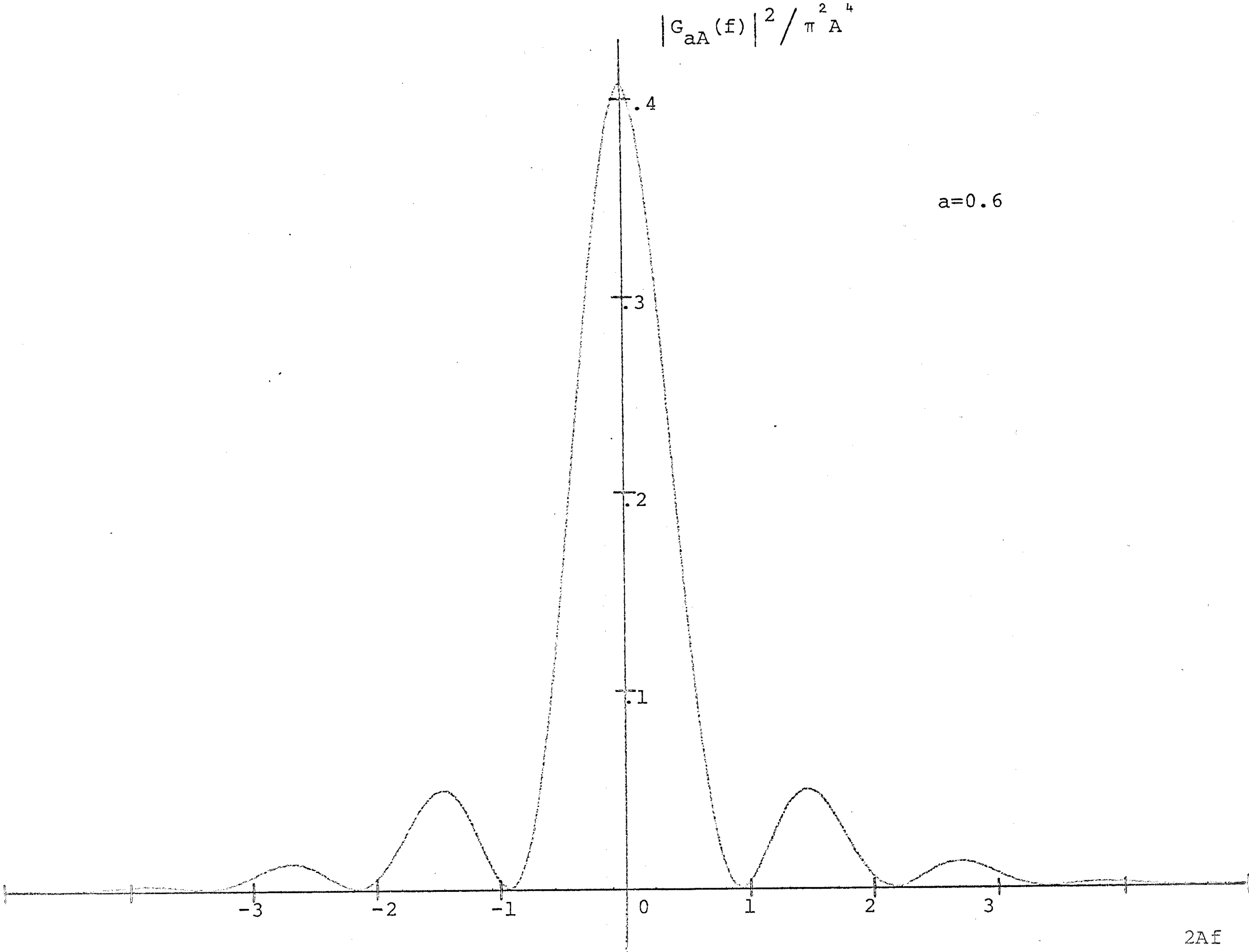

Fig. 16

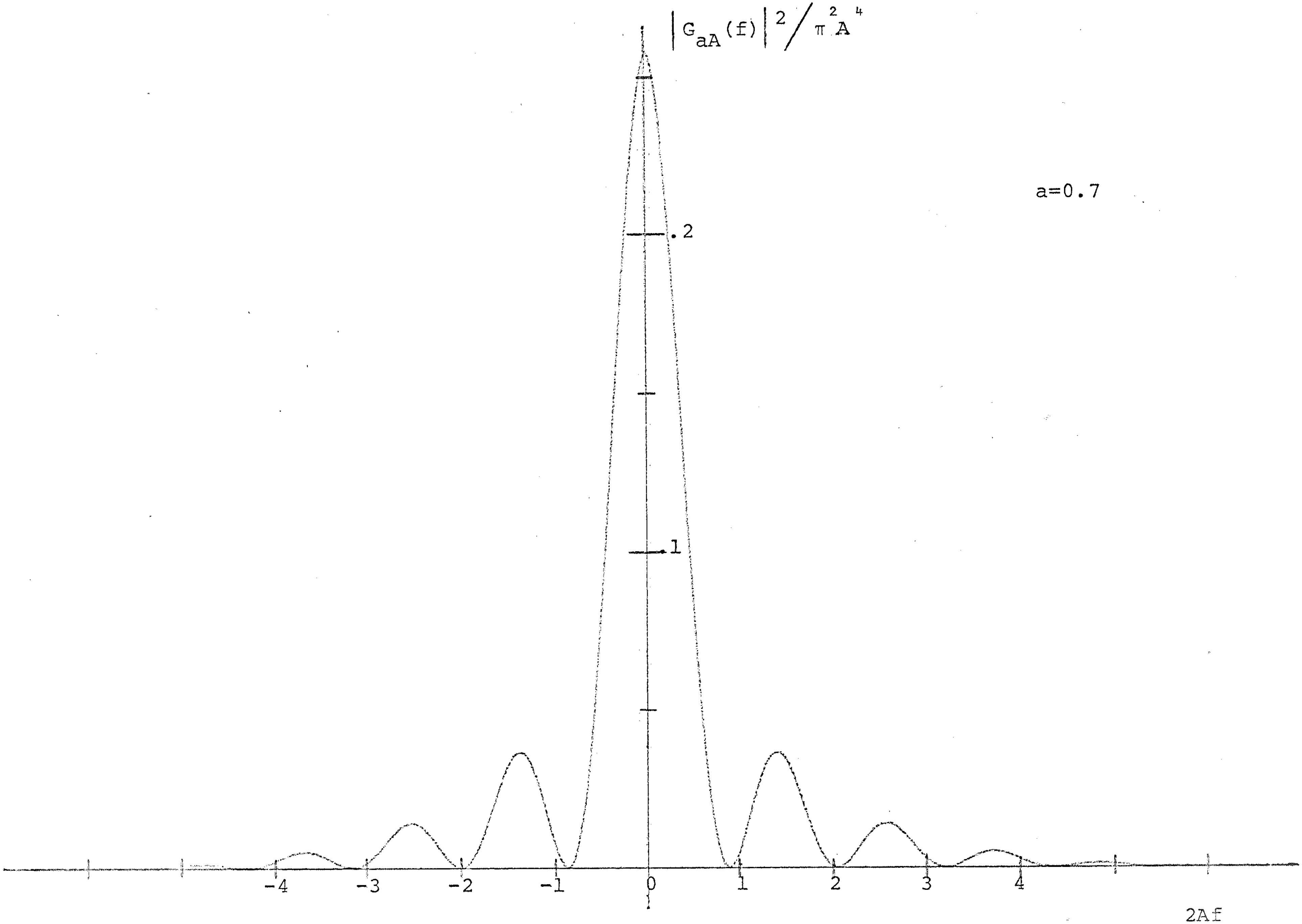

Fig. 17

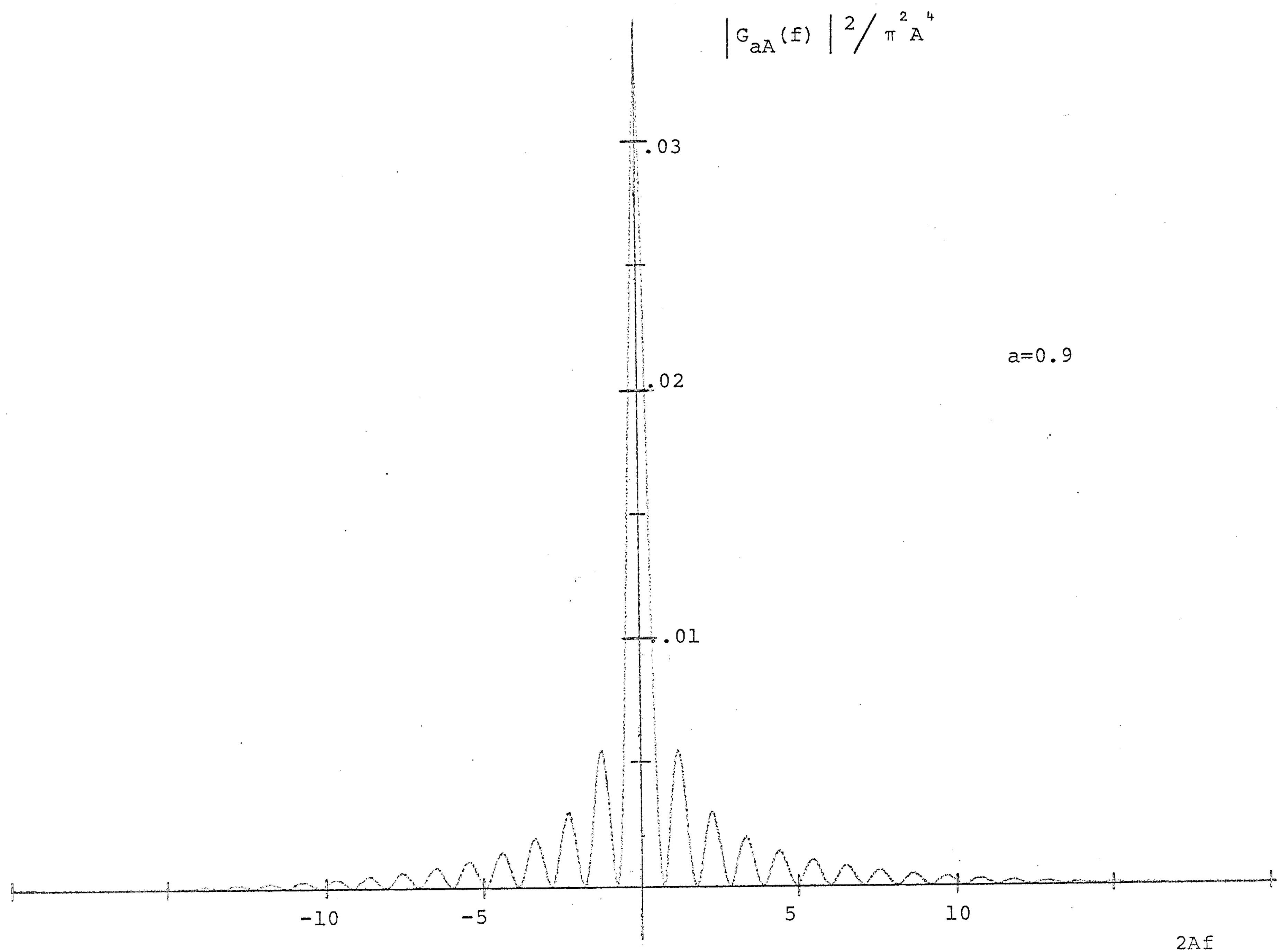

Fig. 18

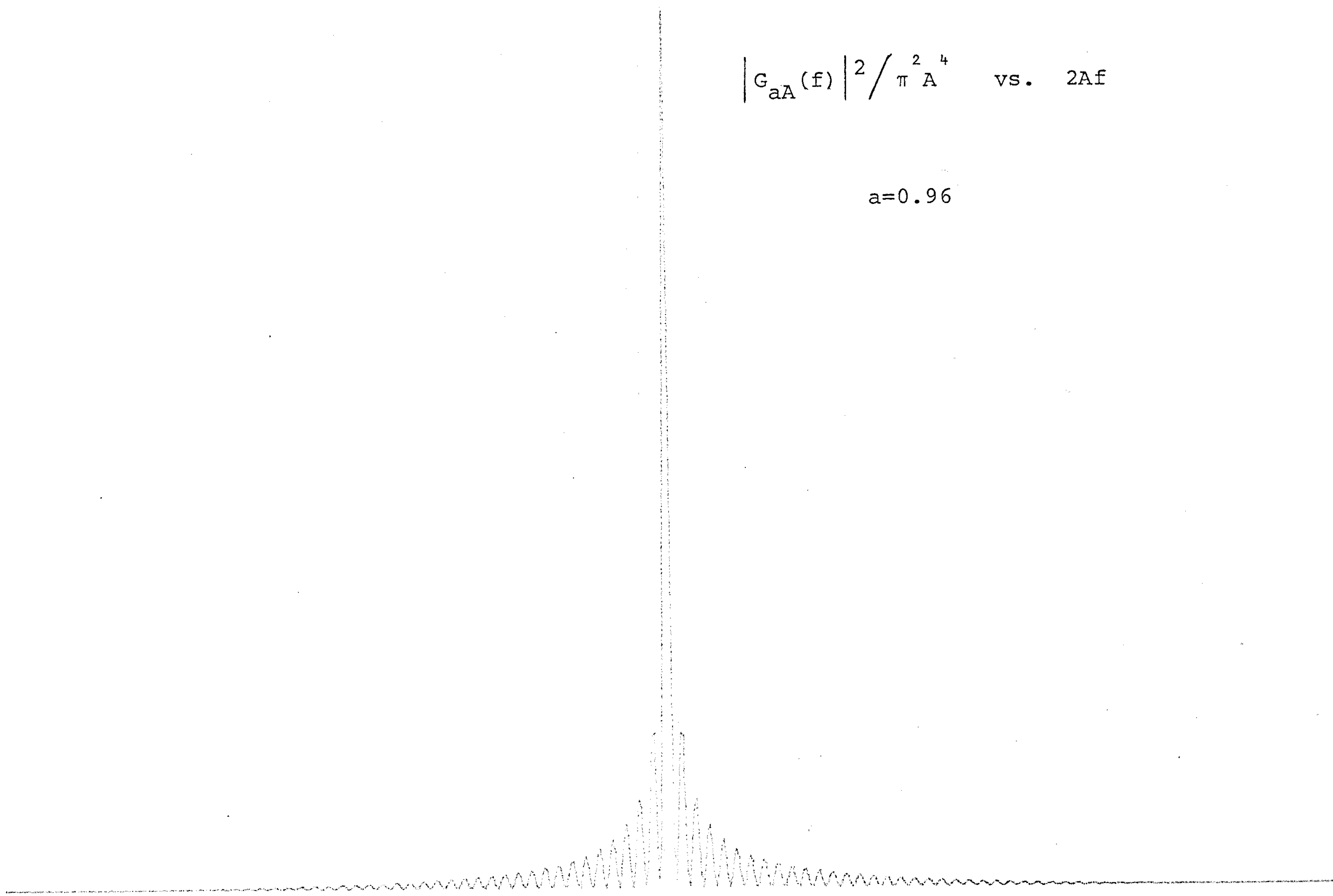

Fig. 19

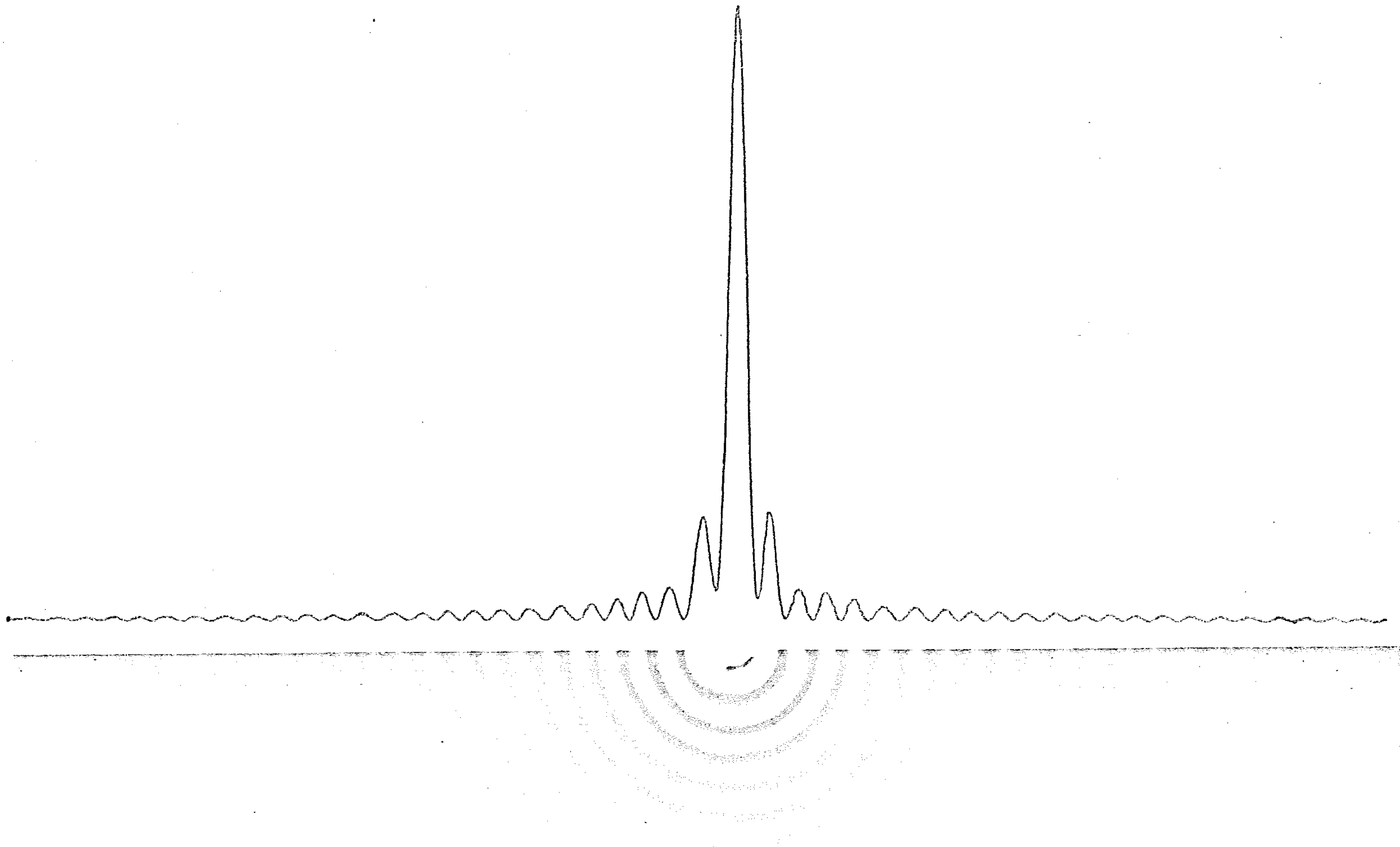

Fig. 20 Photograph and photomultiplier scan of power spectrum of $ring_a(r)$. $a=0.96$.

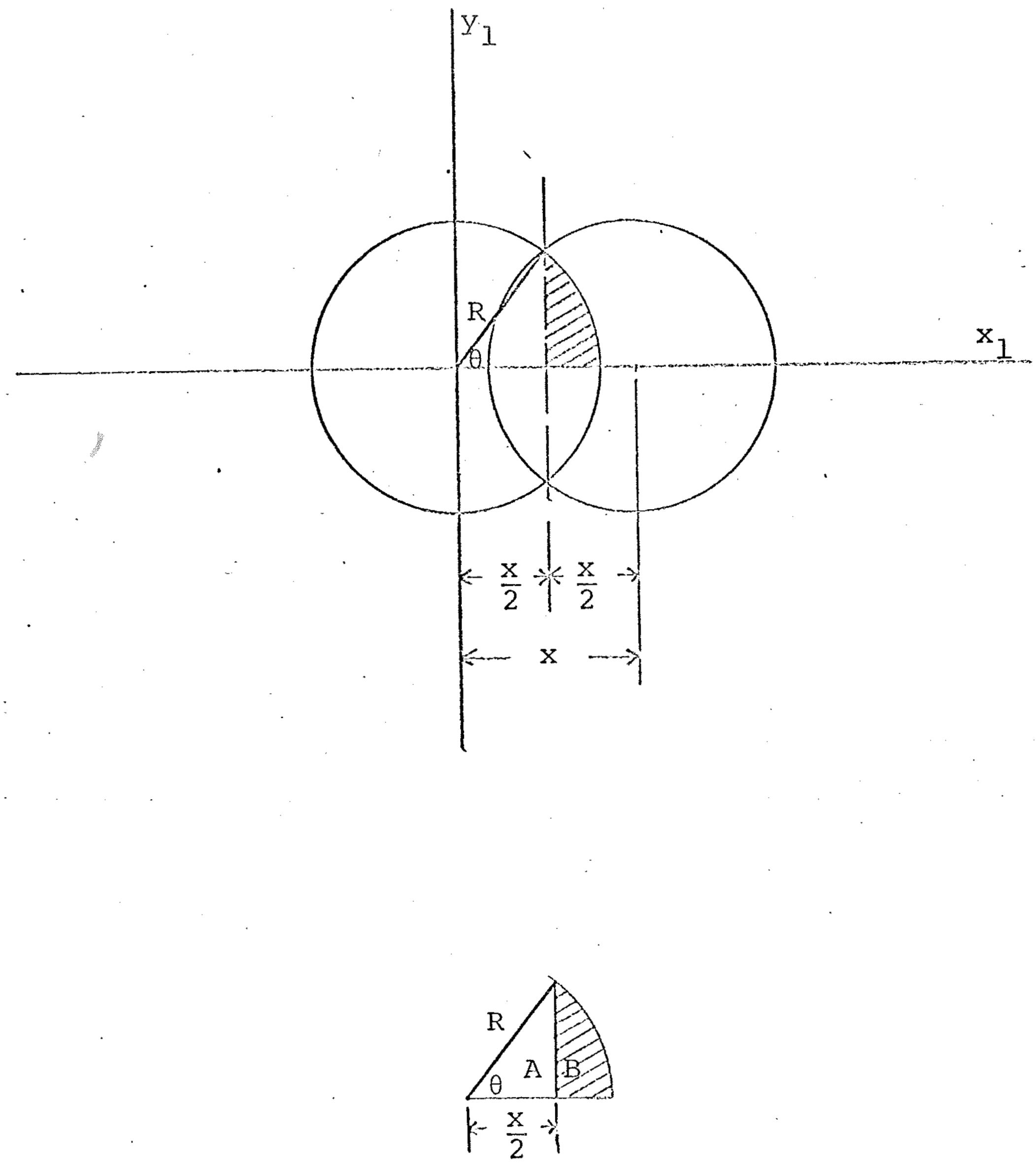

Fig. 21

$$\phi_{RR}(x) = \pi R^2 \, F\left(\frac{x}{2R}\right) \tag{22}$$

A plot of $F(S)$ vs. S is shown in Fig. 22. A photomultiplier scan of the autocorrelation of a circular aperture, found by measuring the Fourier transform of the power spectrum, is shown in Fig. 23. Discrepancies are due to nonlinear effects in the two-step photographic process and phase variations across the transparency.

In order to calculate the autocorrelation function of a circular ring it is necessary to find the area of overlap as the ring is slid across itself. To find the autocorrelation function $\phi_{oo}(x)$ of $\mathrm{ring}_a(r)$ given by (15) note from (15) and (19) that

$$\phi_{oo}(x) = \phi_{11}(x) + \phi_{aa}(x) - 2\phi_{a1}(x) \tag{23}$$

where

$$\phi_{11}(x) = \pi \, F\left(\frac{x}{2}\right) \tag{24}$$

is the autocorrelation function of $\mathrm{circ}(r)$ and

$$\phi_{aa}(x) = \pi a^2 \, F\left(\frac{x}{2a}\right) \tag{25}$$

is the autocorrelation function of $\mathrm{circ}(r/a)$. $\phi_{a1}(x)$ is the cross-correlation of $\mathrm{circ}(r)$ and $\mathrm{circ}(r/a)$ and can be found with the aid of Figs. 24 and 25.

In the range $0 \leq x \leq (1-a)$ the area of overlap of $\mathrm{circ}(r)$ and $\mathrm{circ}(r/a)$ is just the area of $\mathrm{circ}(r/a)$ or πa^2. The area of overlap in the range $(1-a) \leq x \leq \sqrt{1-a^2}$ can be found from Fig. 24 to be given by

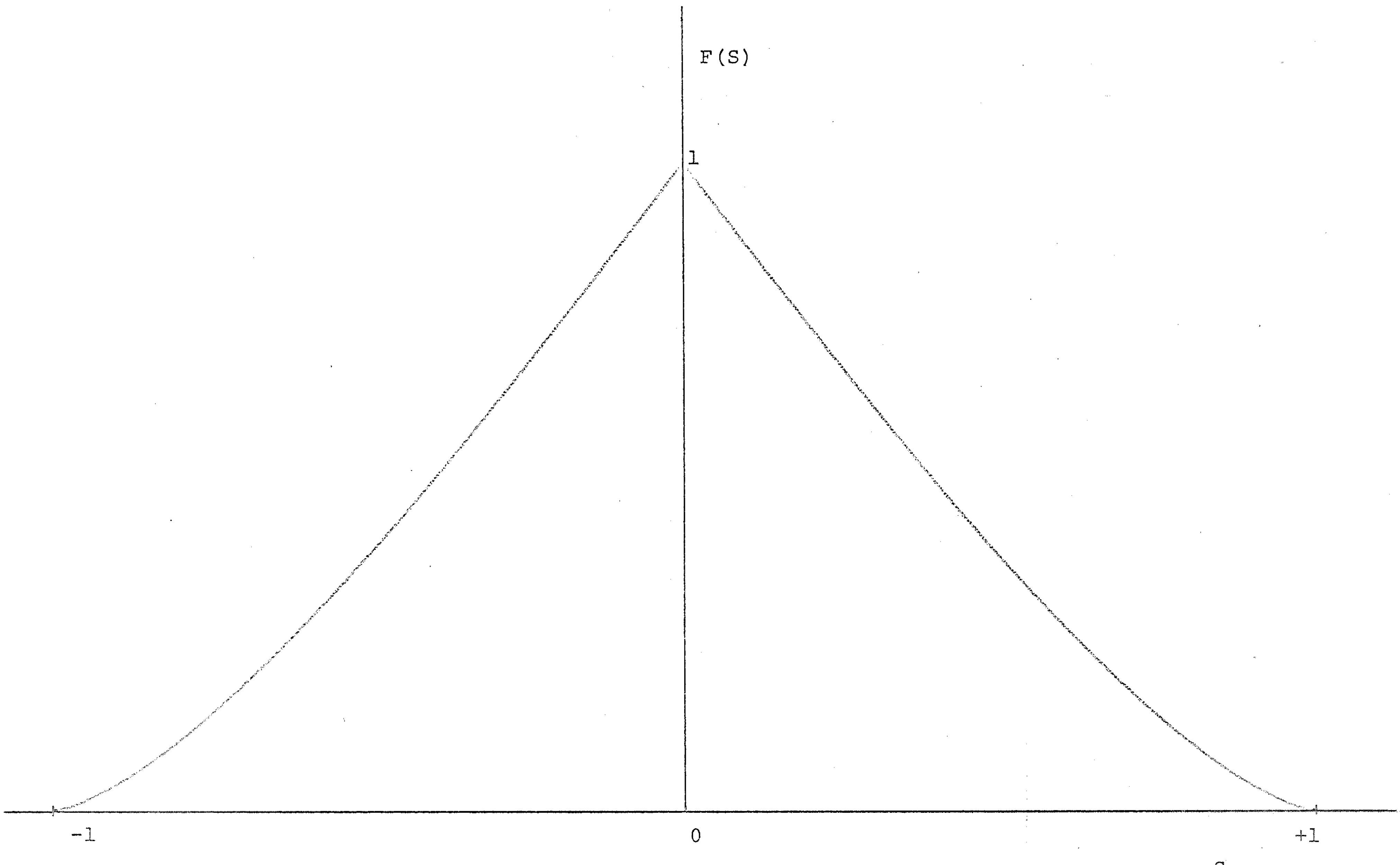

Fig. 22

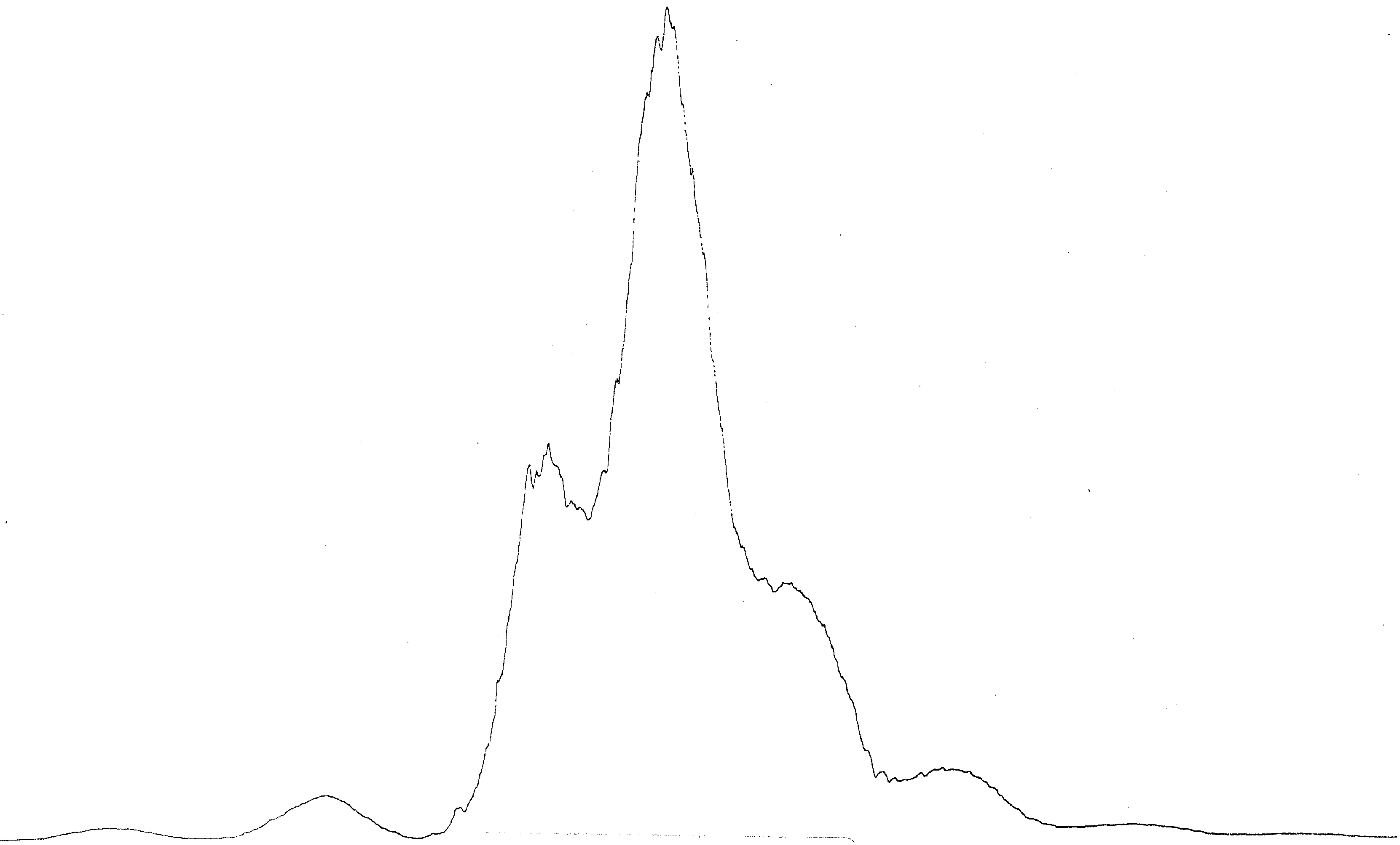

Fig. 23 Photomultiplier scan of the autocorrelation of circ (r).

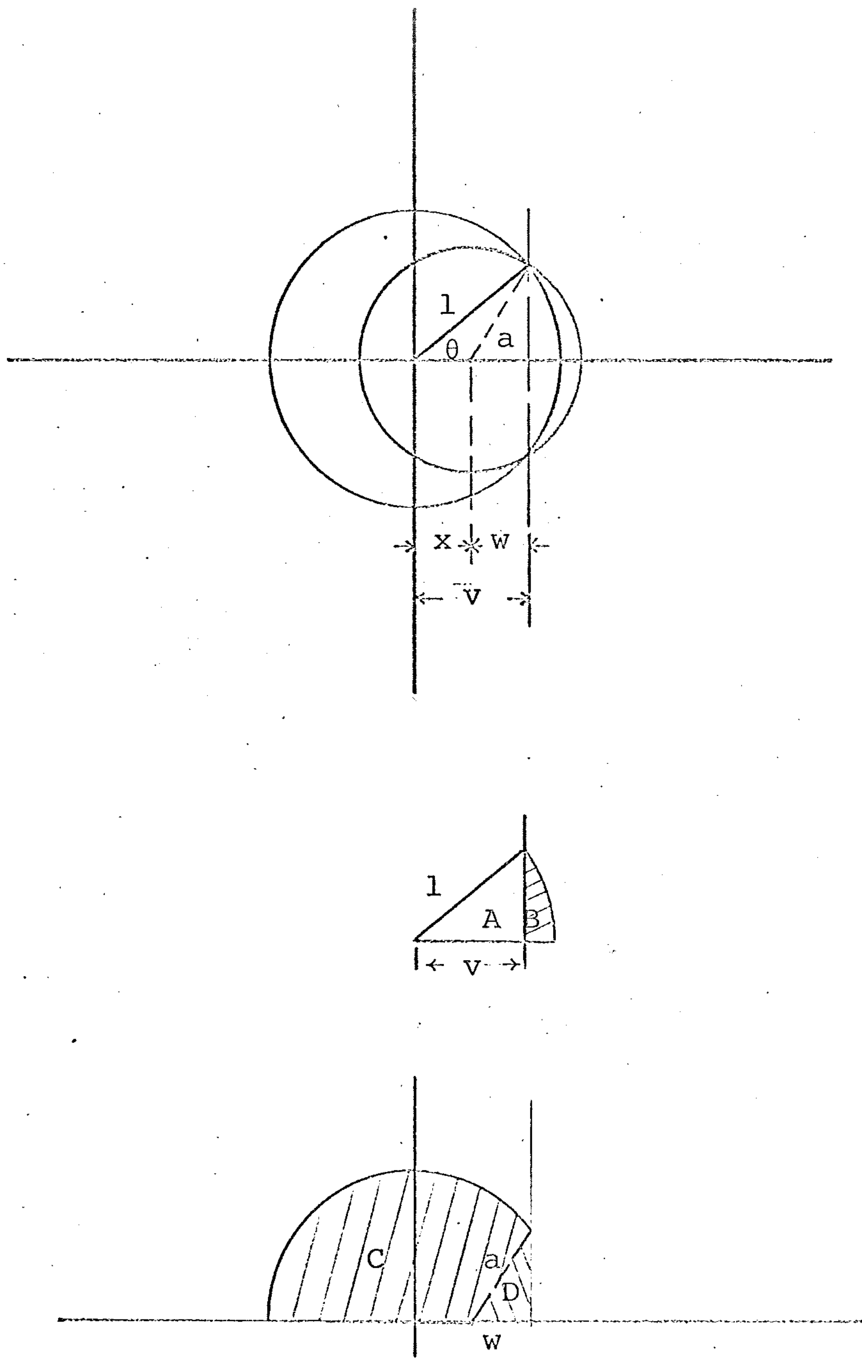

Fig. 24

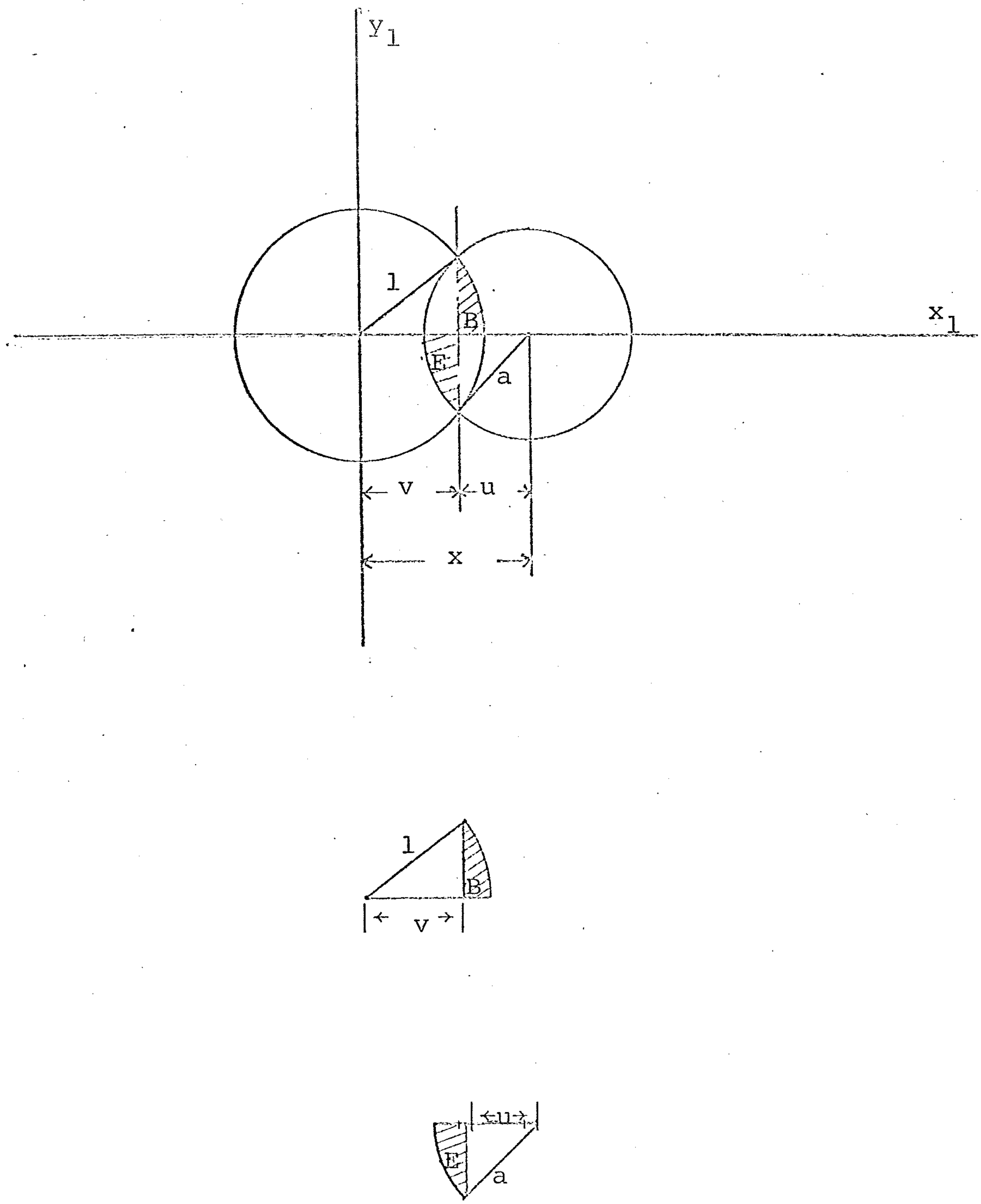

Fig. 25

$$\phi_{a1}(x) = 2\ \text{area}(B) + 2\ \text{area}(C) + 2\ \text{area}(D)$$

$$= \left[\cos^{-1}(v) - v\sqrt{1 - v^2}\right] + \left[\pi a^2 - a^2 \cos^{-1}\left(\frac{w}{a}\right)\right]$$

$$+ \left[a^2 \left(\frac{w}{a}\right)\sqrt{1 - \left(\frac{w}{a}\right)^2}\right]$$

$$= \frac{\pi}{2} F(v) + \pi a^2 - \frac{\pi a^2}{2} F\left(\frac{w}{a}\right) \tag{26}$$

where

$$v = \frac{x^2 + 1 - a^2}{2x} \tag{27}$$

$$w = \frac{1 - a^2 - x^2}{2x} \tag{28}$$

The area of overlap in the range $\sqrt{1 - a^2} \leq x \leq (1+a)$ can be found from Fig. 25 to be given by

$$\phi_{a1}(x) = 2\ \text{area}(B) - 2\ \text{area}(E)$$

$$= \frac{\pi}{2} F(v) + \frac{\pi}{2} F\left(\frac{u}{a}\right) \tag{29}$$

where

$$u = \frac{x^2 + a^2 - 1}{2x} \tag{30}$$

Therefore, from (23) - (30) the autocorrelation function of $\text{ring}_a(r)$ can be written as

$$\phi_{oo}(x) = \begin{cases} \pi F\left(\frac{x}{2}\right) + \pi a^2 F\left(\frac{x}{2a}\right) - 2\pi a^2 & 0 \leq x \leq (1-a) \\ \pi F\left(\frac{x}{2}\right) + \pi a^2 F\left(\frac{x}{2a}\right) - \pi F(v) + \pi a^2 F\left(\frac{w}{a}\right) - 2\pi a^2 & (1-a) \leq x \leq \sqrt{1-a^2} \\ \pi F\left(\frac{x}{2}\right) + \pi a^2 F\left(\frac{x}{2a}\right) - \pi F(v) - \pi a^2 F\left(\frac{u}{a}\right) & \sqrt{1 - a^2} \leq x \leq (1+a) \end{cases}$$

(31)

where v, w, and u are given by (27), (28) and (30). Plots of $\phi_{oo}(x)$ for different values of a are shown in Figs. 26-30. A photomultiplier scan of the autocorrelation of a circular ring with a = .96 is shown in Fig. 31.

4.2 Random Two-hole Pattern

As an example of a random diffracting screen, let the signal in the input plane be two circular holes of radius R separated by a distance d with the line of centers oriented at an angle θ to the x-axis as shown in Figure 32. Let θ be a random variable with a uniform probability density. A circular aperture centered at the origin can be denoted by

$$g_o(\underset{\sim}{r}) = \mathrm{circ}\left(\frac{r}{R}\right) \tag{32}$$

The Fourier transform of $g_o(\underset{\sim}{r})$ is

$$G_o(\underset{\sim}{f}) = \left(\frac{R^2}{2}\right)\frac{J_1(2\pi R f_o)}{R f_o} \tag{33}$$

where $f_o = \sqrt{f_x^{\,2} + f_y^{\,2}}$ and J_1 is a Bessel function of the first kind, order one. The two hole signal in Figure 32 can then be written as

$$g(\underset{\sim}{r}) = g_o(\underset{\sim}{r}) * [\delta(\underset{\sim}{r} - \underset{\sim}{r}_1) - \delta(\underset{\sim}{r} - \underset{\sim}{r}_2)] \tag{34}$$

The Fourier transform of (34) is

$$G(f) = G_o(\underset{\sim}{f})\left[e^{-j2\pi\underset{\sim}{f}\cdot\underset{\sim}{r}_1} + e^{-j2\pi\underset{\sim}{f}\cdot\underset{\sim}{r}_2}\right] \tag{35}$$

Making the substitutions $\underset{\sim}{r}_1 = \underset{\sim}{r}_o - \frac{1}{2}\underset{\sim}{d}$ and $\underset{\sim}{r}_2 = \underset{\sim}{r}_o + \frac{1}{2}\underset{\sim}{d}$

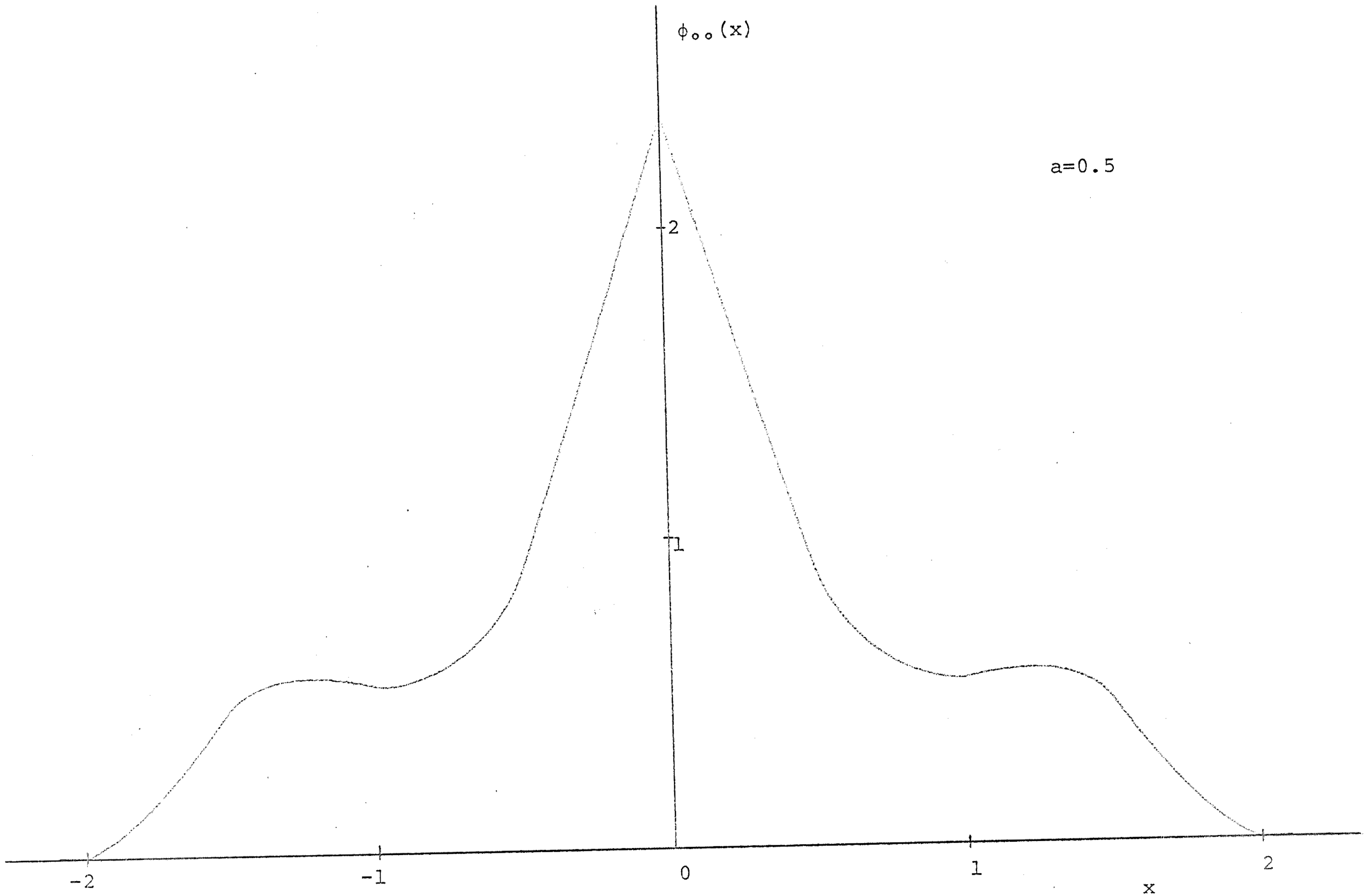

Fig. 26

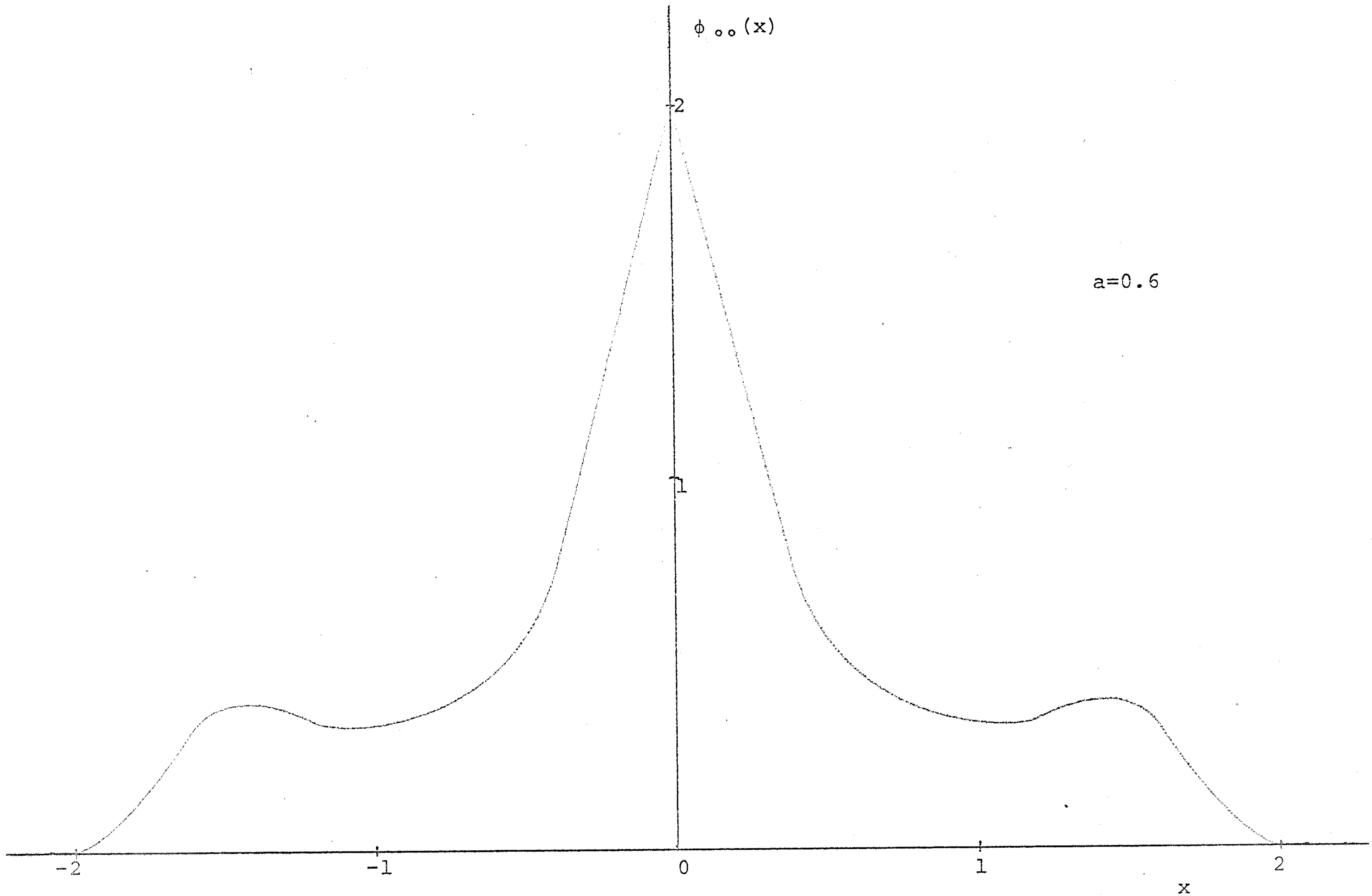

Fig. 27

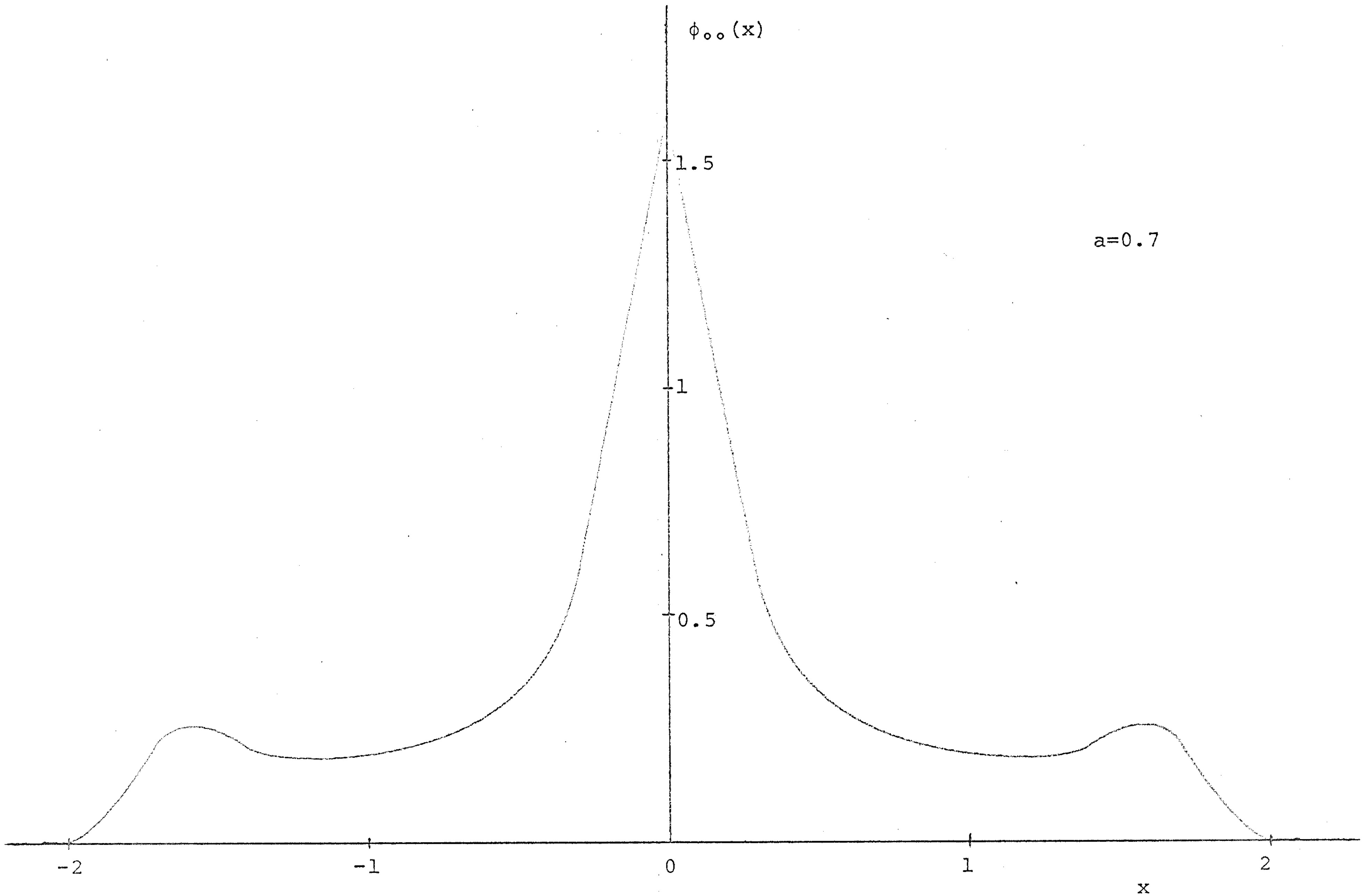

Fig. 28

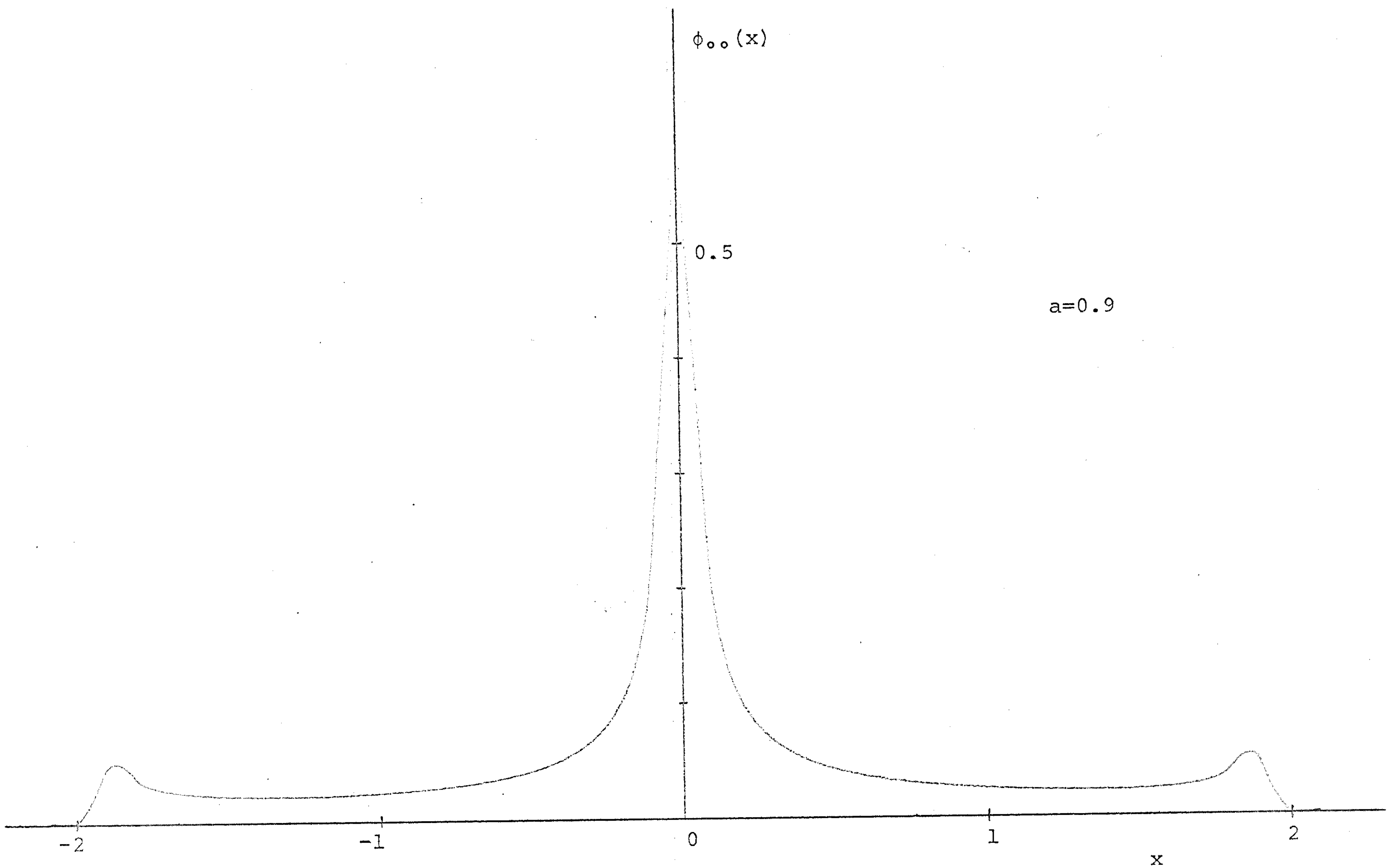

Fig.29

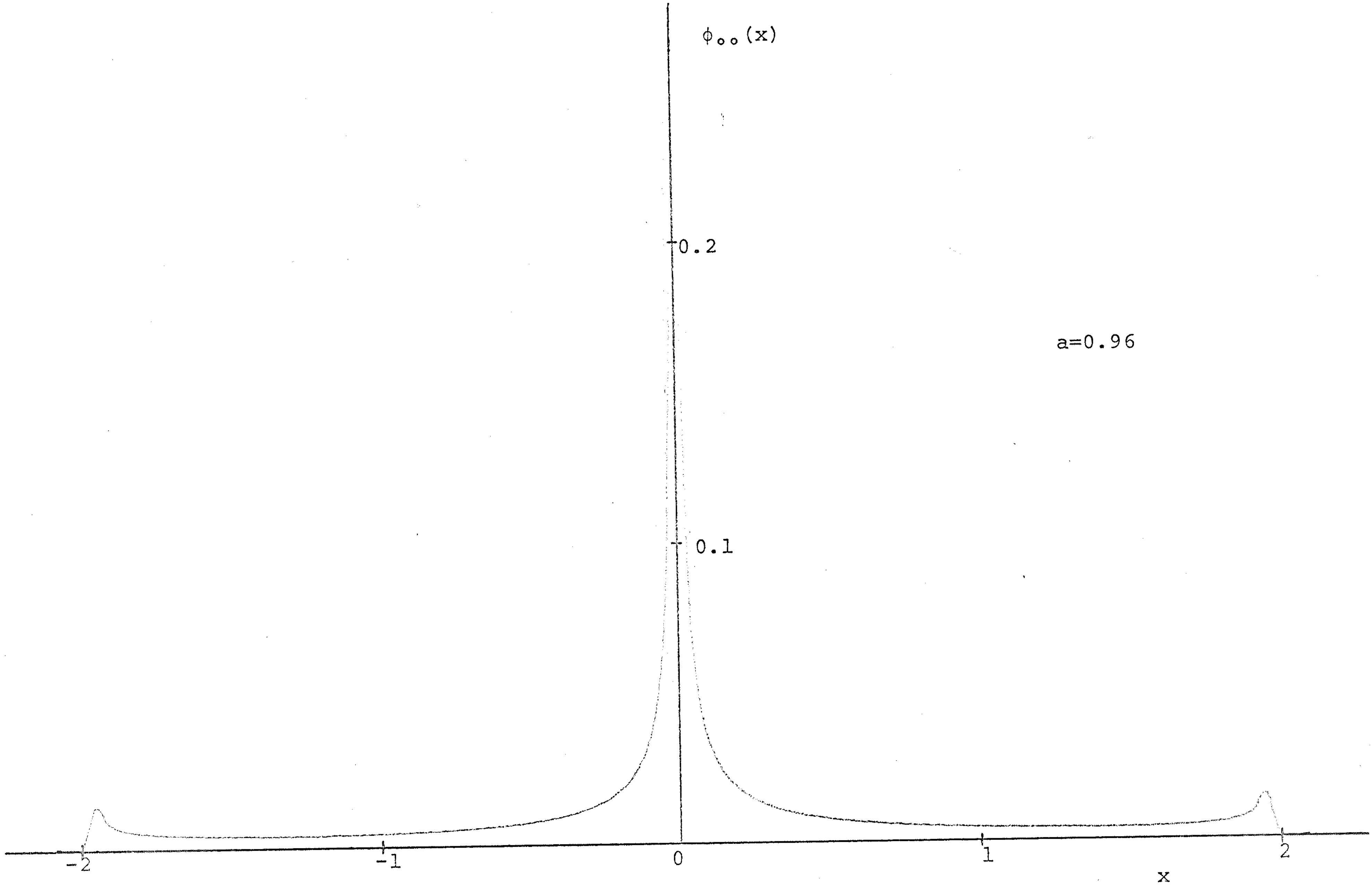

Fig. 30

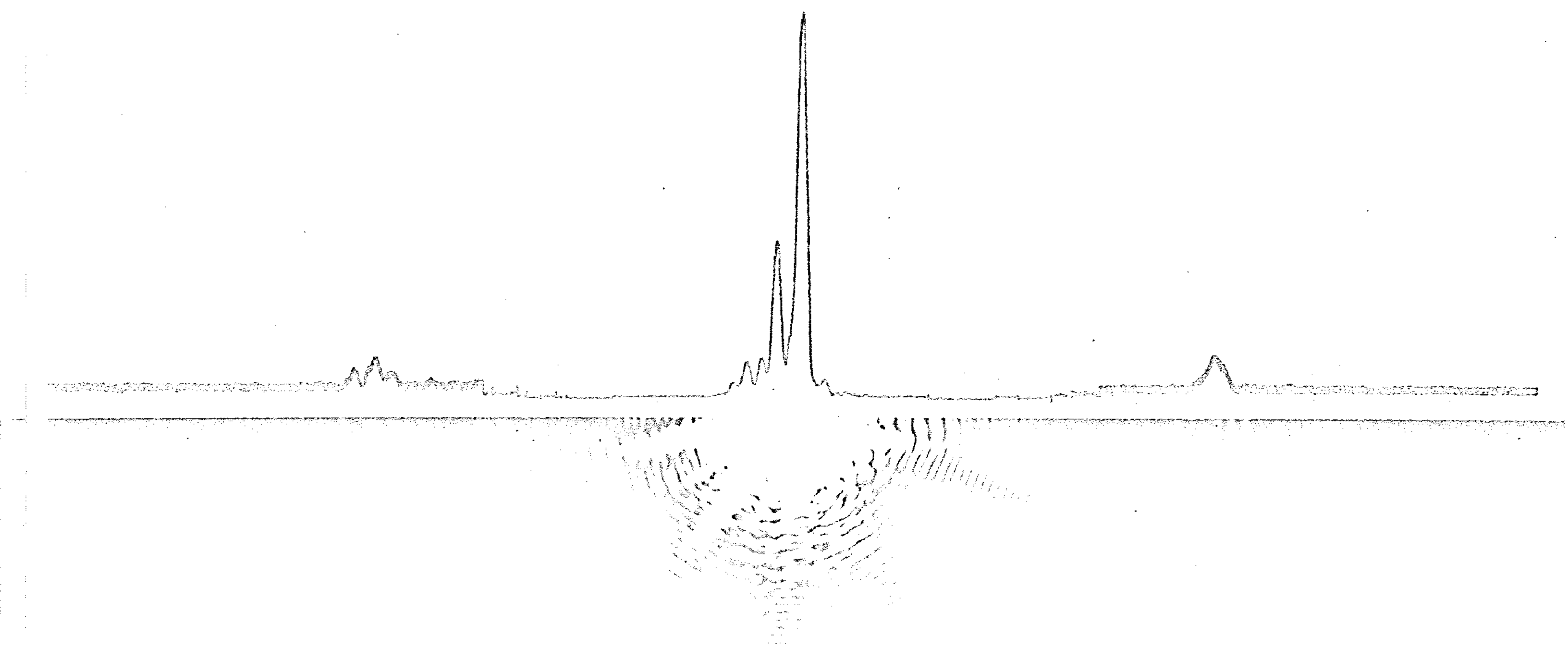

Fig. 31 Photograph and photomultiplier scan of the autocorrelation of $ring_a(r)$. $a=0.96$

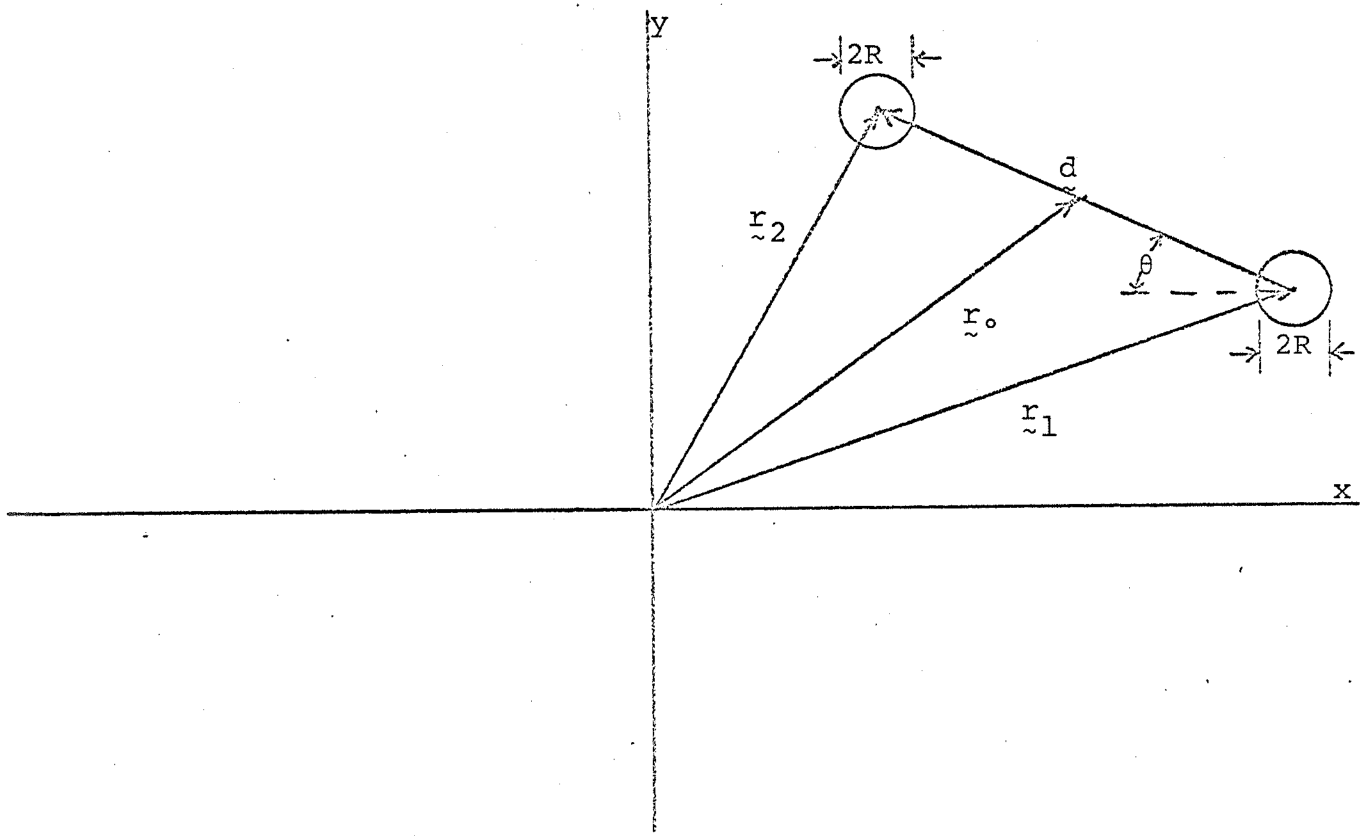

Fig. 32

Geometry of Two-hole Pattern

Eq. (35) can be written in the form

$$G(\underset{\sim}{f}) = e^{-j2\pi \underset{\sim}{f}\cdot \underset{\sim}{r}_o} \; 2\, G_o(\underset{\sim}{f}) \cos\pi \underset{\sim}{f}\cdot\underset{\sim}{d} \tag{36}$$

The intensity in the transform plane will then be proportional to $G(\underset{\sim}{f})G^*(\underset{\sim}{f})$ where

$$G(\underset{\sim}{f})G^*(\underset{\sim}{f}) = 2G_o^{\,2}(\underset{\sim}{f})\,[1 + \cos 2\pi\, \underset{\sim}{f}\cdot\underset{\sim}{d}] \tag{37}$$

Figure 33 shows the transform pattern of a two-hole aperture which closely follows Eq. (37). Note that the cosine modulation of the envelope is related to the separation distance d .

To obtain the power spectrum of the random process an ensemble average over all orientations of the two hole signal is required. From (37) one can calculate

$$\begin{aligned} G(\underset{\sim}{f})G^*(\underset{\sim}{f}) &= 2G_o^{\,2}(\underset{\sim}{f}) + 2G_o^{\,2}(\underset{\sim}{f}) \int_0^{2\pi} \frac{1}{2\pi} \cos[2\pi f_o d \cos(\theta-\psi)]\,d\theta \\ &= 2G_o^{\,2}(f)\,[1 + J_o(2\pi f_o d)] \end{aligned} \tag{38}$$

where $\underset{\sim}{f}\cdot\underset{\sim}{d} = f_o d \cos(\theta-\psi)$ has been used and $\psi = \tan^{-1}(f_y/f_x)$. From (38) one notes that the power spectrum is proportional to the single hole transform given by (33) which is modulated by a J_o Bessel function term that contains information about the separation distance d . A plot of (38) for the case $d = 6R$ is shown in Fig. 34.

An array of these two-hole random patterns as plotted on an oscilloscope by the computer program described in Section 3 is shown in Fig. 35. The power spectrum of this pattern as measured in the

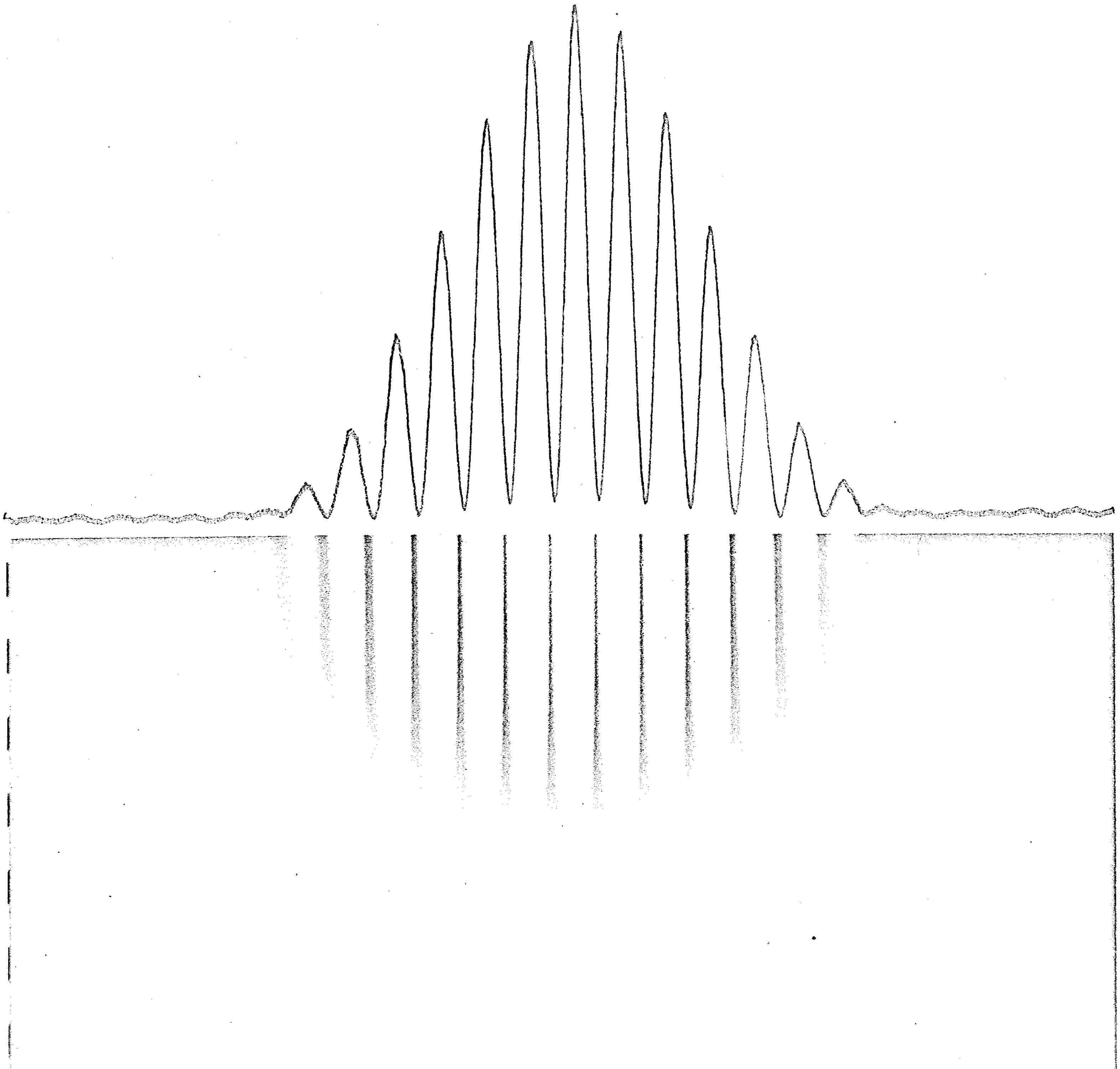

Fig. 33 Photograph and photomultiplier scan of the transform pattern of a two-hole aperture.

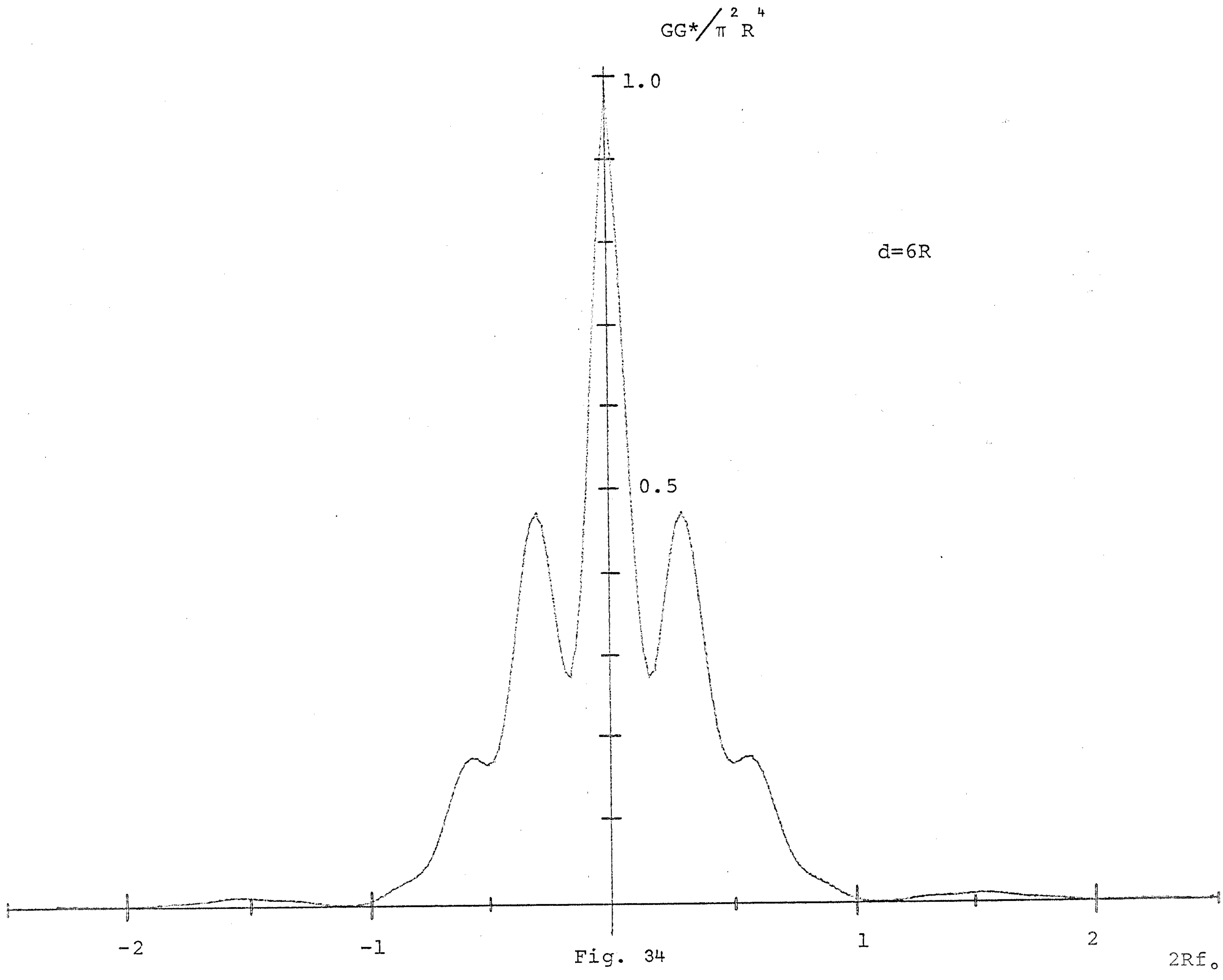

Fig. 34

Fig. 35 Random two-hole pattern produced by digital computer and oscilloscope.

transform plane is shown in Fig. 36. This pattern is a certain representation of the random process $G(\underset{\sim}{f})G^*(\underset{\sim}{f})$. An ensemble average of all such representations should yield the power spectral density function similar to that shown in Fig. 34. The envelope function $G_o^{\,2}(f)$ containing information about the hole radius R is apparent in the single representation of Fig. 36. The J_o Bessel function modulation in (38) should cause light diffracted by a signal proportional to Fig. 36, to form a circle in the transform plane proportional to d . The autocorrelation function of the two-hole random pattern obtained by measuring the Fourier transform of the power spectrum is shown in Fig. 37. A circular ring can be seen surrounding the central peak and is proportional to the distance d separating the two holes of each random pattern. One would expect this type of ring since if the original random pattern were shifted a distance d in any direction there should be an equal probability that two of the paired holes will overlap. A second autocorrelation measurement using the holographic technique described in Technical Report No. 70-2 was made of this random pattern and the result is shown in Fig. 38. Again the circular ring surrounding the central peak is evident. The outer rings and periodic appearance of Figs. 37 and 38 are due to the fact that the two-hole patterns in Fig. 35 were arranged in a periodic array. This is not apparent in Fig. 35 but reveals itself in the autocorrelation measurement.

Power spectrum and autocorrelation measurements can be useful in characterizing random spatial signals and recognizing various statistical parameters. Improved techniques are being developed that will allow ensemble averages to be made.

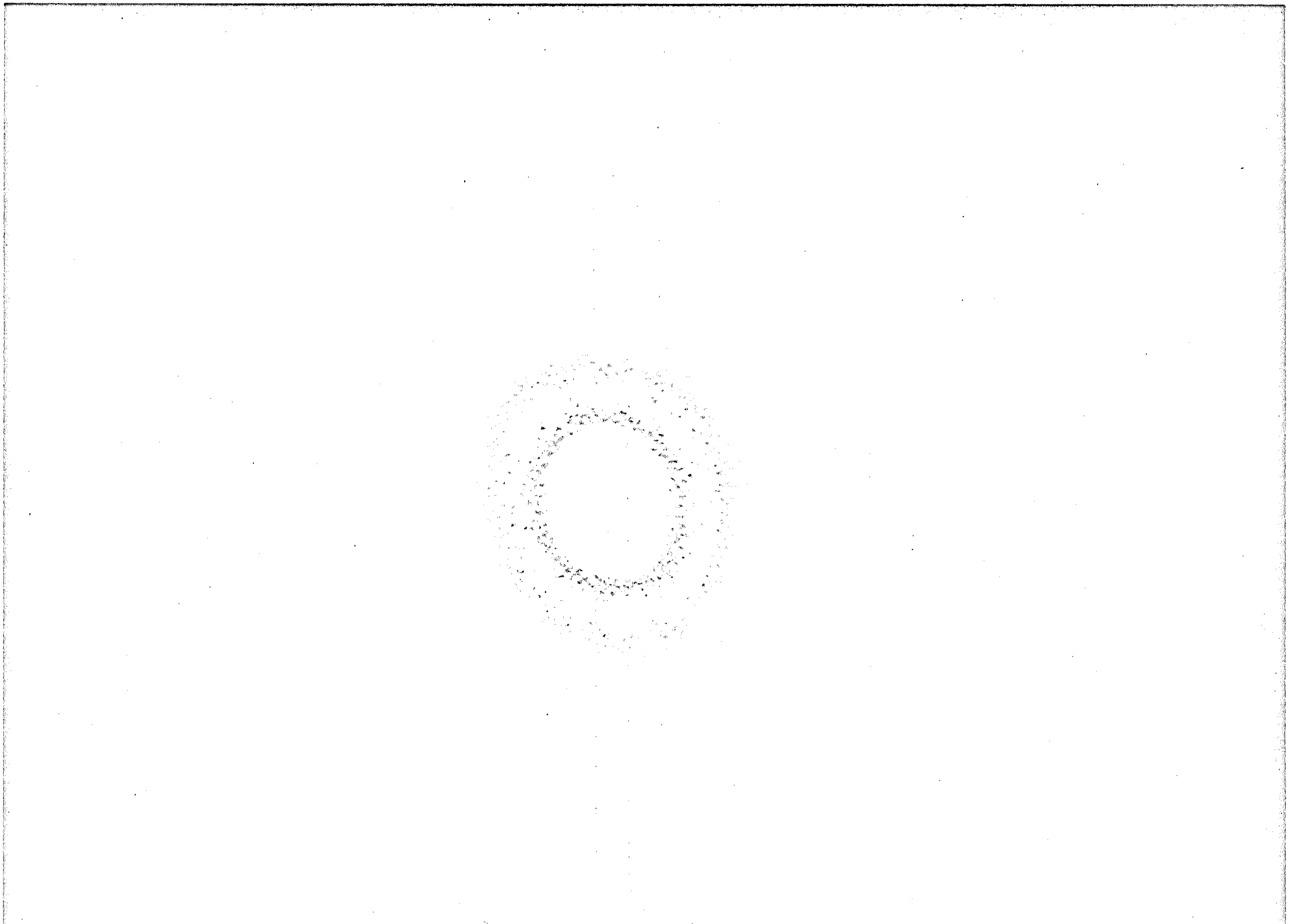

Fig. 36 Power spectrum measurement of random two-hole pattern.

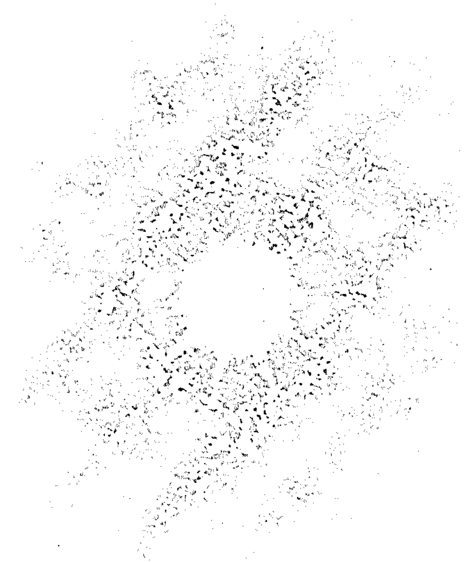

Fig. 37 Autocorrelation measurement of random two-hole pattern.

Fig. 38 Autocorrelation measurement of two-hole random pattern using holographic technique.

References

1. Lendaris, G. G., and G. L. Stanley, "Diffraction-Pattern Sampling for Automatic Pattern Recognition," Proc. IEEE, 58, 198-216, February 1970.

2. Goodman, J. W., Introduction to Fourier Optics, McGraw-Hill Book Co., New York, 1968.

APPENDIX 1

COMPUTER PROGRAM LISTINGS

```
// JOB T
// FOR
*ONE WORD INTEGERS
*LIST ALL
      FUNCTION RANS(K7,IRAN,NCALL)
      GO TO (5,10),K7
5     IF(NCALL-1) 7,6,7
6     IX=IRAN+10
7     CALL RANDU(IX,IY,TFL)
      IX=IY
      RANS=.0625*TFL+.0625
      RETURN
10    RANS=.0625
      RETURN
      END
// DUP
*STORE      WS  UA  RANS
```

```
// FOR
*ONE WORD INTEGERS
*LIST ALL
      FUNCTION RANC(K6,IRAN,NCALL)
      GO TO (5,10),K6
5     IF(NCALL-1) 7,6,7
6     IX=IRAN+8
7     CALL RANDU(IX,IY,YFL)
      IX=IY
      RANC=.1*YFL+.2
      RETURN
10    RANC=.3
      RETURN
      END
// DUP
*STORE      WS  UA  RANC
```

```
// FOR
*ONE WORD INTEGERS
*LIST ALL
      SUBROUTINE OVLAP(X,Y,INC,IGO,KO)
      DIMENSION PT(225,2)
      GO TO (35,1),KO
1     PT(INC,1)=X
      PT(INC,2)=Y
      IF(INC-1) 10,5,10
5     IGO=2
      RETURN
10    N=INC-1
      IGO=2
      DO 30 I=1,N
      IF(IGO-1) 15,30,15
15    DIST=SQRT((PT(INC,1)-PT(I,1))**2 + (PT(INC,2)-PT(I,2))**2)
      IF(DIST-.65) 20,20,25
20    IGO=1
      GO TO 30
25    IGO=2
30    CONTINUE
      RETURN
35    IGO=2
      RETURN
      END
// DUP
*STORE      WS  UA  OVLAP
```

```
// FOR
*ONE WORD INTEGERS
*LIST ALL
      SUBROUTINE PTLOC(IRAN,NCALL,XH1,YH1,XH2,YH2,IRAD,NSPOT)
      COMMON CRAD,SPOT
      PI=3.1415926
42    FSTOD=PI/2.
      IF(NCALL-1) 10,5,10
5     IX=IRAN
10    CALL RANDU (IX,IY,YFL)
      IX=IY
      GO TO (60,15),NSPOT
C     DOUBLE SPOT
15    ANGLE=PI*YFL
      GO TO (20,21),IRAD
20    CALL RANDU(IX,IY,TFL)
      IX=IY
      R=TFL*(CRAD-(SPOT+.005))+(SPOT+.005)
      GO TO 14
21    R= CRAD-(SPOT+.005)
14    IF(ANGLE-FSTOD) 16,22,25
C      COMPUTE POINT COORDINATES
16    XH1=  R*COS(ANGLE)
      YH1=  R*SIN(ANGLE)
C      ADJUST POINTS TO PROPER QUADRANT
      XH2=-XH1
      YH2=-YH1
      RETURN
22    XH1=0.
      YH1=  R
      XH =0.
      YH2=-  R
      RETURN
25    ANG=PI-ANGLE
      XH1=-  R*COS(ANG)
      YH1=  R*SIN(ANG)
      XH2=-XH1
      YH =-YH1
      RETURN
C      SINGLE POINT COORDINATE LOCATION
60    ANGLE=2.*PI*YFL
      GO TO (65,70),IRAD
65    CALL RANDU(IX,IY,TFL)
      IX=IY
      R=TFL*(CRAD-(SPOT+.005))
      GO TO 75
70    R=CRAD-(SPOT+.005)
75    XH1=R*COS(ANGLE)
      YH1=R*SIN(ANGLE)
      XH2=0.0
      YH2=0.0
      RETURN
99    END
// DUP
*STORE [illegible] WS UA PTLOC
```

```
// FOR
*ONE WORD INTEGERS
*LIST ALL
      SUBROUTINE DSPOT(X,Y)
      COMMON CRAP,SPOT
C      PEN UP (PRECATUION)
      CALL RSCL(1,IER)
      R=SPOT
      XSTRT=(X+.0625)*3276.7
      IXSTR=XSTRT
      YSTRT=Y*3276.7
      IYSTR=YSTRT
C      MOVE PEN TO INITIAL POINT
      CALL LTDA(6,IXSTR,IER)
      CALL LTDA(7,IYSTR,IER)
      CALL DELAY(.4)
C      PEN DOWN
      CALL SSCL(1,IER)
      CALL DELAY(.1)
      DIV=(2.*3.14159)/20.
C      DRAW FOUR CONCENTRIC CIRCLES
      IF(R-.1250) 20,15,15
15    L=25
      GO TO 55
20    IF(R-.1093) 30,25,25
25    L=21
      GO TO 55
30    IF(R-.0937) 40,35,35
35    L=18
      GO TO 55
40    IF(R-.0718) 50,45,45
45    L=15
      GO TO 55
50    L=12
55    DO 10 J=1,L
      THETA=0.0
      DO 5 I=1,20
      X1=R*COS(THETA)
      Y1=R*SIN(THETA)
       XOUT=(X+X1)*3276.7
       YOUT=(Y+Y1)*3276.7
      IXOUT=XOUT
      IYOUT=YOUT
      CALL LTDA(6,IXOUT,IER)
      CALL LTDA(7,IYOUT,IER)
      THETA=THETA+DIV
5     CONTINUE
      R=R-.005
10    CONTINUE
C      PEN UP
      CALL RSCL(1,IER)
      CALL DELAY(.1)
      RETURN
      END
// DUP
*STORE       WS  UA  DSPOT
```

```
// FOR
*ONE WORD INTEGERS
*LIST ALL
      SUBROUTINE CIRCL(X,Y)
      COMMON CRAD,SPOT
C      PEN UP (PRECAUTION)
      CALL RSCL(1,IER)
      PI=3.1415926
      DIV=(2.*PI)/125.
      THETA=0.0
      R=CRAD
      IXOUT=(X+ R )*3276.7
      IYOUT=Y*3276.7
C      MOVE PEN TO FIRST POINT
      CALL LTDA(6,IXOUT,IER)
      CALL LTDA(7,IYOUT,IER)
      CALL DELAY(.4)
C      PEN DOWN
      CALL SSCL(1,IER)
      CALL DELAY(.1)
C      PLOT CIRCLE
      DO 20 I=1,125
      Y1=  R*SIN(THETA)
      X1=  R*COS(THETA)
      IXOUT=(X+X1)*3276.7
      IYOUT=(Y+Y1)*3276.7
      CALL LTDA(6,IXOUT,IER)
      CALL LTDA(7,IYOUT,IER)
      THETA=THETA+DIV
20    CONTINUE
C      PEN UP
      CALL RSCL(1,IER)
      CALL DELAY(.1)
      RETURN
      END
// DUP
*STORE      WS  UA  CIRCL
```

```
// FOR
*IOCS(1132 PRINTER,DISK,CARD,TYPEWRITER,KEYBOARD)
*ONE WORD INTEGERS
*LIST ALL
      INTEGER ROWS,COLS
      DIMENSION KEY(16)
      COMMON GRAD,SPOT
C      WRITE SWITCH CONFIGURATION
4     WRITE(1,2000)
      WRITE(1,2001)
      WRITE(1,2005)
      WRITE(1,2010)
      WRITE(1,2015)
      WRITE(1,2020)
      WRITE(1,2025)
      WRITE(1,2030)
      WRITE(1,2031)
      WRITE(1,2032)
      WRITE(1,2035)
      PAUSE 1111
C      READ SWITCHES
      DO 5 I=1,10
5     CALL DATSW(I,KEY(I))
      CALL DATSW(0,K0)
      K1=KEY(1)
      K2=KEY(2)
      K3=KEY(3)
      K4=KEY(4)
      K5=KEY(5)
      K6=KEY(6)
      K7=KEY(7)
       K8=KEY(8)
      K9=KEY(9)
      K10=KEY(10)
      WRITE(1,2040)
      WRITE(1,2041)
      READ(6,2045) IRAN
C      PEN UP
      CALL PSCL(1,IER)
C      SELECT STATIC TEST MODE
6     CALL SAVD(3,IER)
      II=0
C      LOAD DACS WITH ZEROES
      CALL LTDA(6,II,IER)
      CALL LTDA(7,II,IER)
      WRITE(1,2050)
      PAUSE 2222
      GO TO (130,10),K8
10    GO TO (12,11),K2
11    WRITE(1,2055)
      READ(6,2060) ROWS
      WRITE(1,2065)
      CALL LTDA(6,III,IER)
      READ(6,2060) COLS
C      UNIFORM PATTERN GENERATION SECTION
12    DO 100 I=1,4096
      R=ROWS+1
      CALL DATSW(1,K1)
      GO TO (120,15),K1
15    IF(I-1) 20,20,25
20    MINC=10./R
```

```
      GO TO 30
25    YINC=YINC+10./R
30    DO 100 J=1,COLS
      NCALL=I+J-1
      CRAD=RANC(K6,IRAN,NCALL)
      C=COLS+1
      CALL DATSW(1,K1)
      GO TO (100,31),K1
31    IF(J-1) 40,35,40
35    XINC=10./C
      GO TO 45
40    XINC=XINC+10./C
45    GO TO (50,55),K5
50    CALL CIRCL(XINC,YINC)
55    GO TO (65,60),K2
60    GO TO (65,100),K3
65    SPOT=RANS(K7,IRAN,NCALL)
      CALL PTLOC(IRAN,NCALL,XH1,YH1,XH2,YH2,KEY(4),K2)
      VOLX1=XINC+XH1
      VOLY1=YINC+YH1
      CALL DSPOT(VOLX1,VOLY1)
      GO TO (70,100),K3
70.   VOLX2=XINC+XH2
      VOLY2=YINC+YH2
      CALL DSPOT(VOLX2,VOLY2)
100   CONTINUE
120   CONTINUE
130   GO TO (129,201),K8
C      RANDOM PATTERN GENERATION SECTION
129   JRAN=IRAN+2
      KRAN=JRAN+2
      GO TO(132,131),K9
131   WRITE(1,2056)
      READ(6,2060) ROWS
      NF=0
132   DO 200 K=1,ROWS
      NCALL=K
      CRAD=RANC(K6,IRAN,NCALL)
133   CALL DATSW(1,K1)
      GO TO (200,135),K1
135   CALL RANDU(JRAN,IY,Y)
136   JRAN=IY
      YO=Y*9.4+.3
      CALL RANDU(KRAN,IX,Y)
141   KRAN=IX
      XO=Y*9.4 +.3
      CALL OVLAP(XO,YO,K,IGO,K9)
      GO TO (143,144),IGO
143   NF=NF+1
      GO TO 133
144   WRITE (3,1234) XO,YO
1234  FORMAT ('COORDINATE OF THE CIRCLE',2X,F10.5,4X,F10.5)
      GO TO (145,150),K5
145   CALL CIRCL(XO,YO)
150   GO TO (160,155),K2
155   GO TO (160,200),K3
160   SPOT=RANS(K7,IRAN,NCALL)
      CALL PTLOC(IRAN,NCALL,XH1,YH1,XH2,YH2,KEY(4),K2)
      VOLX1=XO+XH1
      VOLY1=YO+YH1
```

```
      CALL DSPOT(VOLX1,VOLY1)
      GO TO (165,200),K3
  165 VOLX2=XO+XH2
      VOLY2=YO+YH2
      CALL DSPOT(VOLX2,VOLY2)
  200 CONTINUE
      NT=NF+ROWS
      WRITE(1,2080) ROWS,NT
  201 WRITE(1,2070)
      PAUSE 3333
C      REPLOT OR NEW PLOT
      CALL DATSW(9,K9)
      GO TO(6,205),K9
  205 WRITE(1,2075)
      PAUSE 4444
      CALL DATSW(10,K10)
      GO TO (4,210),K10
 2000 FORMAT('T U R N  O N',4X,'F O R'/)
 2001 FORMAT(4X,'SW 0',6X,'OVERLAP')
 2005 FORMAT(4X,'SW 1',6X,'INTERUPT')
 2010 FORMAT(4X,'SW 2',6X,'SINGLE RANDOM SPOTS')
 2015 FORMAT(4X,'SW 3',6X,'PAIRS OF RANDOM SPOTS')
 2020 FORMAT(4X,'SW 4',6X,'RANDOM SPOT LOCATION RADIUS')
 2025 FORMAT(4X,'SW 5',6X,'CIRCLES AROUND PATTERNS')
 2030 FORMAT(4X,'SW 6',6X,'RANDOM CIRCLE RADIUS')
 2031 FORMAT(4X,'SW 7',6X,'RANDOM SPOT SIZE')
 2032 FORMAT(4X,'SW 8',6X,'RANDOM PATTERN LOCATION'/)
 2035 FORMAT('SELECT SWITCHES *** PUSH START'/)
 2040 FORMAT('ENTER RANDOM VARIABLE')
 2041 FORMAT('ODD NUMBER(      ) 1 TO 32750')
 2045 FORMAT(11X,I5)
 2050 FORMAT('POSITION THE PEN IN THE LOWER LEFT CORNER OF GRID'/'X-Y SC
     1ALES 1V/IN'/'PUSH START'/)
 2055 FORMAT('ENTER NUMBER OF PATTERNS'/'ROWS(    ) MAX-15')
 2056 FORMAT('ENTER NUMBER OF PATTERNS'/'NO. (    ) MAX-225')
 2060 FORMAT(5X,I3)
 2065 FORMAT('COLS(    ) MAX-15')
 2070 FORMAT(/'SW 9 ON TO REPLOT *** PUSH START'/)
 2075 FORMAT(/'SW 10 ON FOR NEW PLOT *** PUSH START'/)
 2080 FORMAT('TOTAL TRIALS FOR ',I3,' POINTS IS ',I4/)
  210 CALL EXIT
      END
// XEQ
```

APPENDIX 2

NOMOGRAPHS FOR HOLOGRAPHIC IMAGING

by

Richard E. Haskell

Coherent Optics Laboratory
Technical Report No. 70-1, May 1970

This work was supported in part
by NASA under Grant NGR 23-054-003

School of Engineering
Oakland University
Rochester, Michigan 48063

I. HOLOGRAPHIC IMAGING

The holographic imaging of point sources can be described using the geometry of Fig. 1. An object beam in the form of a spherical wave originates from a point source at O. Neglecting constant phase factors, the complex amplitude of this wave at the z = 0 plane can be written as $\underset{\sim}{U}_o = K_o\, e^{jkr_o}$ where $K_o = A_o/r_o$. Similarly the reference beam originating from a point source at R can be written as $\underset{\sim}{U}_r = K_r\, e^{jkr_r}$. If a photographic film is placed in the plane z = 0 the intensity recorded by the film is proportional to

$$|\underset{\sim}{U}_o + \underset{\sim}{U}_r|^2 = \underset{\sim}{U}_o\underset{\sim}{U}_o^* + \underset{\sim}{U}_r\underset{\sim}{U}_r^* + \underset{\sim}{U}_o\underset{\sim}{U}_r^* + \underset{\sim}{U}_o^*\underset{\sim}{U}_r \qquad (1)$$

Assuming that the amplitude transmittance of the resulting hologram is proportional to this intensity function and if the reconstruction beam in Fig. 1b is of the form $U_c = K_c\, e^{jkr_c}$ then the wave transmitted by the hologram located in the z = 0 plane of Fig. 1b will be proportional to

$$\underset{\sim}{U}_T = \underset{\sim}{U}_c\underset{\sim}{U}_o\underset{\sim}{U}_o^* + \underset{\sim}{U}_c\underset{\sim}{U}_r\underset{\sim}{U}_r^* + \underset{\sim}{U}_c\underset{\sim}{U}_o\underset{\sim}{U}_r^* + \underset{\sim}{U}_c\underset{\sim}{U}_o^*\underset{\sim}{U}_r \qquad (2)$$

The first two terms on the right-hand side of (2) are d-c terms representing the main zero-order diffracted reconstruction beam. The third term $\underset{\sim}{U}_+ = \underset{\sim}{U}_c\underset{\sim}{U}_o\underset{\sim}{U}_r^*$ is the primary beam and the fourth term $\underset{\sim}{U}_- = \underset{\sim}{U}_c\underset{\sim}{U}_o^*\underset{\sim}{U}_r$ is the conjugate beam.

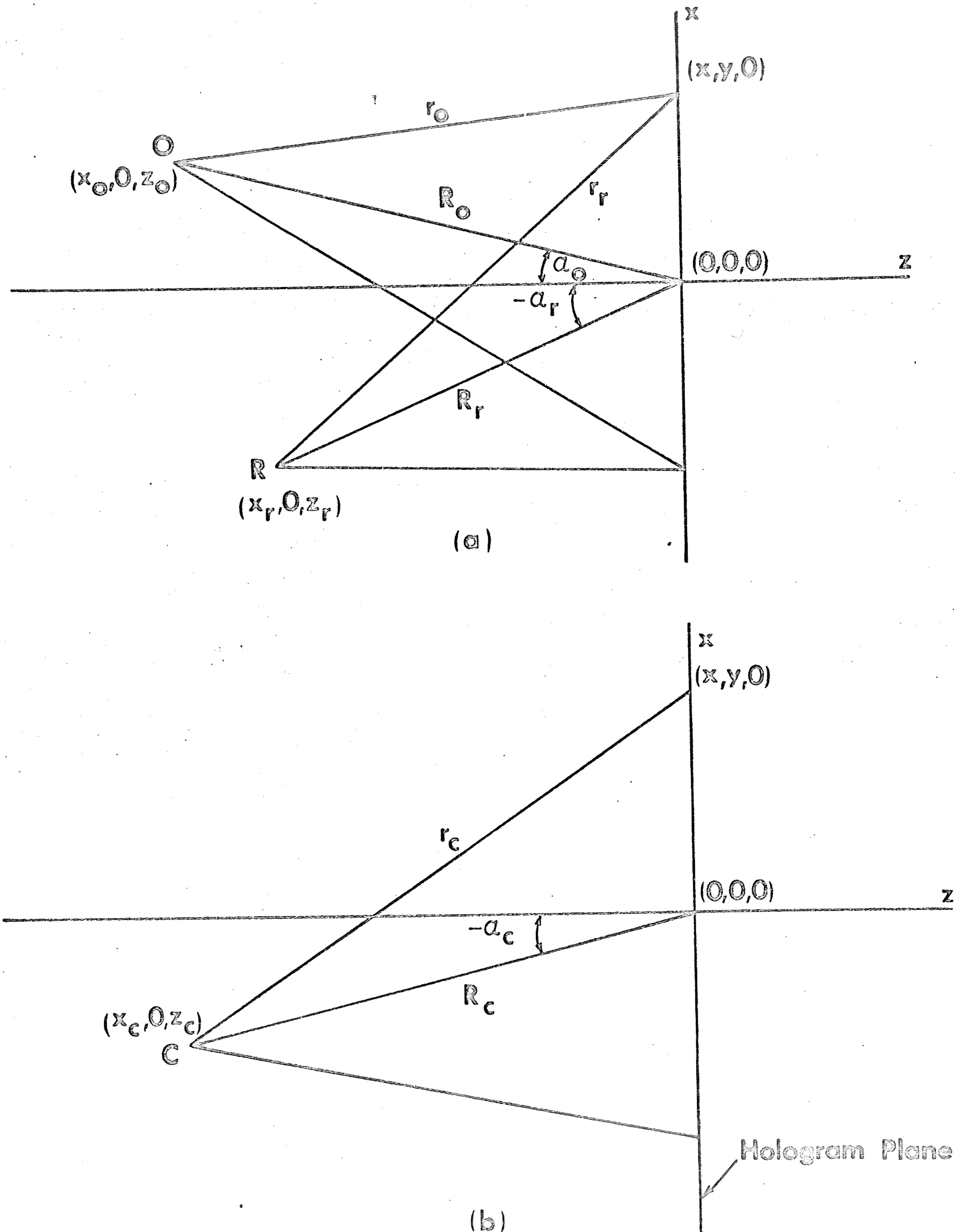

Fig. 1
a) Recording and
b) Reconstruction geometry for point source holographic imaging

It follows that

$$\underset{\sim}{U}_{\pm} = K_{\pm} e^{jkr_i^{\pm}} \tag{3}$$

where

$$r_i^{\pm} = r_c \pm (r_o - r_r) \tag{4}$$

Thus the primary and conjugate beams $\underset{\sim}{U}_{\pm}$ are spherical waves diverging from or converging to a point specified by image coordinates that can be determined from (4).

From Fig. 1a note that

$$\begin{aligned} r_o &= \left[(x-x_o)^2 + y^2 + z_o^2\right]^{1/2} \\ &= \left[R_o^2 + x^2 + y^2 - 2xx_o\right]^{1/2} \end{aligned} \tag{5}$$

where $R_o^2 = x_o^2 + z_o^2$. Expanding (5) in a binominal series about R_o one can approximate r_o by the expression

$$r_o \approx R_o + \frac{x^2+y^2}{2R_o} - x \sin \alpha_o \tag{6}$$

where $\sin \alpha_o = x_o/R_o$. Analogous expressions can be written for r_r, r_c, and r_i. If this is done then by using (3) and (4) one can write

$$\underset{\sim}{U}_{\pm} = K_{\pm}\, e^{jkR_i}\, e^{jk\frac{x^2+y^2}{2R_i}}\, e^{-jkx \sin \Theta_i}$$

$$= K_c K_o K_r\, e^{jk[R_c \pm (R_o - R_r)]}\, e^{jk\frac{x^2+y^2}{2}\left[\frac{1}{R_c} \pm \left(\frac{1}{R_o} - \frac{1}{R_r}\right)\right]}$$

$$\cdot\, e^{-jkx[\sin \alpha_c \pm (\sin \alpha_o - \sin \alpha_r)]} \tag{7}$$

For this equation to be true for all x it is necessary that

$$\frac{1}{R_i} = \frac{1}{R_c} \pm \left(\frac{1}{R_o} - \frac{1}{R_r}\right) \tag{8}$$

and

$$\sin \alpha_i = \sin \alpha_c \pm (\sin \alpha_o - \sin \alpha_r) \tag{9}$$

Eqs. (8) and (9) have been obtained by Champagne[1] and give the image coordinates R_i, α_i in terms of the coordinates R, α for the object, reference, and reconstruction beams. If R_i is positive the image is virtual while if R_i is negative the image is real. The plus sign is associated with the primary wave and the minus sign with the conjugate wave.

II. CONSTRUCTION AND USE OF HOLOGRAPHIC NOMOGRAPHS

Eqs. (8) and (9) permit a wide range of possible image point locations depending upon the particular choices of R_o, R_r, R_c, α_o, α_r, and α_c. As an aid in determining image point locations, two nomographs of Eqs. (8) and (9) have been constructed. Parallel-scale nomographs can easily be constructed for an equation of the form[2]

$$f_3(w) = f_1(u) + f_2(v) \tag{10}$$

By introducing the two auxiliary variables R_f and α_f defined by the equations

$$\frac{1}{R_f} = \frac{1}{R_o} - \frac{1}{R_r} \tag{11}$$

and

$$\sin \alpha_f = \sin \alpha_o - \sin \alpha_r \tag{12}$$

Eqs. (8) and (9) may be written in the form

$$\frac{1}{R_i} = \frac{1}{R_c} \pm \frac{1}{R_f} \tag{13}$$

and

$$\sin \alpha_i = \sin \alpha_c \pm \sin \alpha_f \tag{14}$$

Eqs. (11) - (14) are each of the form of Eq. (10) and can therefore be solved by a parallel-scale nomograph. The R-nomograph shown in Fig. 2 can be used to solve both Eq. (11) for R_f and Eq. (13) for R_i. Similarly, the α-nomograph shown in Fig. 3 can be used to solve both Eq. (12) for α_f and Eq. (14) for α_i.

The R-nomograph for determing R_i is used in the following manner. A straight line is drawn between R_o on the left-hand axis and R_r on the right hand axis. The intersection of this line with the R_f axis determines a particular value of R_f. If a second straight line is now drawn from this value of R_f to R_c on the left-hand axis the intersection of this second line with the R_i axis determines the image distance R_i for the primary wave. The value of R_i for the conjugate wave is determined by connecting the second straight line from $-R_f$ to R_c. The α-nomograph shown in Fig. 3 works in an exactly analogous manner. This procedure will be illustrated by two examples.

Example 1: Let the object be a point source located at $R_o = 15$ (units arbitrary), $\alpha_o = 0°$ and let the reference beam come from a point source located at $R_r = 60$, $\alpha_r = 20°$. Let the reconstruction beam be the same as the reference beam, i.e., $R_c = 60$, $\alpha_c = 20°$. On the R-nomograph in Fig. 4 the straight line joining $R_o = 15$ and $R_r = 60$ gives a value of $R_f = 20$. To find the primary wave draw a straight line from $R_f = 20$ to $R_c = 60$ which gives the image distance $R_i = 15$. To find the angle α_i for the primary wave draw a straight line in Fig. 5 from $\alpha_o = 0°$ to $\alpha_r = 20°$. A straight line drawn from $\alpha_f = -20°$ to $\alpha_c = 20°$ determines that $\alpha_i = 0°$ for the primary wave. That is, the primary image is a virtual point source located at $R_i = 15$, $\alpha_i = 0°$ which is the same as the object as expected. To find the conjugate image return to Fig. 4 and draw a straight line from $-R_f$ (i.e., $R_f = -20$) to $R_c = 60$ which gives a value of $R_i = -30$. In Fig. 5 a straight line from $-\alpha_f$ ($\alpha_f = +20°$) to $\alpha_c = 20°$ shows that for the conjugate wave $\alpha_i = 43°$. Thus, the conjugate image is a real image located at $R_i = -30$, $\alpha_i = 43°$.

Example 2: In Example 1 the primary image was a virtual image and the conjugate image was a real image. As an example of a case in which the primary image is real and the conjugate image is virtual let $R_o = 100$, $\alpha_o = 0°$, $R_r = 20$, $\alpha_r = -15°$, $R_c = 50$, and $\alpha_c = -15°$. Then from Figs. 6 and 7 the primary image is a real image located at $R_i = -50$, $\alpha_i = 0°$ and the conjugate image is a virtual image located at $R_i = 16.6$, $\alpha_i = -31°$.

Sample copies of the two nomographs are included at the end of this report.

REFERENCES

1. E.B. Champagne, J. Opt. Soc. Am., 57, 51, (1967).

2. J.E. Gibson, Introduction to Engineering Design, pp. 50-55, Holt, Rinehart and Winston, Inc., New York, 1968.

R-NOMOGRAPH FOR HOLOGRAPHIC IMAGING

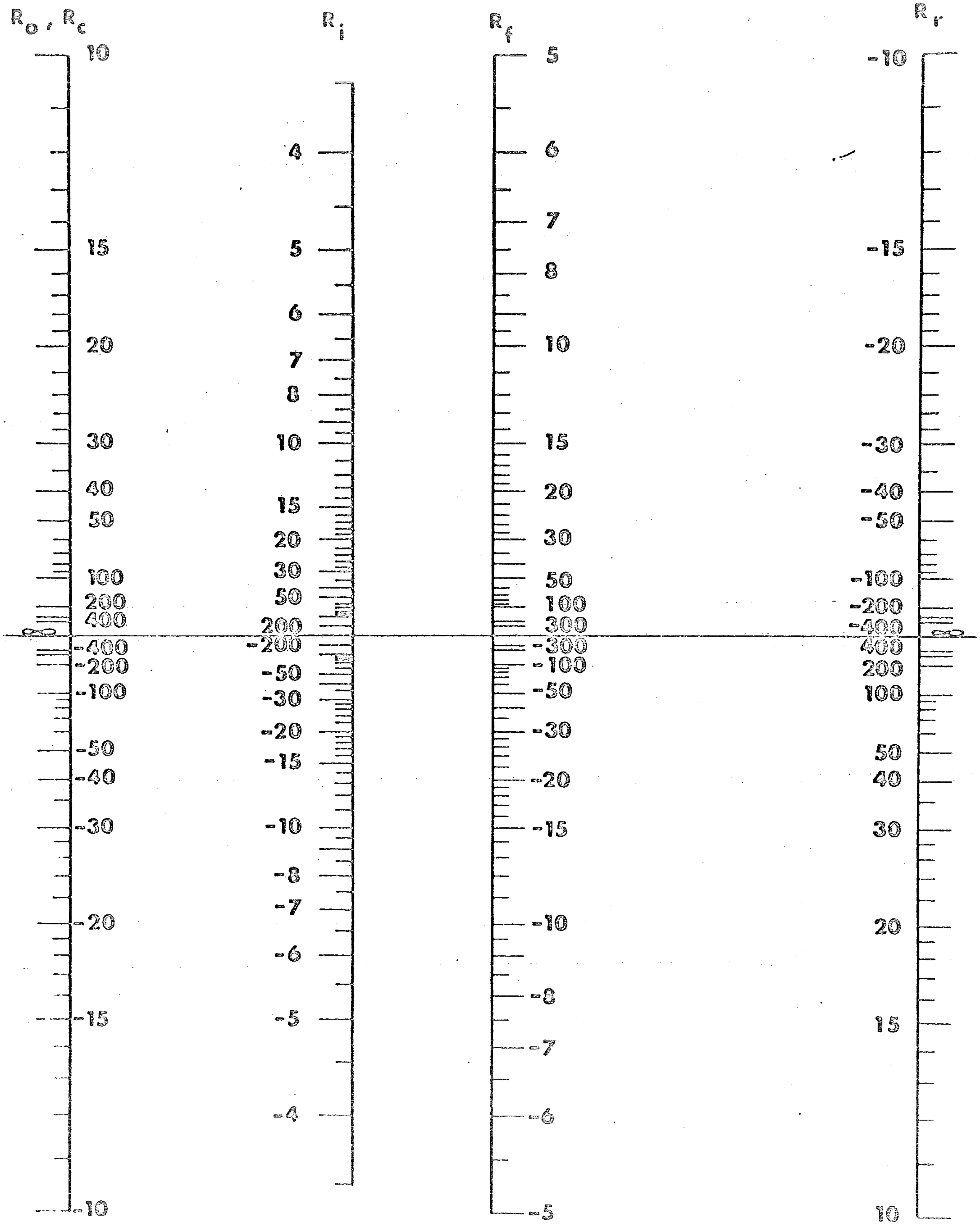

Fig. 2

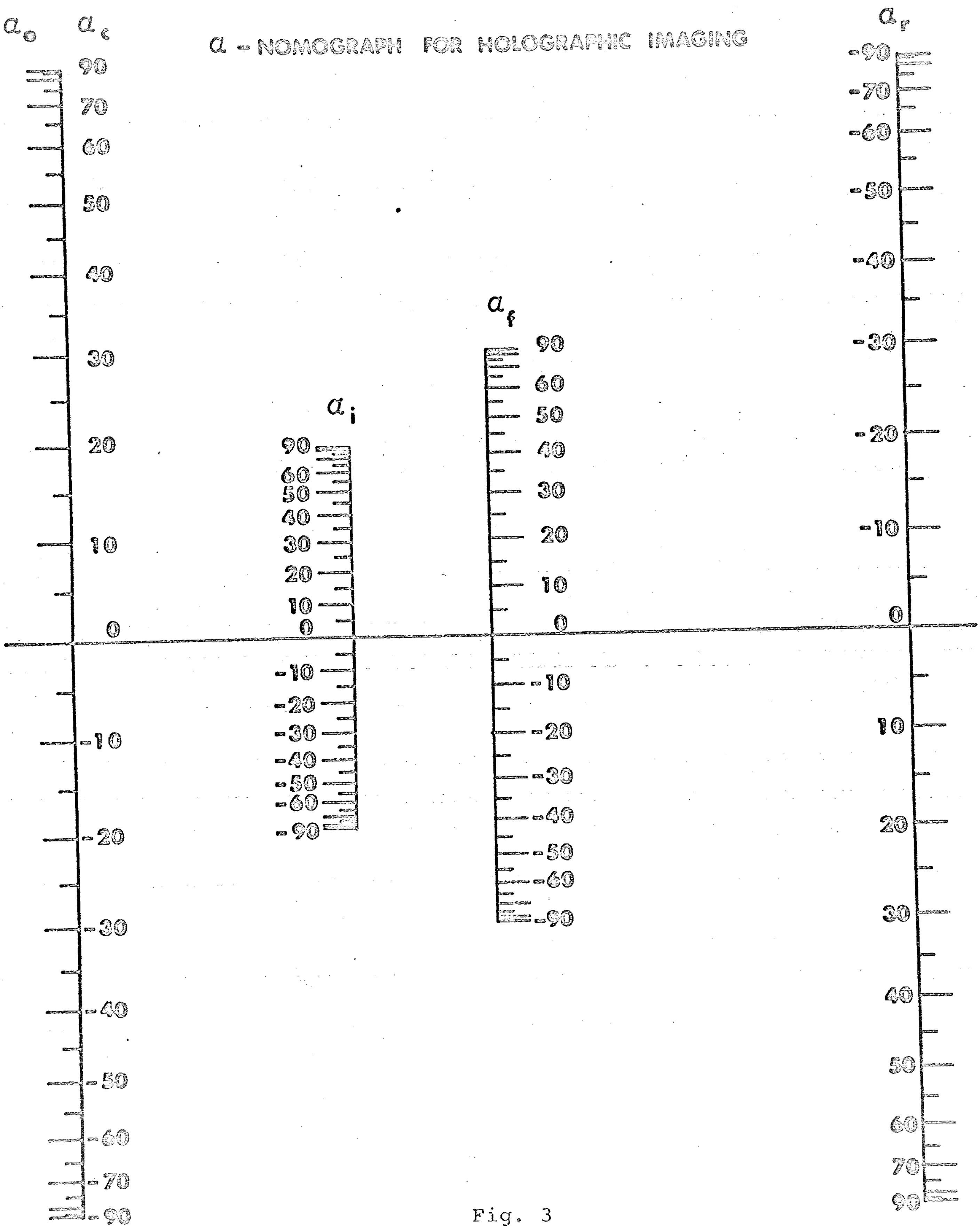

Fig. 3

R - NOMOGRAPH FOR HOLOGRAPHIC IMAGING

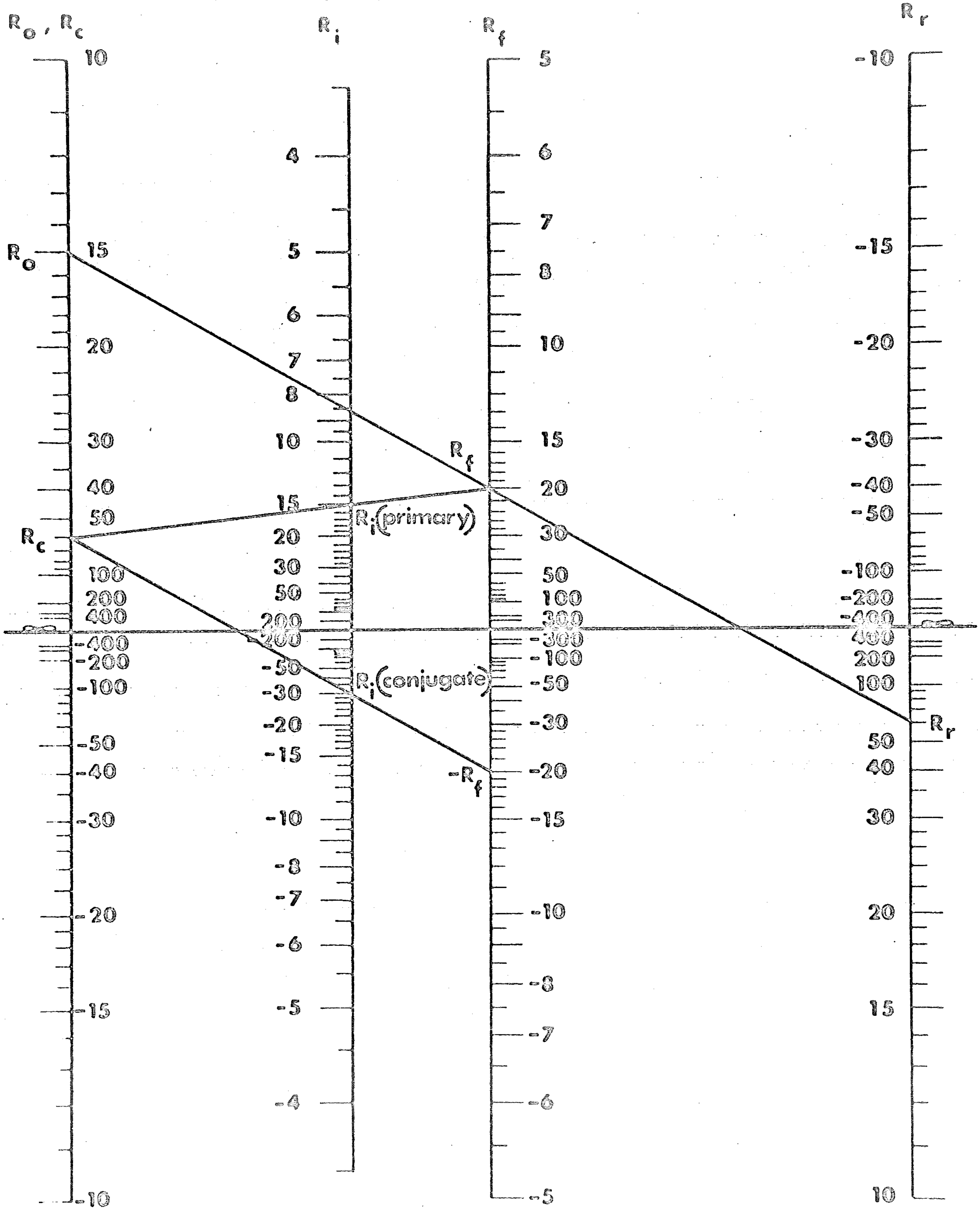

Fig. 4
Solution for Example 1.
Units are arbitrary.

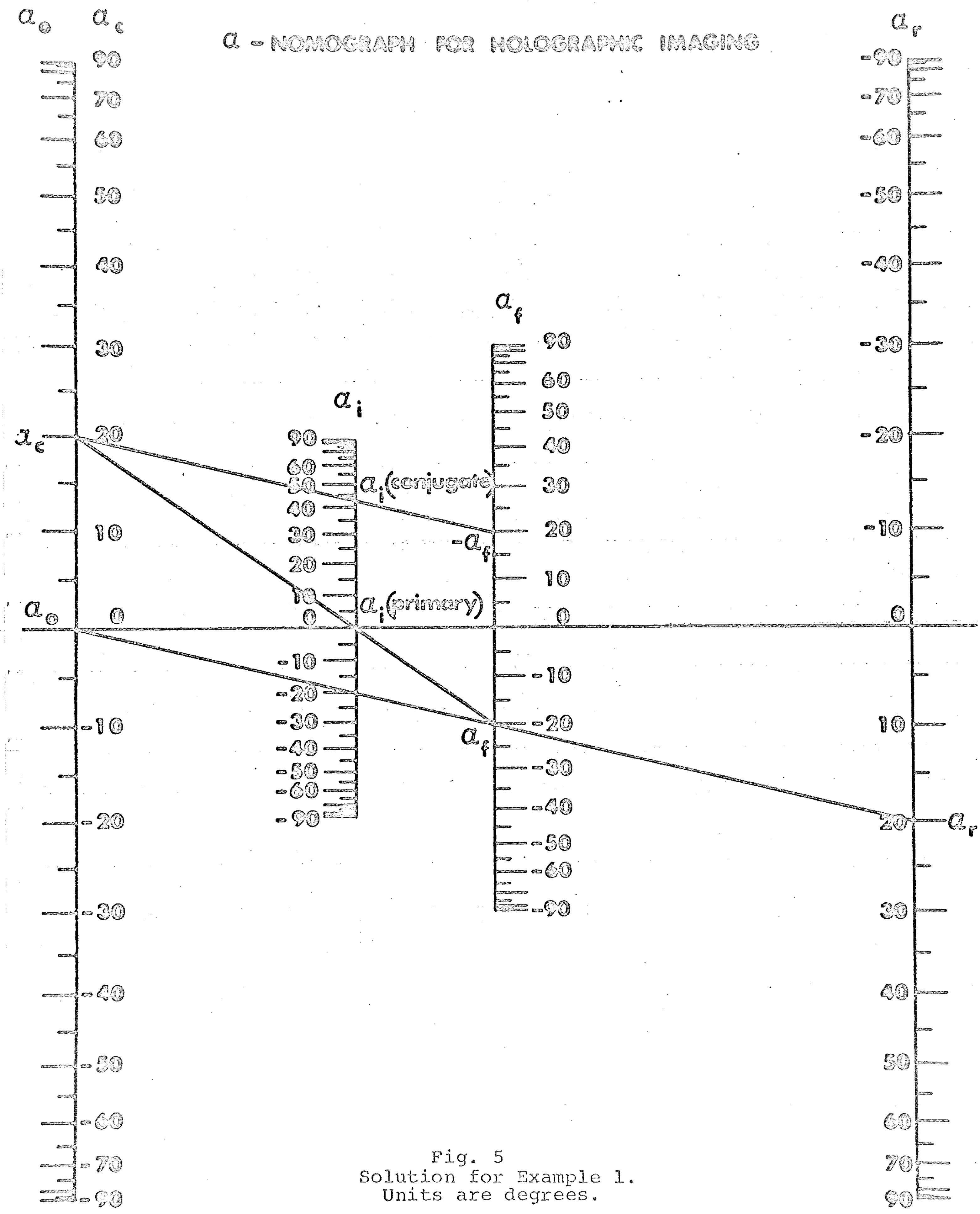

Fig. 5
Solution for Example 1.
Units are degrees.

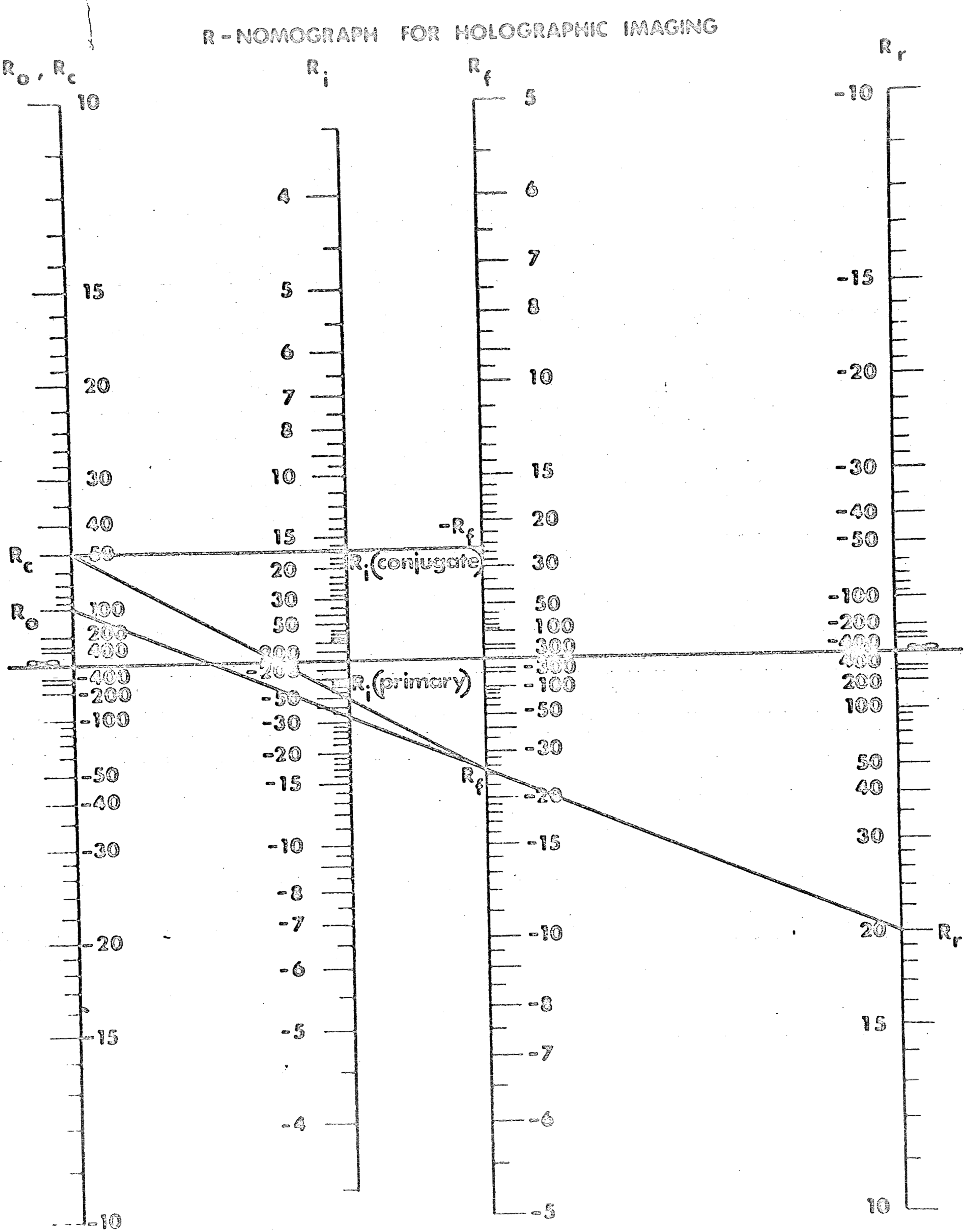

Fig. 6
Solution for Example 2.

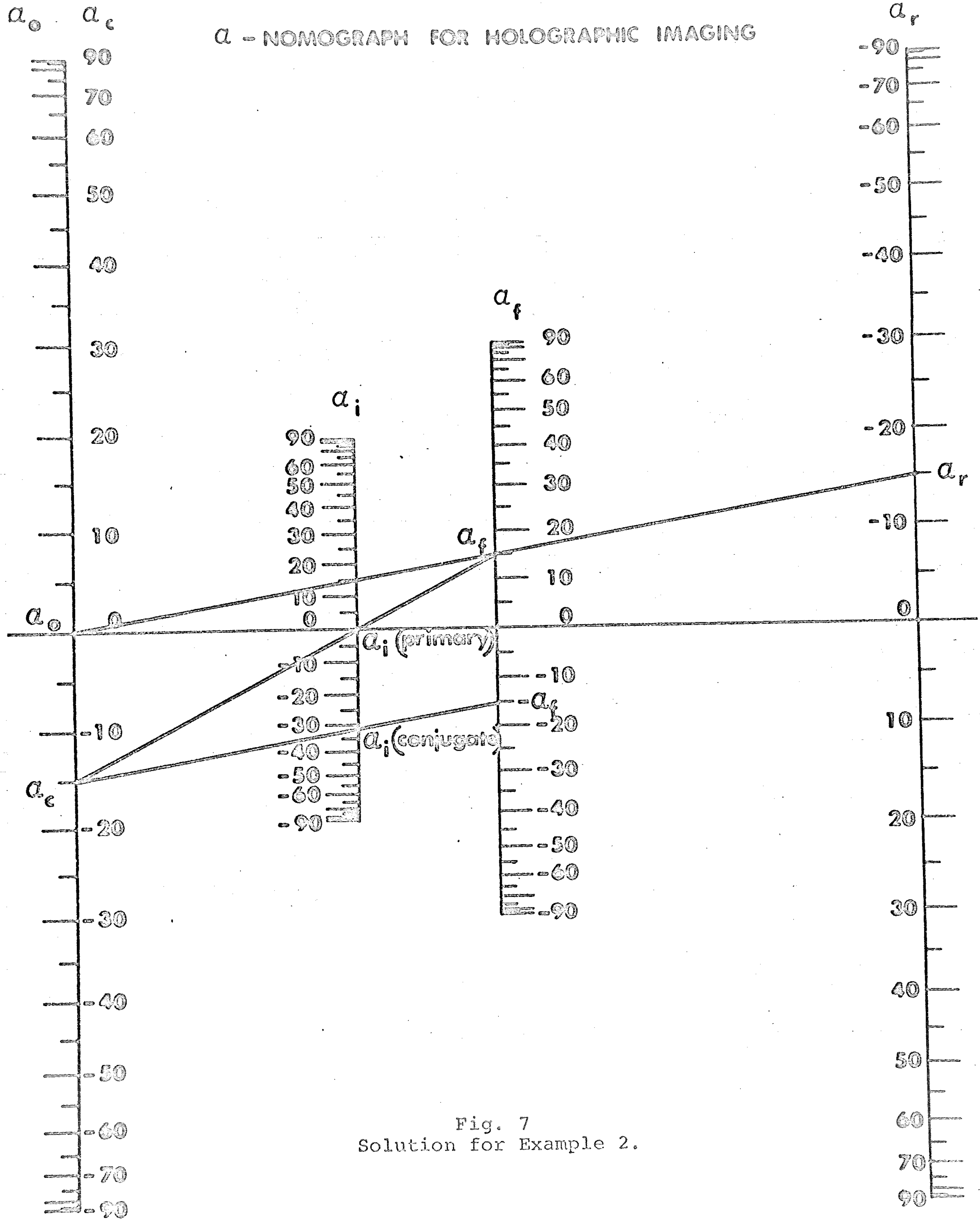

Fig. 7
Solution for Example 2.

R-NOMOGRAPH FOR HOLOGRAPHIC IMAGING

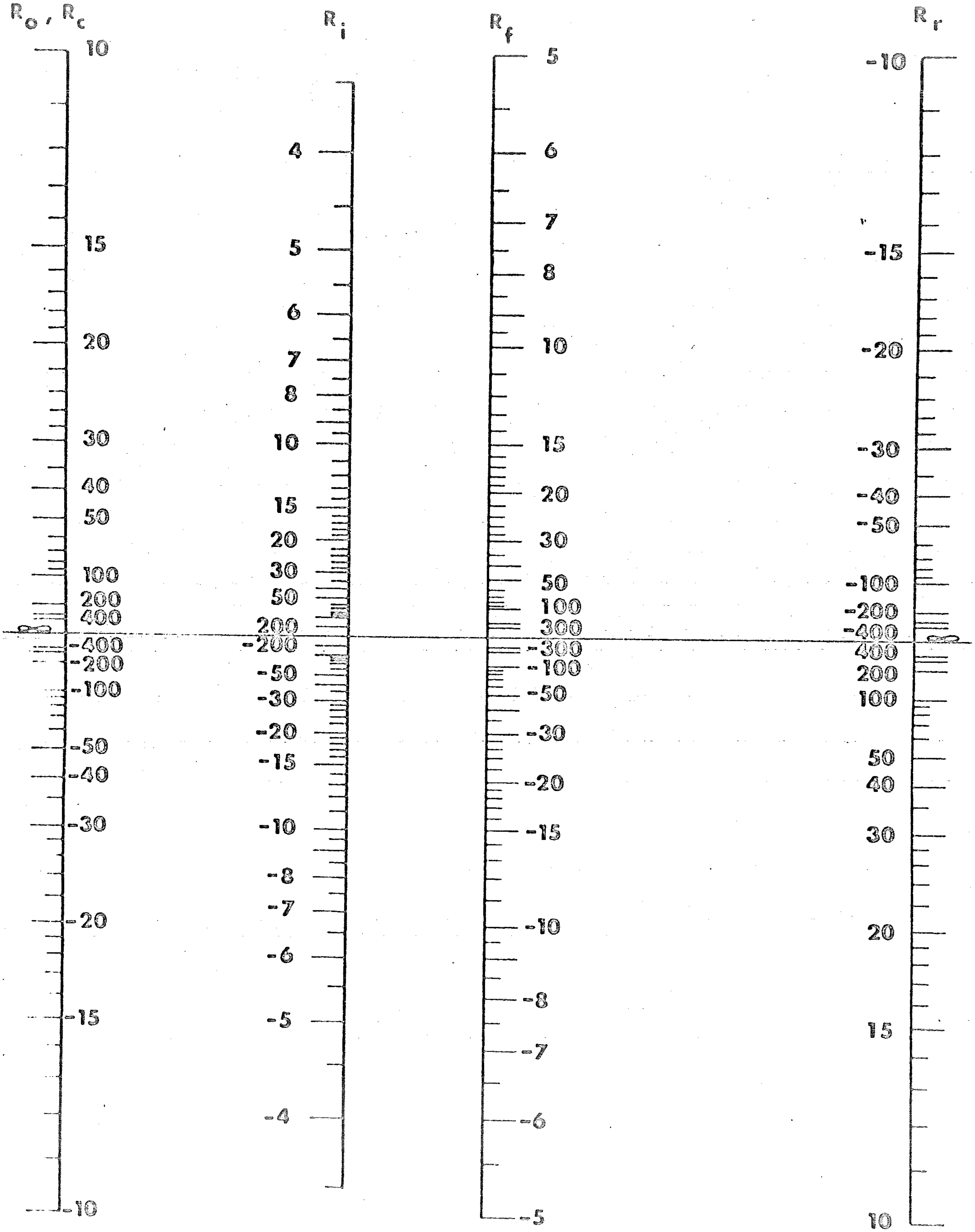

α - NOMOGRAPH FOR HOLOGRAPHIC IMAGING

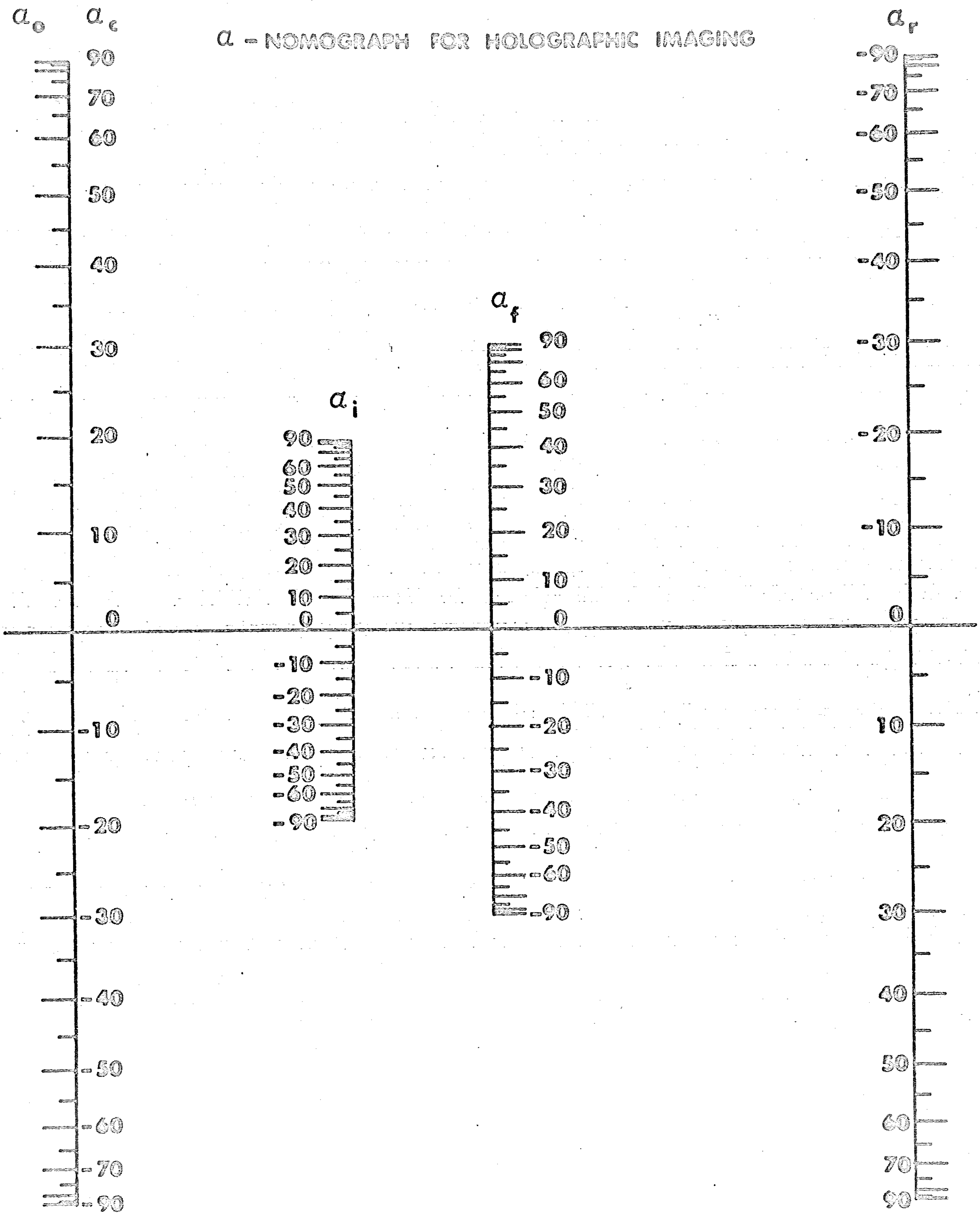

APPENDIX 3

HOLOGRAPHIC CORRELATION -- THEORY AND EXPERIMENTS

by

Richard E. Haskell

Coherent Optics Laboratory
Technical Report No. 70-2, June, 1970

This work was supported in part by
NASA under Grant NGR 23-054-033.

School of Engineering
Oakland University
Rochester, Michigan 48063

HOLOGRAPHIC CORRELATION -- THEORY AND EXPERIMENTS

Optical data processing and spatial filtering techniques have been used in a variety of applications.[1] An historical review of spatial filtering and optical information processing has been given by Goodman.[2] Vander Lugt[3] has shown how complex spatial filters can be made holographically. When a Vander Lugt filter is used the cross-correlation (or autocorrelation) is displayed in one region of the output plane and the convolution is displayed in another region of the output plane.

Most of the applications of the Vander Lugt filter have involved identification systems. For example, a filter of a fingerprint is made and when used in the optical processing system will produce an autocorrelation signal in the output plane when "matched" with the same fingerprint. Since the autocorrelation signal is much stronger than any cross-correlation signal the system can identify a given fingerprint. This application is typical of the binary nature of these types of identification systems. That is, one simply wants to know if an unknown signal is a specific one or not.

In this report the extent to which actual measurements of the entire cross-correlation (or autocorrelation) and convolution patterns can be made is examined. Such measurements may prove useful in helping to recognize unknown spatial patterns.

The technique consists essentially of making a Vander Lugt filter. A schematic of the optical system used for the experiments described below is shown in Figure 1. A detailed analysis of this system is given in the appendix. The operation of the system is as follows. A laser beam is passed through a microscope objective and pinhole located at P_1. This point source of coherent light is imaged by lens 1 onto the p-q plane. A spatial signal $\underset{\sim}{g}_1(x,y)$ is inserted in the x-y plane. The resulting diffraction pattern in the p-q plane is proportional to the Fourier transform $\underset{\sim}{G}_1(f_x,f_y)$ of the spatial signal $\underset{\sim}{g}_1(x,y)$ where f_x and f_y are spatial frequencies and are related to the coordinates p and q by $f_x = p/\lambda d_3$ and $f_y = q/\lambda d_3$, where λ is the wavelength of the light.

A reference beam is introduced from a point source P_2 located at coordinates $(x_r,0)$ in the x-y plane. A photographic plate is inserted in the p-q plane and a holographic recording is made. The developed hologram has a grating-like structure in those areas where the two beams interfere; that is, in the regions corresponding to the Fourier transform of $\underset{\sim}{g}_1(x,y)$.

The processed hologram is reinserted in the p-q plane and the reference beam is removed. If the same signal $\underset{\sim}{g}_1(x,y)$ is kept in the x-y plane, the same Fourier transform distribution of light will appear in the p-q plane. Since all of this area has a grating-like structure due to the holographic recording, the light will be diffracted as in a diffraction grating. One of the first-order diffraction components essentially reconstructs the reference beam. Lens 2 images the x-y plane onto the r-s plane. This means that point P_2 is imaged at a point along the negative r axis. The reconstructed reference beam therefore tends to become a focus at that point. However, as shown in the appendix, the light distribution at this point is proportional to the autocorrelation of $\underset{\sim}{g}_1(x,y)$.

If after the processed hologram is reinserted in the p-q plane, a second signal $\underset{\sim}{g}_2(x,y)$ is placed in the x-y plane its Fourier transform will be different from that of $\underset{\sim}{g}_1(x,y)$. Only that part of its transform which is the same as that of $\underset{\sim}{g}_1(x,y)$ will result in diffracted light which falls on the grating-like structure of the hologram in the p-q plane. It is shown in the appendix that where an autocorrelation appeared in the r-s plane previously, the light distribution in this case is proportional to the cross-correlation of the two signals $\underset{\sim}{g}_1(x,y)$ and $\underset{\sim}{g}_2(x,y)$. It is also shown in the appendix that the other first-order diffraction component is imaged along the positive r-axis and is proportional to the convolution of $\underset{\sim}{g}_1(x,y)$ and $\underset{\sim}{g}_2(x,y)$.

Experimental Results

A non-symmetrical 3-slit pattern shown schematically at the top of Fig. 2 was used to make a Vander Lugt filter in the optical system of Fig. 1. Fig. 2 shows the predicted form of the autocorrelation function $\phi_{gg}(x)$ and the convolution $g(x) * g(x)$. The slit pattern is actually two-dimensional with the y-variation being simply a wide single slit. The autocorrelation (or convolution) of such a single slit is just a triangular function whose width is twice the width of the slit. The output images recorded along the -r and +r axes in Fig. 1 are shown in Fig. 3. These images are recognized as good representations of the autocorrelation function $\phi_{gg}(x)$ and the convolution $g(x) * g(x)$ shown in Fig. 2.

As a second experiment, with the same holographic filter in place a different two-slit signal h(x) shown in Fig. 4 was inserted in the input x-y plane of Fig. 1. The predicted cross-correlation $\phi_{gh}(x)$ and convolution $g(x) * h(x)$ are shown in Fig. 4. The two diffracted images measured in the output plane are shown in Fig. 5 and are again seen to be good representations of the cross-correlation and convolution of the two signals.

A number of other experiments have been performed including autocorrelation measurements of random patterns. Such measurements may prove useful in determining the statistical nature of various random spatial signals. As real time holographic recording techniques are perfected such real-time correlation measurements could find wide applications.

ACKNOWLEDGMENT

The experiments described in this report were performed by Y.Y. Hung and J. Moran.

APPENDIX

Analysis of Holographic Correlator

A wave analysis of an optical system can be carried out by determining the complex amplitude of the wave $\underset{\sim}{U}(x,y)$ at any plane perpendicular to the optical axis. If $\underset{\sim}{U}'(x_1,y_1)$ is the complex amplitude of the wave at plane $z = 0$ then the complex amplitude $\underset{\sim}{U}(x_o,y_o)$ at a parallel plane a distance z away is given by the Huygen-Fresnel principle[2,4] as shown in Figure 6. Referring to Figure 6 one sees that the effect of traveling a distance d in free space is to change $\underset{\sim}{U}'(x_1,y_1)$ to $\underset{\sim}{U}(x_o,y_o)$ through the relation

$$\underset{\sim}{U}(x_o,y_o) = \underset{\sim}{K}\iint_{-\infty}^{\infty}\underset{\sim}{U}'(x_1,y_1)e^{j\frac{k}{2d}[(x_o-x_1)^2 + (y_o-y_1)^2]}\,dx_1dy_1 \qquad (1)$$

where $\underset{\sim}{K}$ is a complex constant and $\underset{\sim}{U}'(x_1,y_1)$ is assumed to be zero outside the aperture. The result for light from a point source traveling a distance d is found by letting $\underset{\sim}{U}'(x_1,y_1) = \delta(x_1,y_1)$ in (1) from which

$$\underset{\sim}{U}_d(x_o,y_o) = \underset{\sim}{K}\,e^{j\frac{k}{2d}(x_o{}^2+y_o{}^2)} \qquad (2)$$

The effect of a thin lens is to multiply the amplitude function $\underset{\sim}{U}(x,y)$ that enters the lens by some complex amplitude $\underset{\sim}{\psi}(x,y)$. To determine $\underset{\sim}{\psi}(x,y)$ recognize that light from a point source which enters a lens after traveling a distance f equal to the focal length will emerge from the lens as a plane wave.

That is

$$\underset{\sim}{U}_f(x,y)\ \underset{\sim}{\psi}(x,y) = \text{constant}$$

and thus from (2) it follows that

$$\underset{\sim}{\psi}(x,y) = e^{-j \frac{k}{2f} (x^2 + y^2)} \tag{3}$$

represents the effect of a lens.

Fourier transform of $\underset{\sim}{g}(x,y)$

Consider first only that portion of Figure 1 that is shown in Figure 7 and let $\underset{\sim}{U}_\ell(u,v)$ be the light amplitude just to the left of the lens. From (2), $\underset{\sim}{U}_\ell(u,v)$ is given by

$$\underset{\sim}{U}_\ell(u,v) = \underset{\sim}{K}_1\ e^{j\frac{k}{2d_1} (u^2 + v^2)} \tag{4}$$

The effect of the lens is to multiply (4) by $\underset{\sim}{\psi}(u,v)$ from (3). Thus, if $\underset{\sim}{U}_\ell'(u,v)$ is the light amplitude just to the right of the lens then

$$\underset{\sim}{U}_\ell'(u,v) = \underset{\sim}{U}_\ell(u,v)\ \underset{\sim}{\psi}(u,v) \tag{5}$$

The focal length f_1 of lens 1 is related to d_1 and D_1 by the lens formula

$$\frac{1}{f_1} = \frac{1}{d_1} + \frac{1}{D_1} \tag{6}$$

Substituting (3) and (4) into (5) and using (6) one can write

$$\underset{\sim}{U}_{\ell}'(u,v) = K_1 e^{-j\frac{k}{2D_1}(u^2+v^2)} \tag{7}$$

Let $\underset{\sim}{U}_o(x,y)$ be the light amplitude just to the left of the signal film $\underset{\sim}{g}(x,y)$ and let $\underset{\sim}{U}_o'(x,y)$ be the light amplitude just to the right of the film. Eq. (1) can be used to find $\underset{\sim}{U}_o(x,y)$ in terms of $\underset{\sim}{U}_{\ell}'(u,v)$. Thus

$$\underset{\sim}{U}_o(x,y) = \underset{\sim}{K}_2 \iint_{-\infty}^{\infty} \underset{\sim}{U}_{\ell}'(u,v)\, e^{j\frac{k}{2d_2}[(x-u)^2+(y-v)^2]}\, dudv \tag{8}$$

To the right of the film $\underset{\sim}{U}_o'(x,y)$ is given by

$$\underset{\sim}{U}_o'(x,y) = \underset{\sim}{U}_o(x,y)\, \underset{\sim}{g}(x,y) \tag{9}$$

Let $\underset{\sim}{U}_t(p,q)$ be the light amplitude at the p-q plane and use (1) again to write

$$\underset{\sim}{U}_t(p,q) = \underset{\sim}{K}_3 \iint_{-\infty}^{\infty} \underset{\sim}{U}_o'(x,y)\, e^{j\frac{k}{2d_3}[(p-x)^2+(q-y)^2]}\, dxdy \tag{10}$$

Combining (7) - (10), $\underset{\sim}{U}_t(p,q)$ can be written as

$$\underset{\sim}{U}_t(p,q) = \underset{\sim}{K}_4 \iiiint_{-\infty}^{\infty} \underset{\sim}{g}(x,y)\, e^{j\frac{k}{2}\rho}\, dudvdxdy \tag{11}$$

where

$$\rho = -\frac{u^2 + v^2}{D_1} + \frac{x^2 + y^2 + u^2 + v^2 - 2xu - 2yv}{d_2}$$

$$+ \frac{p^2 + q^2 + x^2 + y^2 - 2px - 2qy}{d_3} \tag{12}$$

It is first necessary to do the integration over u and v. To this end let the parts of ρ containing u and v be represented by ρ_u and ρ_v respectively. Thus,

$$\rho_u = u^2 \left(-\frac{1}{D_1} + \frac{1}{d_2}\right) - 2u \left(\frac{x}{d_2}\right)$$

$$\rho_v = v^2 \left(-\frac{1}{D_1} + \frac{1}{d_2}\right) - 2v \left(\frac{y}{d_2}\right) \tag{13}$$

Since

$$\int_{-\infty}^{\infty} e^{jC_1(u-C_2)^2} du = C_3 \int_{-\infty}^{\infty} e^{j\frac{\pi}{2}\zeta^2} d\zeta = \text{constant}$$

it is desirable to complete the squares in (13) and write

$$\rho_u = \frac{d_3}{d_2 D_1} \left(u - \frac{xD_1}{d_3}\right)^2 - x^2 \frac{D_1}{d_2 d_3} = \rho_u' - x^2 \frac{D_1}{d_2 d_3}$$

$$\rho_v = \frac{d_3}{d_2 D_1} \left(v - \frac{yD_1}{d_3}\right)^2 - y^2 \frac{D_1}{d_2 d_3} = \rho_v' - y^2 \frac{D_1}{d_2 d_3} \tag{14}$$

where the fact that $D_1 = d_2 + d_3$ has been used. Collecting (14) and the remaining terms in (12) one can write

$$\rho = \rho_u' + \rho_v' + \left(\frac{1}{d_2} + \frac{1}{d_3} - \frac{D_1}{d_2 d_3}\right)(x^2 + y^2)$$

$$+ \frac{p^2 + q^2}{d_3} - \frac{2}{d_3}(px + qy) \tag{15}$$

The terms ρ_u' and ρ_v' give a constant when integrated over u and v. The coefficient of $(x^2 + y^2)$ in (15) is identically zero. Thus, Eq. (11) can be written as

$$\underset{\sim}{U}_t(p,q) = \underset{\sim}{K}_t \, e^{j \frac{k}{2d_3}(p^2+q^2)} \iint_{-\infty}^{\infty} \underset{\sim}{g}(x,y) \, e^{-j \frac{k}{d_3}(px + qy)} \, dxdy \tag{16}$$

Since $k = 2\pi/\lambda$ where λ is the wavelength of the light, (16) can be rewritten as

$$\underset{\sim}{U}_t(p,q) = \underset{\sim}{K}_t \, e^{j\frac{k}{2d_3}(p^2 + q^2)} \, \underset{\sim}{G}(f_x, f_y) \tag{17}$$

where

$$\underset{\sim}{G}(f_x, f_y) = \iint_{-\infty}^{\infty} \underset{\sim}{g}(x,y) \, e^{-j2\pi(f_x x + f_y y)} \, dxdy \tag{18}$$

is the Fourier transform of $\underset{\sim}{g}(x,y)$ and

$$f_x = \frac{p}{\lambda d_3}$$

$$f_y = \frac{q}{\lambda d_3} \tag{19}$$

are the spatial frequencies. Eq. (17) shows that to within a quadratic phase factor $\underset{\sim}{U}_t(p,q)$ is proportional to the two-dimensional Fourier transform of the spatial signal $\underset{\sim}{g}(x,y)$.

Holographic Recording

The point source at P_2 can be represented by the delta function $\delta(x-x_r, y)$. Thus, using Eq. (1) the light amplitude of the reference beam in the p-q plane due to this point source is given by

$$\underset{\sim}{U}_r(p,q) = \underset{\sim}{K}_r \iint_{-\infty}^{\infty} \delta(x-x_r,y)\, e^{j\frac{k}{2d_3}[(p-x)^2+(q-y)^2]}\, dxdy$$

$$= \underset{\sim}{K}_r\, e^{j\frac{k}{2d_3}[(p-x_r)^2+q^2]}$$

$$= \underset{\sim}{K}_r\, e^{j\frac{kx_r^2}{2d_3}}\, e^{j\frac{k}{2d_3}(p^2+q^2)}\, e^{-j\frac{kpx_r}{d_3}} \tag{20}$$

In deriving (20) it is assumed that x_r is small enough so that the paraxial approximation used in obtaining Eq. (1) is valid. The constant phase factor $e^{jkx_r^2/2d_3}$ in (20) is of no importance and will be dropped for convenience. By introducing the spatial frequency f_x from (19) one can write (20) in the form

$$\underset{\sim}{U}_r(p,q) = \underset{\sim}{K}_r\, e^{j\frac{k}{2d_3}(p^2+q^2)}\, e^{-j2\pi x_r f_x} \tag{21}$$

The total light field at the p-q plane is the sum of the fields $\underset{\sim}{U}_t(p,q)$ from (17) and $\underset{\sim}{U}_r(p,q)$ from (21). A photographic plate is inserted in the p-q plane and records the intensity of this total field. The intensity is given by

$$I = |\underset{\sim}{U}_t + \underset{\sim}{U}_r|^2 = |\underset{\sim}{U}_t|^2 + |\underset{\sim}{U}_r|^2 + \underset{\sim}{U}_t\underset{\sim}{U}_r^* + \underset{\sim}{U}_t^*\underset{\sim}{U}_r \tag{22}$$

It is assumed that the amplitude transmittance of the resulting hologram is proportional (with a negative sign) to the exposure which in turn is proportional to the intensity (22). Thus, absorbing these proportionality constants in the other constants a filter function $\underset{\sim}{H}(f_x,f_y)$ representing the amplitude transmittance of the hologram in the p-q plane [frequence plane; see (19)] can be written using (17), (21) and (22) in the form

$$\begin{aligned}\underset{\sim}{H}(f_x,f_y) \;=\; & |\underset{\sim}{K}_t|^2\,|\underset{\sim}{G}_1|^2 + |\underset{\sim}{K}_r|^2 \\ & + \underset{\sim}{K}_t\underset{\sim}{K}_r^*\,\underset{\sim}{G}_1(f_x,f_y)\,e^{j2\pi x_r f_x} \\ & + \underset{\sim}{K}_t^*\underset{\sim}{K}_r\underset{\sim}{G}_1^*(f_x,f_y)\,e^{-j2\pi x_r f_x}\end{aligned} \tag{23}$$

where the signal used in making the filter $\underset{\sim}{H}(f_x,f_y)$ has been designated as $\underset{\sim}{g}_1(x,y)$ with a Fourier transform $\underset{\sim}{G}_1(f_x,f_y)$.

Reconstruction

In the reconstruction process let $\underset{\sim}{g}_1(x,y)$ be replaced by a second signal $\underset{\sim}{g}_2(x,y)$ whose Fourier transform is $\underset{\sim}{G}_2(f_x,f_y)$. Figure 8 shows that part of Figure 1 that is relevant to the reconstruction process. In this case the reference beam is removed so that the total field $\underset{\sim}{U}_t(p,q)$ is proportional to

$\underset{\sim}{G}_2(f_x, f_y)$ according to (17). Thus

$$\underset{\sim}{U}_c(p,q) = \underset{\sim}{K}_c \, e^{j \frac{k}{2d_3} (p^2 + q^2)} \underset{\sim}{G}_2(f_x, f_y) \tag{24}$$

The hologram in the p-q plane has an amplitude transmittance $\underset{\sim}{H}(f_x, f_y)$ given by (23) where f_x and f_y are related to p and q by (19). Thus to the right of the p-q plane $\underset{\sim}{U}_c'(p,q)$ is given by

$$\underset{\sim}{U}_c'(p,q) = \underset{\sim}{U}_c(p,q) \, \underset{\sim}{H}(f_x, f_y) \tag{25}$$

Eq. (25) can be combined with (23) and (24) and written as

$$\underset{\sim}{U}_c'(p,q) = \underset{\sim}{K}_c \, e^{j \frac{k}{2d_3} (p^2 + q^2)} \underset{\sim}{T}(f_x, f_y) \tag{26}$$

where

$$\underset{\sim}{T}(f_x, f_y) = \underset{\sim}{T}_o(f_x, f_y) + \underset{\sim}{T}_+(f_x, f_y) + \underset{\sim}{T}_-(f_x, f_y) \tag{27}$$

and

$$\underset{\sim}{T}_o(f_x, f_y) = |\underset{\sim}{K}_t|^2 \, |\underset{\sim}{G}_1|^2 \, \underset{\sim}{G}_2 + |\underset{\sim}{K}_r|^2 \, \underset{\sim}{G}_2 \tag{28}$$

$$\underset{\sim}{T}_+(f_x, f_y) = \underset{\sim}{K}_t \underset{\sim}{K}_r^* \, \underset{\sim}{G}_1(f_x, f_y) \, \underset{\sim}{G}_2(f_x, f_y) \, e^{j2\pi x_r f_x} \tag{29}$$

$$\underset{\sim}{T}_-(f_x, f_y) = \underset{\sim}{K}_t^* \underset{\sim}{K}_r \, \underset{\sim}{G}_1^*(f_x, f_y) \, \underset{\sim}{G}_2(f_x, f_y) \, e^{-j2\pi x_r f_x} \tag{30}$$

Referring to Figure 8, Eq. (1) can be used to write the field to the left of the lens $\underset{\sim}{U}_m(\tilde{u},\tilde{v})$ as

$$\underset{\sim}{U}_m(\tilde{u},\tilde{v}) = \underset{\sim}{K}_5 \iint_{-\infty}^{\infty} \underset{\sim}{U}_c'(p,q)\, e^{j\frac{k}{2d_4}[(\tilde{u}-p)^2 + (\tilde{v}-q)^2]}\, dpdq \qquad (31)$$

Substituting (26) into (31) and making the change of variables given by (19) one can write (31) in the form

$$\underset{\sim}{U}_m(\tilde{u},\tilde{v}) = \underset{\sim}{K}_6 \iint_{-\infty}^{\infty} e^{j\frac{k\lambda^2 d_3}{2}(f_x{}^2+f_y{}^2)}\, \underset{\sim}{T}(f_x,f_y)\, e^{j\frac{k}{2d_4}[(\tilde{u}-\lambda d_3 f_x)^2+(\tilde{v}-\lambda d_3 f_y)^2]}\, df_x df_y \qquad (32)$$

If f_2 is the focal length of lens 2 then from (3) the field $\underset{\sim}{U}_m'(\tilde{u},\tilde{v})$ to the right of lens 2 is given by

$$\underset{\sim}{U}_m'(\tilde{u},\tilde{v}) = \underset{\sim}{U}_m(\tilde{u},\tilde{v})\, e^{-j\frac{k}{2f_2}(\tilde{u}^2 + \tilde{v}^2)} \qquad (33)$$

Finally, using (1) the field $\underset{\sim}{U}_i(r,s)$ in the r-s image plane is given by

$$\underset{\sim}{U}_i(r,s) = \underset{\sim}{K}_7 \iint_{-\infty}^{\infty} \underset{\sim}{U}_m'(\tilde{u},\tilde{v})\, e^{j\frac{k}{2d_5}[(r-\tilde{u})^2 + (s-\tilde{v})^2]}\, d\tilde{u}d\tilde{v} \qquad (34)$$

Combining (32), (33) and (34) the field $\underset{\sim}{U}_i(r,s)$ can be written as

$$\underset{\sim}{U}_i(r,s) = \underset{\sim}{K}_8 \iiiint_{-\infty}^{\infty} \underset{\sim}{T}(f_x,f_y)\, e^{j\frac{k}{2}\mu}\, d\tilde{u}d\tilde{v}df_x df_y \qquad (35)$$

where

$$\mu = \mu_{\tilde{u}} + \mu_{\tilde{v}} + \lambda^2 d_3{}^2 \left(\frac{1}{d_3} + \frac{1}{d_4}\right) \left(f_x{}^2 + f_y{}^2\right) + \frac{r^2+s^2}{d_5} \tag{36}$$

and

$$\mu_{\tilde{u}} = \tilde{u}^2 \left(\frac{1}{d_4} - \frac{1}{f_2} + \frac{1}{d_5}\right) - 2\tilde{u}\left(\frac{\lambda d_3 f_x}{d_4} + \frac{r}{d_5}\right) \tag{37}$$

$$\mu_{\tilde{v}} = \tilde{v}^2 \left(\frac{1}{d_4} - \frac{1}{f_2} + \frac{1}{d_5}\right) - 2\tilde{v}\left(\frac{\lambda d_3 f_y}{d_4} + \frac{s}{d_5}\right) \tag{38}$$

In order to do the integration over $\tilde{u}$ and $\tilde{v}$ in (35) it is necessary to complete the squares in (37) and (38) as was done in (13). If this is done and use is made of the lens formula

$$\frac{1}{f_2} = \frac{1}{D_2} + \frac{1}{d_5} \tag{39}$$

then (37) and (38) can be written in the form

$$\mu_{\tilde{u}} = \mu_{\tilde{u}}' - \left(\frac{\lambda d_3 f_x}{d_4} + \frac{r}{d_5}\right)^2 \frac{d_4 D_2}{d_3} \tag{40}$$

and

$$\mu_{\tilde{v}} = \mu_{\tilde{v}}' - \left(\frac{\lambda d_3 f_y}{d_4} + \frac{s}{d_5}\right)^2 \frac{d_4 D_2}{d_3} \tag{41}$$

where

$$\mu_{\tilde{u}}' = \frac{d_3}{d_4 D_2}\left[\tilde{u} - \left(\frac{\lambda d_3 f_x}{d_4} + \frac{r}{d_5}\right)\frac{d_4 D_2}{d_3}\right]^2 \tag{42}$$

and

$$\mu_{\tilde{v}}' = \frac{d_3}{d_4 D_2}\left[\tilde{v} - \left(\frac{\lambda d_3 f_y}{d_4} + \frac{s}{d_5}\right)\frac{d_4 D_2}{d_3}\right]^2 \tag{43}$$

Substituting (40) and (41) into (36) one obtains

$$\mu = \mu_{\tilde{u}}' + \mu_{\tilde{v}}' + \lambda^2 d_3{}^2\left(\frac{1}{d_3} + \frac{1}{d_4} - \frac{D_2}{d_3 d_4}\right)\left(f_x{}^2 + f_y{}^2\right)$$

$$+ (r^2 + s^2)\left(\frac{1}{d_5} - \frac{d_4 D_2}{d_5{}^2 d_3}\right) - \frac{D_2 2\lambda}{d_5}\,(f_x r + f_y s) \tag{44}$$

The terms $\mu_{\tilde{u}}'$ and $\mu_{\tilde{v}}'$ give a constant when integrated over $\tilde{u}$ and $\tilde{v}$ in (35). The coefficient of $(f_x{}^2 + f_y{}^2)$ in (44) is identically zero. Thus, Eq. (35) can be written as

$$\underset{\sim}{U}_i(r,s) = \underset{\sim}{K}_i\, e^{j\frac{k}{2d_5}\left(1-\frac{d_4 D_2}{d_5 d_3}\right)(r^2+s^2)} \iint_{-\infty}^{\infty} \underset{\sim}{T}(f_x,f_y)\, e^{-j\frac{kD_2\lambda}{d_5}(f_x r+f_y s)}\, df_x df_y \tag{45}$$

If one introduces the reduced coordinates

$$r' = -\frac{r}{M}$$

$$s' = -\frac{s}{M} \tag{46}$$

where

$$M = \frac{d_5}{D_2} \tag{47}$$

is the magnification between the x-y and r-s planes, then (45) can be written as

$$\underset{\sim}{U}_i(r',s') = \underset{\sim}{K}_i\, e^{j\frac{kM}{2D_2}\left(1-\frac{d_4}{Md_3}\right)(r'^2+s'^2)} \iint_{-\infty}^{\infty} \underset{\sim}{T}(f_x,f_y)\, e^{j2\pi(f_x r'+f_y s')}\, df_x df_y \tag{48}$$

Thus, to within a quadratic phase factor $\underset{\sim}{U}_i(r',s')$ is proportional to the inverse Fourier transform of $\underset{\sim}{T}(f_x,f_y)$. That is, if $\underset{\sim}{T}(f_x,f_y)$ is the Fourier transform of $\underset{\sim}{t}(r',s')$ then

$$\underset{\sim}{U}_i(r',s') = \underset{\sim}{K}_i\, e^{j\frac{kM}{2D_2}\left(1-\frac{d_4}{Md_3}\right)(r'^2+s'^2)}\, \underset{\sim}{t}(r',s') \tag{49}$$

Since $\underset{\sim}{T}(f_x,f_y)$ is made up of three parts as indicated in Eqs. (27)-(30), then $\underset{\sim}{t}(r',s')$ will also be made up of three corresponding parts $\underset{\sim}{t}_o$, $\underset{\sim}{t}_+$ and $\underset{\sim}{t}_-$. The $\underset{\sim}{t}_o$ term is the inverse transform of $\underset{\sim}{T}_o$ and is displayed at the origin of the r-s plane. It has no particular significance or usefulness. The other two terms, however, are useful and are separated in space in the r-s plane. They will each be considered separately below.

Convolution Measurement

Consider first the term $\underset{\sim}{T}_+(f_x,f_y)$ given by (29). In the image plane $\underset{\sim}{t}_+(r',s')$ is given by the inverse Fourier transform of (29). That is,

$$\underset{\sim}{t}_+(r',s') = \underset{\sim}{K}_t \underset{\sim}{K}_r^* \iint_{-\infty}^{\infty} \underset{\sim}{G}_1(f_x,f_y)\, \underset{\sim}{G}_2(f_x,f_y)\, e^{j2\pi x_r f_x}\, e^{j2\pi(f_x r'+f_y s')}\, df_x df_y \tag{50}$$

From the definitions of $\underset{\sim}{G}_1(f_x,f_y)$ and $\underset{\sim}{G}_2(f_x,f_y)$ Eq. (50) can be written as

$$\underset{\sim}{t}_+(r',s') = \underset{\sim}{K}_+ \iint_{-\infty}^{\infty} \iint_{-\infty}^{\infty} \underset{\sim}{g}_1(x_1,y_1)\, e^{-j2\pi(f_x x_1 + f_y y_1)}\, dx_1 dy_1$$

$$\cdot \iint_{-\infty}^{\infty} \underset{\sim}{g}_2(x_2,y_2)\, e^{-j2\pi(f_x x_2 + f_y y_2)}\, dx_2 dy_2\; e^{j2\pi x_r f_x}$$

$$\cdot\; e^{j2\pi(f_x r' + f_y s')}\, df_x df_y \tag{51}$$

Interchanging the order of integration and integrating one obtains

$$\underset{\sim}{t}_+(r',s') = \underset{\sim}{K}_+ \iint_{-\infty}^{\infty} \underset{\sim}{g}_1(x_1,y_1) \iint_{-\infty}^{\infty} \underset{\sim}{g}_2(x_2,y_2) \int_{-\infty}^{\infty} e^{-j2\pi f_x(x_1+x_2-x_r-r')}\, df_x \;\cdot$$

$$\cdot \int_{-\infty}^{\infty} e^{-j2\pi f_y(y_1+y_2-s')}\, df_y dx_2 dy_2 dx_1 dy_1$$

$$= \underset{\sim}{K}_+ \iint_{-\infty}^{\infty} \underset{\sim}{g}_1(x_1,y_1) \iint_{-\infty}^{\infty} \underset{\sim}{g}_2(x_2,y_2)\, \delta(x_1+x_2-x_r-r')\, \delta(y_1+y_2-s')\, dx_2 dy_2 dx_1 dy_1$$

$$= \underset{\sim}{K}_+ \iint_{-\infty}^{\infty} \underset{\sim}{g}_1(x_1,y_1)\; \underset{\sim}{g}_2(r'+x_r-x_1,\; s'-y_1)\, dx_1 dy_1 \tag{52}$$

Eq. (52) is a two-dimensional convolution integral centered at $r' = -x_r$, $s' = 0$. Thus, $\underset{\sim}{t}_+(r',s')$ can be written as

$$\underset{\sim}{t}_+(r',s') = \underset{\sim}{K}_+\; \underset{\sim}{g}_1(r'+x_r,s') * \underset{\sim}{g}_2(r'+x_r,s') \tag{53}$$

Since r',s' are reduced coordinates defined by (46) the convolution $\underset{\sim}{t}_+$ will be centered at the coordinates $r = Mx_r$, $s = 0$.

Correlation Measurement

Consider now the term $\underset{\sim}{T}_-(f_x,f_y)$ given by (30). In the image plane $\underset{\sim}{t}_-(r',s')$ is given by the inverse Fourier transform of (30). That is,

$$\underset{\sim}{t}_-(r',s') = \underset{\sim}{K}_t{}^*\underset{\sim}{K}_r \iint_{\infty}^{\infty} \underset{\sim}{G}_1{}^*(f_x,f_y)\,\underset{\sim}{G}_2(f_x,f_y)\,e^{-j2\pi x_r f_x}\,e^{j2\pi(f_x r'+f_y s')}\,df_x df_y$$

from which

$$\underset{\sim}{t}_-(r',s') = \underset{\sim}{K} \iint_{\infty}^{\infty} \iint_{\infty}^{\infty} \underset{\sim}{g}_1{}^*(x_1,y_1)\; e^{j2\pi(f_x x_1+f_y y_1)}\; dx_1 dy_1$$

$$\cdot \iint_{\infty}^{\infty} \underset{\sim}{g}_2(x_2,y_2)\,e^{-j2\pi(f_x x_2+f_y y_2)}\,dx_2 dy_2\,e^{-j2\pi x_r f_x}\,e^{j2\pi(f_x r'+f_y s')}\,df_x df_y \tag{54}$$

Interchanging the order of integration and integrating one obtains

$$\underset{\sim}{t}_-(r',s') = \underset{\sim}{K}_- \iint_{\infty}^{\infty} \underset{\sim}{g}_1{}^*(x_1,y_1) \iint_{\infty}^{\infty} \underset{\sim}{g}_2(x_2,y_2) \int_{\infty}^{\infty} e^{-j2\pi f_x(x_2-x_1+x_r-r')}\,df_x$$

$$\cdot \int_{\infty}^{\infty} e^{-j2\pi f_y(y_2-y_1-s')}\,df_y dx_2 dy_2 dx_1 dy_1$$

$$= \underset{\sim}{K}_- \iint_{\infty}^{\infty} \underset{\sim}{g}_1{}^*(x_1,y_1) \iint_{\infty}^{\infty} \underset{\sim}{g}_2(x_2,y_2)\,\delta(x_2-x_1+x_r-r')\,\delta(y_2-y_1-s')\,dx_2 dy_2 dx_1 dy_1$$

$$= \underset{\sim}{K}_- \iint_{\infty}^{\infty} \underset{\sim}{g}_1{}^*(x_1,y_1)\,\underset{\sim}{g}_2(x_1+r'-x_r,\; y_1+s')\;dx_1 dy_1 \tag{55}$$

Eq. (55) is the cross-correlation $\phi_{g_1^* g_2}$ of $\underset{\sim}{g}_1^*$ and $\underset{\sim}{g}_2$ centered at $r' = x_r$, $s' = 0$ or $r = -Mx_r$, $s = 0$. That is

$$\underset{\sim}{t}_-(r',s') = \underset{\sim}{K}_- \, \phi_{g_1^* g_2}(r'-x_r,s') \tag{56}$$

If $\underset{\sim}{g}_1$ and $\underset{\sim}{g}_2$ are the same real signal then $\underset{\sim}{t}_-(r',s')$ will record the autocorrelation function.

REFERENCES

1. Cutrona, L.J., et. al., IRE Trans. Inform. Theory, IT-6, 386 (1960).

2. Goodman, J.W., Introduction to Fourier Optics, McGraw-Hill Book Co., New York, 1968.

3. Vander Lugt, A.B., IEEE Trans. Inform. Theory, IT-10, 2 (1964).

4. Born, M., and E. Wolf, Principles of Optics, 2nd rev. ed., Pergamon Press, New York, 1964.

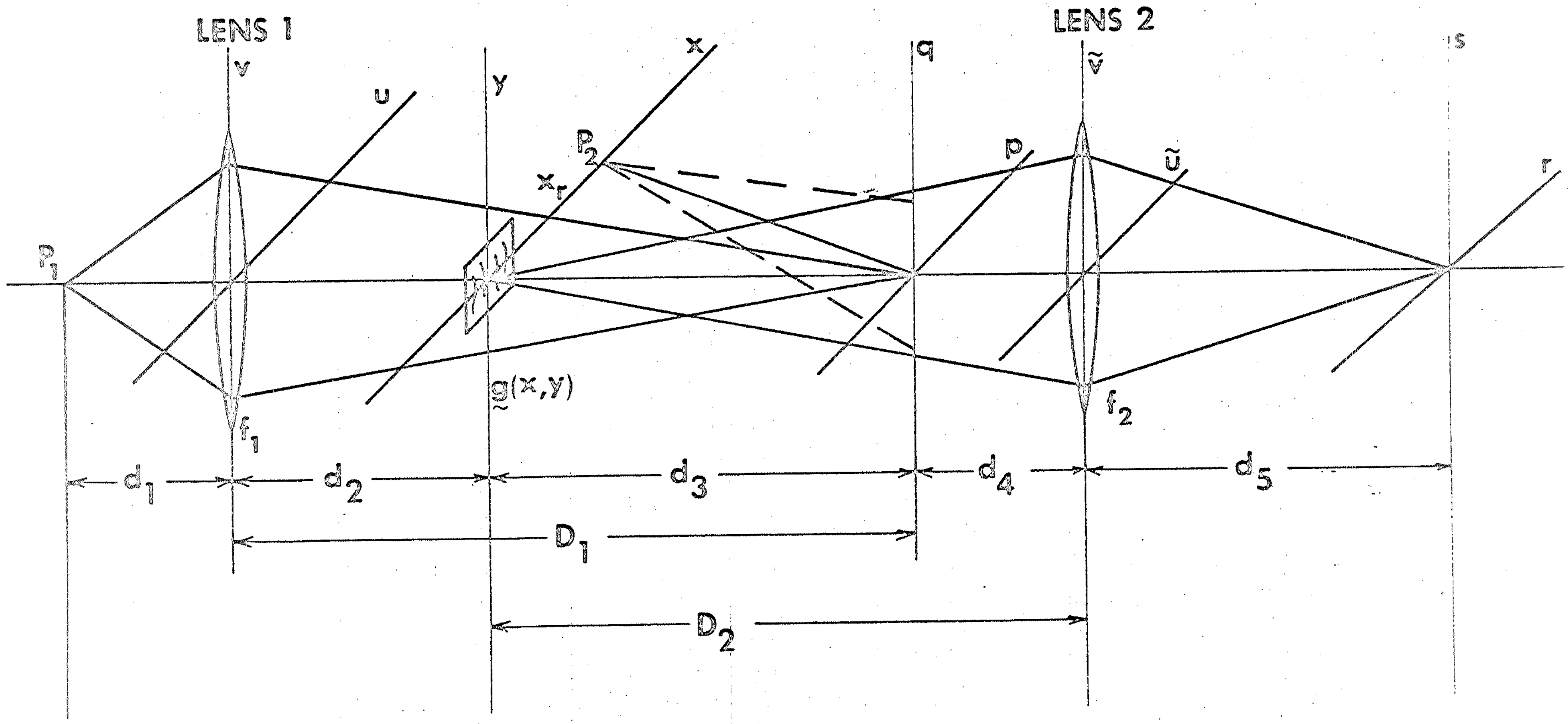

Fig. 1

Optical system used for holographic correlation

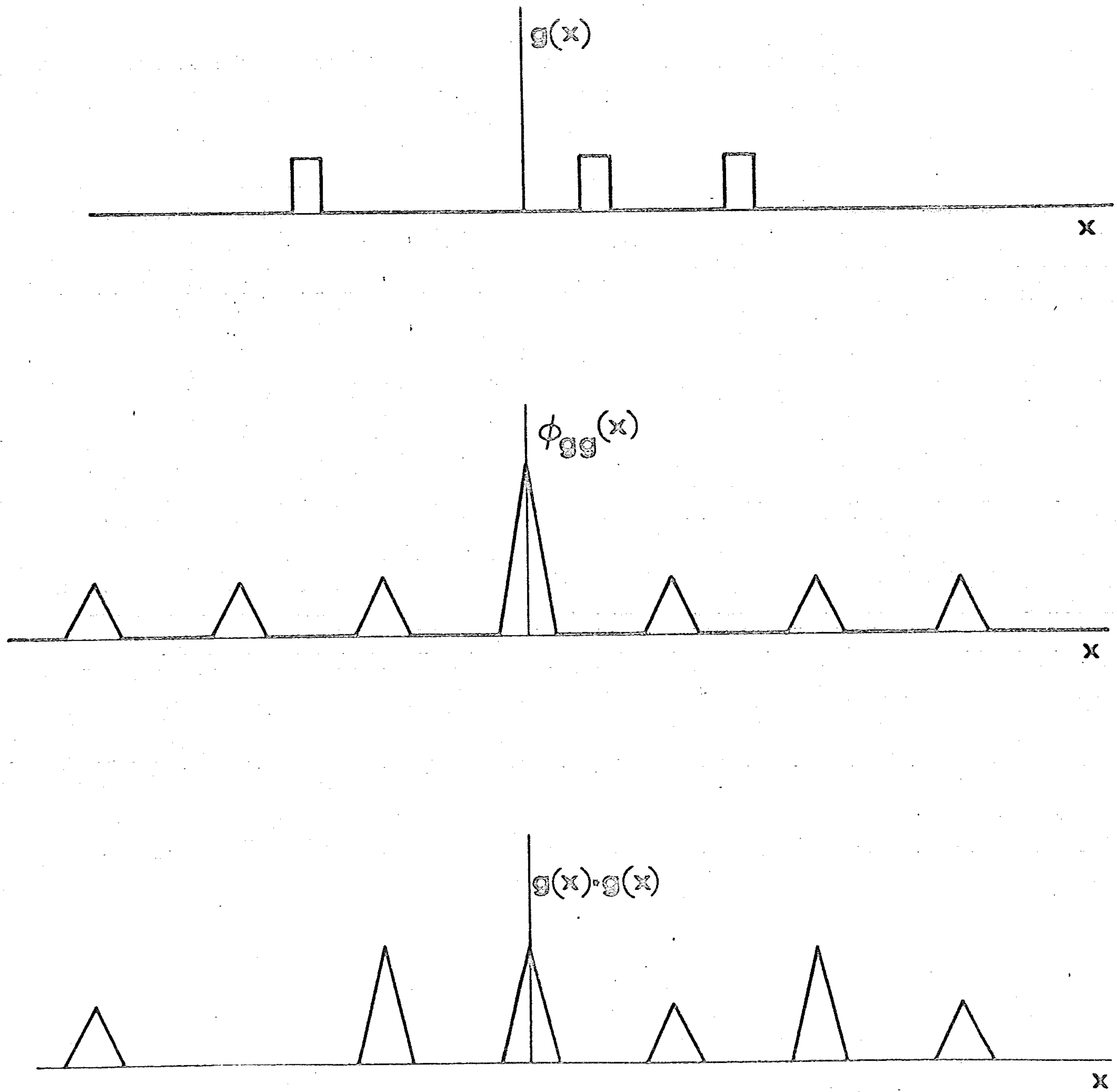

Fig. 2
Test signal g(x) showing the autocorrelation function $\phi_{gg}(x)$ and the convolution $g(x) * g(x)$.

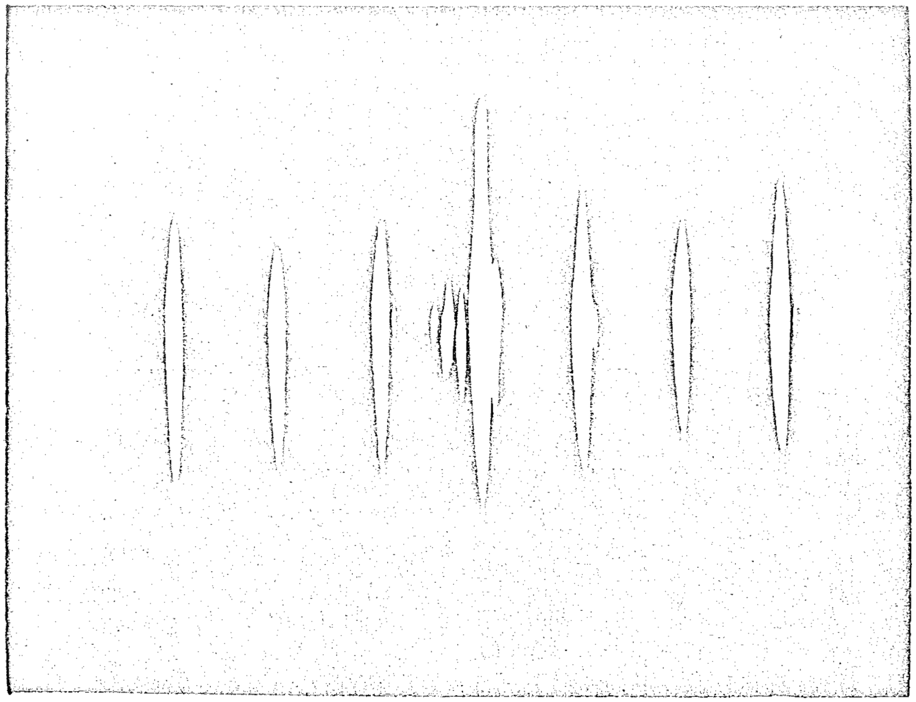

(a)

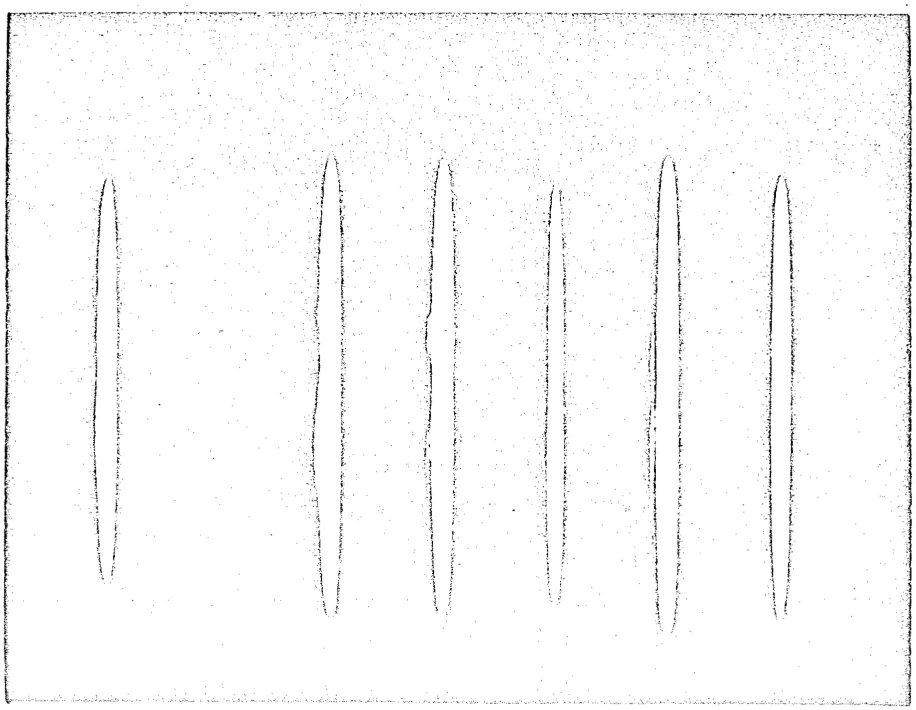

(b)

Fig. 3
Photographs of
a) $\phi_{gg}(x)$ and
b) $g(x) * g(x)$ for the signal shown in Fig. 2.

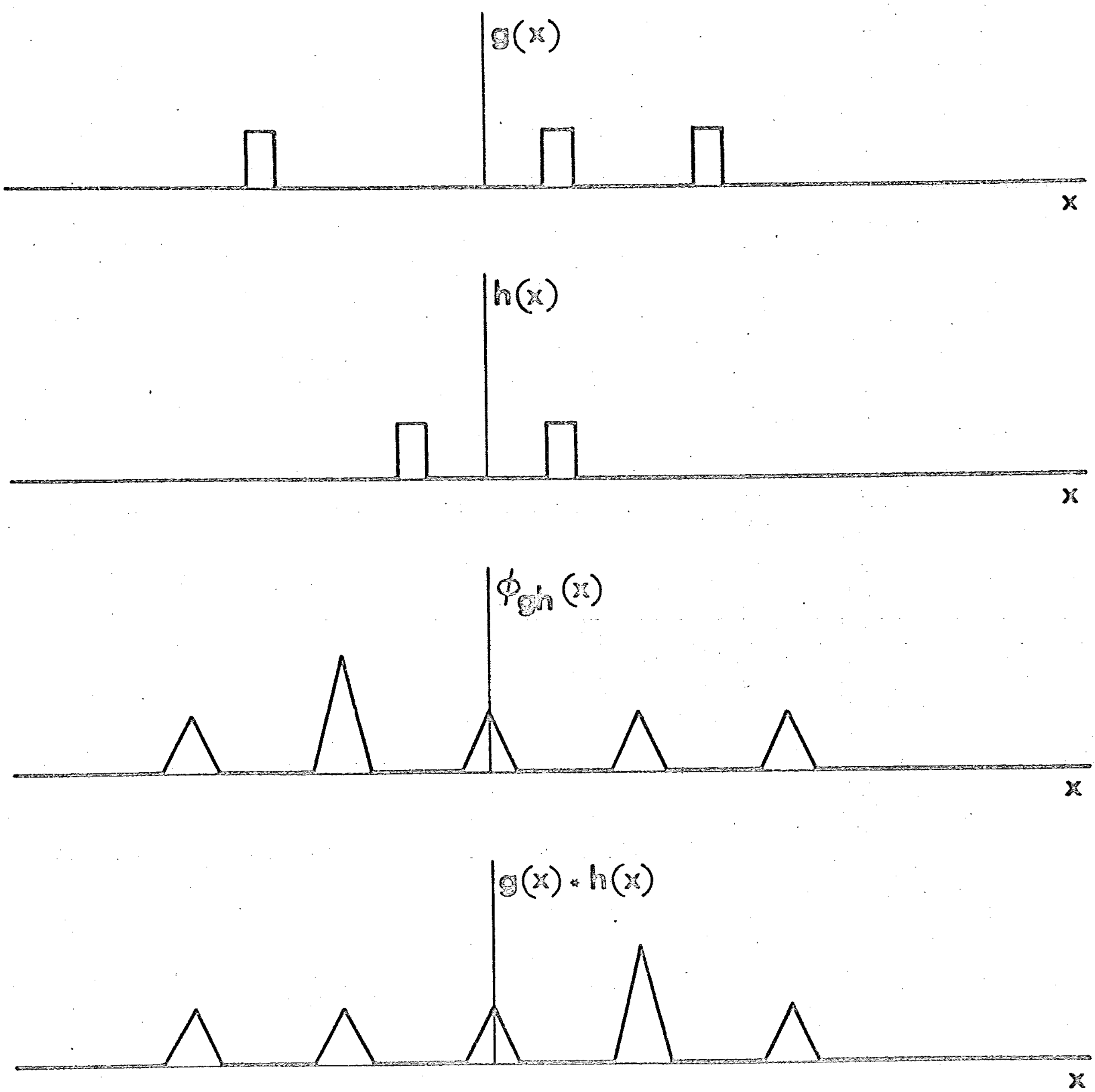

Fig. 4
Cross-correlation $\phi_{gh}(x)$ and convolution $g(x) * h(x)$ of the two signals $g(x)$ and $h(x)$

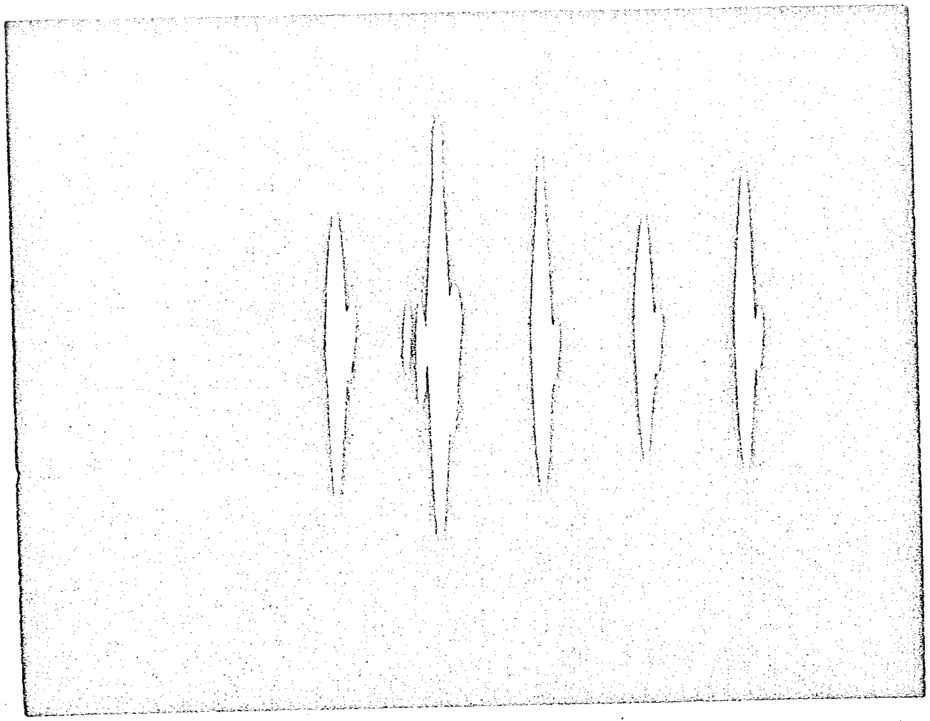

(a)

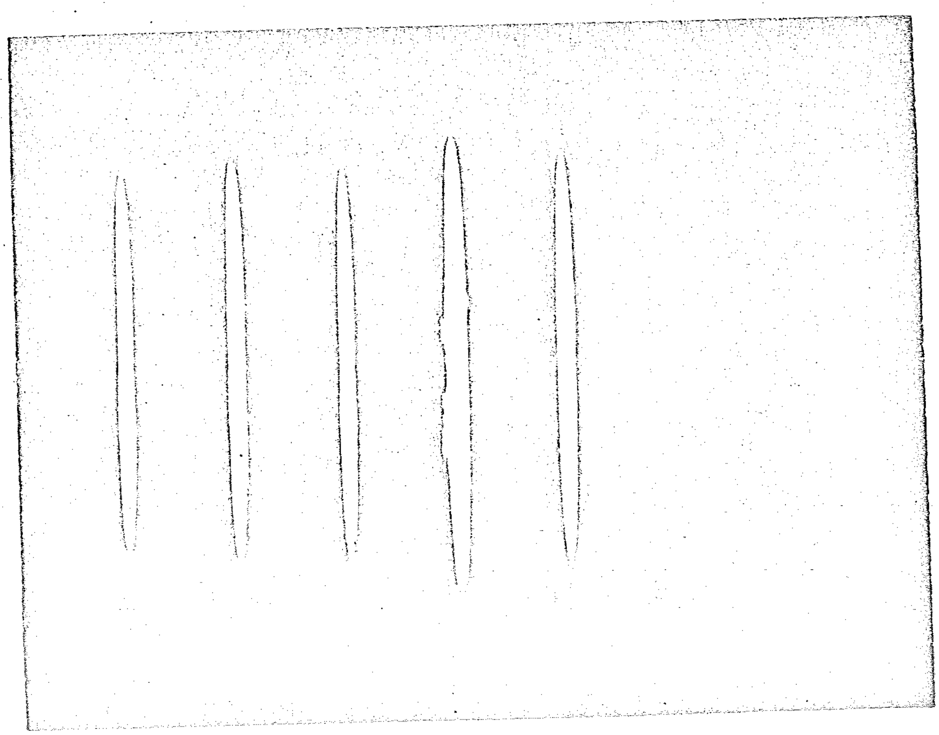

(b)

Fig. 5
Photographs of
a) $\phi_{gh}(x)$ and
b) $g(x) * h(x)$ for the signal shown in Fig. 4.

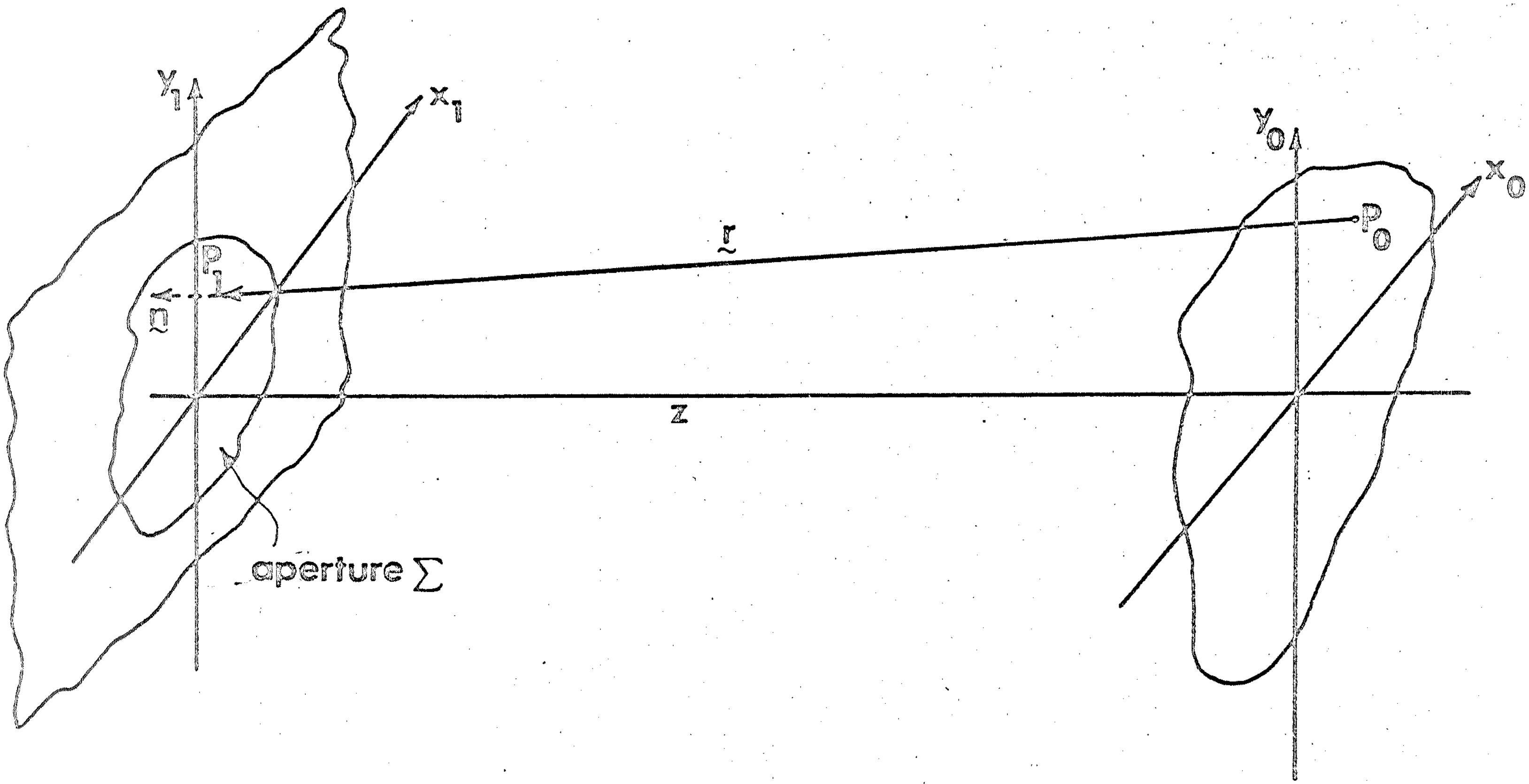

$$r \approx z\left[1 + \frac{1}{2}\left(\frac{x_0 - x_1}{z}\right)^2 + \frac{1}{2}\left(\frac{y_0 - y_1}{z}\right)^2\right] \qquad \text{(Paraxial Approximation)}$$

$$\underset{\sim}{U}(x_0, y_0) = \frac{1}{j\lambda}\iint_{\Sigma} \underset{\sim}{U}'(x_1, y_1)\,\frac{e^{jkr}}{r}\cos(\underset{\sim}{n}, \underset{\sim}{r})\,dx_1 dy_1$$

$$\approx \frac{e^{jkz}}{j\lambda z}\iint_{-\infty}^{\infty} \underset{\sim}{U}'(x_1, y_1)\, e^{j\frac{k}{2z}\left[(x_0 - x_1)^2 + (y_0 - y_1)^2\right]} dx_1\, dy_1$$

Fig. 6
Fresnel Diffraction at
an Aperture

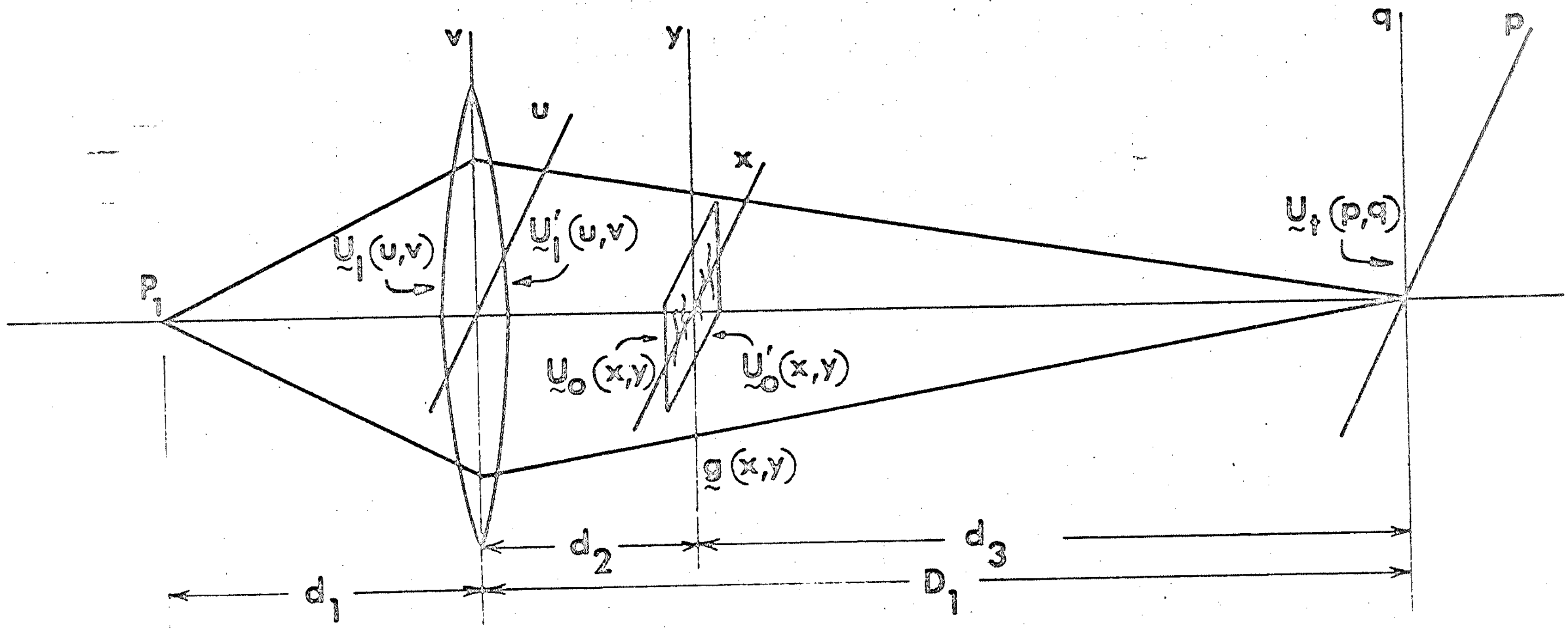

Fig. 7
Geometry for producing the
Fourier transform of $\underset{\sim}{g}(x,y)$

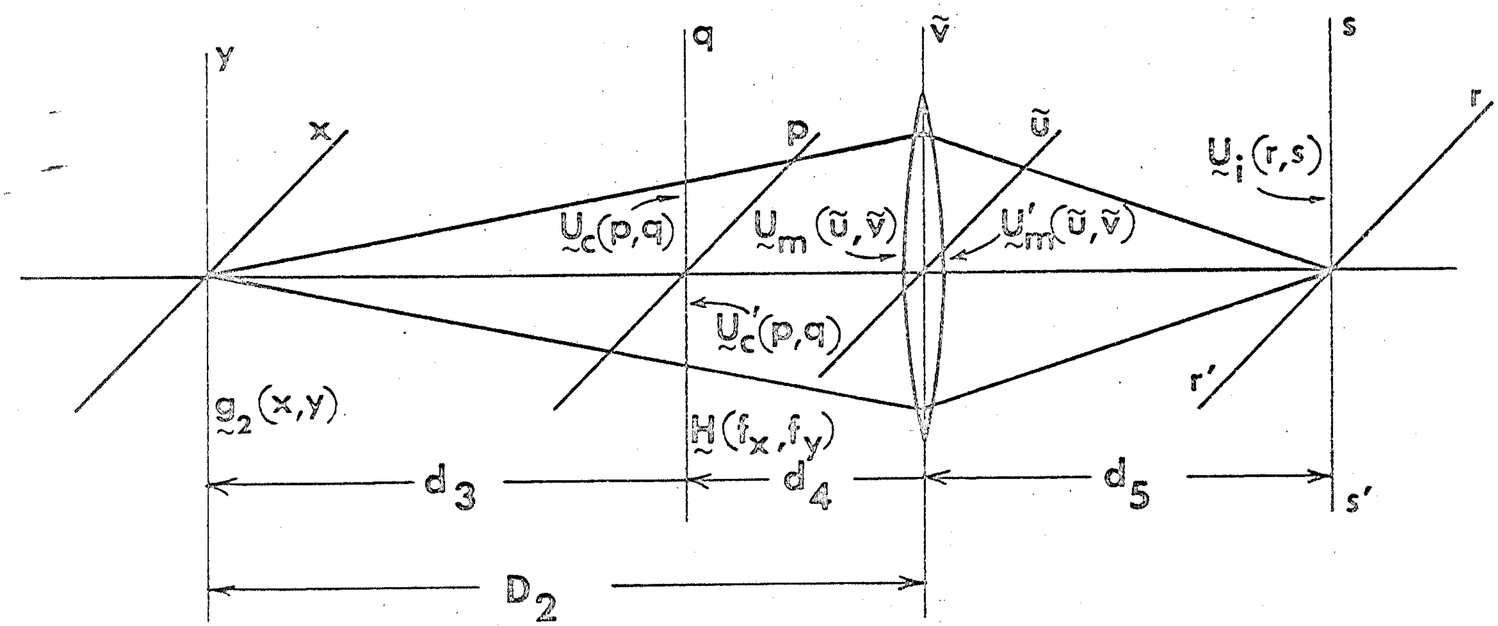

Fig. 8
Geometry for analyzing
the reconstruction process

APPENDIX 4

COHERENT OPTICAL PROCESSING

USING A SINGLE SPHERICAL MIRROR

by
Richard E. Haskell

Coherent Optics Laboratory
Technical Report No. 70-3, June 1970

This work was supported in part by

NASA under Grant NGR 23-054-003.

School of Engineering
Oakland University
Rochester, Michigan 48063

COHERENT OPTICAL PROCESSING USING A SINGLE SPHERICAL MIRROR

1. Introduction

Optical data processing and spatial filtering techniques have been used in a variety of applications.[1] An historical review of spatial filtering and optical information processing has been given by Goodman.[2] The standard optical processing system contains a collimating lens, a transforming lens, and an imaging (or second transforming) lens. By appropriately locating the input plane, the same lens can be used for both transforming and imaging the input signal. As will be shown below, the incident wave need not be a plane wave so that the collimating lens can also be eliminated. A schematic of the resulting single lens system is shown in Fig. 1. The single lens in this system can be replaced by a spherical mirror resulting in an optical processor that uses no lenses at all following the input pinhole. Two possible configurations of such an optical processor for use with transmitting and reflecting signals respectively are shown in Figs. 2 and 3. An analysis of the optical processing system in Fig. 1 is given in Section 2. The effects of the finite size of the mirror and the input signal are discussed in Section 3. Some Fourier transforms and spatial filtering experiments using a single spherical mirror are presented in Section 4.

2. Analysis of the Optical Processing System

A wave analysis of the optical system in Figure 1 can be carried out by determining the complex amplitude of the wave $\underset{\sim}{U}(x,y)$ at any plane perpendicular to the optical axis. If $\underset{\sim}{U}'(x_1,y_1)$ is the complex amplitude of the wave at plane z = 0, then the complex amplitude $\underset{\sim}{U}(x_o,y_o)$ at a parallel plane a distance z away is given by the Huygen-Fresnel principle[2,3] as shown in Figure 4. Referring to Figure 4 one sees that the effect of traveling a distance d in free space is to change $\underset{\sim}{U}'(x_1,y_1)$ to $\underset{\sim}{U}(x_o,y_o)$ through the relation

$$\underset{\sim}{U}(x_o,y_o) = \underset{\sim}{K}\iint_{-\infty}^{\infty}\underset{\sim}{U}'(x_1,y_1)\,e^{j\frac{k}{2d}[(x_o-x_1)^2 + (y_o-y_1)^2]}\,dx_1dy_1 \qquad (1)$$

where $\underset{\sim}{K}$ is a complex constant and $\underset{\sim}{U}'(x_1,y_1)$ is assumed to be zero outside the aperture. The result for light from a point source on the axis traveling a distance d is found by letting $\underset{\sim}{U}'(x_1,y_1) = \delta(x_1,y_1)$ in (1) from which

$$\underset{\sim}{U}_d(x_o,y_o) = \underset{\sim}{K}\;e^{j\frac{k}{2d}(x_o^2 + y_o^2)} \qquad (2)$$

The effect of the lens (or spherical mirror) is to multiply the incident amplitude function $\underset{\sim}{U}(x,y)$ by some complex amplitude $\underset{\sim}{\psi}(x,y)$. To determine $\underset{\sim}{\psi}(x,y)$ recognize that light from a point source which is incident on the lens (or mirror) after traveling a distance f equal to the focal length will be transmitted (or reflected) as a plane wave. That is

$$\underset{\sim}{U}_f(x,y)\ \underset{\sim}{\psi}(x,y) = \text{constant}$$

and thus from (2) it follows that

$$\underset{\sim}{\psi}(x,y) = e^{-j\frac{k}{2f}(x^2 + y^2)} \tag{3}$$

represents the effect of the lens (or sperical mirror) where f is the focal length of the lens (or mirror).

Refer now to Figure 1 where $\underset{\sim}{U}_1(x,y)$ is the light amplitude just to the left of the signal plane. From (2) $\underset{\sim}{U}_1(x,y)$ is given by

$$\underset{\sim}{U}_1(x,y) = \underset{\sim}{K}_1\ e^{j\frac{k}{2d_1}(x^2 + y^2)} \tag{4}$$

To the right of the input plane $\underset{\sim}{U}_2(x,y)$ is given by

$$\underset{\sim}{U}_2(x,y) = \underset{\sim}{U}_1(x,y)\ \underset{\sim}{g}(x,y) \tag{5}$$

Equation (1) can be used to find $\underset{\sim}{U}_3(u,v)$ in terms of $\underset{\sim}{U}_2(x,y)$. Thus

$$\underset{\sim}{U}_3(u,v) = \underset{\sim}{K}_2 \iint_{-\infty}^{\infty} \underset{\sim}{U}_2(x,y)\, e^{j\frac{k}{2d_2}[(u-x)^2 + (v-y)^2]}\ dxdy \tag{6}$$

The effect of the lens (or mirror) is to multiply $\underset{\sim}{U}_3(u,v)$ by $\psi(u,v)$ given by (3). Thus

$$\underset{\sim}{U}_4(u,v) = \underset{\sim}{U}_3(u,v)\ e^{-j\frac{k}{2f}(u^2 + v^2)} \tag{7}$$

Using (1) again $\underset{\sim}{U}_5(p,q)$ can be written as

$$\underset{\sim}{U}_5(p,q) = \underset{\sim}{K}_3 \iint_{-\infty}^{\infty} \underset{\sim}{U}_4(u,v)\ e^{j\frac{k}{2d_3}[(p-u)^2 + (q-v)^2]}\ dudv \tag{8}$$

If a filter with a complex transmittance $\underset{\sim}{H}(p,q)$ is inserted in the p-q plane, then $\underset{\sim}{U}_6(p,q)$ is given by

$$\underset{\sim}{U}_6(p,q) = \underset{\sim}{U}_5(p,q)\ \underset{\sim}{H}(p,q) \tag{9}$$

Finally the light amplitude in the output plane $\underset{\sim}{U}_7(r,s)$ is given by

$$\underset{\sim}{U}_7(r,s) = \underset{\sim}{K}_4 \iint_{-\infty}^{\infty} \underset{\sim}{U}_6(p,q)\ e^{j\frac{k}{2d_4}[(r-p)^2 + (s-q)^2]} \tag{10}$$

It is convenient to first evaluate $\underset{\sim}{U}_5(p,q)$. Combining Equations (4) through (8) one can write

$$\underset{\sim}{U}_5(p,q) = \underset{\sim}{K}_5 \iiiint_{-\infty}^{\infty} \underset{\sim}{g}(x,y)\ e^{j\frac{k}{2}\rho}\ dudv\ dxdy \tag{11}$$

where

$$\rho = \frac{x^2+y^2}{d_1} + \frac{u^2+v^2+x^2+y^2-2ux-2vy}{d_2} - \frac{u^2+v^2}{f}$$

$$+ \frac{p^2+q^2+u^2+v^2-2pu-2qv}{d_3} \tag{12}$$

It is first necessary to do the integration over u and v. To this end let the parts of ρ containing u and v be represented by ρ_u and ρ_v respectively. Thus

$$\rho_u = u^2\left(\frac{1}{d_2} - \frac{1}{f} + \frac{1}{d_3}\right) - 2u\left(\frac{x}{d_2} + \frac{p}{d_3}\right)$$

$$\rho_v = v^2\left(\frac{1}{d_2} - \frac{1}{f} + \frac{1}{d_3}\right) - 2v\left(\frac{y}{d_2} + \frac{q}{d_3}\right) \qquad (13)$$

Since

$$\int_{-\infty}^{\infty} e^{jC_1(u-C_2)^2}\, du = C_3 \int_{-\infty}^{\infty} e^{j\frac{\pi}{2}\xi^2}\, d\xi = \text{constant}$$

it is desirable to complete the squares in (13) and write

$$\rho_u = \rho_u' - \frac{d_2L_1}{d_1}\left(\frac{x}{d_2} + \frac{p}{d_3}\right)^2$$

$$\rho_v = \rho_v' - \frac{d_2L_1}{d_1}\left(\frac{y}{d_2} + \frac{q}{d_3}\right)^2 \qquad (14)$$

where

$$\rho_u' = \frac{d_1}{d_2L_1}\left[u - \frac{d_2L_1}{d_1}\left(\frac{x}{d_2} + \frac{p}{d_3}\right)\right]^2$$

$$\rho_v' = \frac{d_1}{d_2L_1}\left[u - \frac{d_2L_1}{d_1}\left(\frac{y}{d_2} + \frac{q}{d_3}\right)\right]^2 \qquad (15)$$

and the lens formula $1/f = 1/L_1 + 1/d_3$ has been used. Combining (14) with the remaining terms in (12) one can write ρ in the form

$$\rho = \rho_u' + \rho_v' + \left(\frac{1}{d_1} + \frac{1}{d_2} - \frac{L_1}{d_1d_2}\right)\left(x^2 + y^2\right)$$

$$+ \left(\frac{1}{d_3} - \frac{d_2L_1}{d_1{d_3}^2}\right)\left(p^2 + q^2\right) - \frac{2L_1}{d_1d_3}(xp + yq) \qquad (16)$$

The terms ρ_u' and ρ_v' give a constant when integrated over u and v. The coefficient of $(x^2 + y^2)$ in (16) is identically zero. Thus (11) can be written as

$$\underset{\sim}{U}_5(p,q) = \underset{\sim}{K}_6 \, e^{j\frac{k}{2d_3}\left(1 - \frac{d_2L_1}{d_1d_3}\right)\left(p^2 + q^2\right)} \iint_{-\infty}^{\infty} \underset{\sim}{g}(x,y) \, e^{-j\frac{2\pi L_1}{\lambda d_1 d_3}(xp + yq)} \, dxdy$$

$$= \underset{\sim}{K}_6 \, e^{j\frac{k}{2d_3}\left(1 - \frac{d_2L_1}{d_1d_3}\right)\left(p^2 + q^2\right)} \underset{\sim}{G}\left(\frac{L_1 p}{\lambda d_1 d_3}, \frac{L_1 q}{\lambda d_1 d_3}\right) \tag{17}$$

where $\underset{\sim}{G}(f_x, f_y)$ is the two-dimensional Fourier transform of $\underset{\sim}{g}(x,y)$ with spatial frequencies $f_x = L_1p/\lambda d_1 d_3$ and $f_y = L_1 q/\lambda d_1 d_3$.

A filter with an impulse response $\underset{\sim}{h}(x,y)$ and a transfer function $\underset{\sim}{H}(f_x, f_y)$ is to be inserted in the p-q plane. Then from (17), (9) and (10), $\underset{\sim}{U}_7(r,s)$ can be written as

$$\underset{\sim}{U}_7(r,s) = \underset{\sim}{K}_7 \iint_{-\infty}^{\infty} \underset{\sim}{G}\left(\frac{L_1 p}{\lambda d_1 d_3}, \frac{L_1 q}{\lambda d_1 d_3}\right) \underset{\sim}{H}\left(\frac{L_1 p}{\lambda d_1 d_3}, \frac{L_1 q}{\lambda d_1 d_3}\right) e^{j\frac{k}{2}\mu} \, dpdq \tag{18}$$

where

$$\mu = \frac{1}{d_3}\left(1 - \frac{d_2L_1}{d_1d_3}\right)\left(p^2 + q^2\right) + \frac{1}{d_4}\left(r^2 + s^2 + p^2 + q^2 - 2rp - 2sq\right) \tag{19}$$

The coefficient of $(p^2 + q^2)$ in (19) is

$$\frac{1}{d_3} + \frac{1}{d_4} - \frac{d_2 L_1}{d_1 {d_3}^2} \tag{20}$$

Applying the lens formula to Figure 1 one can write

$$\frac{1}{f} = \frac{1}{L_1} + \frac{1}{d_3} = \frac{1}{d_2} + \frac{1}{L_2} \tag{21}$$

By cross-multiplying and combining terms in (21) one can show that

$$\frac{L_1}{d_1 d_3} = \frac{L_2}{d_2 d_4} \tag{22}$$

Substituting (22) into (20) one obtains

$$\frac{1}{d_3} + \frac{1}{d_4} - \frac{L_2}{d_3 d_4} = 0$$

so that the coefficient of $(p^2 + q^2)$ in (19) vanishes. Thus, (18) reduces to

$$\underset{\sim}{U}_7(r,s) = \underset{\sim}{K}_7 \, e^{j\frac{k}{2d_4}(r^2+s^2)} \iint_{-\infty}^{\infty} \underset{\sim}{G}\left(\frac{L_1 p}{\lambda d_1 d_3}, \frac{L_1 q}{\lambda d_1 d_3}\right) \underset{\sim}{H}\left(\frac{L_1 p}{\lambda d_1 d_3}, \frac{L_1 q}{\lambda d_1 d_3}\right)$$

$$e^{-j\frac{2\pi}{\lambda d_4}(rp + sq)} \, dpdq \tag{23}$$

In terms of the spatial frequencies $f_x = L_1 p/\lambda d_1 d_3$, $f_y = L_1 q/\lambda d_1 d_3$ and the reduced coordinates $r' = -(d_2/L_2)\, r$, $s' = -(d_2/L_2)\, s$ Equation (23) can be written as

$$\underset{\sim}{U}_7(r', s') = \underset{\sim}{K}_8 \, e^{j\frac{kL_2^2}{2d_4d_2^2}(r'^2 + s'^2)} \iint_{-\infty}^{\infty} \underset{\sim}{G}(f_x, f_y) \, \underset{\sim}{H}(f_x, f_y)$$

$$e^{j2\pi(f_x r' + f_y s')} \, df_x df_y \tag{24}$$

where (22) has been used. Thus to within a quadratic phase factor $\underset{\sim}{U}_7(r', s')$ is proportional to the inverse Fourier transform of the product $\underset{\sim}{G}(f_x, f_y)\,\underset{\sim}{H}(f_x, f_y)$. The light intensity in the output plane will therefore be proportional to the magnitude squared of this inverse Fourier transform or alternatively to the magnitude squared of the convolution of the input signal $\underset{\sim}{g}(x,y)$ with the impulse response $\underset{\sim}{h}(x,y)$. In particular, if no filter is used $\underset{\sim}{H}(p,q) = 1$, $\underset{\sim}{h}(x,y) = \delta(x,y)$ and the output intensity reduces to

$$I(r,s) = \left| \underset{\sim}{K}_8 \, \underset{\sim}{g}\left(- \frac{d_2}{L_2} r, \; - \frac{d_2}{L_2} s \right) \right|^2 \tag{25}$$

which as expected is an inverted image of $\underset{\sim}{g}(x,y)$ that has been magnified by an amount L_2/d_2.

3. Design Criteria for the Optical Processor

In designing the lensless processor for a particular application a compromise is often required between the magnification $M = L_2/d_2$, the actual size of the diffraction pattern in the transform (filter) plane, and the maximum spatial frequency that can be faithfully transmitted by the system in the absence of any filtering in the transform plane. This maximum spatial frequency can be determined from the coherent transfer function which is equal to the pupil function of the spherical mirror $P(\lambda L_2 f_x', \lambda L_2 f_y')$[2,3]. This coherent transfer function is defined as the ratio of the frequency spectrum of the image to the frequency spectrum of the image predicted by geometrical optics. The spatial frequencies f_x' and f_y' are associated with the image coordinates. However, the spatial frequencies f_x and f_y related to the Fourier transform in (17) are associated with the input signal. These two sets of spatial frequencies are related by the magnification through the expression $f_{x,y} = Mf'_{x,y}$. Thus, in terms of the input spatial frequencies the coherent transfer function is given by $P(\lambda L_2 f_x/M, \lambda L_2 f_y/M) = P(\lambda d_2 f_x, \lambda d_2 f_y)$. For a lens (or spherical mirror) of diameter D the cut-off frequency f_o is thus given by

$$f_o = \frac{D}{2\lambda d_2} \tag{26}$$

This cut-off frequency f_o corresponds to the spatial frequency of an on-axis object whose diffracted light just makes it through the aperture of the lens (or spherical mirror). This is illustrated in Figure 5 where the solid line passing through the center of an object of width a belongs to the bundle of rays which converge to a point in the transform plane a distance p_o from the axis. This distance corresponds to the maximum spatial frequency

$$f_o = \frac{L_1 p_o}{\lambda d_1 d_3} \tag{27}$$

which will be passed by an aperture of diameter D. From the geometry of Figure 5 one can readily show that

$$p_o = \frac{D\ d_1 d_3}{2\ d_2 L_1} \tag{28}$$

so that one can obtain (26) by substituting (28) into (27). Equation (26) is derived by considering the optical system to be space-invariant (isoplanatic). One would then expect this cut-off frequency f_o to apply to all points in the image. In fact, it does not as shown by the bundle of dashed rays in Figure 5. Light that is diffracted in the signal plane at a distance a/2 from the axis will only pass through the aperture of diameter D if the spatial frequency is less than $f_a = L_1 p_a/\lambda d_1 d_3$ as shown in Figure 5. From the geometry of this figure one can show that f_a is related to the cut-off frequency f_o given by (26) by the equation

$$f_a = f_o \left(1 - \frac{L_1}{d_1} \frac{a}{D}\right) \tag{29}$$

Thus the vignetting effect of the finite aperture reduces the maximum spatial frequency that can be faithfully transmitted by the system proportionately to the ratio a/D.

4. Experimental Results

The preceding analysis will apply to the spherical mirror configurations of Figs. 2 and 3 provided the effects of the beamsplitters can be ignored. The most important effects will be the finite size of the beamsplitters and multiple reflections. In practice it is often possible to eliminate the beamsplitters altogether. In the following experiments no beamsplitters were used. The diverging light was reflected directly from a 20 cm. diameter spherical mirror with a focal length of 164 cm. Because of the long focal length a slight tilting of the mirror would separate the transform plane and the output plane from the incoming light beam without significantly affecting the images in these planes. Figures 6 - 9 show a number of signals and their power spectra as measured in the transform plane of Fig. 1. In each case the signal completely filled an aperture in the signal plane 6.5 cm. in diameter. These signals are larger than those which can be used in conventional optical processing systems using standard size lenses (35 mm signals are a standard size). For the measurements shown in Figs. 6 - 9 the distances in Fig. 1 had the following values: d_1=112cm., d_2=109cm., and d_3=636cm.

The spatial filtering capability of the single spherical mirror system was illustrated by a number of experiments. Fig. 10a shows a grating in which the line frequency varies logarithmically from 0.5 lines /mm to 5 lines/mm. A filter consisting of a periodic bar pattern was inserted in the transform plane. The resulting filtered version of the transform plane is shown in Fig. 10b. The resulting output image is shown in Fig. 10c. Since the filter will block all the harmonies of certain spatial frequencies entire regions of the original signal, corresponding to these spatial frequencies, will become darkened as shown in Fig. 10c. In this measurement the distances in Fig. 1 had the following values: d_1=284 cm., d_2=328 cm., d_3=224 cm., and d_4=104cm.

As a second filtering experiment the words "yes" and "no" were recorded on a glass photographic plate and the plate was then bleached and thus became completely transparent. However, there is a phase variation across the glass plate due to changes in the refractive index and thickness of the emulsion where the words are located. The resulting image in the output plane of Fig. 1 is shown in Fig. 11a. A filter which blocked the undiffracted d.c. light was inserted in the transform plane and the resulting image in the output plane is shown in Fig. 11b.

The d.c. filter used for the experiment of Fig. 11 was made by simply recording photographically the point of light (in the form of an Airy disc) which appears in the transform plane when there is no signal in the input plane. When this filter is reinserted in the transform plane the image in the output plane is as shown in Fig. 12. If a transparent object is now inserted in the input plane any light which is diffracted around the d.c. filter will appear in the output plane. This is illustrated in Figs. 13 - 15 where three samples of automobile windshields with different surface qualities were inserted in the input plane. Phase variations due to defects in the glass become visible in the output plane.

Due to the fact that spherical (or parabolic) mirrors can be made larger than lenses of the same quality it may prove useful to use spherical mirrors in optical processing and testing systems where the signals or objects are of large extent.

References

1. Cutrona, L.J., et. al., IRE Trans. Inform. Theory, IT-6, 386 (1960).

2. Goodman, J.W., Introduction to Fourier Optics, McGraw-Hill Book Co., New York, 1968.

3. Born, M., and E. Wolf, Principles of Optics, 2nd rev. ed. Pergamon Press, New York, 1964.

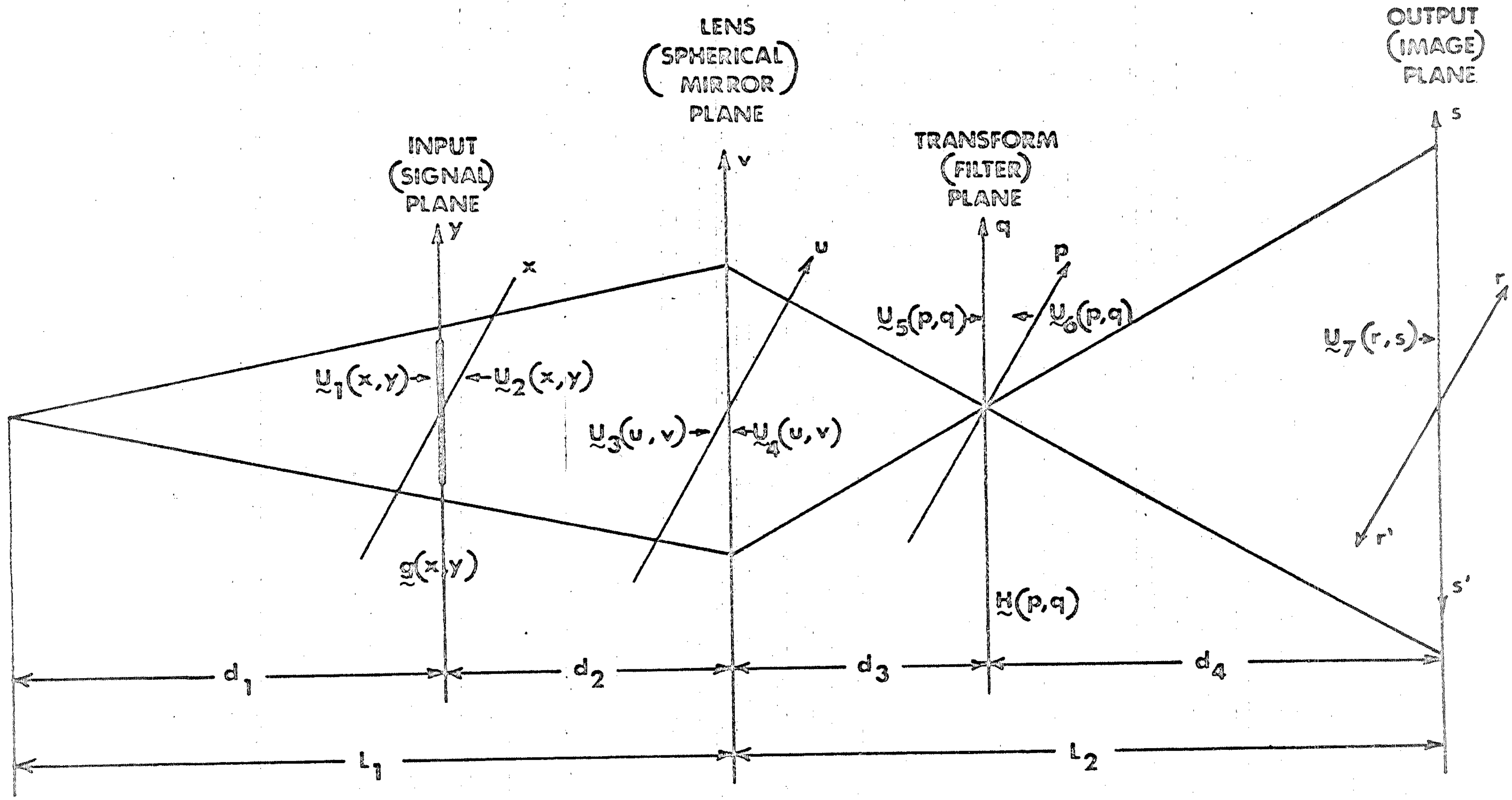

Fig. 1 Single lens (or spherical mirror) optical processing system.

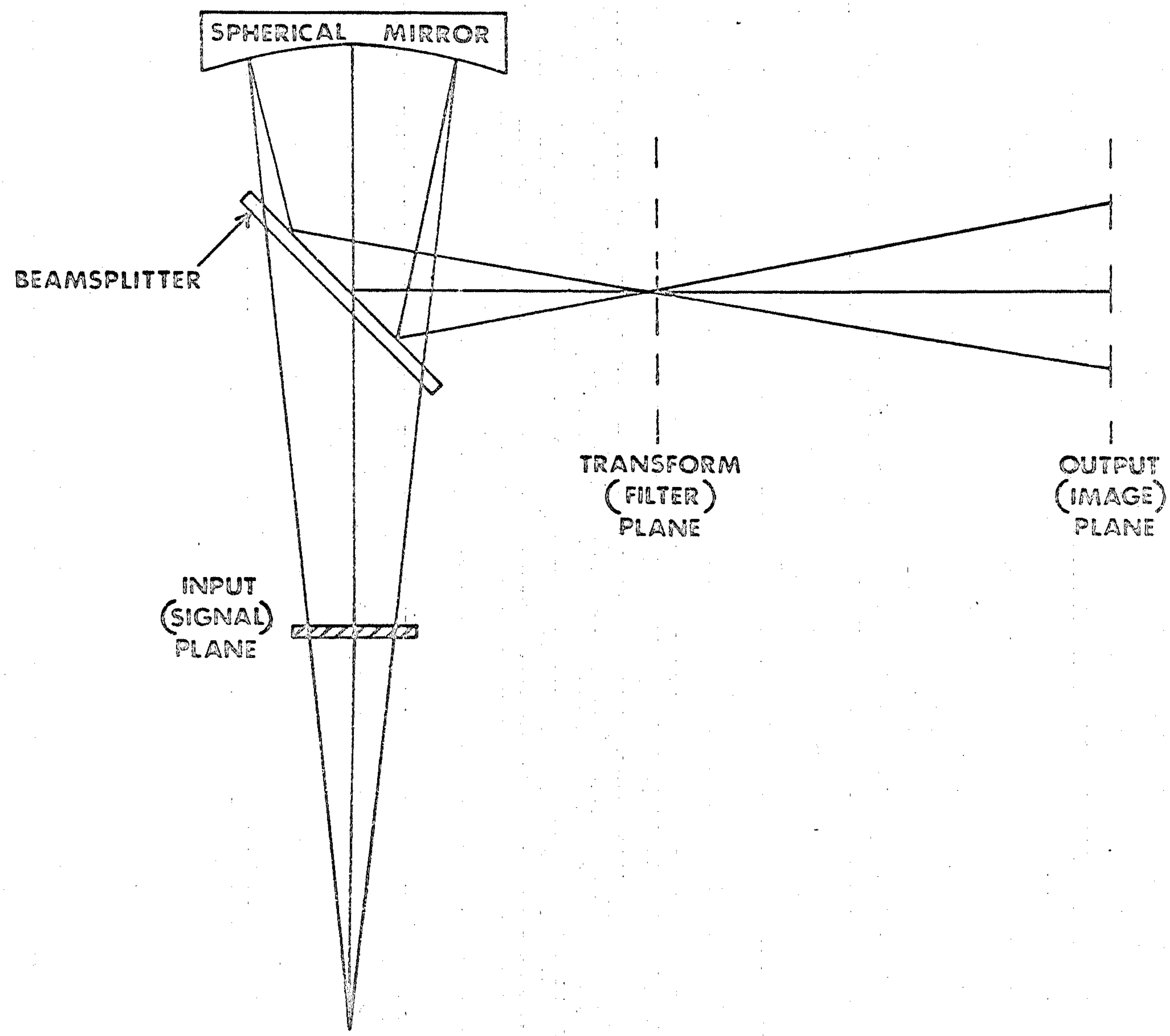

Fig. 2 Optical processor for transmitting signals using a single spherical mirror.

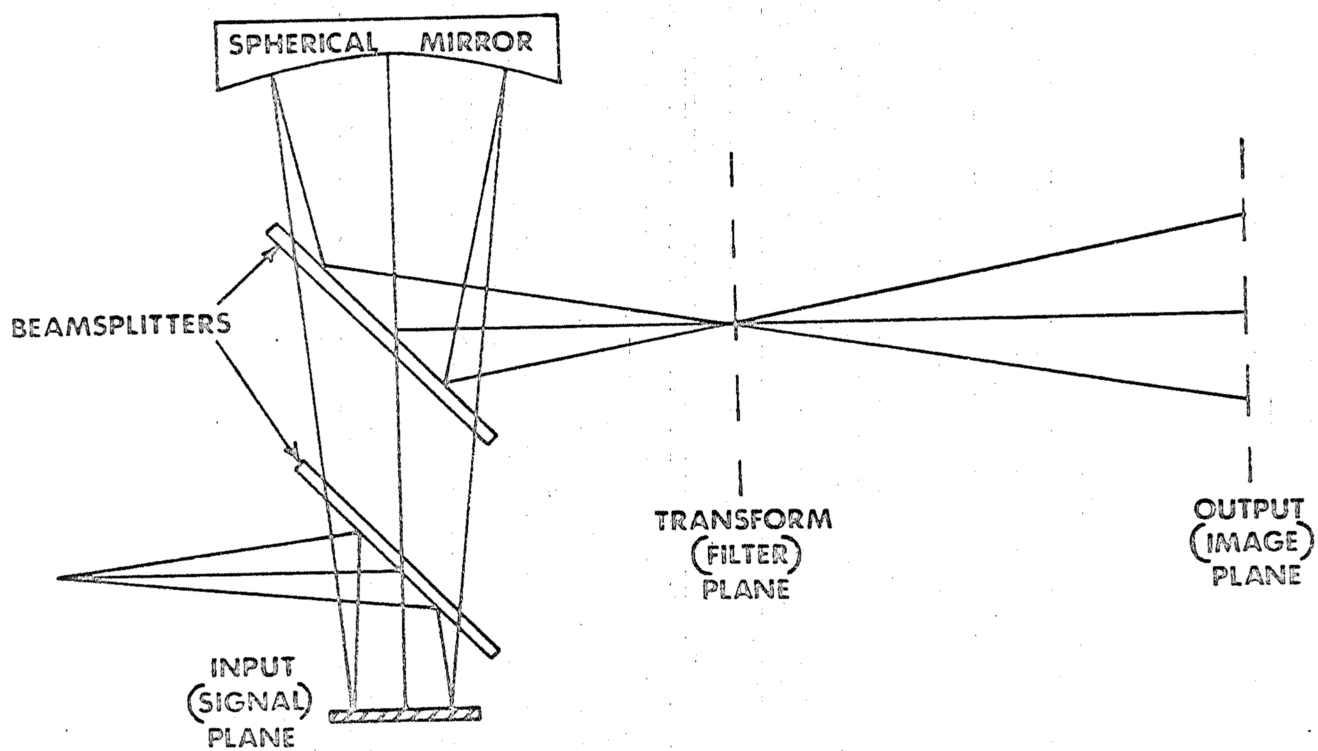

Fig. 3 Optical processor for reflecting signals using a single spherical mirror.

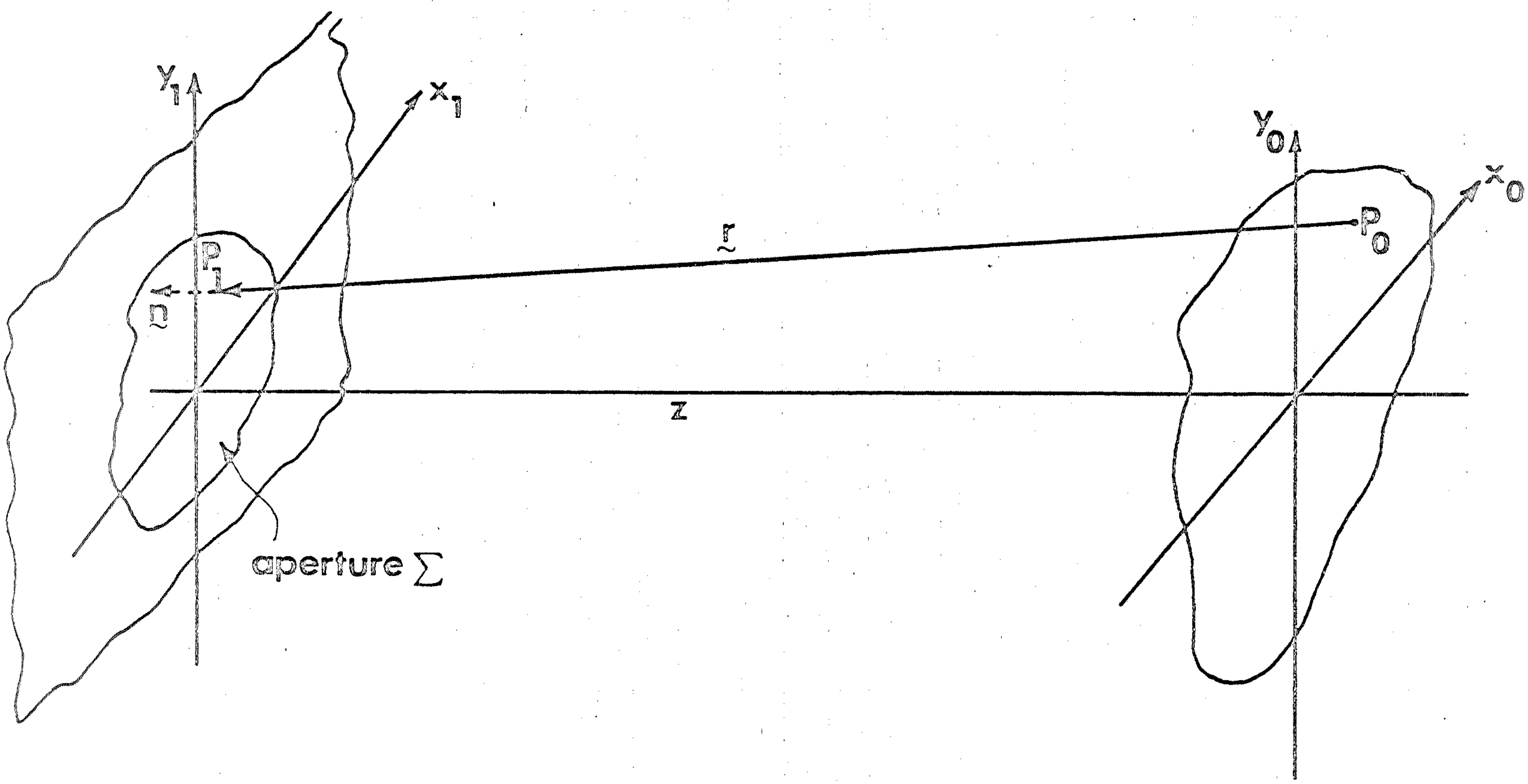

$$r \approx z\left[1+\frac{1}{2}\left(\frac{x_0-x_1}{z}\right)^2+\frac{1}{2}\left(\frac{y_0-y_1}{z}\right)^2\right] \qquad \text{(Paraxial Approximation)}$$

$$\underset{\sim}{U}(x_0, y_0) = \frac{1}{j\lambda}\iint_{\Sigma} \underset{\sim}{U}'(x_1, y_1)\,\frac{e^{jkr}}{r}\cos(\underset{\sim}{n},\underset{\sim}{r})\,dx_1 dy_1$$

$$\approx \frac{e^{jkz}}{j\lambda z}\iint_{-\infty}^{\infty} \underset{\sim}{U}'(x_1, y_1)\, e^{j\frac{k}{2z}\left[(x_0-x_1)^2+(y_0-y_1)^2\right]}\,dx_1 dy_1$$

Fig. 4 Fresnel diffraction at an aperture.

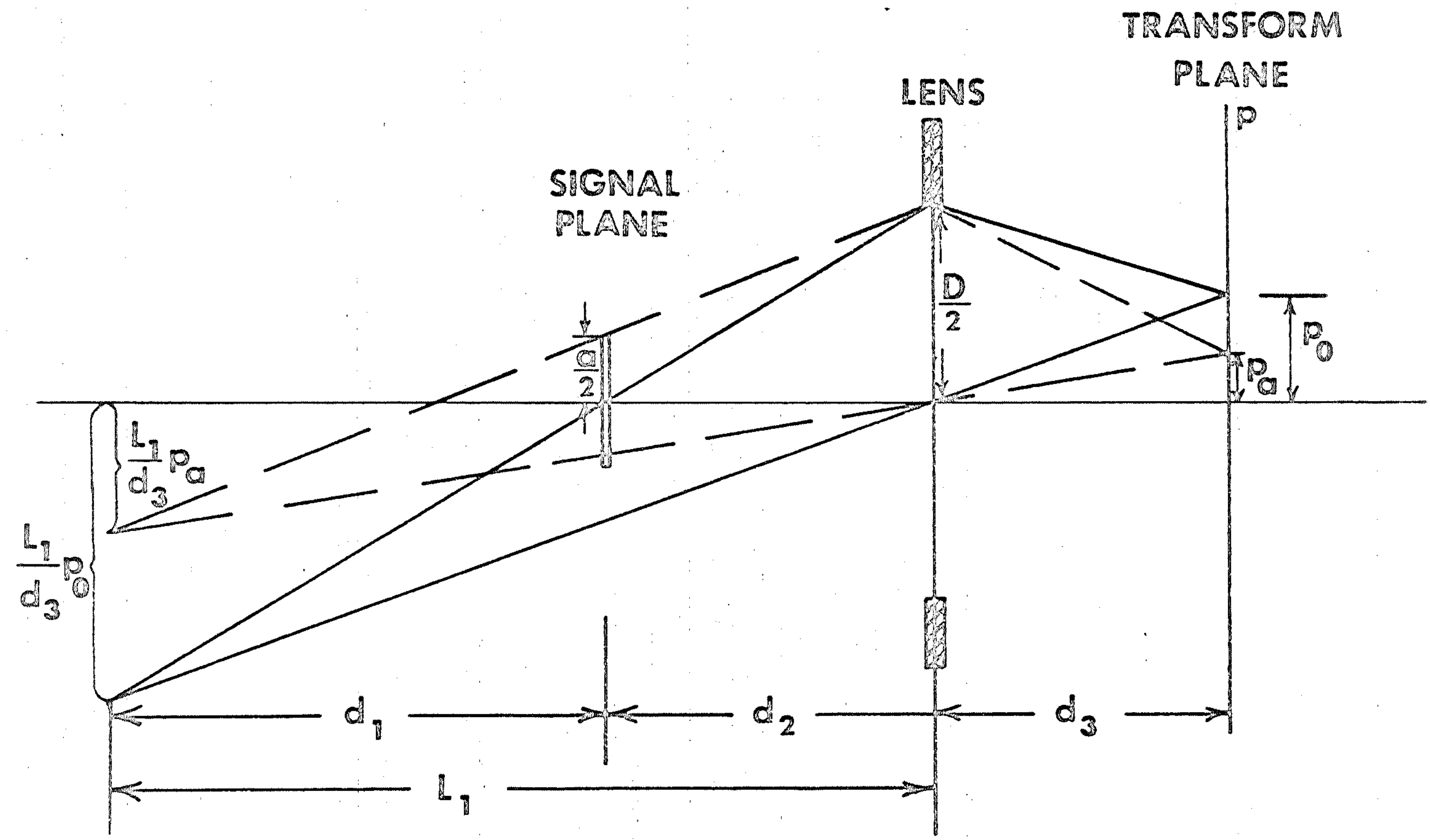

Fig. 5 Geometry for determining the maximum spatial frequency transmitted by a lens.

(a)

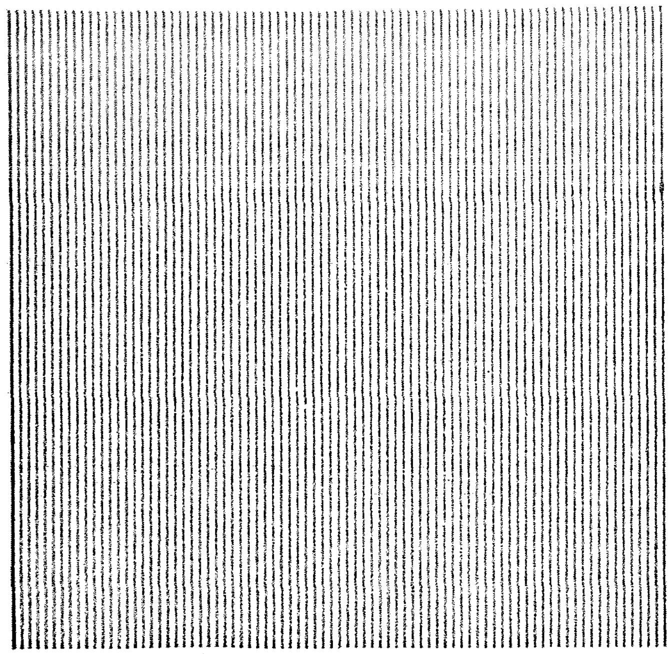

(b)

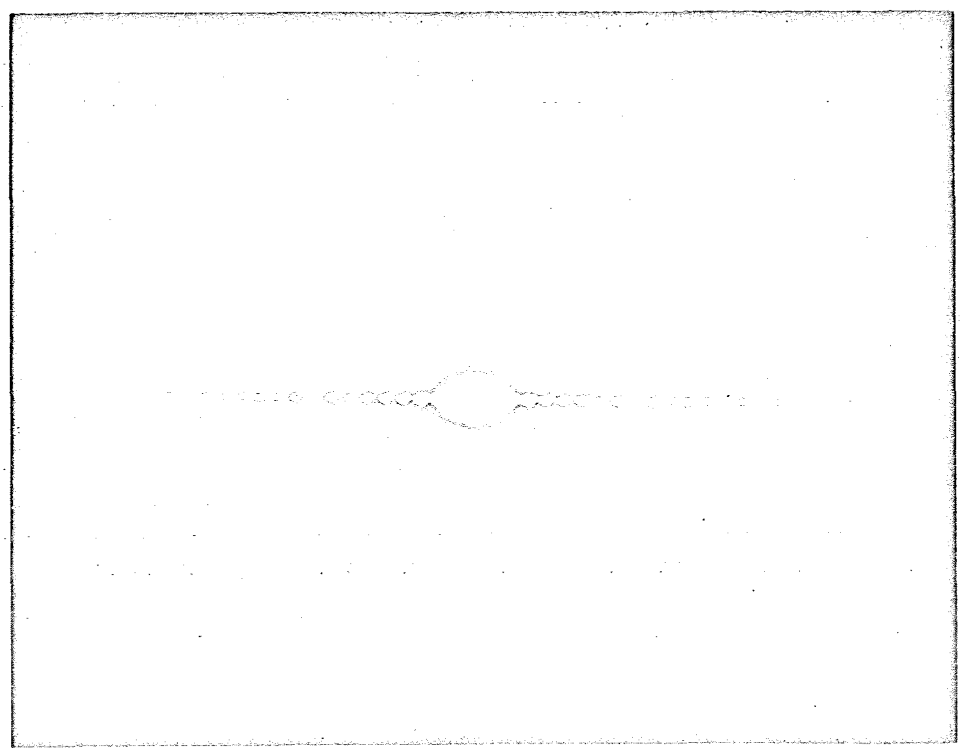

Fig. 6 a) Signal pattern
b) Power spectrum of a).

(a)

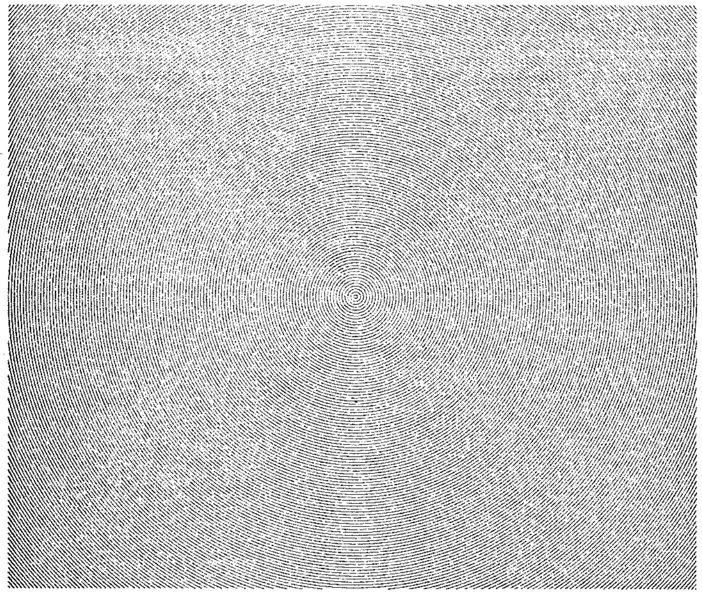

(b)

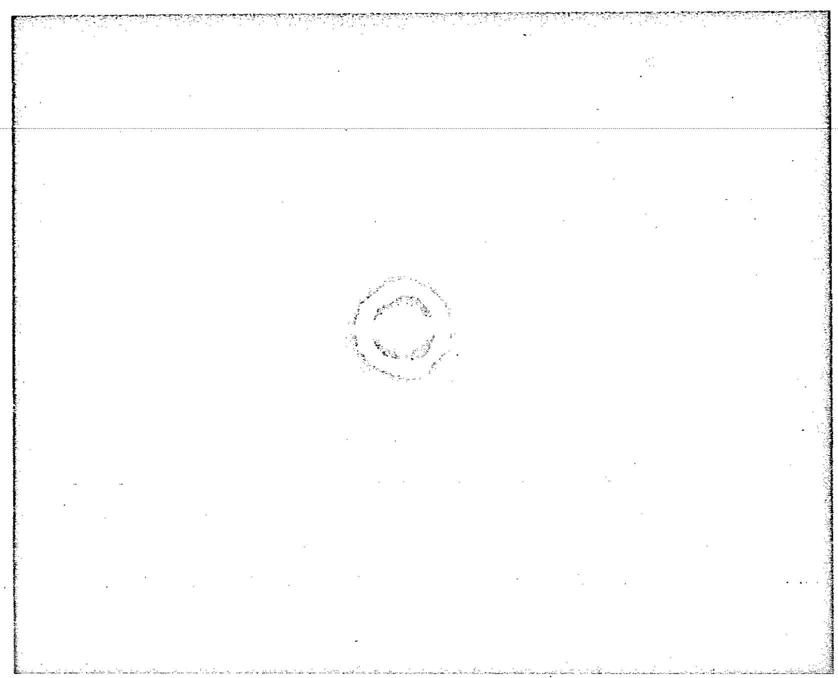

Fig. 7 a) Signal pattern
b) Power spectrum of a).

(a)

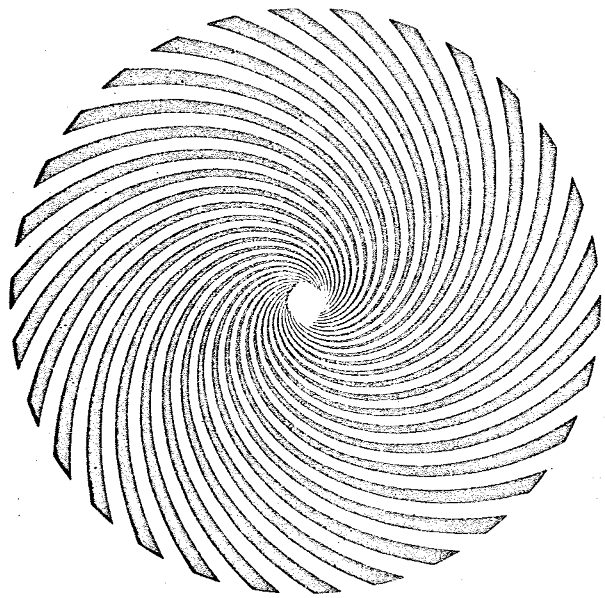

(b)

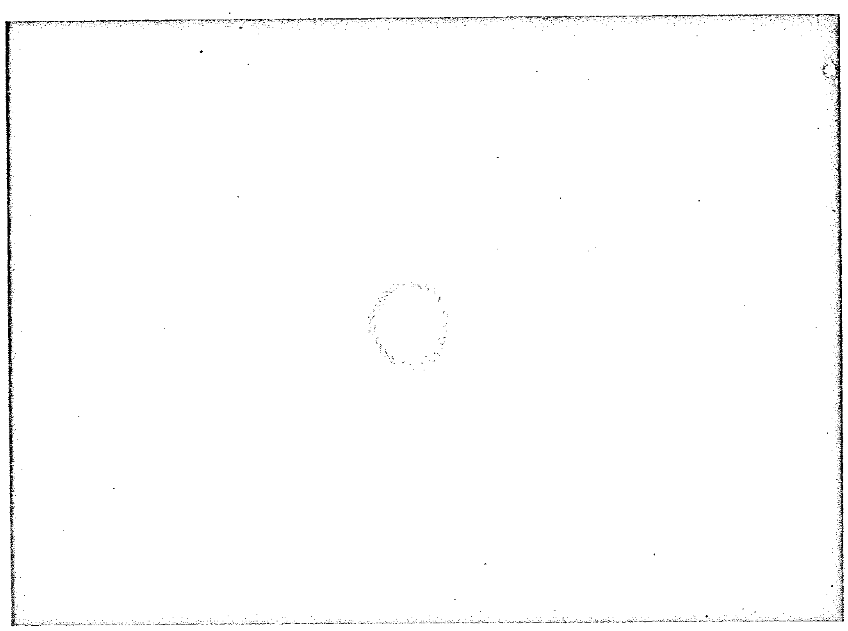

Fig. 8 a) Signal pattern
b) Power spectrum of a).

(a)

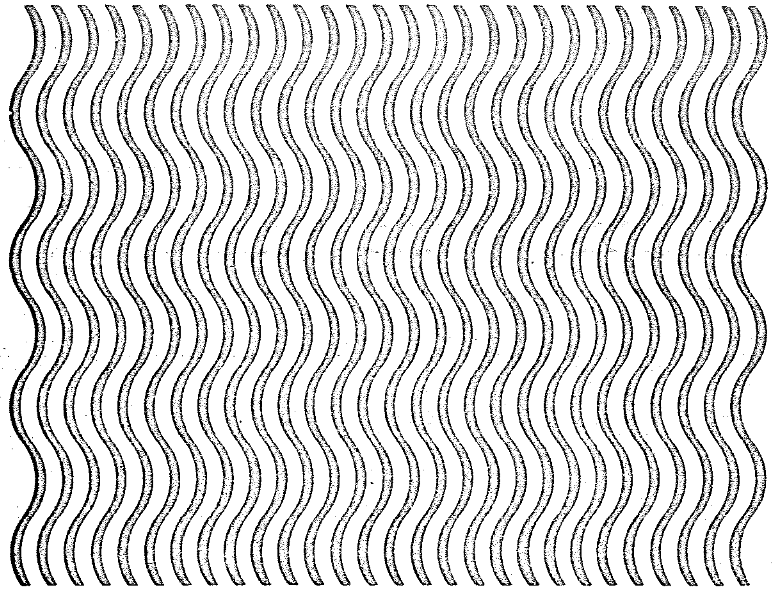

(b)

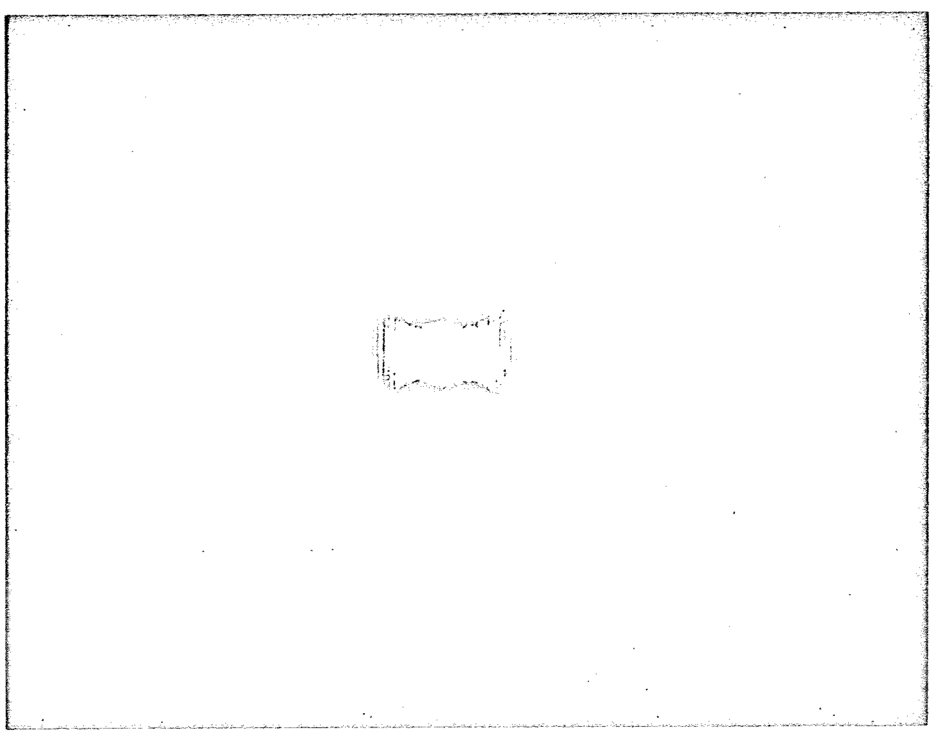

Fig. 9 a) Signal pattern
b) Power spectrum of a).

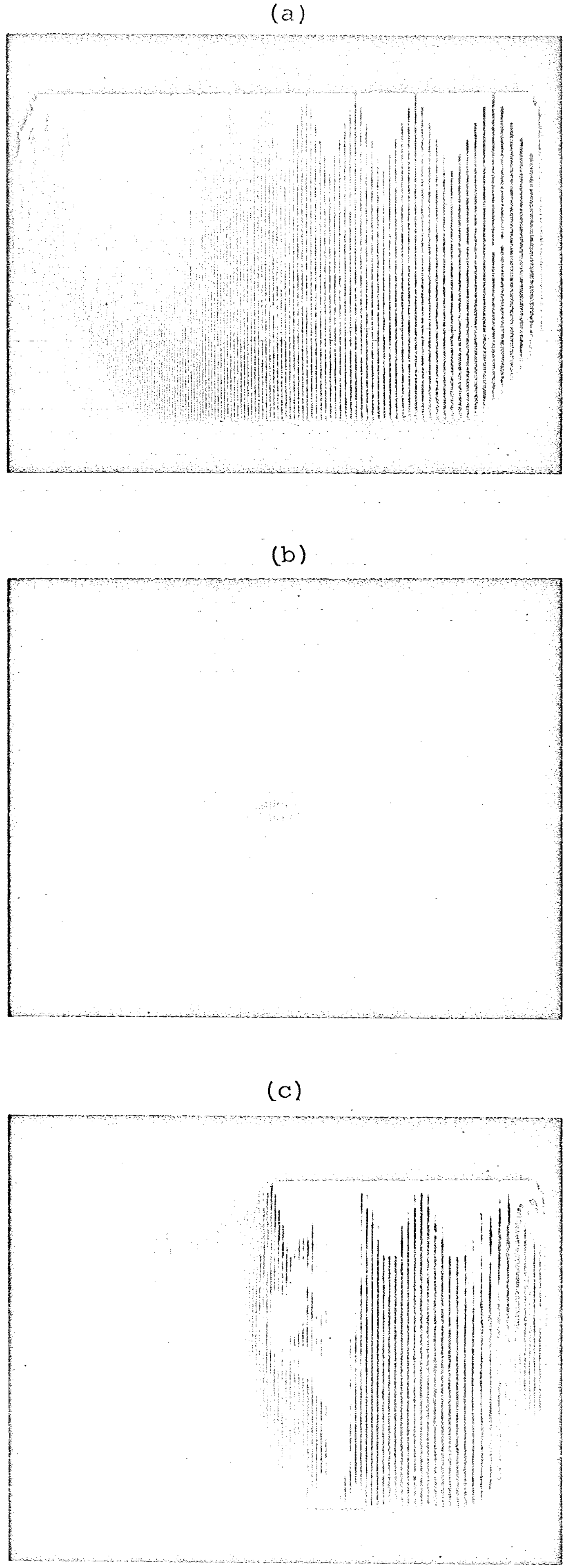

Fig. 10 a) Signal pattern,
b) Filtered power spectrum,
c) Filtered output image.

(a)

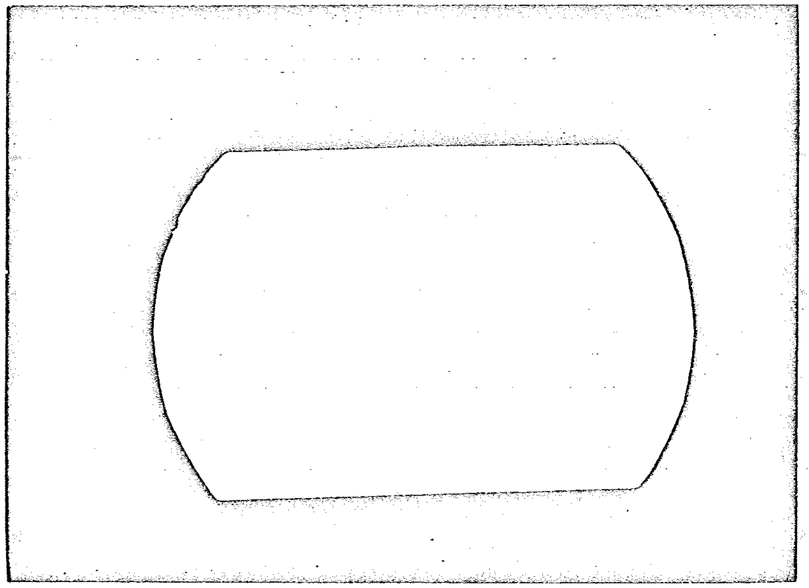

(b)

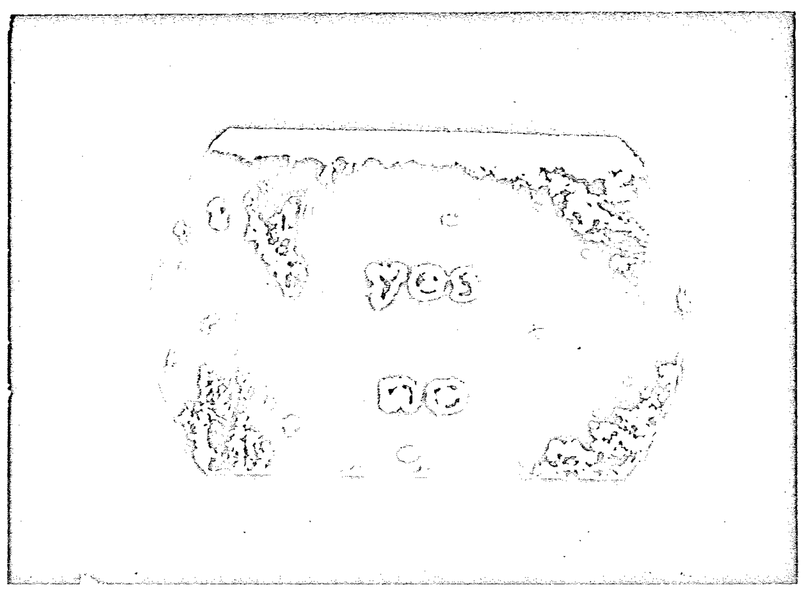

Fig. 11 a) image in output plane with no filtering, b) image in output plane with d.c. filtering.

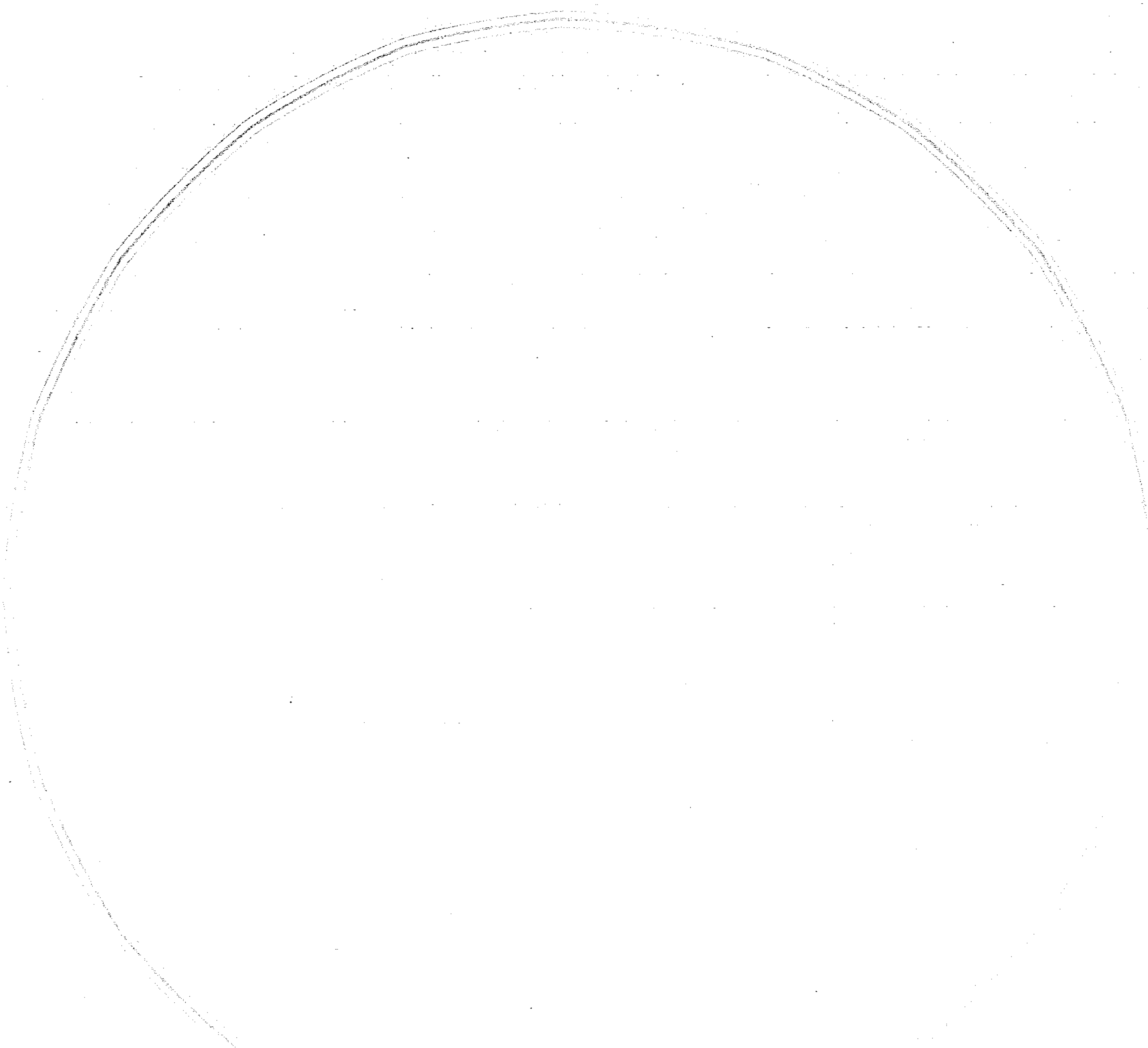

Fig. 12 Output image with no input signal and d.c. filter in transform plane.

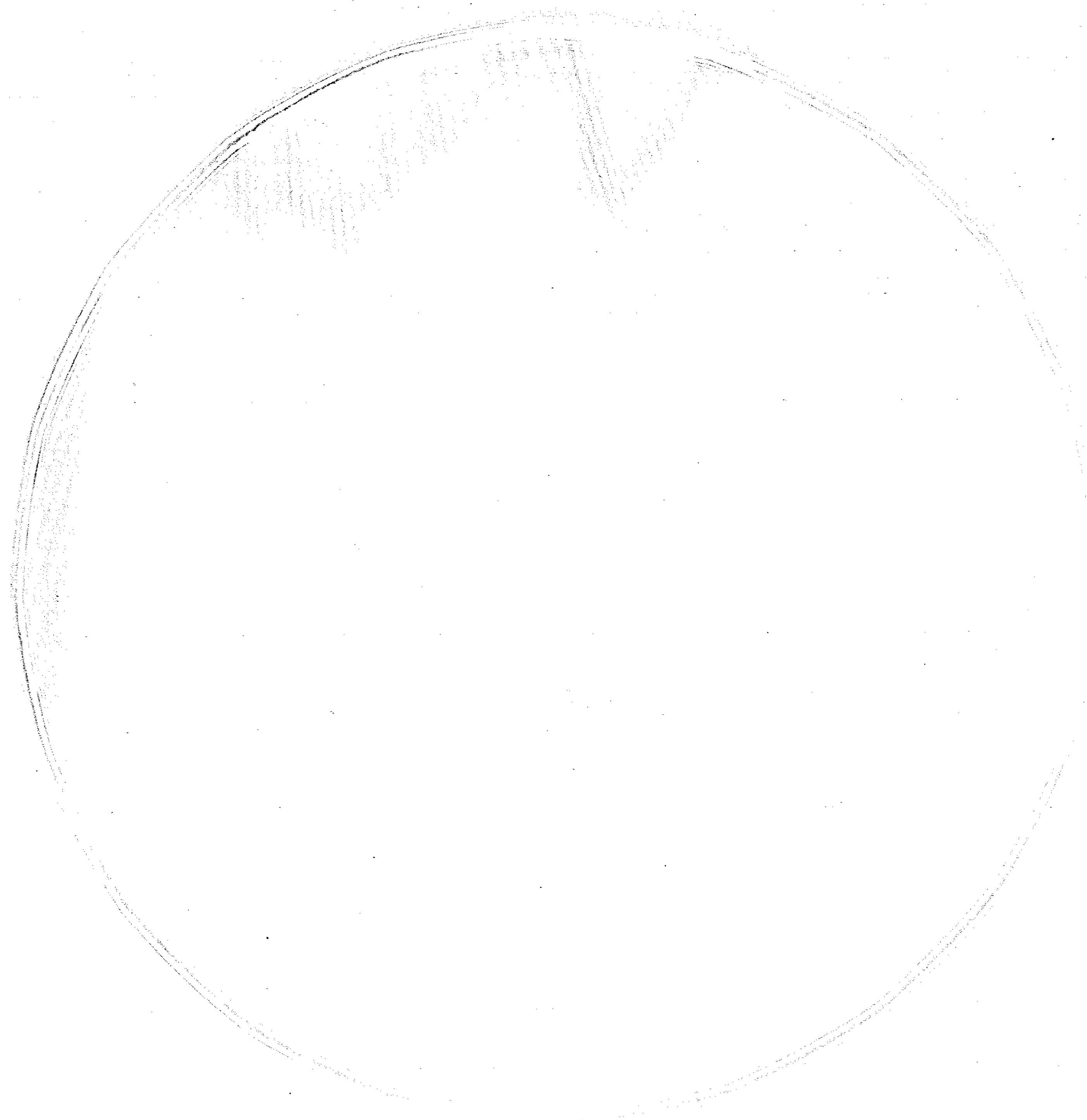

Fig. 13 Output image of good quality windshield sample.

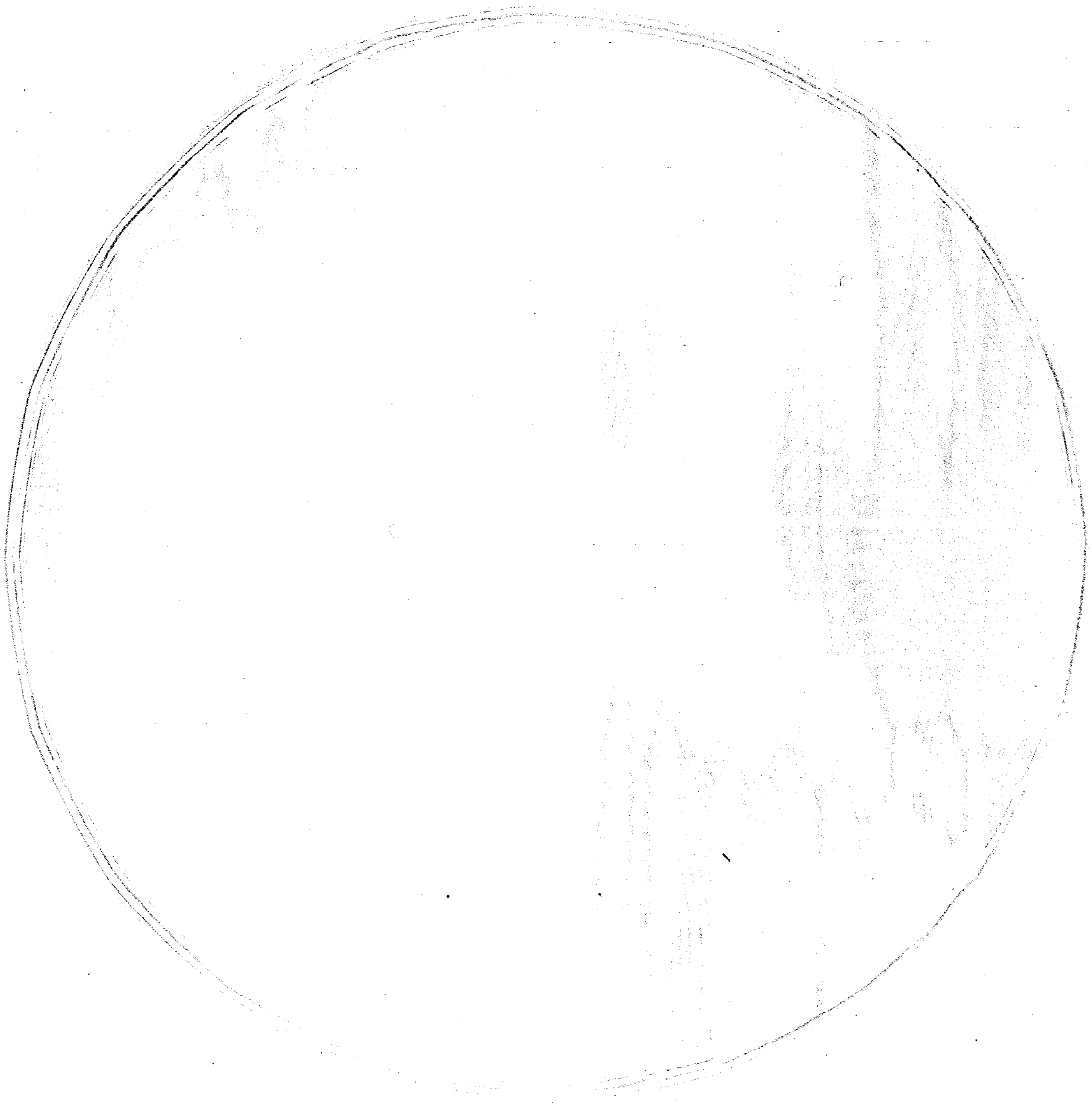

Fig. 14 Output image of poor quality windshield sample.

Fig. 15 Output image of windshield sample with line defects.

APPENDIX 5

FOURIER TRANSFORMING PROPERTIES OF HOLOGRAMS*

by

Richard E. Haskell

Technical Report No. 70-4, September, 1970.

This work was supported in part by NASA under Grant NGR 23-054-003.

*Presented at the Optical Society of America meeting, Hollywood, Florida, October 1, 1970.

School of Engineering
Oakland University
Rochester, Michigan 48063

FOURIER TRANSFORMING PROPERTIES
OF HOLOGRAMS*

Richard E. Haskell

School of Engineering
Oakland University
Rochester, Michigan 48063

ABSTRACT

Holograms are shown to possess ~~a~~ Fourier transforming properties in addition to their well-known imaging properties. Under certain circumstances a direct analogy exists between the Fourier transforming properties of lenses and holograms. It is possible to locate Fourier transform planes in the reconstruction of both the primary and conjugate waves. The existance of the Fourier transform planes depends on the proper selection of the reference and reconstruction beams. A pair of nomographs for point source holographic imaging have been developed and are used to locate the Fourier transform planes. Power spectrum measurements made holographically without the use of lenses are presented. A complete derivation of the Fourier transforming properties of holograms is given.

Holography can be used to produce images without the use of a lens as the imaging element. It is well-known that in addition to their imaging properties, lenses also possess Fourier transforming properties when illuminated with coherent light. In this paper it is shown that holograms also possess Fourier transforming properties.

The holographic imaging of point sources has been discussed by Champagne.[1] The equations for determining the image coordinates of point source holograms are obtained in Section I and two nomographs are introduced for rapidly finding the image coordinates of both the primary image and the conjugate image. These nomographs are useful for visualizing the general imaging properties of holograms and, in particular, for determining whether the image is real or virtual. In Section II it is shown how these nomographs can be used to locate Fourier transform planes and experimental results are presented. A detailed analysis of these results is given in Section III. The entire discussion is limited to plane holograms.

I. HOLOGRAPHIC IMAGING

The holographic imaging of point sources can be described using the geometry of Fig. 1. An object beam in the form of a spherical wave originates from a point source at O. Neglecting constant phase factors, the complex amplitude of this wave at the z = 0 plane can be written as $\underset{\sim}{U}_o = K_o\ e^{jkr_o}$

where $K_o = A_o/r_o$. Similarly the reference beam originating from a point source at R can be written as $\underset{\sim}{U}_r = K_r\, e^{jkr_r}$. If a photographic film is placed in the plane z = 0 the intensity recorded by the film is proportional to

$$|\underset{\sim}{U}_o + \underset{\sim}{U}_r|^2 = \underset{\sim}{U}_o\underset{\sim}{U}_o^* + \underset{\sim}{U}_r\underset{\sim}{U}_r^* + \underset{\sim}{U}_o\underset{\sim}{U}_r^* + \underset{\sim}{U}_o^*\underset{\sim}{U}_r \tag{1}$$

Assuming that the amplitude transmittance of the resulting hologram is proportional to this intensity function and if the reconstruction beam in Fig. 1b is of the form $\underset{\sim}{U}_c = K_c\, e^{jkr_c}$ then the wave transmitted by the hologram located in the z = 0 plane of Fig. 1b will be proportional to

$$\underset{\sim}{U}_T = \underset{\sim}{U}_c\underset{\sim}{U}_o\underset{\sim}{U}_o^* + \underset{\sim}{U}_c\underset{\sim}{U}_r\underset{\sim}{U}_r^* + \underset{\sim}{U}_c\underset{\sim}{U}_o\underset{\sim}{U}_r^* + \underset{\sim}{U}_c\underset{\sim}{U}_o^*\underset{\sim}{U}_r \tag{2}$$

The first two terms on the right-hand side of (2) are d-c terms representing the main zero-order diffracted reconstruction beam. The third term $\underset{\sim}{U}_+ = \underset{\sim}{U}_c\underset{\sim}{U}_o\underset{\sim}{U}_r^*$ is the primary beam and the fourth term $\underset{\sim}{U}_- = \underset{\sim}{U}_c\underset{\sim}{U}_o^*\underset{\sim}{U}_r$ is the conjugate beam. It follows that

$$\underset{\sim}{U}_\pm = K_\pm\, e^{jkr_i^\pm} \tag{3}$$

where

$$r_i^\pm = r_c \pm (r_o - r_r) \tag{4}$$

Thus the primary and conjugate beams $\underset{\sim}{U}_{\pm}$ are spherical waves diverging from or converging to a point specified by image coordinates that can be determined from (4).

From Fig. 1a note that

$$r_o = \left[(x-x_o)^2 + y^2 + z_o^2\right]^{1/2}$$

$$= \left[R_o^2 + x^2 + y^2 - 2xx_o\right]^{1/2} \tag{5}$$

where $R_o^2 = x_o^2 + z_o^2$. Expanding (5) in a binomial series about R_o one can approximate r_o by the expression

$$r_o \approx R_o + \frac{x^2+y^2}{2R_o} - x \sin \alpha_o \tag{6}$$

where $\sin \alpha_o = x_o/R_o$. Analogous expressions can be written for r_r, r_c and r_i. If this is done then by using (3) and (4) one can write

$$\underset{\sim}{U}_{\pm} = K_{\pm}\, e^{jkR_i}\, e^{jk\frac{x^2+y^2}{2R_i}}\, e^{-jkx \sin \theta_i}$$

$$= K_c K_o K_r\, e^{jk[R_c \pm (R_o - R_r)]}\, e^{jk\frac{x^2+y^2}{2}\left[\frac{1}{R_c} \pm \left(\frac{1}{R_o} - \frac{1}{R_r}\right)\right]}$$

$$\cdot\, e^{-jkx[\sin \alpha_c \pm (\sin \alpha_o - \sin \alpha_r)]} \tag{7}$$

For this equation to be true for all x it is necessary that

$$\frac{1}{R_i} = \frac{1}{R_c} \pm \left(\frac{1}{R_o} - \frac{1}{R_r}\right) \tag{8}$$

and

$$\sin \alpha_i = \sin \alpha_c \pm (\sin \alpha_o - \sin \alpha_r) \tag{9}$$

Eqs. (8) and (9) have been obtained by Champagne[1] and give the image coordinates R_i, α_i in terms of the coordinates R, α for the object, reference, and reconstruction beams. If R_i is positive the image is virtual while if R_i is negative the image is real. The plus sign is associated with the primary wave and the minus sign with the conjugate wave.

Eqs. (8) and (9) permit a wide range of possible image point locations depending upon the particular choices of R_o, R_r, R_c, α_o, α_r, and α_c. As an aid in determining image point locations two nomographs[2] of Eqs. (8) and (9) have been constructed as shown in Figures 2 and 3. Two auxiliary variables R_f and α_f have been introduced and are defined by the equations

$$\frac{1}{R_f} = \frac{1}{R_o} - \frac{1}{R_r} \tag{10}$$

and

$$\sin \alpha_f = \sin \alpha_o - \sin \alpha_r \tag{11}$$

The R-nomograph for determing R_i is used in the following manner. A straight line is drawn between R_o on the left-hand axis and R_r on the right hand axis. The intersection of this line with the R_f axis determines a particular value of R_f. If a second straight line is now drawn from this value of R_f to R_c on the left-hand axis the intersection of this second line with the R_i axis determines the image distance R_i for the primary wave. The value of R_i for the conjugate wave is determined by connecting the second straight line from $-R_f$ to R_c. The α-nomograph works in an exactly analogous manner. This procedure will be illustrated by two examples.

Example 1: Let the object be a point source located at R_o = 15 (units arbitrary), $\alpha_o = 0°$ and let the reference beam come from a point source located at $R_r = 60$, $\alpha_r = 20°$. Let the reconstruction beam be the same as the reference beam, i.e., $R_c = 60$, $\alpha_c = 20°$. On the R-nomograph in Fig. 2 the straight line joining $R_o = 15$ and $R_r = 60$ gives a value of $R_f = 20$. To find the primary wave draw a straight line from $R_f = 20$ to $R_c = 60$ which gives the image distance $R_i = 15$. To find the angle α_i for the primary wave draw a straight line in Fig. 3 from $\alpha_o = 0°$ to $\alpha_r = 20°$. A straight line drawn from $\alpha_f = -20°$ to $\alpha_c = 20°$ determines that $\alpha_i = 0°$ for the primary wave. That is, the primary image is a virtual point source located at $R_i = 15$, $\alpha_i = 0°$ which is the same as the object as expected. To find the conjugate image return to Fig. 2 and draw a straight line from $-R_f$ (i.e., $R_f = -20$) to $R_c = 60$ which gives a value of $R_i = -30$. In Fig. 3 a straight line from $-\alpha_f$ ($\alpha_f = +20°$) to $\alpha_c = 20$ shows that for the conjugate wave $\alpha_i = 43°$ Thus, the conjugate image is a real image located at $R_i = -30$, $\alpha_i = 43°$.

Example 2: In Example 1 the primary image was a virtual image and the conjugate image was a real image. As an example of a case in which the primary image is real and the conjugate image is virtual let $R_o = 100$, $\alpha_o = 0°$, $R_r = 20$, $\alpha_r = -15°$, $R_c = 50$, and $\alpha_c = -15°$. Then from Figs. 4 and 5 the primary image is a real image located at $R_i = -50$, $\alpha_i = 0°$ and the conjugate image is a virtual image located at $R_i = 16.6$, $\alpha_i = -31°$.

II. HOLOGRAPHIC SPECTRUM ANALYSIS

It is well known that in addition to their imaging properties, lenses can produce two-dimensional Fourier transforms of spatial signals when illuminated with coherent light.[3] In particular, if coherent light from a point source P shown in Fig. 6 is imaged onto the p-q plane and if a transparency with an amplitude transmittance $\underset{\sim}{g}(x,y)$ is inserted in the x-y plane, then the complex amplitude of light $\underset{\sim}{U}_f(p,q)$ in the p-q plane is given by

$$\underset{\sim}{U}_f(p,q) = \underset{\sim}{K}_f \; e^{j\frac{k}{2d_3}\left(1 - \frac{d_2(d_1+d_2)}{d_1 d_3}\right)(p^2+q^2)} \; \underset{\sim}{G}(f_x,f_y) \qquad (12)$$

where

$$\underset{\sim}{G}(f_x,f_y) = \iint_{-\infty}^{\infty} \underset{\sim}{g}(x,y) \; e^{-j2\pi(f_x x + f_y y)} \, dxdy \qquad (13)$$

is the two-dimensional Fourier transform of $\underset{\sim}{g}(x,y)$ and

$$f_x = \frac{(d_1+d_2)}{\lambda d_1 d_3}\, p \qquad f_y = \frac{(d_1+d_2)}{\lambda d_1 d_3}\, q \tag{14}$$

are the spatial frequencies. If the point source P is moved out to infinity so that the transparency is illuminated with a plane wave then d_3 will reduce to the focal length of the lens and the quadratic phase factor in (12) reduces to $\exp\left[\frac{jk}{2d_3}\left(1 - \frac{d_2}{d_3}\right)\right]$ and the spatial frequencies reduce to the more familiar forms $f_x = p/\lambda d_3$ and $f_y = q/\lambda d_3$. If the signal transparency is now placed in the front focal plane of the lens ($d_2 = d_3$) the quadratic phase factor will vanish altogether. Since it is always the intensity $|\underset{\sim}{U}_f|^2$ that is measured the quadratic phase factor in (12) is generally of no consequence.

Referring to Fig. 6 it is seen that independent of the location of the x-y plane the Fourier transform of $\underset{\sim}{g}(x,y)$ appears in the image plane of the point source P. This suggests that if the lens is replaced by a photographic plate and a hologram is recorded using a point source reference wave, and if a reconstruction beam is chosen that will produce a real image of the point source P, then perhaps at the location of this real image the Fourier transform of $\underset{\sim}{g}(x,y)$ will be displayed. In Section III this will, in fact, be shown to be true for both the primary and conjugate waves.

A number of experiments have been performed which demonstrate this result. Consider the recording and reconstruction geometries shown in Fig. 7. The values of R_r, R_o, R_c, α_r, and α_o are those of Example 1 in Section I. From Fig. 2 it can be seen that the conjugate wave produces a real image of P at a distance $R_i = -30$. If the reconstruction angle α_c is taken equal to $-\alpha_r$ rather than $+\alpha_r$ as in Fig. 3, then instead of being equal to 43° the image angle α_i for the conjugate wave is 0° as shown in Fig. 7b. The three slit signal shown in Fig. 8a was used for $\underset{\sim}{g}(x,y)$ in both the lens system of Fig. 6 and the holographic system of Fig. 7. The light intensity recorded in the p-q plane of Fig. 6 is shown in Fig. 8b and the light intensity recorded in the Fourier transform plane of Fig. 7b is shown in Fig. 8c.

As an example of using the primary wave for Fourier transform measurements consider the recording and reconstruction geometries of Fig. 9. The values of R_o, R_r, R_c, α_o, α_r, and α_c correspond to those of Example 2 in Section I. The primary wave produces an image of P at P' in a Fourier transform plane. Fig. 10 shows a signal and its power spectrum ($|\underset{\sim}{G}|^2$) as measured with a lens and as measured holographically in the transform plane of Fig. 9b.

III. THEORY

In this section a theory will be presented which verifies the existance of Fourier transform planes in holographic imaging, locates these planes, and determines the scale factor which relates the spatial frequencies to the spatial coordinates. The geometry for the analysis is shown in Fig. 11. The signal $\underset{\sim}{g}(x,y)$ is in the x-y plane and the hologram is recorded in the u-v plane. Upon reconstruction one wants the Fourier transform of $\underset{\sim}{g}(x,y)$ to appear in the p-q plane.

The analysis is carried out by determining the complex amplitude of the wave $\underset{\sim}{U}(x,y)$ at various planes perpendicular to the optical axis. If $\underset{\sim}{U}'(x_1,y_1)$ is the complex amplitude of the wave at the plane z = 0 then the complex amplitude $\underset{\sim}{U}(x_o,y_o)$ at a parallel plane a distance z away is given by the Huygen-Fresnel principle[3] as shown in Fig. 12. Referring to this figure one sees that the effect of traveling a distance d in free space is to change $\underset{\sim}{U}'(x_1,y_1)$ to $\underset{\sim}{U}(x_o,y_o)$ through the relation

$$\underset{\sim}{U}(x_o,y_o) = \underset{\sim}{K} \iint_{-\infty}^{\infty} \underset{\sim}{U}'(x_1,y_1)\, e^{j\frac{k}{2d}\left[(x_o-x_1)^2 + (y_o-y_1)^2\right]} dx_1 dy_1 \tag{15}$$

where $\underset{\sim}{K}$ is a complex constant and $\underset{\sim}{U}'(x_1,y_1)$ is assumed to be zero outside the aperture. Just to the left of the signal film in Fig. 11 $\underset{\sim}{U}_1(x,y)$ is the result of light from a point source traveling a distance d_1. To find $\underset{\sim}{U}_1(x,y)$ let $\underset{\sim}{U}'(x_1,y_1) = \delta(x_1,y_1)$ in (15) from which

$$\underset{\sim}{U}_1(x,y) = \underset{\sim}{K}_1\, e^{j\frac{k}{2d_1}(x^2+y^2)} \tag{16}$$

To the right of the signal film $\underset{\sim}{U}_2(x,y)$ is given by

$$\underset{\sim}{U}_2(x,y) = \underset{\sim}{U}_1(x,y)\ \underset{\sim}{g}(x,y) \tag{17}$$

where $\underset{\sim}{g}(x,y)$ is the amplitude transmittance of the signal film.

Let $\underset{\sim}{U}_o(u,v)$ be the resulting object beam in the plane of the hologram. From (15) this object beam can be written as

$$\underset{\sim}{U}_o(u,v) = \underset{\sim}{K}_2 \iint_{-\infty}^{\infty} \underset{\sim}{U}_2(x,y)\ e^{j\frac{k}{2d_2}\left[(u-x)^2+(v-y)^2\right]}\ dxdy \tag{18}$$

Substituting (16) and (17) into (18) one can write

$$\underset{\sim}{U}_o(u,v) = \underset{\sim}{K}_o \iint_{-\infty}^{\infty} \underset{\sim}{g}(x,y)\ e^{j\frac{k}{2}\rho_o}\ dxdy \tag{19}$$

where

$$\rho_o = \frac{1}{d_1}(x^2+y^2) + \frac{1}{d_2}(u^2+v^2+x^2+y^2-2ux-2vy) \tag{20}$$

The reference wave from a point source Q can be written as [see Eq. (6)]

$$\underset{\sim}{U}_r(u,v) = \underset{\sim}{K}_r\ e^{jk\left(\frac{u^2+v^2}{2R_r} - u \sin \alpha_r\right)} \tag{21}$$

Similarly, during the reconstruction process the reconstruction wave from a point source S can be written as

$$\underset{\sim}{U}_c(u,v) = \underset{\sim}{K}_c \; e^{jk\left(\frac{u^2+v^2}{2R_c} - u \sin \alpha_c\right)} \tag{22}$$

The hologram will record the intensity of the sum of the object wave $\underset{\sim}{U}_o(u,v)$ and the reference wave $\underset{\sim}{U}_r(u,v)$ as given by Eq. (1). Upon reconstruction the total field $\underset{\sim}{U}_r(u,v)$ to the right of the hologram in Fig. 11 will be the sum of four terms as shown in Eq. (2). Only the primary and conjugate terms need to be considered since they will be separated from each other and from the d-c terms in the p-q plane. Just to the right of the hologram the primary wave will be designated as

$$\underset{\sim}{U}_4^+ = \underset{\sim}{U}_c \underset{\sim}{U}_o \underset{\sim}{U}_r^* \tag{23}$$

and the conjugate wave will be designated as

$$\underset{\sim}{U}_4^- = \underset{\sim}{U}_c \underset{\sim}{U}_o^* \underset{\sim}{U}_r \tag{24}$$

Eq. (15) can then be used to write the field in the p-q plane as

$$\underset{\sim}{U}_5^{\pm}(p,q) = \underset{\sim}{K}_5 \iint_{-\infty}^{\infty} \underset{\sim}{U}_4^{\pm} \; e^{j\frac{k}{2d_3}\left[(p-u)^2 + (q-v)^2\right]} \, du dv \tag{25}$$

where the upper signs refer to the primary wave and the lower signs refer to the conjugate wave. Combining Eqs. (19) - (25) one can write

$$\underset{\sim}{U}_5^{\pm}(p,q) = \underset{\sim}{K}_6 \iiiint_{-\infty}^{\infty} \underset{\sim}{g}_{\pm}(x,y)\; e^{j\frac{k}{2}\rho_{\pm}}\, dudvdxdy \tag{26}$$

where $\underset{\sim}{g}_{+}(x,y) = \underset{\sim}{g}(x,y)$, $\underset{\sim}{g}_{-}(x,y) = \underset{\sim}{g}^{*}(x,y)$, and

$$\rho_{\pm} = \pm\rho_o + (u^2+v^2)\left(\frac{1}{R_c} \mp \frac{1}{R_r}\right) - 2u\,(\sin\alpha_c \mp \sin\alpha_r)$$

$$+ \frac{1}{d_3}\,(p^2 + q^2 + u^2 + v^2 - 2pu - 2qv) \tag{27}$$

It is first necessary to do the integration over u and v. To this end let the parts of $\rho_{\pm}$ containing u and v be represented by ρ_u and ρ_v respectively. Then (27) can be written as

$$\rho_{\pm} = \rho_u + \rho_v + (x^2+y^2)\left(\pm\frac{1}{d_1} \pm \frac{1}{d_2}\right) + \frac{p^2+q^2}{d_3} \tag{28}$$

where

$$\rho_u = u^2\left(\pm\frac{1}{d_2} \mp \frac{1}{R_r} + \frac{1}{R_c} + \frac{1}{d_3}\right) - 2u\left(\pm\frac{x}{d_2} \mp \sin\alpha_r + \sin\alpha_c + \frac{p}{d_3}\right) \tag{29}$$

and

$$\rho_v = v^2\left(\pm\frac{1}{d_2} \mp \frac{1}{R_r} + \frac{1}{R_c} + \frac{1}{d_3}\right) - 2v\left(\pm\frac{y}{d_2} + \frac{q}{d_3}\right) \tag{30}$$

From the imaging equations (8) and (9)

$$\mp \frac{1}{R_r} + \frac{1}{R_c} = \frac{1}{R_i} \mp \frac{1}{R_o} \tag{31}$$

and

$$\mp \sin \alpha_r + \sin \alpha_c = \mp \sin \alpha_o + \sin \alpha_i \tag{32}$$

If α_o is taken equal to zero and α_c is selected to make α_i equal to zero as in Figs. 7 and 9, then (32) shows that the sin terms are eliminated in (29). From Figs. 7, 9 and 11 set $R_i = -d_3$ and $R_o = d_1+d_2$ in (31). The coefficient of u^2 and v^2 in (29) and (30) then reduces to $\pm\, d_1/d_2(d_1+d_2)$. Since

$$\int_{-\infty}^{\infty} e^{jC_1(u-C_2)^2}\, du = C_3 \int_{-\infty}^{\infty} e^{j\frac{\pi}{2}\,\xi^2}\, d\xi = \text{constant}$$

it is desirable to complete the squares in (29) and (30) and write

$$\rho_u = \rho_u' \mp \frac{d_2(d_1+d_2)}{d_1} \left(\frac{p}{d_3} \pm \frac{x}{d_2}\right)^2 \tag{33}$$

$$\rho_v = \rho_v' \mp \frac{d_2(d_1+d_2)}{d_1} \left(\frac{q}{d_3} \pm \frac{y}{d_2}\right)^2 \tag{34}$$

where

$$\rho_u' = \frac{\pm\, d_1}{d_2(d_1+d_2)} \left[u \mp \frac{d_2(d_1+d_2)}{d_1} \left(\frac{p}{d_3} \pm \frac{x}{d_2}\right)\right]^2 \tag{35}$$

with a similar expression for ρ_v' with u replaced by v, p replaced by q, and x replaced by y.

Substituting (33) and (34) into (28) one obtains

$$\rho_{\pm} = \rho_u' + \rho_v' + (x^2+y^2)\left(\pm \frac{1}{d_1} \pm \frac{1}{d_2} \mp \frac{d_1+d_2}{d_1 d_2}\right)$$

$$+ \frac{(p^2+q^2)}{d_3}\left(1 \mp \frac{d_2(d_1+d_2)}{d_1 d_3}\right) - 2\left(\frac{d_1+d_2}{d_1 d_3}\right)(px + qy) \tag{36}$$

The terms ρ_u' and ρ_v' give a constant when (26) is integrated over u and v. The coefficient of (x^2+y^2) in (36) is identically zero. Thus, (26) can be written as

$$\underset{\sim}{U}_5^{\pm} = \underset{\sim}{K}_7 e^{j\frac{k}{2d_3}\left(1\mp\frac{d_2(d_1+d_2)}{d_1 d_3}\right)(p^2+q^2)} \iint_{-\infty}^{\infty} \underset{\sim}{g}_{\pm}(x,y)\, e^{-j2\pi(f_x x+f_y y)}\, dxdy \tag{37}$$

where

$$f_x = \frac{(d_1+d_2)}{\lambda d_1 d_3}\, p \qquad f_y = \frac{(d_1+d_2)}{\lambda d_1 d_3}\, q \tag{38}$$

Eqs. (37) and (38) should be compared with Eqs. (12), (13) and (14). In particular, the holographic system in Fig. 11 produces the same spectrum measurement in the p-q plane as the lens system shown in Fig. 6 with the same scale factor for the spatial frequencies in terms of d_1, d_2 and d_3.

IV. CONCLUSION

It has been shown both theoretically and experimentally that under certain conditions holograms possess Fourier transforming properties similar to lenses. Thus holograms not only contain information about the image of an object but may also contain information about the Fourier transform of the object. From (37) and (26) one sees that the primary wave $\underset{\sim}{U}_5^+$ is proportional (to within a quadratic phase factor) to the Fourier transform of $\underset{\sim}{g}(x,y)$ while the conjugate wave $\underset{\sim}{U}_5^-$ is proportional to the Fourier transform of $\underset{\sim}{g}^*(x,y)$. Also note that the quadratic phase factor in (37) can be eliminated for the primary wave by using plane wave illumination as discussed for the lens following Eq. (14). However, the quadratic phase factor can never be eliminated for the conjugate wave.

In equation (32) α_o and α_i were set equal to zero for analytical convenience. This is not necessary and leaving the sine terms in simply centers the transform plane at the image location of point P in Fig. 11. In fact, experimentally, it may be desirable to pick an α_o other than zero in order to minimize aberrations and to pick an α_i other than zero in order to maximize the intensity of the diffracted light due to volume hologram effects.

By referring to the nomographs in Figs. 2 and 4 one can show that the image of $\underset{\sim}{g}(x,y)$ in Fig 7b occurs between the hologram plane and the Fourier transform plane, while in

Fig. 9b the image of $\underset{\sim}{g}(x,y)$ occurs to the right of the Fourier transform plane. Thus, in this latter case which uses the primary wave in the reconstruction it would be possible to obtain a filtered version of the output image by means of spatial filtering in the transform plane. This would then be an optical processing system which uses no lenses at all.

ACKNOWLEDGMENTS

The author wishes to acknowledge helpful discussions with Dr. E. B. Champagne of GC Optronics and Dr. J. D. Hovanesian of Oakland University, and to thank Y. Y. Hung and J. Moran who performed the experiments, and W. Gelbach who developed a computer program for plotting the nomographs.

References and Footnotes

* Work supported in part by NASA under Grant NGR 23-054-003.

1. E. B. Champagne, J. Opt. Soc. Am., 57, 51, (1967).

2. Sample copies of these nomographs may be obtained by writing the author.

3. See e.g. J. W. Goodman, Introduction to Fourier Optics, McGraw-Hill Book Company, New York, (1968).

List of Figures

Fig. 11 Recording and reconstruction geometry for theory developed in Section III.

Fig. 12 Fresnel diffraction at an aperture.

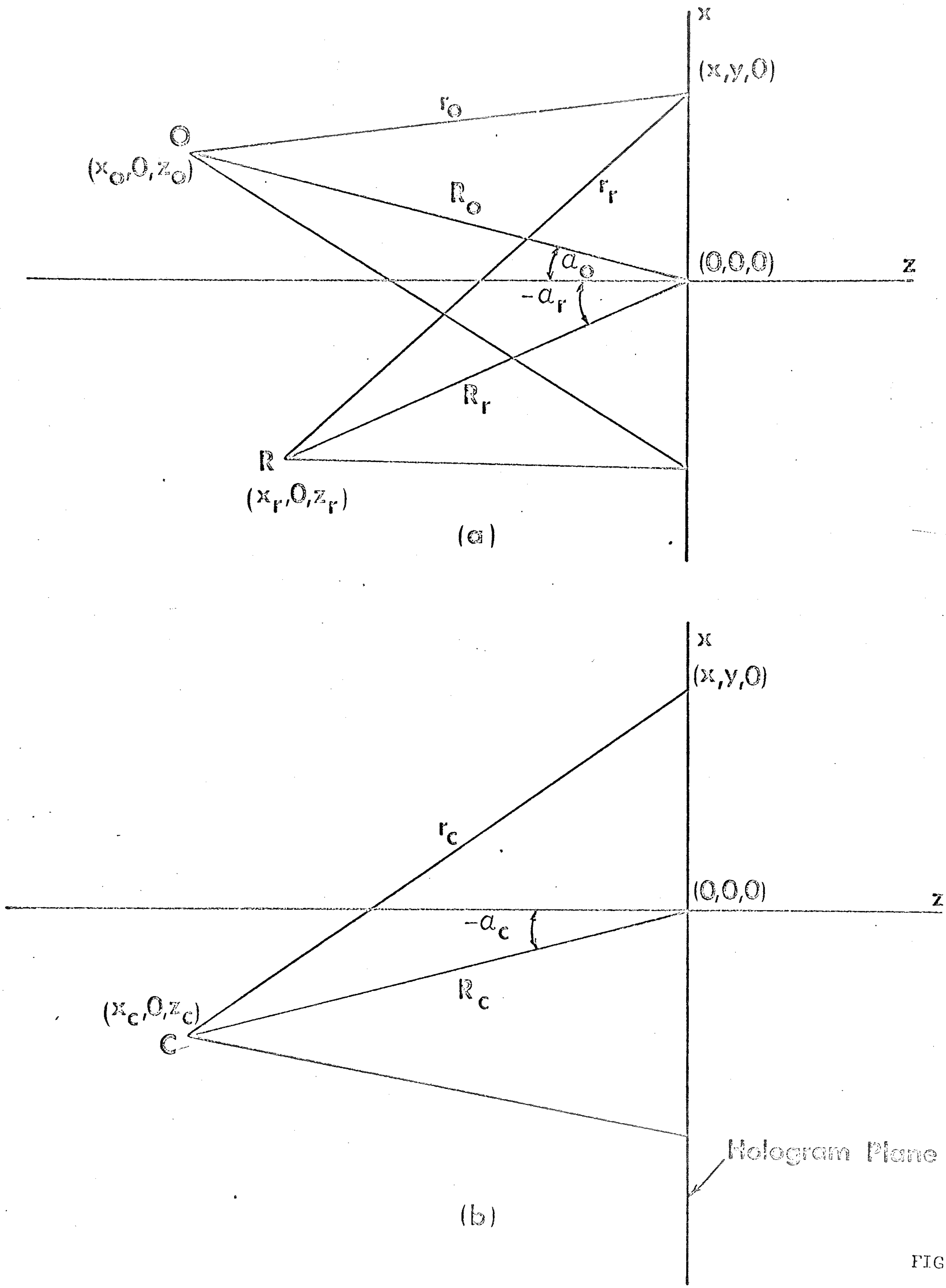
x
(x,y,0)
r_o
O
$(x_o,0,z_o)$
R_o
r_r
a_o
(0,0,0)
z
$-a_r$
R_r
R
$(x_r,0,z_r)$
(a)
x
(x,y,0)
r_c
(0,0,0)
z
$-a_c$
R_c
$(x_c,0,z_c)$
C
Hologram Plane
(b)

FIG. 1

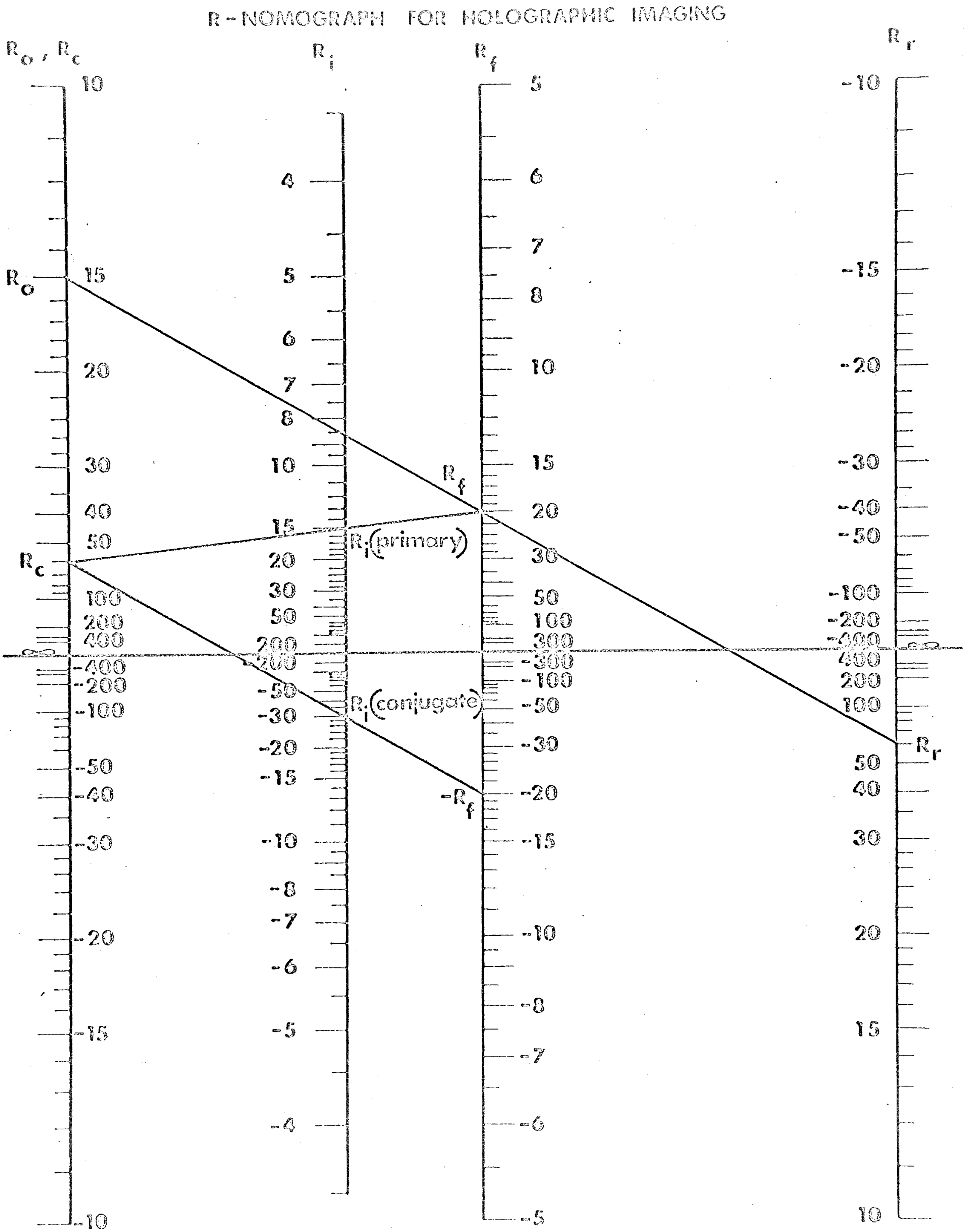
R - NOMOGRAPH FOR HOLOGRAPHIC IMAGING
R_o, R_c
R_i
R_f
R_r
R_o
R_c
R_f
R_i(primary)
R_i(conjugate)
$-R_f$
R_r
∞

FIG. 2

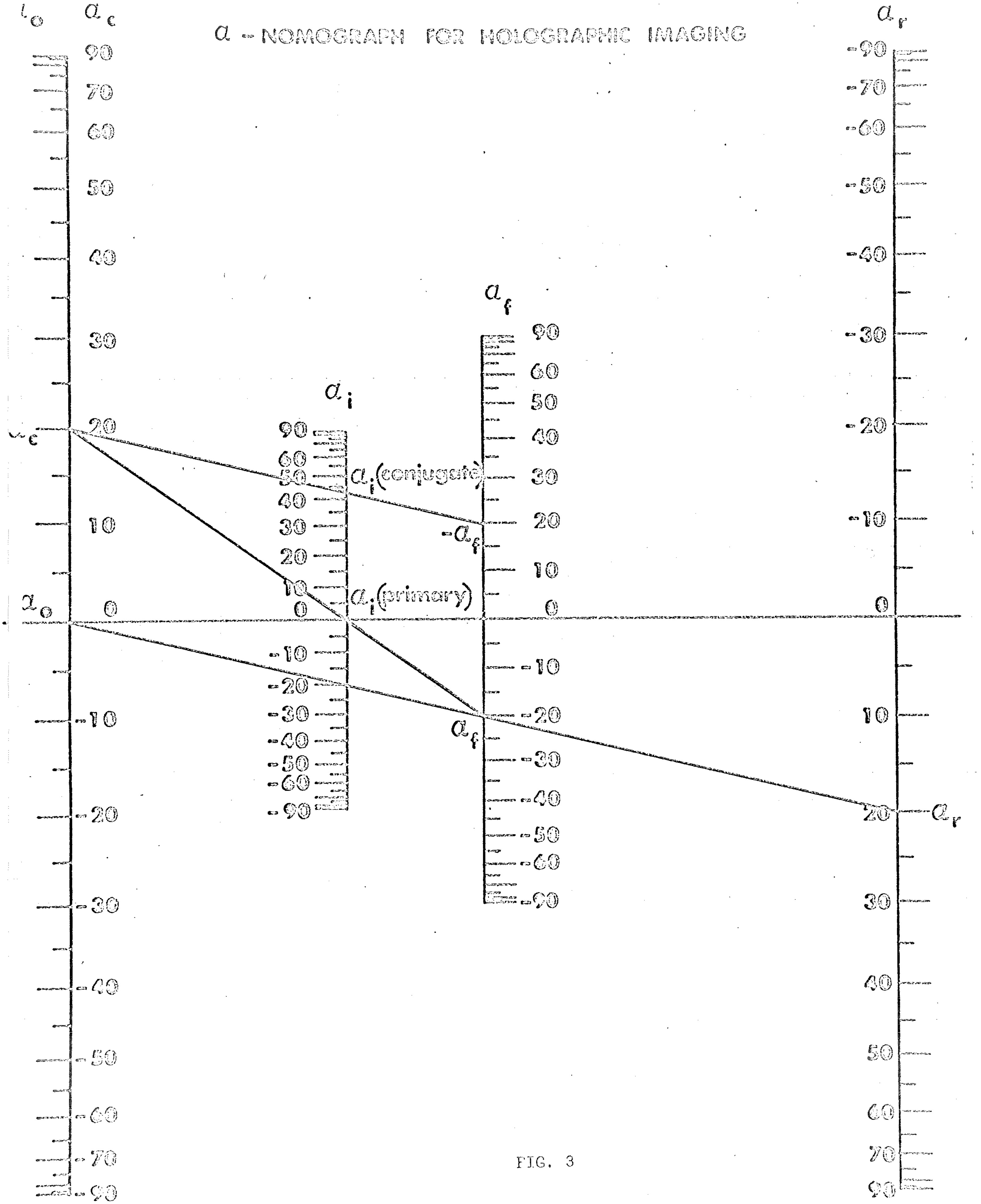

α - NOMOGRAPH FOR HOLOGRAPHIC IMAGING
α_o
α_c
α_i
α_f
α_r
α_i (conjugate)
α_i (primary)
-α_f

FIG. 3

R-NOMOGRAPH FOR HOLOGRAPHIC IMAGING

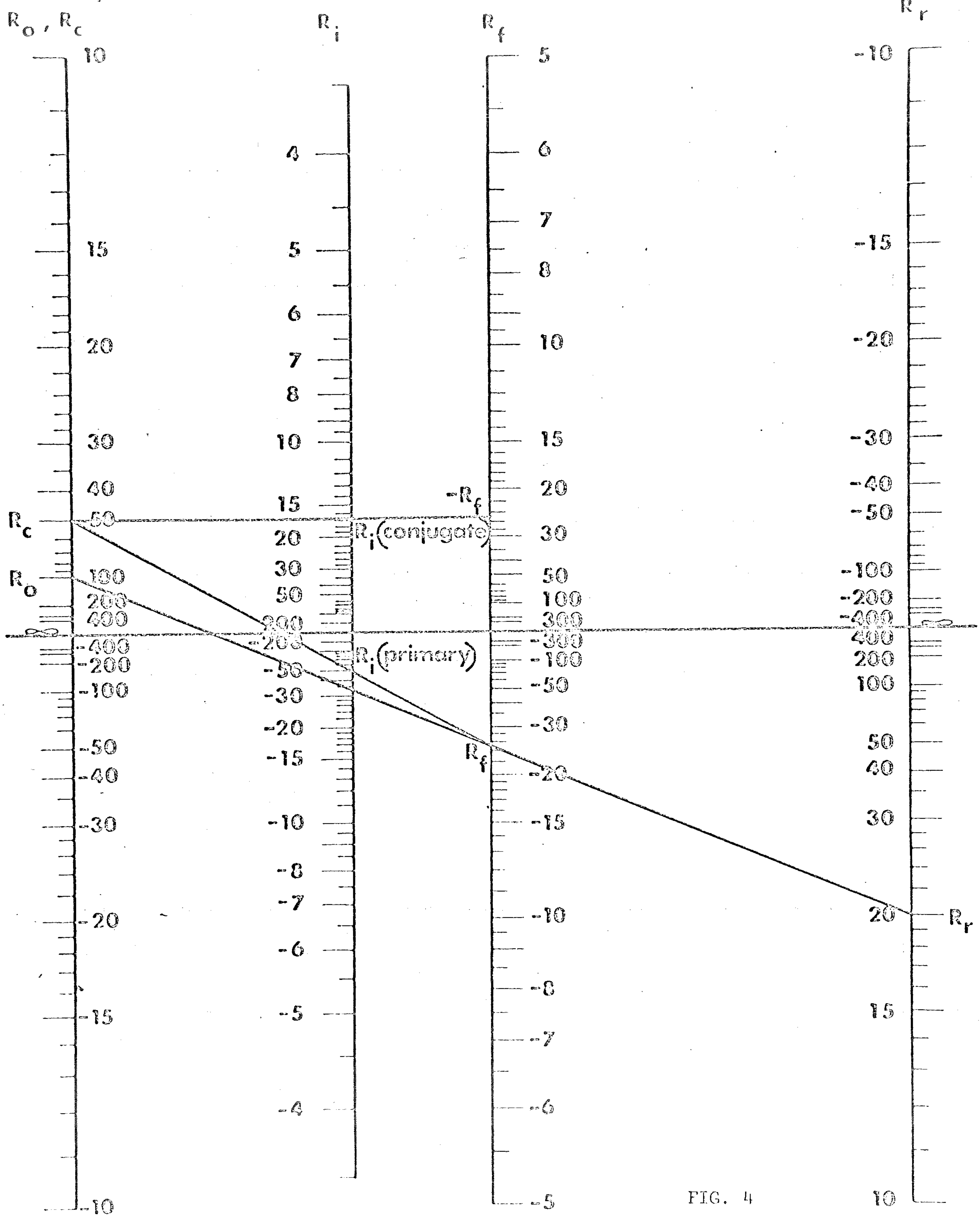

FIG. 4

α - NOMOGRAPH FOR HOLOGRAPHIC IMAGING

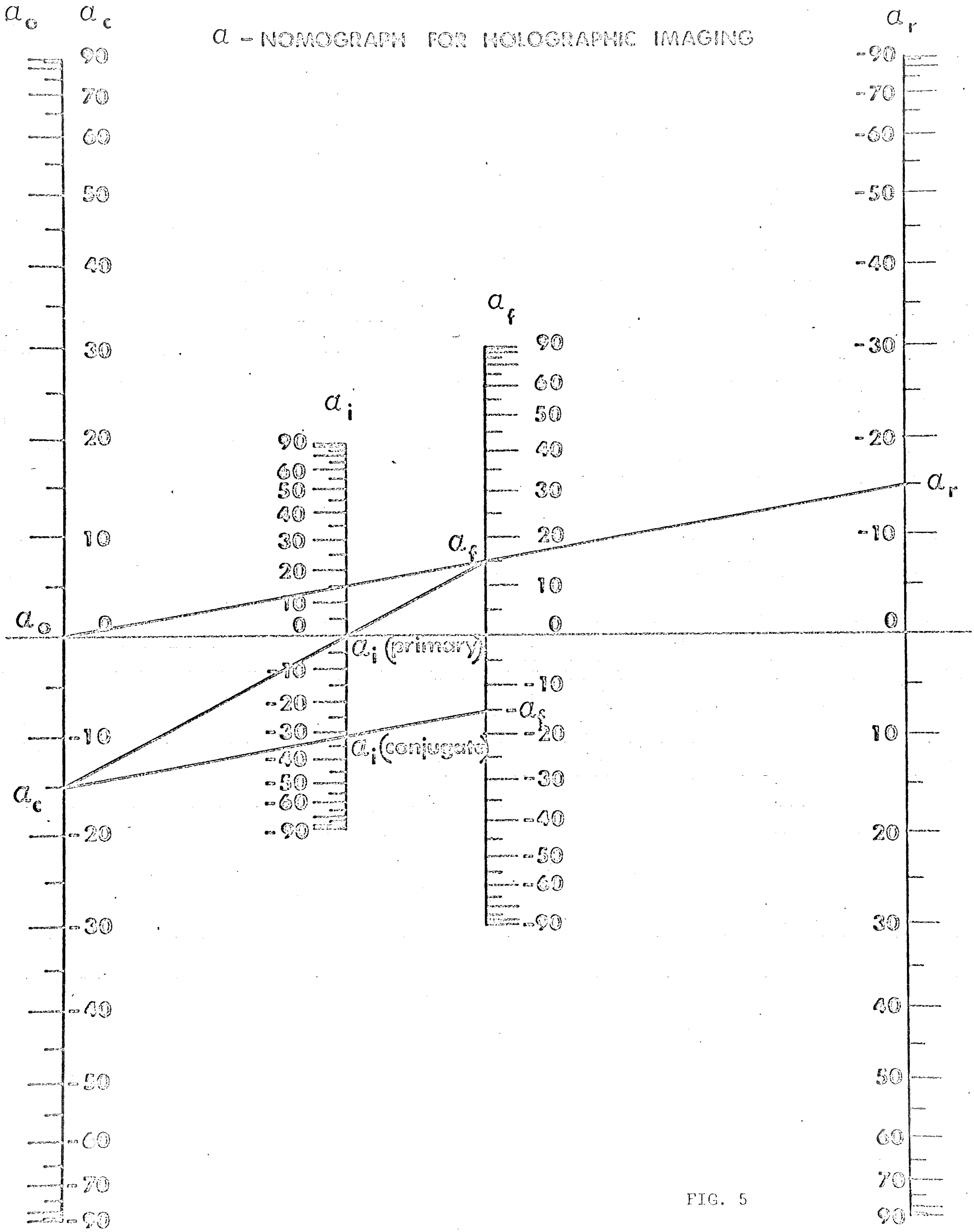

FIG. 5

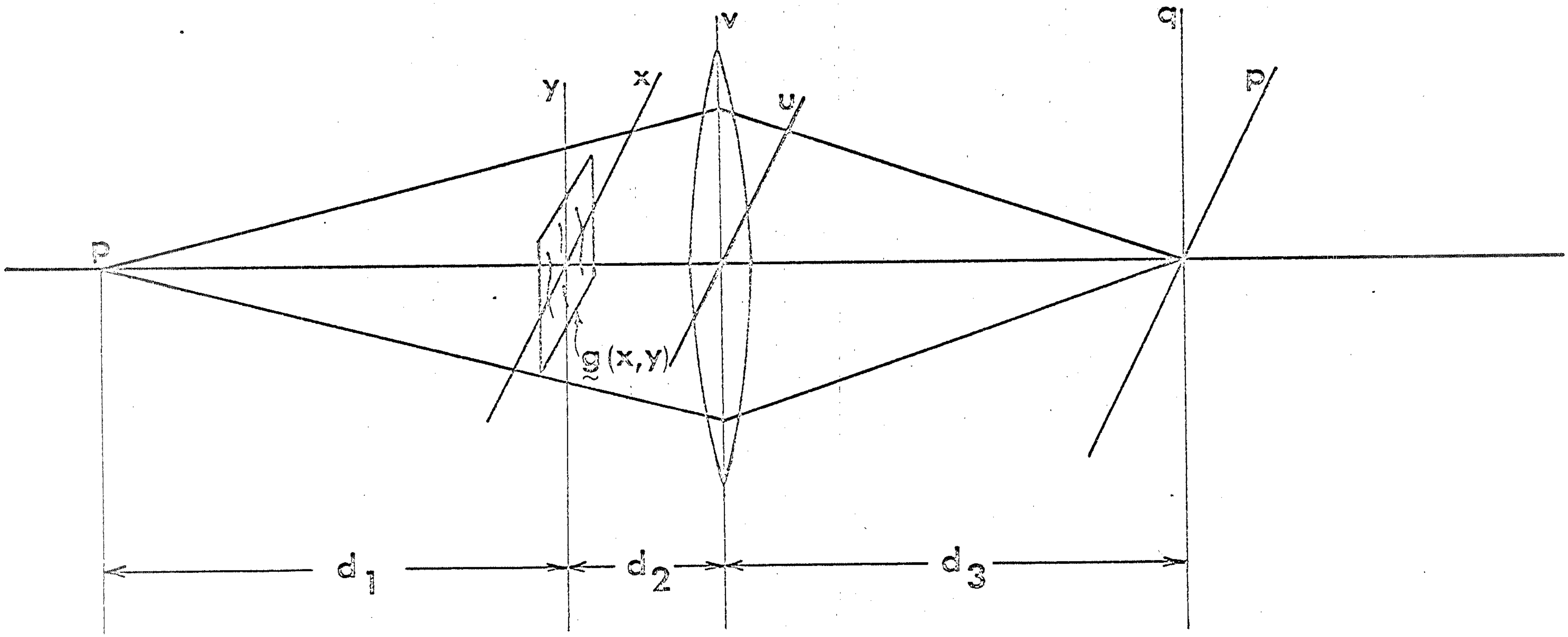

FIG. 6

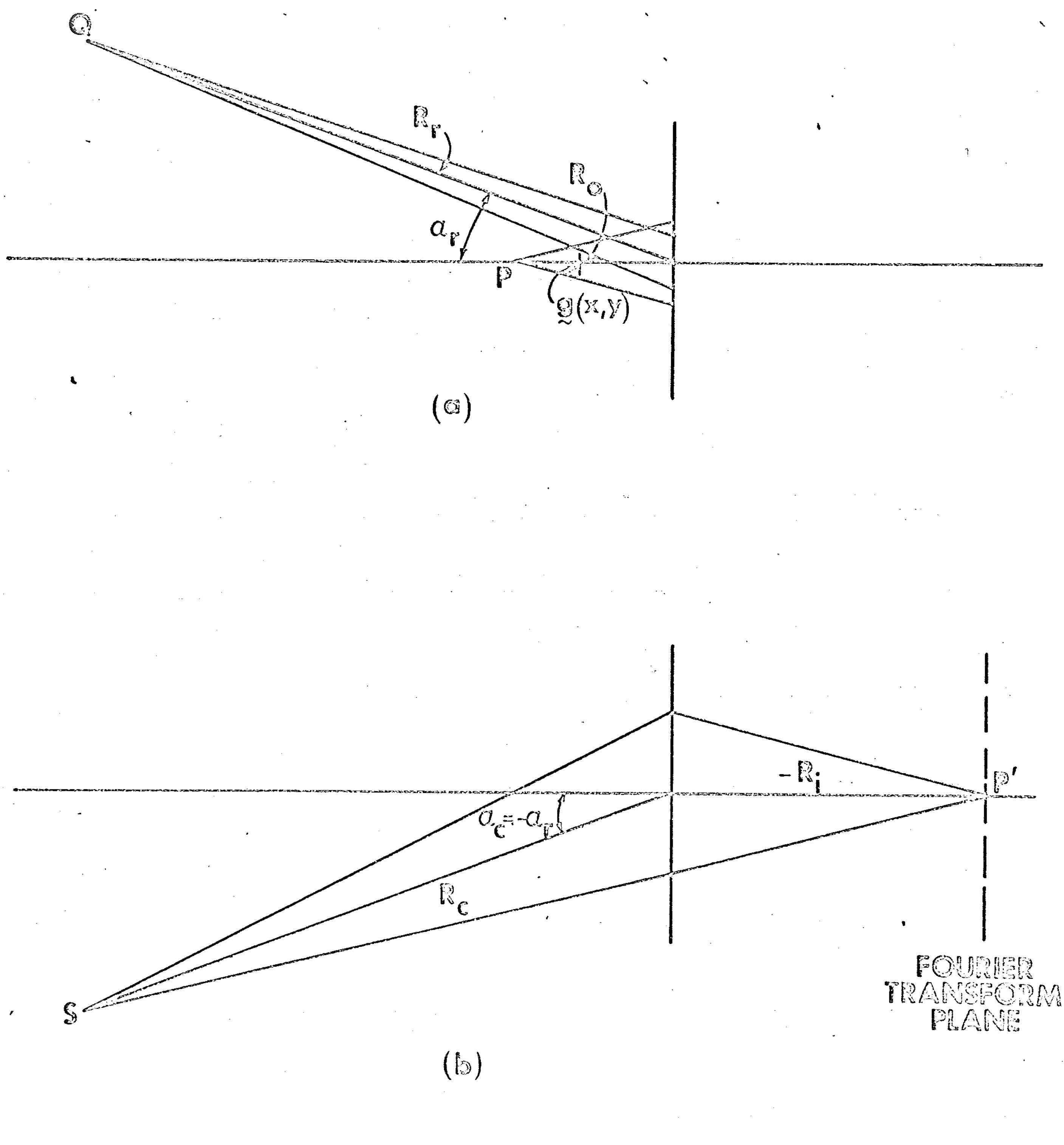

FIG. 7

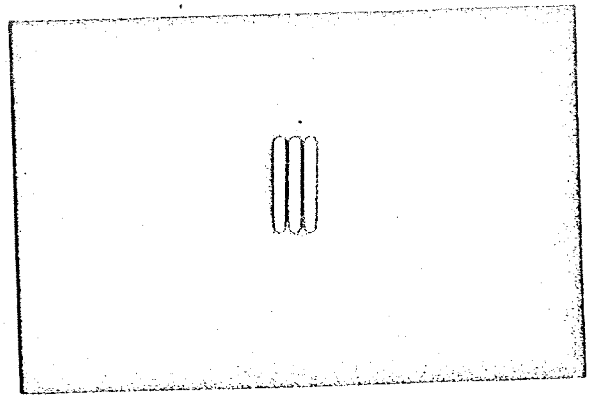

(a)

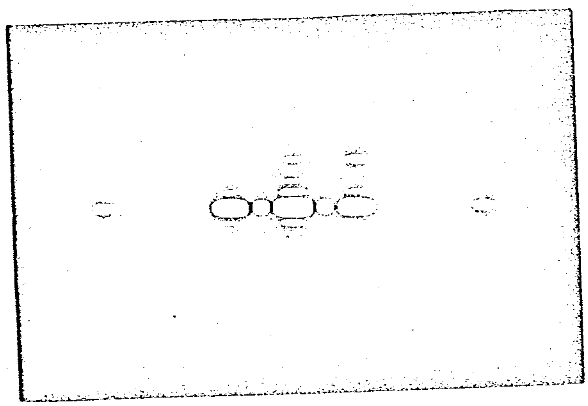

(b)

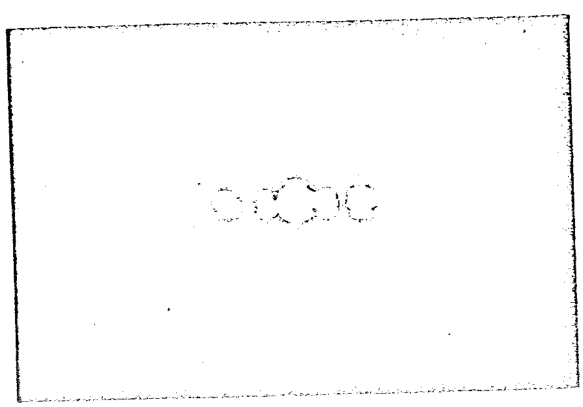

(c)

FIG. 8

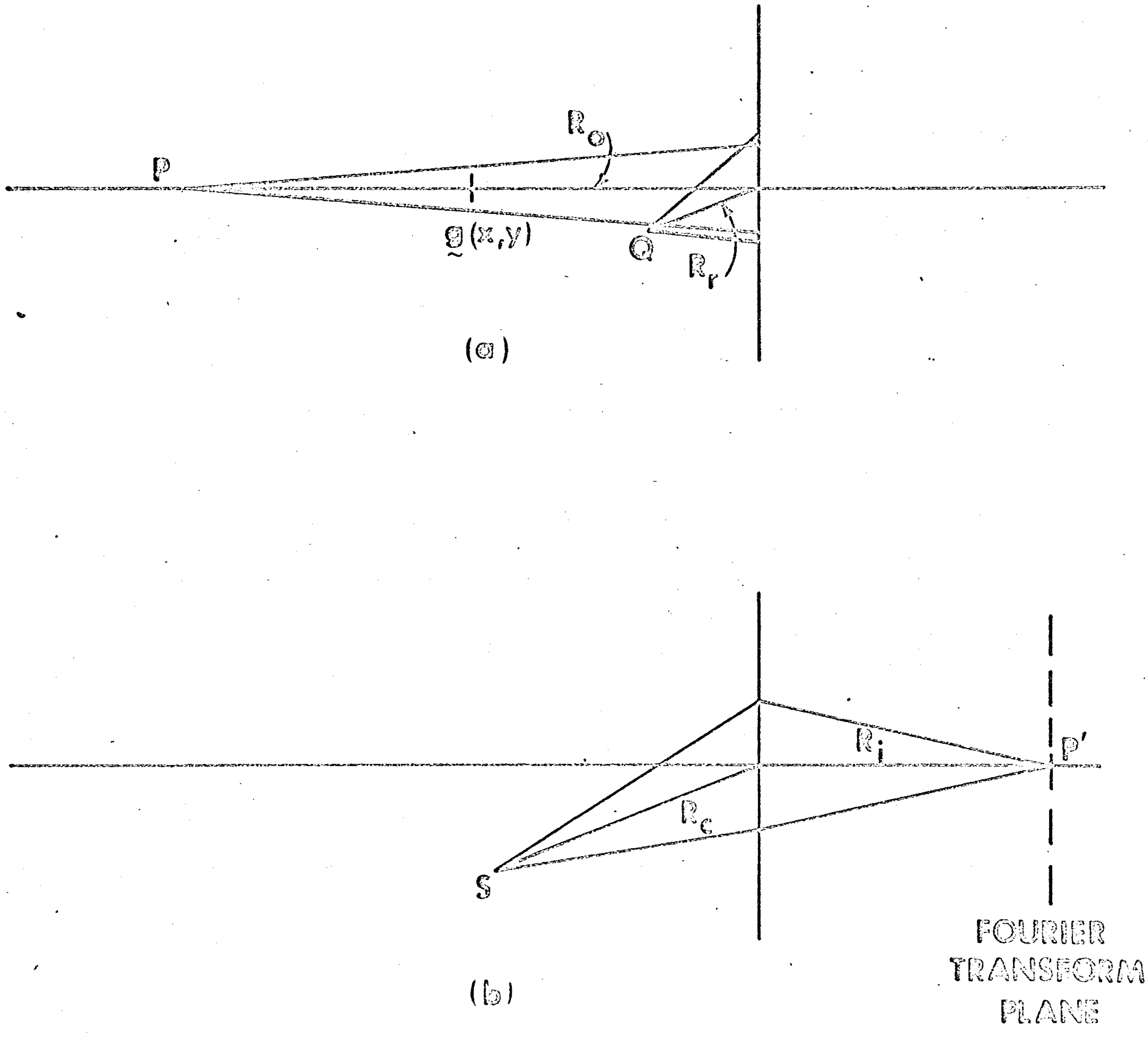

FIG. 9

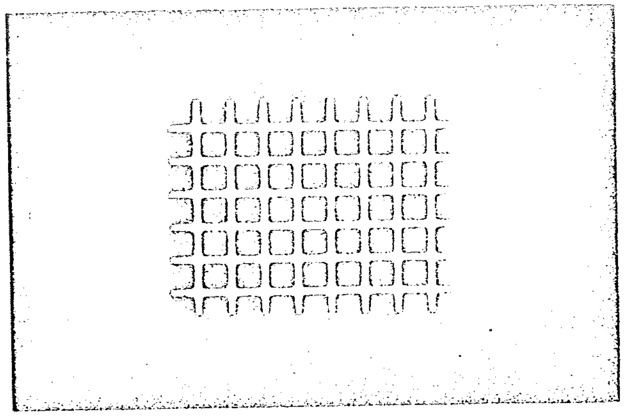
(a)

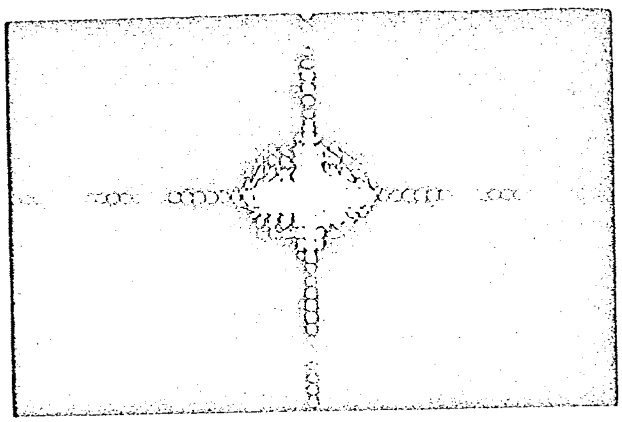
(b)

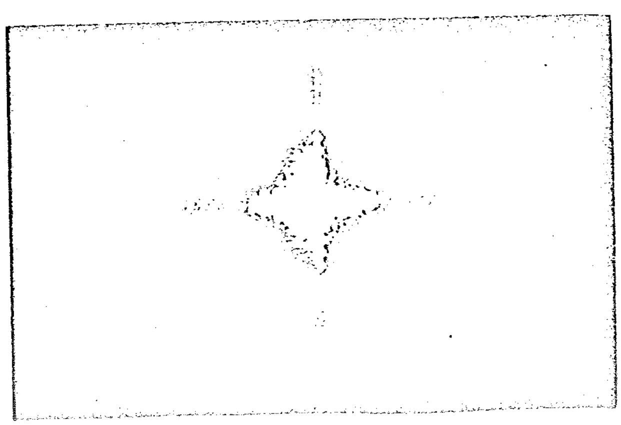
(c)

FIG. 10

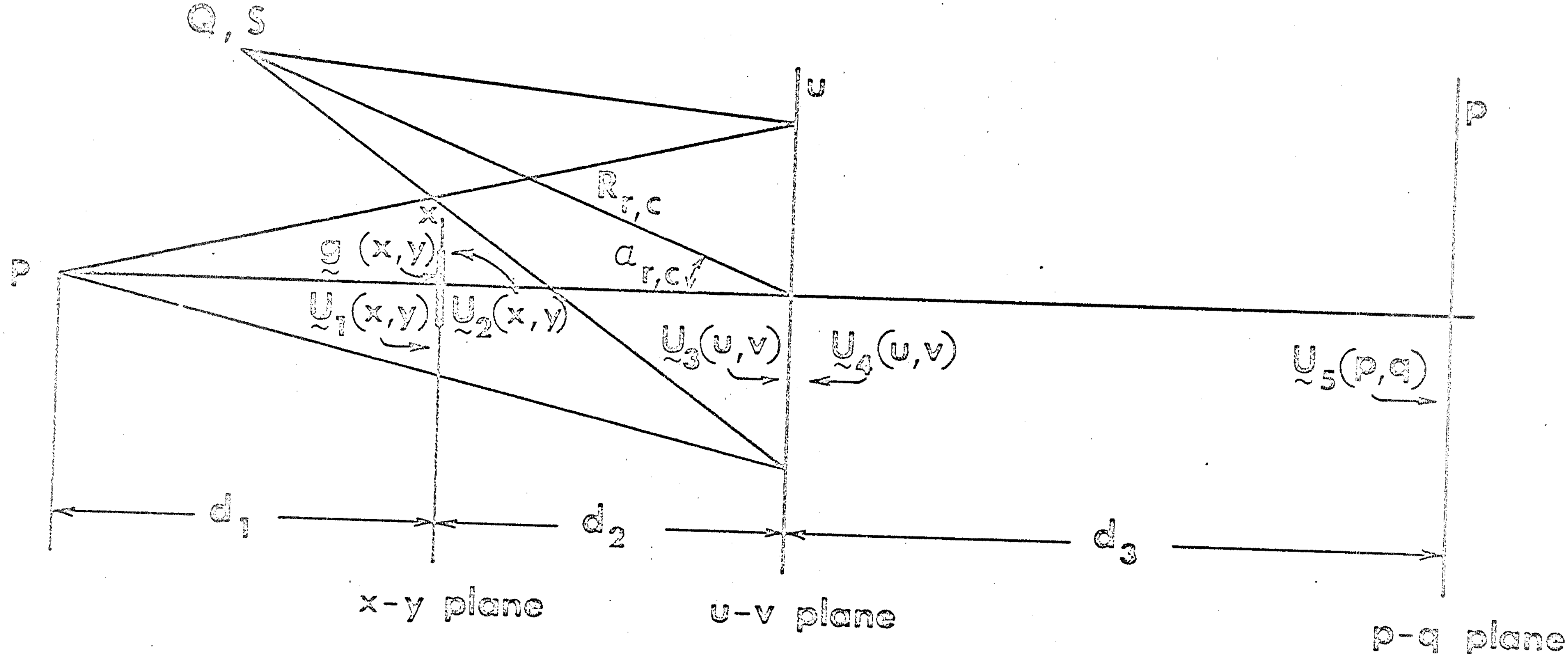
Q, S
u
p
R r,c
x
g (x,y)
P
a r,c
U 1(x,y)
U 2(x,y)
U 3(u,v)
U 4(u,v)
U 5(p,q)
d 1
d 2
d 3
x-y plane
u-v plane
p-q plane

FIG. 11

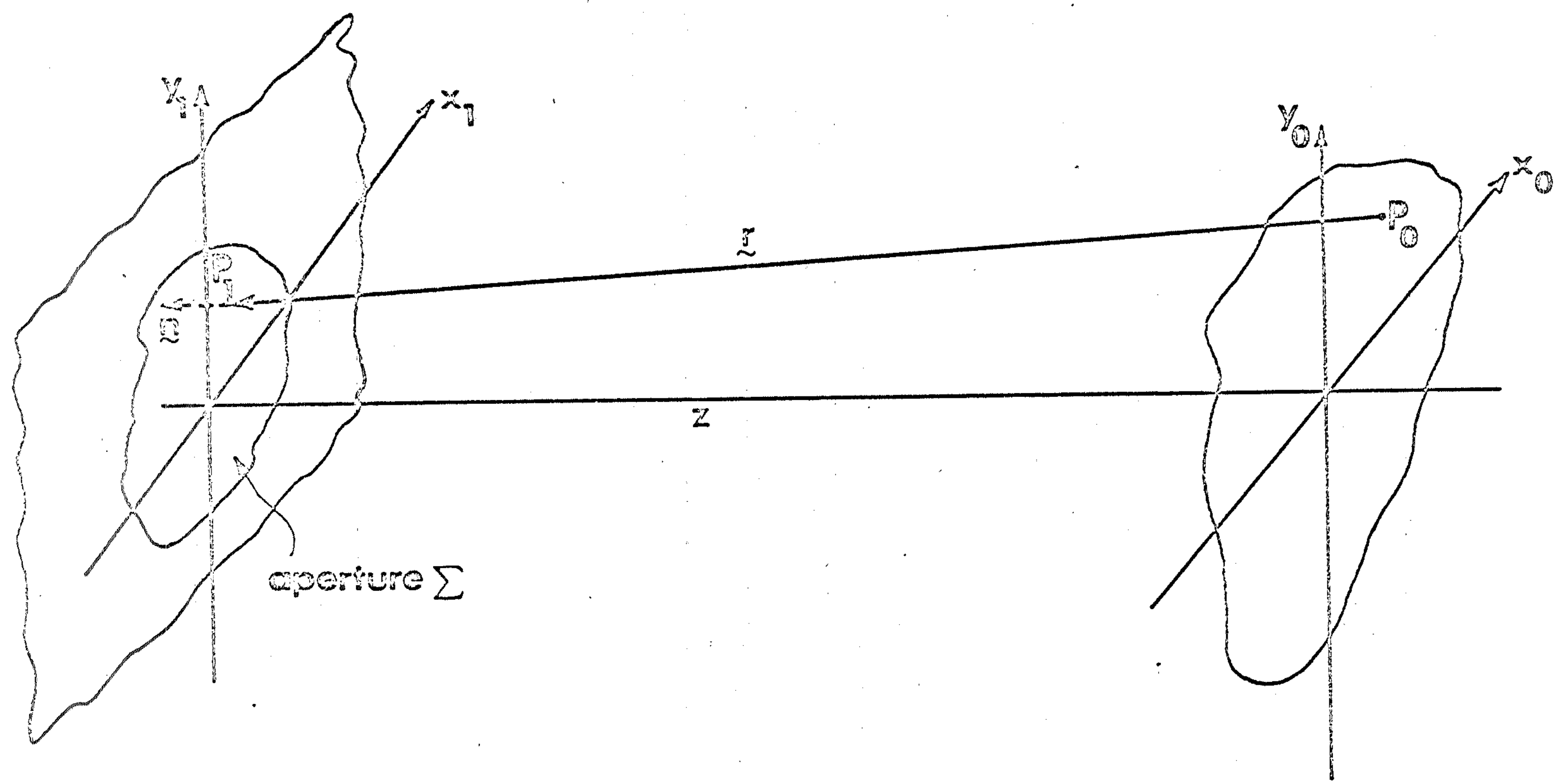

$$r \approx z\left[1 + \frac{1}{2}\left(\frac{x_0 - x_1}{z}\right)^2 + \frac{1}{2}\left(\frac{y_0 - y_1}{z}\right)^2\right] \qquad \text{(Paraxial Approximation)}$$

$$\underset{\sim}{U}(x_0, y_0) = \frac{1}{j\lambda}\iint_{\Sigma} \underset{\sim}{U}'(x_1, y_1)\,\frac{e^{jkr}}{r}\cos(\underset{\sim}{n}, \underset{\sim}{r})\,dx_1 dy_1$$

$$\approx \frac{e^{jkz}}{j\lambda z}\iint_{-\infty}^{\infty} \underset{\sim}{U}'(x_1, y_1)\, e^{j\frac{k}{2z}\left[(x_0 - x_1)^2 + (y_0 - y_1)^2\right]} dx_1\, dy_1$$

FIG. 12